10-21-2021

Quantifying How Coastal Flooding and Stormwater Runoff Drive Spatiotemporal Variability in Carbon and Nutrient Processing in Urban Aquatic Ecosystems

Matthew A. Smith
msmit275@fiu.edu

FLORIDA INTERNATIONAL UNIVERSITY

Miami, Florida

QUANTIFYING HOW COASTAL FLOODING AND STORMWATER RUNOFF DRIVE SPATIOTEMPORAL VARIABILITY IN CARBON AND NUTRIENT PROCESSING IN URBAN AQUATIC ECOSYSTEMS

A dissertation submitted in partial fulfillment of the

requirements for the degree of

DOCTOR OF PHILOSOPHY

in

BIOLOGY

by

Matthew Smith

2021

To: Dean Michael R. Heithaus
College of Arts, Sciences and Education

This dissertation, written by Matthew Smith, and entitled Quantifying How Coastal Flooding and Stormwater Runoff Drive Spatiotemporal Variability in Carbon and Nutrient Processing in Urban Aquatic Ecosystems, having been approved in respect to style and intellectual content, is referred to you for judgment.

We have read this dissertation and recommend that it be approved.

Omar Abdul-Aziz

Evelyn Gaiser

René Price

Tiffany Troxler

John Kominoski, Major Professor

Date of Defense: October 21, 2021

The dissertation of Matthew Smith is approved.

Dean Michael R. Heithaus
College of Arts, Sciences and Education

Andre G. Gil
Vice President for Research and Economic Development
and Dean of the University Graduate School

Florida International University, 2021

DEDICATION

I dedicate this dissertation to my family, Dwight, Vira, Chris, and Kate, whose support was essential to the completion of this work.

ACKNOWLEDGMENTS

I thank my advisor, Dr. John Kominoski, for his endless support and expertise. John has challenged me to think critically, ask carefully, and communicate clearly. His guidance pushed me to put forth my best work and I could not have succeeded without his mentorship. I'm fortunate to have such an excellent scientist as a mentor and I will cherish your advice for years to come.

My committee members, Dr. Evelyn Gaiser, Dr. Tiffany Troxler, Dr. Renè Price, and Dr. Omar Abdul-Aziz, were invaluable contributors to this dissertation and to my development as a scientist. I thank them for their support and critical advice over the years. This dissertation represents research projects that involved many collaborators, whom I thank for their contributions, including Dr. Nancy Grimm, Dr. Olga Barbosa, Dr. Elizabeth Cook, Dr. Jennifer Morse and many others.

I thank my wonderful lab mates of past and present: Sean, Shelby, Ben, Ximena, Dong Yoon, Andrea, Kenny, Sophia, Ryan, & Chris. I thank the entire Urban Resilience to Extremes Sustainability Research Network (UREx SRN) for providing countless opportunities to develop my interdisciplinary research. I thank the leadership and members of the Florida International University CREST Center for Aquatic Chemistry and Environment for their support and technical assistance.

I am extremely grateful for the exemplary work of the undergraduate students I have had the privilege of mentoring, including Andreina Contreras, Alessandra Puig-Santana, Gonzalo Eyzaguirre, and Daniel Reed.

This dissertation was funded by the National Science Foundation (NSF) Grant No. SES-1444755, Urban Resilience to Extremes Sustainability Research Network (UREx SRN). Additional funding was provided by the NSF Center for Research Excellence in Science and Technology (CREST) (Grant No. HRD-1547798).

ABSTRACT OF THE DISSERTATION

QUANTIFYING HOW COASTAL FLOODING AND STORMWATER RUNOFF DRIVE SPATIOTEMPORAL VARIABILITY IN CARBON AND NUTRIENT PROCESSING IN URBAN AQUATIC ECOSYSTEMS

by

Matthew Smith

Florida International University, 2021

Miami, Florida

Professor John Kominoski, Major Professor

Coastal river networks alter the transport and transformation of dissolved organic carbon (DOC) and dissolved organic matter (DOM), which vary in concentration and composition across spatiotemporal scales. Climate-induced shifts in rainfall and tidal variation in coastal regions can significantly alter DOC and DOM regimes by influencing the timing and delivery of fresh versus saltwater to coastal waterways. While the sources of pollution in urban ecosystems are well understood, the influence of flooding on biogeochemical cycling is uncertain. Most research on DOC and DOM in urban aquatic systems to-date has not been done in low-lying coastal areas, despite the majority of the world's cities residing in coastal regions. Thus, quantifying changes in the hydrologic and land-use drivers of DOM source and composition change is needed to understand its role in metabolic processing and export to downstream aquatic ecosystems.

In Chapter 2, I evaluated time-variable interactions among water source contributions in urban canals and found that terrestrially-sourced DOC and DOM is pulsed to urban canals and supplemented by microbially-sourced DOM during the wet season at high tide. In Chapter 3, I compared the source and composition of DOM across urban canals and found that interactions between runoff and tides in-

creased bioavailability and increases in recently produced DOM corresponded with elevated indicators of human waste from groundwater inputs. In Chapter 4, I examined the role of hydrologic and landscape variables on water column versus whole system nutrient uptake capacity of urban wetlands. We found that nutrient uptake in the water column represents a significant portion of total uptake and increases in the stoichiometric availability of labile carbon can stimulate sequestration of nitrate and phosphorus in nutrient-limited urban wetlands. Finally, Chapter 5 investigated how urbanization has impacted the spatiotemporal variability of high discharge events across regional climates. Here, I introduce the urban flow-shunt flood-pulse concept to better explain how spatiotemporal synchrony of urban stream discharge occurs following extreme precipitation across regional climates. Together, this research shows that urban aquatic systems serve as biogeochemical hotspots where transformations of DOC and DOM are influenced by the source, magnitude, and timing of water contributions to coastal environments.

TABLE OF CONTENTS

CHAPTER PAGE

1. Introduction 1
1.1 Bibliography 8

2. Linking seasonal changes in organic matter composition and nutrients to shifting hydraulic gradients in coastal urban canals using a Bayesian mixing model 14
2.1 Abstract 15
2.2 Introduction 16
2.3 Methods 19
2.4 Results 25
2.5 Discussion 31
2.6 Conclusions 35
2.7 Bibliography 36
2.8 Tables 42
2.9 Figures 44
2.10 Supplemental Information 54

3. Stormwater runoff and tidal flooding transform dissolved organic matter composition and increase bioavailability in urban coastal ecosystems 60
3.1 Abstract 61
3.2 Introduction 62
3.3 Methods 66
3.4 Results 72
3.5 Discussion 78
3.6 Conclusions 85
3.7 Bibliography 87
3.8 Tables 98
3.9 Figures 103
3.10 Supplemental Information 111

4. Dissolved organic matter composition and phosphorus limitation mediate water-column and whole-system nutrient uptake in urban wetlands 120
4.1 Abstract 121
4.2 Introduction 122
4.3 Methods 125
4.4 Results 132
4.5 Discussion 136
4.6 Conclusions 142
4.7 Bibliography 143
4.8 Tables 153

4.9 Figures . . . 157

5. Synchronizing hydrology in urban watersheds: flow-shunt flood-pulse concept . . . 164
5.1 Abstract . . . 165
5.2 Introduction . . . 166
5.3 Methods . . . 169
5.4 Results . . . 172
5.5 Discussion . . . 175
5.6 Conclusions . . . 180
5.7 Bibliography . . . 182
5.8 Tables . . . 191
5.9 Figures . . . 192
5.10 Supplemental Information . . . 202

6. CONCLUSIONS . . . 204
6.1 Bibliography . . . 207

VITA . . . 209

LIST OF TABLES

TABLE PAGE

2.1 Mean (± standard deviation) values for hydrologic variables, water physicochemistry, and DOM optical properties in surface, ground, and marine water from June 2018 to May 2019 . 42

2.2 Coefficients, variance, and significance of multiple linear regression model to explain differences in DOC concentrations of surface canal waters. 43

2.3 List of USGS, SFWMD, NOAA, and Miami-Dade County DERM hydrologic variable collection sites for rainfall, groundwater, canal stage/flow, and marine water. 58

2.4 DOM Fluorescence indices analyzed in this study, indicating the calculation and interpretation according to referenced literature. 59

3.1 Land use and cover characteristics of canal drainage basins in Miami, FL, USA. 98

3.2 Mean (± standard deviation) values for hydrologic variables, water physicochemistry, optical properties, and autotrophic and heterotrophic biological stocks including process rates in surface water and groundwater during dry (November-April) and wet (May-October) seasons from June 2018 to May 2019. 99

3.3 Results of two-way ANOVA with balanced design of effects of tide and season on % BDOC. 100

3.4 Emission and excitation maxima and characteristics of modeled EEM-PARAFAC components 101

3.5 Statistical comparisons of EEM-PARAFAC components across seasons, tides, and location with percent bioavailable DOC (BDOC) as a covariate using two-way repeated measures analysis of covariance (ANCOVA). 102

3.6 List of USGS/SFWMD collection sites for canal stage/flow, groundwater, and rainfall. 118

3.7 Results of two-way repeated measures ANOVA on mean values for water physicochemistry and autotrophic and heterotrophic biological stocks and process rates in each canal basin during dry (November-April) and wet (May-October) season between June 2018 to May 2019. 119

4.1 Physicochemical characteristics of urban wetland sites in Valdivia, Chile. 153

4.2 Fluorescence excitation-emission matrices of dissolved organic carbon (DOC) in riparian wetlands. 154

4.3 First-order loss rates (k; h-1) for field and water column uptake of nitrate ($NO3^-$), ammonium ($NH4^+$), and soluble reactive phosphorus (SRP) across a gradient of watershed imperviousness. 155

4.4 Structural equation modeling fit statistics of whole system (WS) and water column (WC) uptake of nitrate ($NO3^-$) and soluble reactive phosphorus (SRP). 156

5.1 Watershed characteristics of non-urban and urban watersheds using NLCD 2016 and GAGESII dataset information. 191

5.2 List of streamflow statistics from Archfeld et al. (2013) 202

LIST OF FIGURES

FIGURE PAGE

2.1 Graphic representation of the various hydrologic (freshwater and saltwater) contributions to surface canals in an urban coastal karstic system. 46

2.2 Map of canal surface water (red circles), groundwater (yellow circles), marine (blue circles), and rainwater collection sites in Miami, FL. Water control structures are represented by grey squares in each canal basin. 47

2.3 Mean (a) canal stage (m; NGVD29) and surface flow (cfs) across three water control structures (G-93, S-26, S-27) and (b) mean groundwater level (m; NGVD29) at three USGS wells control structures (F-319, F-179, F-45) from June 1, 2018 to May 31, 2019. 48

2.4 Stable isotopic composition ($\delta\ ^{18}O$ and $\delta\ ^{2}H$) of surface waters in three canal drainage basins: Coral Gables (CG), Wagner Creek (WC), and Little River (LR). Also depicted are the $\delta\ ^{18}O$ and $\delta\ ^{2}H$ values of shallow groundwater (GW; gold diamonds), and marine water (MW; blue squares) relative to each canal basin. The bold black line represents the global meteoric water line (GMWL) with a slope of +8 and an intercept of +10 ‰. The thin gray line represents the best fit line for surface canal samples. 49

2.5 Best fit fractional contributions of monthly mean groundwater (GW), marine water (MW), rainwater (RW), and stormwater (SW) from the Bayesian mixing model (2H/HIX/FI) across all study canal basins. Mean salinity (ppt) concentrations (± 0.95 C.I) are also represented. 50

2.6 Relationships between distance upstream (m) and mean annual (a) dissolved organic carbon (DOC) concentrations, (b) humification index (HIX), (c) biological index (BIX), (d) fluorescence index (FI), and (e) fractional groundwater contributions across all three coastal canals. Points represent the seasonal mean at each site (± SE, n = 6). 51

2.7 The dashed horizontal line represents the mean GW contribution to the Coral Gables (CG) canal during the month of October (x = 0.215 ± 0.20) and the dotted line represents the annual mean GW contribution during the entire study period (x = 0.194 ± 0.20). 52

2.8 Results of a principal component analysis (PCA) represented by principal components (PC1 and PC2) scores during the (a) wet season, (b) dry season, (c) across a range of salinity (0-30 ppt), and (d) the model loadings. Model parameters include water isotopes ($\delta^{18}O$ and $\delta^{2}H$), optical properties (HIX, BIX, FI), fractional source contributions of (GW, MW, RW, SW), and canal to marine head differential (CMHD). Axes are labeled with the percent variability explained by each principal component. 53

2.9 Relationship between HIX and BIX of DOM corresponding to canal water (CW) and groundwater (GW) samples. Shaded areas represent a 0.95 confidence interval. 54

2.10 Relationships between DOC concentration and BIX during (a) wet and dry seasons I 2018-2019 and (b) three consecutive King Tide events in October 2018. The shaded area represents a 0.95 confidence interval. 55

2.11 Relationship between the groundwater-to-marine head difference (m) and surface water nutrients in Biscayne Bay including (a) TP and (b) NOX. Significant R2 values are shown (P ¡ 0.05). Shaded regions represent 95% confidence intervals. . . . 56

2.12 Relationship between turbidity and chlorophyll-a concentrations across three marine water sites in Biscayne Bay. 57

3.1 Map of sampling locations and land use/cover in three canal drainage basins including Coral Gables (CG), Wagner Creek (WC), and Little River (LR). Grab sampling locations are designated by yellow circles (n=12). Coordinates are presented in decimal degrees. 105

3.2 Daily cumulative rainfall and canal stage in three study canals from June 2018 to May 2019. Data represent stage (m; NAVD29) measured at (1) 15-minute intervals and (2) 3-day moving average. Four sampling events are represented by solid black lines. 106

3.3 Comparison of (a) dissolved organic carbon (DOC), (b) percent bioavailable DOC (BDOC), and ratios of % BDOC to (c) bacterial abundance (BA; 106 cells mL^{-1}) and (d) bacterial productivity (BP, µg C L d^{-1}). Drainage basins are ordered by increasing septic:stormwater (WC, LR, CG). The direction of arrows indicates the upstream-downstream location within each canal. 107

3.4 Excitation-emission plots of five EEM-PARAFAC components (C1, C2, C3, C4, C5) validated in this study. Orange hues indicate higher and blue hues lower fluorescence intensities. . 108

3.5 Principal component analysis (PCA) for water quality parameters. PCA score plots show differences (a) wet and dry season versus (b) high and low tide. PCA loading plot (c) depicts the distribution of variables including EEM-PARAFAC components, DOM fluorescence indices, and % BDOC. Axes are labeled with the percent variability explained by each principal component. 109

3.6 Seasonal relationships between the standardized percentage of components and (a,b) % BDOC, (c,d) log10 Escherichia coli (E. coli) concentrations, as well as fluorescence intensity in raman units (RU) with (d,f) $\log_{10}$ Enterococci concentrations. Significant R^2 values are shown ($P < 0.05$). Shaded regions represent 95% confidence intervals. 110

3.7 Seasonal average (a) salinity (ppt), (b) surface water temperature (deg C), and (c) dissolved oxygen (mg/L) in upstream and downstream locations in three drainage basins of Miami, FL from June 2018 to May 2019. Significant seasonal differences were observed in salinity ($P < 0.05$) while differences in surface water temperature and dissolved oxygen and were seen across seasons and basins ($P < 0.01$). Significant interactions between season and basin were observed with temperature ($P < 0.01$). 111

3.8 Comparison of dissolved N:P molar ratios in surface water samples. Samples were analyzed by canal location along an inland-coastal gradient (upstream-downstream) and by season (wet and dry). Repeated measures ANOVA followed by Tukey's honest significant differences (HSD) post hoc test showed a significant difference among locations ($P = 0.04$), but not seasons ($P > 0.05$). A significant interaction among location*season was observed ($F_{1,34} = 4.90$; $P = 0.03$). 112

3.9 Average % BDOC proportions across all 12 sites in (a) wet and dry seasons and (b) low and high tides. Drainage basins are ordered by their respective septic:stormwater ratio (WC, LR, CG). 113

3.10 Seasonal rainfall and tidal relationships between Septic:Stormwater ratios and bioavailable DOC (BDOC; %). . . . 114

3.11 Emission and excitation loadings from splits used in split-half analysis of the 5-component PARAFAC model (Fig. 5) validated for 146 samples. 115

3.12 Relationships between percent contributions of five components across a gradient of septic:stormwater. 116

3.13 Comparison of PARAFAC components across season and tide. Significant differences were determined by two-way repeated measures ANOVA with Tukey's HSD. 117

4.1 Wetland study locations along a gradient of imperviousness in Valdivia, Chile (n = 9). 158

4.2 Conceptual causal model linking land use and ambient biogeochemistry to nutrient uptake through direct and indirect links in shallow urban and non-urban wetlands. 159

4.3 Water chemistry and dissolved organic matter composition variables in wetlands represented by low, medium, and high levels of watershed imperviousness. Grey-scale shading used on boxplots to indicate increasing imperviousness. Describe the box plots (median, upper and lower quartiles, and 95% confidence intervals as error bars). 160

4.4 Comparison of whole system maximum (n=18) and water column (n=36) daily nutrient uptake (U_{vol}; mg m^{-3} d^{-1}) of (a) nitrate (NO3-) and soluble reactive phosphorus (SRP) in wetlands along a gradient of watershed imperviousness. Circles represent mean values and error bars represent ± SD. 161

4.5 The best-supported model for nitrate ($NO3^{-}$) in water column and whole system uptake experiments of wetlands along a gradient of imperviousness. Standardized coefficients are reported, and the sign of the coefficient indicates the direction of the correlation between variables. Nonsignificant variables and coefficients were not included in the model (P ¿ 0.05). 162

4.6 The best-supported model for soluble reactive phosphorus (SRP) in water column and whole system uptake experiments of wetlands along a gradient of imperviousness. Standardized coefficients are reported, and the sign of the coefficient indicates the direction of the correlation between variables. Nonsignificant variables and coefficients were not included in the model (P ¿ 0.05). 163

5.1 Diagram illustrating the basic tenets of the flow-shunt concept adapted from Raymond et al. (2016). 194

5.2 Study metropolitan areas of the continental United States including Portland, OR; Syracuse, NY; New York City, NY; Baltimore, MD; Denver, CO; Washington, DC; Phoenix, AZ; Atlanta, GA; Dallas, TX; and Tampa, FL. Level I Ecoregions are represented and study sites are represented white circles. . . . 195

5.3 Pearson correlation coefficients for the observed relationship between seasonal antecedent soil moisture and precipitation in (a) 2000 and (b) 2020 across Level I Ecoregions. 196

5.4 Calculated metrics of stream discharge time series for (a) periodicity of statistically significant power spectra (95% C.I.), (b) signal-to-noise ratios (SNR), (c) lag-one auto-correlation, and (d) cross-correlation (r) coefficients between daily precipitation and stream discharge in urban and non-urban watersheds from 2000 to 2020. See Table 1 for city abbreviations. 197

5.5 Mean values of the seven fundamental daily streamflow statistics (FDSS) with changes in % imperviousness across all study gauges. Shaded regions represent a 95% confidence interval (C.I.). 198

5.6 Calculated Flood Synchrony Scale (FSS; sq km) during 2000 (left) and 2020 (right) in (a) Portland, Oregon, (b) Baltimore, Maryland, and (c) Phoenix, Arizona. Darker hues indicate higher FSS values. 199

5.7 Relationship between Flood Synchrony Scale (FSS; sq km) and (a) change (Δ) in percent watershed imperviousness and (b) total drainage area (sq km) across all study sites. 200

5.8 Conceptual diagram illustrating the the influence of urbanization on the timing, frequency, and magnitude of streamflow anomalies during high-flow flood events. 201

5.9 Comparison of of monthly mean values of gridded precipitation (blue; a,b) and antecedent soil moisture (green; c,d) in January 2000 and January 2020 in the continguous United States. Darker hues indicate higher values. Study locations are represented by white circles. 203

LIST OF ABBREVIATIONS

AFDM Ash-free dry mass

ANOVA Analysis of variance

BIX Biological index (Index of recent autochthonous production)

CDOM Colored dissolved organic matter

CMHD Canal-to-marine head difference

DEM Digital elevation model

DO Dissolved oxygen

DOC Dissolved organic carbon

DOM Dissolved organic matter

EEM Excitation-emission matrix

fDOM Fluorescent dissolved organic matter

FI Fluorescence index

HIX Humification index

HMW High molecular weight

HUC Hydrologic unit code

ISC Impervious surface cover

NLCD National Land Cover Database

NMR Nuclear magnetic resonance

OM Organic matter

PARAFAC Parallel factor analysis

PCA Principal component analysis

PSC Pulse-shunt concept

Q Discharge

RCC River continuum concept

SUVA Specific ultraviolet absorbance

SR Spectral slope ratio

TDN Total dissolved nitrogen

UV ultraviolet

USGS United States Geological Survey

CHAPTER 1

Introduction

Dissolved organic carbon (DOC), is a critical source of energy for aquatic organisms that promotes proper ecosystem functioning and in-stream biogeochemical processing (Findlay et al.; 1993; Tank et al.; 2010; Dick et al.; 2015). In ecosystems that rely on allochthonous inputs of carbon (i.e. net heterotrophic), DOC is a fundamental link between energy and nutrient dynamics (Bernhardt and Likens; 2002; Seybold and McGlynn; 2018). The interdependence of DOC and other key nutrients including nitrogen (N) and phosphorus (P) in aquatic ecosystems is greatly influenced by local hydrologic regime (Ågren et al.; 2014; Maranger et al.; 2018). Climate-induced shifts in seasonal precipitation and tidal amplitude influence the rate of carbon and nutrient transport and transformation along upstream-downstream flowpaths in coastal ecosystems (Regier and Jaffé; 2016). In turn, changing hydrological conditions lead to variable in-stream biogeochemical processing and nutrient transport. In the case of extreme event precipitation or tidal inundation, excess runoff may exceed the water storage capacity of an ecosystem, resulting in localized flooding of variable extent and duration (Poff et al.; 1997). These flood pulses can introduce mixed sources of carbon, and nutrients from the surrounding landscape and alter the timing and concentration of nutrient subsidies to downstream waters (Junk et al.; 1989; Tockner et al.; 2000). In turn, significant flood events may produce biogeochemical "control points" that can have short- or long-term effects on biogeochemical processing and ecosystem health (McClain et al.; 2003; Bernhardt et al.; 2017). As the frequency and magnitude of flood events shift with climate change, there is a critical need to quantify effects of flooding on carbon and nutrient cycling across spatiotemporal scales.

1.0.1 Sources of DOM to aquatic ecosystems

Dissolved organic matter (DOM) is another critical piece of the aquatic carbon pool. The multitude of effects of DOM on aquatic ecosystem function are dependent on the chemical properties determined by its source and the degree to which it undergoes processing. DOM originates from a range of allochthonous (i.e., outside the aquatic system) and autochthonous (i.e., within the aquatic system) sources including plants and soil matter, bacterial or algal production, and exudates from marine phytoplankton (Sobczak et al.; 2002; Asmala et al.; 2016, 2018). Autochthonous DOM is considered to be higher quality (lower C:nutrient) and more bioavailable than allochthonous matter. While the overall pool of autochthonous DOM may be small, it has the ability to stimulate heterotrophic metabolism in aquatic ecosystems (McClain et al.; 2003; Epstein et al.; 2016). However, the composition of DOM varies widely across spatiotemporal scales, especially in coastal drainages. Thus, quantifying changes in the hydrologic and land use drivers of DOM source and composition change is needed to understand its role in metabolic processing and export to downstream water bodies (Parr et al.; 2015).

1.0.2 Biotic and biotic processing of DOC and DOM

Microbial processing and photochemical degradation of DOM are two of most important mechanisms that alter the amount and quality of DOM in aquatic environments. The relative influence of each process is dependent upon the relative source (and composition) of DOM and the physiographic and climatological factors of the surrounding environment. Our ability to quantify the fate of DOM in coastal waters relies on accurate estimations of in-stream biogeochemical processes that contribute

or remove DOM from coastal streams and rivers (Bernal et al.; 2018; Wagner et al.; 2015; Ward et al.; 2017).

As DOC and DOM is transported from headwater streams to the coast, biological processing by microbes, phytoplankton can alter the overall composition of the DOM pool by removing fractions that are labile and or rich in organic nutrients (Hosen et al.; 2021). This process is highly dependent on site-specific biotic (e.g., microbial activities, phytoplankton production) and abiotic (e.g., light) conditions that vary across spatiotemporal scales.

Additionally, solar radiation can elicit changes to the chemical properties of DOM including the breakdown of large molecules to smaller ones (Osburn et al.; 2012), photobleaching (Helms et al.; 2013), or mineralization to CO2 in the atmosphere (Fellman et al.; 2008). Photochemical degradation of DOM can also influence the proportion of inorganic nutrients in the water column which can shift the stoichiometric balance of carbon to nutrients (N or P) and lead to nutrient limitation. Yet, the influence of photochemical changes in DOM are less pronounced in temperate, hydrologically active urban ecosystems where large amounts of water transport occurs underground or rivers with short water residence time.

1.0.3 DOM in urban aquatic systems

Urbanization alters aquatic DOC and DOM composition and processing rates by changing stormwater flow paths and surface-subsurface connectivity (Hosen et al.; 2014). The suite of changes to stream chemistry, biology, and geomorphology caused by urbanization are collectively known as the Urban Stream Syndrome (Walsh et al.; 2005). Urban development significantly alters how water moves through the landscape through the construction of impervious surfaces and subsurface flowpaths that

can shunt water downstream during storm events (also known as engineered headwaters; (Kaushal and Belt; 2012; Fork et al.; 2020). Changes in local hydrology and climate can shift the timing and magnitude of carbon and nutrient delivery from headwaters to streams and rivers. Stormwater runoff is thought to undergo little biogeochemical transformation in headwaters due to short residence time of hydrologically flashy systems. Instead, runoff is transported to coastal waterways (e.g., canals) where carbon and nutrients may undergo further transformation via biotic processes. Given the frequent and substantial contributions of runoff in urban ecosystems, many studies have documented increased DOC concentrations in urban water bodies compared to non-urban areas (Hosen et al.; 2014; Parr et al.; 2015) and that urban-sourced DOM tends to more bioavailable (Fork et al.; 2020). However, most urban aquatic research to-date has not been done in low-lying coastal areas, despite the majority of the world's cities residing in coastal regions.

1.0.4 Urban hydrology shapes DOC and DOM regimes

Urban flooding is becoming increasingly common worldwide due to biophysical alterations to local and regional hydrology through the process of urbanization (Grimm et al.; 2008; Meierdiercks et al.; 2017). Hydrologic modifications including changes in impervious cover and development of complex stormwater infrastructure can shift the local water balance from periodic infiltration to increased surface runoff, creating a range of pulse and press disturbances to aquatic ecosystems downstream (Grimm et al.; 2008; Miller et al.; 2021). In turn, high frequency or long duration flood pulses in urban ecosystems can alter ecosystem biogeochemical processing rates (Meyer et al.; 2005; Walsh et al.; 2005; Roy and Shuster; 2009; Hale et al.; 2016).

Although an expanding body of literature has contributed to the successful characterization of urban stream biogeochemistry (Walsh et al.; 2005; Kaye et al.; 2006; Kaushal and Belt; 2012), considerable gaps remain in understanding how seasonal and event-driven rainfall and tides influence DOC and nutrient dynamics at local and regional scales (Hosen et al.; 2014; Miller et al.; 2021; Ward et al.; 2017). Further, little is known about how urbanization can decouple flows in the surface watershed from the underlying sewershed across spatial and temporal scales. As a result, there is an increasing need to quantify water source contributions to urban coastal waterways across seasons, which is needed to quantify the effects of stormwater runoff and coastal flooding on carbon and nutrient biogeochemical cycling (Moftakhari et al.; 2018).

1.0.5 Advancing ecohydrological theory in urban coastal ecosystems

The role of urban coastal waterways in transporting and transforming carbon and nutrients from headwaters to the ocean is well known. Hydrologic modifications from urbanization, including changes in impervious cover (ISC) and complex stormwater infrastructure can shift the timing and source of water delivery creating a range of pulse and press disturbances to aquatic ecosystems downstream (Blaszczak et al.; 2019; Kaushal and Belt; 2012; Miller et al.; 2021). However, prevailing conceptual models have overlooked the influence of combined terrestrial runoff and coastal dynamics on the timing and composition of carbon and nutrients in urban coastal waters. For example, Walsh et al. (2005) proposed that urban stormwater has become a new class of environmental flow problem: one that requires the reduction of high volumes of water to maintain riverine ecological integrity. Given this new problem,

urban stormwater delivered through conventional drainage systems is delivered to receiving waters unfiltered, through pipes, resulting in more frequent, intense flood pulses of shorter duration and of poor quality. Raymond et al. (2016) went further to propose that episodic hydrologic events result in DOM bypassing headwaters, metabolized in large rivers, and exported to coastal systems. While this Pulse-Shunt Concept has provided a strong framework to identify the timing and magnitude of OM delivery from headwaters to larger river networks, an expanded model is needed to understand how water sources in coastal urban ecosystems influence DOM and nutrient processes. Consequently, high frequency or long duration flood pulses or extreme tide events in coastal urban ecosystems can introduce a range of stressors that differentiate urban and natural ecosystems and biogeochemical processing rates (Meyer et al.; 2005; Walsh et al.; 2005; Hale et al.; 2016).

Although an expanding body of literature has contributed to the successful characterization of urban stream biogeochemistry (Walsh et al.; 2005; Kaye et al.; 2006; Kaushal and Belt; 2012), considerable gaps remain in understanding how seasonal and event-driven rainfall and tides influence DOC and nutrient dynamics at local and regional scales (Hosen et al.; 2014; Miller et al.; 2021; Ward et al.; 2017). In coastal riverine ecosystems, streams or rivers can shift from reactors to pipes with changing hydrological conditions (Casas-Ruiz et al.; 2017). Further, little is known about the quantification of water source contributions from the surrounding landscape during flood pulse events and their influence on downstream water quality. As a result, there is an increasing need to quantify effects of stormwater runoff and coastal flooding on carbon and nutrient biogeochemical cycling (Smith et al.; 2021).

1.0.6 Outline of this dissertation

In this dissertation, I examine how interactions between climate, hydrology, and land use influence the concentration, composition, and ultimate fate of carbon and nutrients in urban coastal aquatic ecosystems. Within each chapter, I test the effects of specific hydro-climatological factors on the source and processing of DOC and DOM that can have both immediate and long-lasting effect on ecosystem processes. The results of this dissertation culminate in a new framework to better understand the spatiotemporal variability of climate-driven flooding on carbon source, transport, and transformation in urban aquatic ecosystems. In Chapter 2, I quantified the relative water source contributions to coastal canal networks to indicate the rising influence of groundwater on carbon and nutrient fluxes. In Chapter 3, I examined how seasonal interactions between stormwater runoff and tidal extension influence the bioavailability of DOM and support evidence of an urban 'priming' effect. In Chapter 4, I experimentally measured the capacity of urban wetlands to remove nutrients and found that optical properties of DOM may be a strong indicator of total removal capacity. Finally, Chapter 5 concludes the dissertation by placing this research in the wider context of the flow-shunt versus flood-pulse paradigm in which spatiotemporal synchrony of urban stream discharge occurs following extreme precipitation events across regional climates.

1.1 Bibliography

Ågren, A., Buffam, I., Cooper, D., Tiwari, T., Evans, C. and Laudon, H. (2014). Can the heterogeneity in stream dissolved organic carbon be explained by contributing landscape elements?, *Biogeosciences* **11**(4): 1199–1213.

Asmala, E., Haraguchi, L., Jakobsen, H. H., Massicotte, P. and Carstensen, J. (2018). Nutrient availability as major driver of phytoplankton-derived dissolved organic matter transformation in coastal environment, *Biogeochemistry* **137**: 93–104.

Asmala, E., Kaartokallio, H., Carstensen, J. and Thomas, D. N. (2016). Variation in riverine inputs affect dissolved organic matter characteristics throughout the estuarine gradient, *Frontiers in Marine Science* **2**: 125.

Bernal, S., Lupon, A., Catalán, N., Castelar, S. and Martí, E. (2018). Decoupling of dissolved organic matter patterns between stream and riparian groundwater in a headwater forested catchment, *Hydrology and Earth System Sciences* **22**(3): 1897–1910.

Bernhardt, E. S., Blaszczak, J. R., Ficken, C. D., Fork, M. L., Kaiser, K. E. and Seybold, E. C. (2017). Control points in ecosystems: Moving beyond the hot spot hot moment concept, *Ecosystems* **20**: 665–682.

Bernhardt, E. S. and Likens, G. E. (2002). Dissolved organic carbon enrichment alters nitrogen dynamics in a forest stream, *Ecology* **83**(6): 1689–1700.

Blaszczak, J. R., Delesantro, J. M., Zhong, Y., Urban, D. L. and Bernhardt, E. S. (2019). Watershed urban development controls on urban streamwater chemistry variability, *Biogeochemistry* **144**: 61–84.

Casas-Ruiz, J. P., Catalán, N., Gómez-Gener, L., von Schiller, D., Obrador, B., Kothawala, D. N., López, P., Sabater, S. and Marcé, R. (2017). A tale of pipes and reactors: Controls on the in-stream dynamics of dissolved organic matter in rivers, *Limnology and Oceanography* **62**: S85–S94.

Dick, J. J., Tetzlaff, D., Birkel, C. and Soulsby, C. (2015). Modelling landscape controls on dissolved organic carbon sources and fluxes to streams, *Biogeochemistry* **122**: 361–374.

Epstein, D. M., Kelso, J. E. and Baker, M. A. (2016). Beyond the urban stream syndrome: organic matter budget for diagnostics and restoration of an impaired urban river, *Urban Ecosystems* **19**: 1623–1643.

Fellman, J. B., D'Amore, D. V., Hood, E. and Boone, R. D. (2008). Fluorescence characteristics and biodegradability of dissolved organic matter in forest and wetland soils from coastal temperate watersheds in southeast alaska, *Biogeochemistry* **88**: 169–184.

Findlay, S., Strayer, D., Goumbala, C. and Gould, K. (1993). Metabolism of streamwater dissolved organic carbon in the shallow hyporheic zone, *Limnology and oceanography* **38**(7): 1493–1499.

Fork, M. L., Osburn, C. L. and Heffernan, J. B. (2020). Bioavailability and compositional changes of dissolved organic matter in urban headwaters, *Aquatic Sciences* **82**.

Grimm, N. B., Faeth, S. H., Golubiewski, N. E., Redman, C. L., Wu, J., Bai, X. and Briggs, J. M. (2008). Global change and the ecology of cities, *science* **319**(5864): 756–760.

Hale, R. L., Scoggins, M., Smucker, N. J. and Suchy, A. (2016). Effects of climate on the expression of the urban stream syndrome, *Freshwater Science* **35**: 421–428.

Helms, J. R., Stubbins, A., Perdue, E. M., Green, N. W., Chen, H. and Mopper, K. (2013). Photochemical bleaching of oceanic dissolved organic matter and its effect on absorption spectral slope and fluorescence, *Marine Chemistry* **155**: 81–91.

Hosen, J. D., Aho, K. S., Fair, J. H., Kyzivat, E. D., Matt, S., Morrison, J., Stubbins, A., Weber, L. C., Yoon, B. and Raymond, P. A. (2021). Source switching maintains dissolved organic matter chemostasis across discharge levels in a large temperate river network, *Ecosystems* **24**: 227–247.

Hosen, J. D., McDonough, O. T., Febria, C. M. and Palmer, M. A. (2014). Dissolved organic matter quality and bioavailability changes across an urbanization gradient in headwater streams, *Environmental Science and Technology* **48**: 7817–7824.

Junk, W. J., Bayley, P. B., Sparks, R. E. et al. (1989). The flood pulse concept in river-floodplain systems, *Canadian special publication of fisheries and aquatic sciences* **106**(1): 110–127.

Kaushal, S. S. and Belt, K. T. (2012). The urban watershed continuum: Evolving spatial and temporal dimensions, *Urban Ecosystems* **15**: 409–435.

Kaye, J. P., Groffman, P. M., Grimm, N. B., Baker, L. A. and Pouyat, R. V. (2006). A distinct urban biogeochemistry?, *Trends in Ecology & Evolution* **21**(4): 192–199.

Maranger, R., Jones, S. E. and Cotner, J. B. (2018). Stoichiometry of carbon, nitrogen, and phosphorus through the freshwater pipe, *Limnology and Oceanography Letters* **3**: 89–101.

McClain, M. E., Boyer, E. W., Dent, C. L., Gergel, S. E., Grimm, N. B., Groffman, P. M., Hart, S. C., Harvey, J. W., Johnston, C. A., Mayorga, E., McDowell, W. H. and Pinay, G. (2003). Biogeochemical hot spots and hot moments at the interface of terrestrial and aquatic ecosystems, *Ecosystems* **6**: 301–312.

Meierdiercks, K. L., Kolozsvary, M. B., Rhoads, K. P., Golden, M. and McCloskey, N. F. (2017). The role of land surface versus drainage network characteristics in controlling water quality and quantity in a small urban watershed, *Hydrological Processes* **31**(24): 4384–4397.

Meyer, J. L., Paul, M. J. and Taulbee, W. K. (2005). Stream ecosystem function in urbanizing landscapes, *Am. Benthol. Soc* **24**: 602–612.

Miller, A. J., Welty, C., Duncan, J. M., Baeck, M. L. and Smith, J. A. (2021). Assessing urban rainfall-runoff response to stormwater management extent, *Hydrological Processes* **35**.

Moftakhari, H. R., AghaKouchak, A., Sanders, B. F., Allaire, M. and Matthew, R. A. (2018). What is nuisance flooding? defining and monitoring an emerging challenge, *Water Resources Research* **54**: 4218–4227.

Osburn, C. L., Handsel, L. T., Mikan, M. P., Paerl, H. W. and Montgomery, M. T. (2012). Fluorescence tracking of dissolved and particulate organic matter quality in a river-dominated estuary, *Environmental Science and Technology* **46**: 8628–8636.

Parr, T. B., Cronan, C. S., Ohno, T., Findlay, S. E., Smith, S. M. and Simon, K. S. (2015). Urbanization changes the composition and bioavailability of dissolved organic matter in headwater streams, *Limnology and Oceanography* **60**: 885–900.

Poff, N. L., Allan, J. D., Bain, M. B., Karr, J. R., Prestegaard, K. L., Richter, B. D., Sparks, R. E. and Stromberg, J. C. (1997). The natural flow regime, **47**: 769–784.

Raymond, P. A., Saiers, J. E. and Sobczak, W. V. (2016). Hydrological and biogeochemical controls on watershed dissolved organic matter transport: pulse-shunt concept.

URL: *http://www.horizon-systems.com/nhdplus/*

Regier, P. and Jaffé, R. (2016). Short-term dissolved organic carbon dynamics reflect tidal, water management, and precipitation patterns in a subtropical estuary, *Frontiers in Marine Science* **3**: 250.

Roy, A. H. and Shuster, W. D. (2009). Assessing impervious surface connectivity and applications for watershed management 1, *JAWRA Journal of the American Water Resources Association* **45**(1): 198–209.

Seybold, E. and McGlynn, B. (2018). Hydrologic and biogeochemical drivers of dissolved organic carbon and nitrate uptake in a headwater stream network, *Biogeochemistry* **138**: 23–48.

Smith, M. A., Kominoski, J. S., Gaiser, E. E., Price, R. M. and Troxler, T. G. (2021). Stormwater runoff and tidal flooding transform dissolved organic matter composition and increase bioavailability in urban coastal ecosystems, *Journal of Geophysical Research: Biogeosciences* **126**.

Sobczak, W. V., Cloern, J. E., Jassby, A. D. and Müller-Solger, A. B. (2002). Bioavailability of organic matter in a highly disturbed estuary: The role of detrital and algal resources, *Proceedings of the National Academy of Sciences* **99**(12): 8101–8105.

Tank, J. L., Rosi-Marshall, E. J., Griffiths, N. A., Entrekin, S. A. and Stephen, M. L. (2010). A review of allochthonous organic matter dynamics and metabolism in streams.

Tockner, K., Malard, F. and Ward, J. (2000). An extension of the flood pulse concept, *Hydrological processes* **14**(16-17): 2861–2883.

Wagner, S., Riedel, T., Niggemann, J., Vahatalo, A. V., Dittmar, T. and Jaffé, R. (2015). Linking the molecular signature of heteroatomic dissolved organic matter to watershed characteristics in world rivers, *Environmental science & technology* **49**(23): 13798–13806.

Walsh, C. J., Roy, A. H., Feminella, J. W., Cottingham, P. D., Groffman, P. M. and Ii, R. P. M. (2005). The urban stream syndrome: current knowledge and the search for a cure, *Am. Benthol. Soc* **24**: 706–723.

Ward, N. D., Bianchi, T. S., Medeiros, P. M., Seidel, M., Richey, J. E., Keil, R. G. and Sawakuchi, H. O. (2017). Where carbon goes when water flows: carbon cycling across the aquatic continuum, *Frontiers in Marine Science* **4**: 7.

CHAPTER 2

Linking seasonal changes in organic matter composition and nutrients to shifting hydraulic gradients in coastal urban canals using a Bayesian mixing model

Matthew A. Smith[1], J.S. Kominoski[1], René M. Price[2], O. Abdul-Aziz[3]

[1]Institute of Environment and Department of Biological Sciences, Florida International University, Miami, Florida 33199, USA

[2]Institute of Environment and Department of Earth and Environment, Florida International University, Miami, Florida 33199, USA

[3]Department of Civil and Environmental Engineering, West Virginia University, Morgantown, West Virginia 26506, USA

2.1 Abstract

The capacity for coastal river networks to alter the transport and transformation of dissolved organic matter (DOM) is widely accepted. Climate-induced shifts in stormwater runoff and tidal extension likely alter fresh and marine water source contributions and associated DOM and nutrient loading rates. However, the ability to trace sources of DOM relies on the use of various hydrologic and geochemical tracking techniques, of which commonly-used spectroscopic indices of DOM source have not been thoroughly explored. Here, we investigate how time-variable interactions among coastal water source contributions influence DOC and nutrient concentrations and DOM composition in urban canals connected to the ocean. We quantified the spatiotemporal variability of DOM quality and nutrient concentrations to determine fractional contributions of marine water, rainwater, stormwater, and groundwater to three coastal urban canal systems of Miami, Florida (USA). We created a Bayesian Monte Carlo (BMC) mixing model using monthly measurements of DOM composition, DOC concentrations, $\delta^{18}O$ and $\delta^{2}H$ isotopic signatures, and chloride (Cl-). Source fractional contributions varied monthly and between seasons, particularly groundwater contributions that averaged 0.17 in the dry season and 0.26 at peak high tide during the height of the subtropical wet season (September - November). Results indicate that the canal-to-marine head difference (CMHD) was a primary driver of groundwater contributions to coastal canals and was linked to synchronous monthly patterns of fDOM and DOC. This relationship indicates the influence of major hydrologic events – such as extreme high tide (> 1 m) and high-flow stormwater discharge – that connect canals to upstream sources of terrestrial DOM. In consideration of the Pulse-Shunt Concept, loading of terrestrially sourced DOC and DOM is pulsed to urban canals and shunted downstream and supple-

mented by microbially sourced DOM during the wet season at high tide. Overall, a combined tracer approach with dual water isotopes and fDOM characteristics reveals differences in short-term fluctuations in water source and fDOM composition that likely influence biogeochemical function in urban canals.

2.2 Introduction

The transport of dissolved organic matter (DOM) from rivers to the coast is a major component of the global carbon cycle (Casas-Ruiz et al.; 2017). Yet, our ability to quantify the fate of DOM in coastal waters relies on accurate estimations of in-stream biogeochemical processes that contribute or remove DOM from coastal streams and rivers (Bernal et al.; 2018; Wagner et al.; 2015; Ward et al.; 2017). Coastal river networks are often identified as active conduits through which DOM can be transported, produced, buried, or mineralized (Raymond et al.; 2016). However, the timing and magnitude of DOM transport relative to processing rates is influenced by various hydrological and biophysical factors that vary across spatiotemporal scales. Therefore, evaluating the factors that promote in-stream processing of DOM versus its passive transport downstream is critical to understand the role of coastal waterways in DOM cycling.

In coastal riverine systems, the concentration and composition of DOM and nutrients differ by source and with changing water levels. As such, headwater streams can shift from reactors to pipes with changing hydrological conditions (Casas-Ruiz et al.; 2017). Major hydrological events, such as high-flow stormwater discharge and extreme high tide (> 1 meter), can shift the hydraulic gradient and lead to prolonged mixing of freshwater and marine water, thereby altering overall DOM composition. This pulse-shunt regime dictates the timing and delivery of DOM based on changes

in (1) drainage network connectivity, hydraulic scaling, DOM bioreactivity, and downstream subsidies (Raymond et al.; 2016). Due to high internal spatial and temporal heterogeneity in the fluxes and biogeochemical processing of DOC, the fate of pulsed terrestrial DOC in receiving estuarine and coastal environments is unclear (Asmala et al.; 2021). A key challenge is to delineate the distinct changes in DOC concentrations and DOM quality across various freshwater and saltwater sources following hydrologic disturbances. While marine and stormwater contributions to coastal waters have been well characterized, the role of coastal groundwater in determining fluxes of DOC concentrations and DOM composition in tidally influenced waterways is uncertain.

Shallow coastal aquifers and permeable karstic environments provide a reaction zone where freshwater and seawater mix to influence groundwater inputs of DOM and nutrients to coastal waters (Moore; 1999; Niencheski et al.; 2007). The subterranean mixing zone is biogeochemically active and can support rapid changes in nutrient speciation and transformation. This freshwater-saltwater boundary migrates in response to seasonal runoff, tidal extension, and groundwater hydraulic gradients. Coastal groundwater nutrient concentrations are often higher than in surface waters and influence nitrogen and phosphorus ratios and may shift surface water N-limiting conditions to P-limiting (Slomp and Cappellen; 2004). Therefore, groundwater inputs to coastal waters via canals may increase nutrient loads and more bioavailable DOM compared to surface waters. Recent studies showed that groundwater-derived dissolved nutrient and organic matter inputs have a strong influence on primary productivity and alter the composition of phytoplankton in coastal waters (Rodellas et al.; 2015). It has also been suggested by Hosen et al. (2021) that autochthonous production can stabilize DOM concentrations and maintain chemostasis at lower flows in large rivers. However, the role of coastal groundwater impacted by anthro-

pogenic pollution (i.e., wastewater) on seasonal fluctuations of DOC and DOM is still relatively unclear (Smith et al.; 2021).

Tracing water sources based on selected DOM quality parameters has potential to provide direct estimates for source contributions of DOM to coastal waterways. There are a variety of indices for characterizing DOM quality, including specific UV absorbance ($SUVA_{254}$), spectral slope to indicate molecular weight (S_R), humification index (HIX), biological index (BIX), and fluorescence index (FI) (Mcknight et al.; 2001; Helms et al.; 2008). Several studies demonstrated the strong capability of combining isotope ratios and fluorescence spectroscopy to trace OM sources in complex and mixed environments (Derrien et al.; 2018; Lee et al.; 2018; Yang et al.; 2015). Further, it has been suggested that some optical properties (e.g., BIX, $SUVA_{254}$, FI) could provide reliable estimates of DOM source independent of local biogeochemical processes (i.e., biodegradation, UV irradiation, adsorption), particularly in systems with short-residence times (Lee et al.; 2018). It is necessary to consider the large variation in DOM concentration among various end-members which can introduce unexpected uncertainties in source estimates (Rudolph et al.; 2020). However, few studies have combined water isotopes with DOM fluorescence to investigate the role of coastal groundwater in shifting DOM quality and nutrient concentrations in coastal canals and nearshore estuarine environments.

The objective of this study was to investigate the influence of seasonal rainfall and tidal extension on relative water source contributions using a combined isotope-fluorescent DOM (fDOM) Bayesian mixing model. We asked the question of how seasonal interactions between canal hydrology and tidal extension influence the amount and composition of DOM and nutrients in coastal urban canals. Using a reach-scale approach, we traced changes in DOM composition along several canals of a coastal estuarine environment using a novel combination of water isotopes and DOM optical

properties. We then determined relevant hydrologic and biogeochemical drivers of changes in DOC and nutrient concentrations in canal and nearshore bay waters. We hypothesized that (1) the gradient in canal-to-marine water hydraulic head would determine the extent of groundwater contributions during the wet season and at high tide and (2) groundwater source contributions and indicators of autochthonous production would explain seasonal changes to the concentration of DOC and DOM quality in surface canal waters. Further, we assumed that Pulse-Shunt Concept processes are important in this system, but we propose that seasonal tidal contributions of bioavailable DOM in groundwater can alter overall DOM composition in urban coastal canals.

2.3 Methods

2.3.1 Site Description and Hydrology

This study was conducted in three coastal drainage basins of Miami, FL (USA). We collected water samples at four locations along inland-to-coastal gradients of three canals that drained into Biscayne Bay (Wagner Creek, WC; Coral Gables, CG; Little River, LR; n = 12; Fig. 2.2). The three drainages represent a range of imperviousness (33-50%), land use, and total drainage area. Canal stage (meters; NGVD29) and flow (cfs) was monitored continuously at 15-minute intervals for the duration of the study period (June 1, 2018 – May 31, 2019) and was collected from South Florida Water Management District (SFWMD) water control structures in each drainage basin (Fig. 2.2; Table S1; SFWMD, 2008). Tides are diurnal and range between 0.63 – 1.17 m throughout the year. Tidal heights can reach upwards of 3 m (MLLW) during periodic perigean spring tide events during the wet season (May –

October). Daily cumulative precipitation (mm) was recorded from a local rain gage located in each basin (n = 3; Fig. 2.2). Precipitation in the region occurs in two distinct seasons: a wet season from June through November and dry season from December to May. Each drainage basin contains a salinity control structure (Fig. 2.2) that serve to maintain higher groundwater levels on the upstream side to limit subsurface saltwater intrusion and limit upstream migration of saltwater in canals during high tide events and storm surge (Sukop et al.; 2018). These structures are located approximately 6.5 km (G93), 9.2 km (S26) to 1.9 km (S27) inland of the coastline and coincide with the position of the saltwater intrusion line in the shallow portion of the underlying aquifer (Fig. 2.2). All structures contain two vertical lift gates that are automatically opened at a stage of 2.5 ft (G93), 2.8 ft (S26), and 1.9 ft (S27) NGVD. Design headwater and tailwater stage varies across each structure (S-27; 3.2 HW, 2.7 TW NGVD; S-26; 4.4 HW, 3.9 TW NGVD; G-93 4.5 HW, 3.0 TW NGVD). We quantified two metrics relative to shifts in the hydraulic gradient including the canal-to-marine hydraulic head difference (CMHD) and groundwater-to-marine hydraulic head difference (GMHD). CMHD and GMHD were calculated as the difference between each respective canal or groundwater well water level and mean sea level at Virginia Key tidal gage station.

2.3.2 Water Quality Determination

Surface water grab samples were collected monthly from twelve canal locations during baseflow from June 2018 through May 2019 (Fig. 1; n = 288). For the purposes of this study, we collected water samples during periods no less than 24 h after a rainfall event to remove the direct influence of rainfall-driven effects on streamflow. Surface grab water samples were collected within 3 h of each other on sampling

days. In addition, triplicate grab water samples were collected quarterly from four distinct end-members (marine water, rainwater, stormwater, groundwater; (n = 48)) to determine baseline concentrations of geochemical parameters (Fig. 1). Three wells were sampled for baseline groundwater quality during wet and dry seasons (n = 12; Table S1). All wells were pre-existing and installed by the United States Geological Survey (USGS). Wells were completed to various depths ranging from 4.6 m (USGS G-3959), 6.0 m (USGS F-319), and 23.5 m (USGS F-179, Table S1). Prior to sampling, the groundwater wells were purged of at least three standing well volumes. All samples were filtered in the field using Whatman 0.7-μ glass fiber filters (GF/F) that were pre-combusted at 500^{o}C and collected in acid-washed, amber HDPE bottles. Samples were transported to the laboratory on ice and stored at 4°C and analyzed within seven days of collection. All water samples were analyzed for dissolved organic carbon (DOC) on a Shimadzu TOC-V total organic carbon analyzer after acidification and purging to remove inorganic C. The net change in longitudinal DOC concentration (Δ DOC; mg C -1) in each canal was calculated as the difference between downstream and upstream concentrations. Hence, positive values indicate net DOC gain, whereas negative values indicate net DOC loss. However, this approach does not denote the significance of in-stream biotic and abiotic processes responsible for net DOC changes. At each sampling location, we also measured water physicochemical parameters [temperature, dissolved oxygen (DO), conductivity, and pH with a YSI multiparameter handheld sonde (YSI Company, Yellow Springs, OH, USA). Water chemistry parameters, including total phosphorus (TP; mg L-1), total Kjeldahl nitrogen (TKN; mg L-1), nitrate + nitrite-nitrogen (NOx-N; mg L-1) were collected and analyzed by the Miami-Dade County Department of Environmental Resources Management (DERM; Lietz, 1999) at the most upstream and downstream sites of this study. Water quality analyses were analyzed

at DERM using EPA methods 365.1, 353.2, and 351.4, for TP, TKN, and NOx, respectively (U.S. EPA, 2018).

$\delta^{18}O$ and $\delta^{2}H$ isotope compositions of water samples were analyzed using a Los Gatos DLT laser isotope analyzer at Florida International University (FIU). This instrument uses infrared absorption spectroscopy to quantify the isotopic composition of water molecules in a sample. Samples were loaded into a 2mL glass vial with split cap septa and placed into an auto-sampler. For each sample, six 1.2-μL aliquots were injected into the instrument. A series of four internal standards and on standard of Vienna Standard Mean Ocean Water were analyzed in between samples. Results of the first aliquot were discarded, and remaining aliquots were analyzed for outliers, with the acceptable values averaged and corrected for per mil scale linearity. Precision of this method was about 0.2‰ for $\delta^{18}O$ and 0.5‰ $\delta^{2}H$. Deuterium excess (d-excess) of each of the water samples was estimated as d = $\delta^{2}H - 8 * \delta^{18}O$ (Dansgaard, 1964).

2.3.3 DOM Fluorescence

DOM fluorescence spectroscopy was also conducted on all samples to determine chemical composition and relative aromaticity. Fluorescence excitation-emission matrices (EEMs) were collected with a Horiba Aqualog (Jobin Yvon Horiba, France) using the methods of Yamashita et al. (n.d.). EEMs were collected on room temperature samples every 3 nm over excitation wavelength intervals between 240 and 455 nm, and an emission wavelength range of λex + 10 nm to λex + 250 nm in a 1 cm quartz cuvette. EEMs were corrected for instruments optics, Raman normalized, and blank subtracted using MATLAB version 2019 software. Three fluorescence indices were calculated including the fluorescence index (FI) indicating

proportion of microbial DOM sources, biological index (BIX) indicating proportion of recently produced DOM, and humification index (HIX) indicating proportion of terrestrial derived DOM (Table 2.2; Jaffé et al. (2008)). Specific ultraviolet absorbance at a wavelength of 254 nm ($SUVA_{254}$) provides a measure of the relative amount of chromophoric C in a sample and is correlated with percent aromaticity of DOM (Weishaar et al.; 2003). $SUVA_{254}$ was determined from measuring the UV absorbance at a 254 nm wavelength on triplicate water samples for all sites. Spectral slopes were calculated for two primary wavelength ranges ($S_{275-295}$, $S_{350-400}$) using nonlinear least-squares for each spectral range where higher S values indicate low molecular weight or decreasing aromaticity (Hansen et al.; 2016). Spectral slope ratio (S_R) was calculated as $S_{275-295}$ divided by $S_{350-400}$ where ratios are negatively correlated to DOM molecular weight (Helms et al.; 2008).

2.3.4 Bayesian Monte Carlo Mixing Model

A Bayesian Monte Carlo (BMC) four end-member mixing model was used to determine the source fraction contributions to three coastal urban canals (Arendt et al.; 2015). BMC has been useful in determining fractional contributions of water source to bulk samples across a range of ecosystems including glacial meltwaters (Cable et al.; 2011; Arendt et al.; 2015), terrestrial headwaters (Yang et al., 2015), and nearshore marine environments following extreme weather events (Rudolph et al.; 2020). Among our sites in each canal, we identified the proportion of contributing end-member sources from marine water ($f$mw), rainwater ($f$rw), stormwater ($f$sw), and groundwater ($f$gw). The sum of the fractional contributions (f) of water sources ($f$mw, $f$rw, $f$sw, $f$gw) in mixed canal water is given in Equation 1.

$$f\text{mw} + f\text{rw} + f\text{sw} + f\text{gw} = 1 \quad (1)$$

To quantify the relative contributions of each end-member to mixed canal water samples, we identified $\delta^{18}O$, $\delta^{2}H$, HIX, BIX, FI, and chloride (Cl^{-}) as geochemical parameters with ranges specific to end-member concentrations. Unique geochemical end-member compositions were defined based on measurements from marine water (n = 12), rainwater (n = 12), stormwater (n = 12), and groundwater (n = 12). We quantified mean values of all three geochemical tracers and incorporated standard deviation within each end-member to allow the model to account for natural variability and uncertainty. We used a Monte Carlo sampling scheme where randomly chosen samples of the prior were retained as samples of the posterior proportional to the estimate likelihood of the misfit between predictions and data (Arendt et al.; 2015). The BMC uses prior and posterior probability density functions based on the known (i.e., end-member concentrations) and the unknown (i.e., relative contributions from end-member to bulk sample) to determine the likelihood of any fractional contribution outcome. The likelihood of a model prediction was calculated by Eq. 2;

$$\mathrm{L}\ \alpha\ \exp\ [(\mathrm{d}^{18}O_p - d^{18}O_o)^2/\sigma^2_{d^{1}8O}]xexp[(HIX_p - HIX_o)^2/\sigma^2_{HIX}]xexp[(FI_p - FI_o)^2/\sigma^2_{FI}](2)$$

where subscripts p and o are the predicted and observed measurements of each variable and σ is the measurement of uncertainty. One million prior and posterior samples were tested for each bulk water sample. Average acceptance rates of each model were determined via the ratio of prior samples to accepted posterior samples (see Eq. 2). These values were used to measure our confidence in each of the model fits. Previous studies that employed similar models suggest that BMC mixing models would provide accurate results if the mean acceptance rates fall between 0.1 and 0.6, with optimal rates between 0.2 and 0.4 (Rosenthal et al.; 2011; Lunn et al.; 2009).

2.3.5 Statistical Analyses

Linear regression was used to determine relationships between monthly mean water quality parameters and water source contributions between sites and seasons. Pearson's bivariate correlation (r) and linear regression analysis (R2) were used to calculate significant relationships among hydrological variables, water source contributions, and DOM optical properties using Bonferroni corrections to account for multiple pairwise comparisons. Relationships with a $p < 0.05$ were selected for multiple regression and models with $R2 > 0.5$ and $p < 0.05$ were considered to represent strong correlations. Principal component analysis (PCA) was used to determine the drivers of spatiotemporal variability in water source contributions and associated DOM characteristics and nutrient concentrations. PCA was conducted using the scikit-learn package in Python (3.6). Prior to statistical analysis, an alpha level of 0.05 was set for all analyses and some data were log-transformed to meet the assumptions of normality and homoscedasticity. To determine the drivers of change in DOC concentrations, we also used multiple linear regression (MLR) models using the scikit-learn package in Python (3.6). Predictor variables were added and removed from the model according to the Bayesian Information Criterion (BIC).

2.4 Results

2.4.1 Rainfall and Hydrology

Over the 12-month period, wet season rainfall occurred from May to October with peak daily rainfall in August 2018 (6.70 mm/day; (Menne et al.; 2012). Daily cumulative rainfall averaged 2.32 mm in the dry season and 4.78 mm in the wet season. Canal stage was variable across all canal reaches with a mean value of 1.20

m (NGVD29) in the dry season and 1.14 m (NGVD29) in the wet season (Fig. 2.3). Canal flow responded rapidly to rain events and closely tracked patterns in total precipitation throughout the year. Mean canal flow ranged from 65.54 cfs in the dry season to 227.54 cfs in the wet season. Canal stage and flow were also influenced by periodic spillway gate openings and closings based on changes in seasonal precipitation and tidal extension (Fig. 2.3). Although canal stage was similar across all canals, freshwater flow was markedly lower in CG compared to LR and WC, due to the greater tidal influence in CG.

2.4.2 DOC and Nutrient Concentrations

DOC concentrations ranged from 2.03 mg C L^{-1} to 10.38 mg C L^{-1} across all canal sites and sampling dates, with a mean value of 5.70 in the dry season and 4.83 in the wet season. DOC was greatest in the LR basin (7.83 mg L^{-1} $\pm$ 1.77) compared to WC (4.25 mg L^{-1} $\pm$ 1.91) and CG (3.72 mg L^{-1} $\pm$ 1.87). Concentrations of DOC were higher in the dry season (5.71 mg L^{-1} $\pm$ 3.02) compared to the wet season (4.83 $\pm$ 2.01). The net change in longitudinal DOC concentrations varied between canals with mean ΔDOC values of 0.76 mg L^{-1} in CG, 1.41 mg L^{-1} in LR, and 2.68 mg L^{-1} in WC. No evident patterns were observed in ΔDOC across seasons. DOC in groundwater averaged 6.80 mg C L^{-1} but did not significantly differ from surface canal water.

Concentrations of TP, NOx, and TKN in surface water were similar among sites and between seasons. Mean TP concentrations ranged from 18.5 to 46.3 μg/L across the three canals (Table 1). Nitrogen concentrations were low to moderate across all canals with mean inorganic NOx concentrations between 0.1 - 0.2 mg L^{-1} and TKN concentrations between 0.5-0.62 mg L^{-1}. Groundwater nutrient concentrations

were slightly higher compared to surface waters, although not significantly different (Table 2.1). N:P molar ratios in surface ranged between 15 to 567 with a mean value of 104, indicating moderate P limitation across all basins and sites. N:P ratios in groundwater were lower than that of surface water with a mean value of 38, but still indicated some degree of P limitation. N:P increased downstream during the wet season, not during the dry season, indicating the influence of pulsed runoff on nutrient availability.

2.4.3 DOM Fluorescence Indices and Source Characteristics

HIX values ranged from 2.73 (dry season) and 29.93 (wet season) with a mean value of 10.45 (Table 1). $SUVA_{254}$, ranged between 1.05 and 12.92 L mg^{-1} m^{-1}, suggesting that canal DOM was a mixture of aromatic (i.e., humic) substances and more protein-like DOM. We observed an increase in $SUVA_{254}$ during the wet season (4.67 L mg^{-1} m^{-1}) compared to the dry season (1.26 L mg^{-1} m^{-1}; Table 2.1). HIX values increased with $SUVA_{254}$ but not with concentrations of DOC, suggesting a mixture of terrestrial and marine derived carbon in the DOC pool. FI ranged between 1.45 and 1.67 and reflected a mixture of terrestrial derived, lignin rich DOM with marine derived protein-like DOM. FI values varied month-to-month but did not differ significantly between wet and dry season. Generally, upstream sites showed higher FI values compared to downstream sites, suggesting an autochthonous source of DOM.

The large variation in HIX and BIX values indicated that humic and proteinaceous OM content changed significantly across canal reaches, likely due to differences in local hydrology and residence time (Fig. S2). Groundwater HIX and BIX values were less variable but showed generally higher BIX compared to surface canal water.

Interestingly, we observed a significant negative relationship between DOC concentration and BIX during the dry season ($R^2 = 0.61$, $P < 0.05$) and during peak tidal events in the wet season ($R^2 = 0.56$, $P < 0.05$), but not in the wet season. (Fig. S3).

Groundwater was characterized by high BIX (0.71-0.83) and FI (1.61-1.83) values compared to surface water (0.58 – 0.81, 1.45 – 1.67 respectively; Table 1). HIX values in groundwater were low ranging from 0.8 – 1.3 compared to surface water (2.6 – 18.2), as seen in other studies (Hosen et al., 2021). Similarly, $SUVA_{254}$ in groundwater was generally low with a mean value of 0.05 L mg^{-1} m^{-1} (Table 1). The minimum value of S_R was 0.92 in surface canal water samples while the maximum S_R of 2.21 was found in in groundwater. $S_{275-295}$ values ranged between 0.0124 nm^{-1} and 0.0209 nm^{-1} and did not differ between basins or seasons.

2.4.4 Water Isotopes

Oxygen isotope ($\delta^{18}O$) values ranged from -2.77 ‰ to +3.19 ‰ , while hydrogen isotope (δ^2H) ranged from -10.22 ‰ to +10.36 ‰ (Fig. 2.4). Average surface values for $\delta^{18}O$ and δ^2H were -1.07 ‰ and -2.87 ‰ in the wet season and -0.60 ‰ and +0.59 ‰ in the dry season. Groundwater samples were generally depleted compared to surface water and marine water values (Fig. 2.4). Groundwater $\delta^{18}O$ and δ^2H values ranged from -2.55 to -0.65 ‰ and -8.93 to -0.26 ‰, respectively. Marine water isotopes sampled from Biscayne Bay varied depending on distance from coast and relative influence of evapotranspiration.

2.4.5 Spatiotemporal Distribution of Water Sources

The mean acceptance rates for our four end-member mixing model ranged from 0.27 to 0.41. Across the three canal systems, the BMC model revealed significant

seasonal differences in source fractional contributions during the wet season ($f$mw =0.46; $f$sw =0.25, $f$rw =0.08, $f$gw = 0.21) and the dry season ($f$mw =0.52; $f$sw =0.22, $f$rw =0.08, $f$gw = 0.17; Fig. 2.5). Groundwater accounts for roughly 21.4 % of total canal inputs during the wet season and 17.4 % during the dry season. Monthly mean $f$gw was greatest in August ($f$gw = 26.3) and lowest in February ($f$gw = 11.4). Contributions of $f$gw increase with distance upstream and mean values are slightly higher in the dry compared to the wet season (Fig. 2.6). Additionally, estimates of $f$gw trend closely with increase with indicators of autochthonous production (i.e., BIX, FI) with distance upstream. While annual estimates of monthly groundwater inputs are low compared to other sources ($f$mw, $f$rw, $f$sw), fgw inputs can account for upwards of 25-30% in canals that drain directly into Biscayne Bay. This finding parallels previous results from Stalker et al. (2009) that suggested groundwater may in part explain the relatively high concentrations of N, P, and DOC in surface waters on the western shoreline of Biscayne Bay (Fig. S2).

2.4.6 King Tide Water Source Contributions

Fractional contributions of $f$mw and $f$gw were elevated during three consecutive perigean spring tide events ($\geq$ 0.52m MLLW) on October 7, 19, and 27, 2018. Across all canal sites, $f$mw increased across rising, peak and ebb tides while $f$gw showed a decreasing trend across tide heights. Interestingly, contributions of $f$gw were saturated with $f$mw by the third tidal event and show no significant trend with rising or ebb tide (Fig. 2.7). Groundwater contributions trended with steadily increasing values of BIX across tide events, with no significant differences between rising and ebb tides (Fig. 2.7).

2.4.7 PCA and Regression Results

PCA revealed a clear seasonality in water sources and DOM composition between wet and dry seasons and among basins (Fig. 2.8). PC 1 and 2 explained 30.32% and 17.68% of the total variance in DOM composition, respectively. PC1 described a gradient of salinity that distinguished marine water from all other sources. PC2 explained differences in DOM source from terrestrial versus autochthonous production. Together, our results show that fractional contributions were thoroughly mixed during the wet season compared to more distinct source groupings and DOM composition in the dry season. Water quality parameters appeared to be driven by groundwater in WC compared to greater tidal influence on water quality in LR and CG. Changes in salinity were driven by increasing seasonal proportions of stormwater and groundwater, as evidenced along PC1 (Fig. 2.8). CMHD trended closely with indicators of fresh DOM (FI, BIX) likely driven by increases in fresh runoff rather than low salinity groundwater inputs.

The MLR model explained 65.8% of the variation in DOC concentrations (Table 2). Our analysis shows positive correlations between DOC and HIX ($p = 0.037$) and $\delta^{18}O$ ($p = 0.010$). We found strong negative relationships between DOC and FI ($p = 0.002$) and CMHD ($p < 0.001$). There was also a weaker negative relationship between DOC and $SUVA_{254}$ ($p = 0.05$). While fgw was not a significant predictor of DOC, it is likely that DOC concentrations are determined by the interaction of several controlling factors.

2.5 Discussion

2.5.1 Role of Coastal Canals in DOM Cycling

The capacity for coastal canals to transport and transform DOC and DOM relies on the proportional contributions from fresh and marine water sources. Most of the uncertainty around estimating biogeochemical processing rates at large scales comes down to the fact that groundwater inputs are rarely directly or indirectly measured. Our combined tracer approach provided reliable estimates of water source contributions to mixed urban canals while still considering the physical and biological constraints on the type and rate of DOM processing. We found multiple lines of evidence that seasonal shifts in the hydraulic gradient between groundwater and marine water significantly alter water source contributions and the concentration and composition of DOC and DOM in urban coastal canals. We found that significant increases in pulsed DOM and nutrient concentrations correspond to changes in the canal-to-marine head difference and increased groundwater contributions during the subtropical wet season. Further, we provide evidence that indicators of autochthonous production and recently produced DOM are elevated during perigean spring tide events and correspond to incremental increases in groundwater (Fig. 2.7). In all, we see that this seasonal pulse-shunt regime can lead to the stabilization of DOC concentrations by inputs of autochthonous production that may be critical to the ecology of such coastal riverine systems.

2.5.2 Groundwater Contributions to the Pulse-Shunt Concept

Results of this study are in agreement with the Pulse-Shunt Concept (Raymond et al.; 2016), which postulates that OM is pulsed into streams during high-flow events and subsequently shunted into larger rivers prior to microbial transformation. Although DOC loading is increased during pulsed events, high flows result in low in-stream processing and decreased microbial but increased terrigenous DOM being exported downstream. In coastal basins, marine pulses from extreme tide events, particularly during the wet season, can supplement these moments with microbially sourced DOM when shallow groundwater connects with surface waters (Fig. 2.7). Although the relative proportion of groundwater contributions may be minor compared to other water sources, we suggest that the importance of nutrients and chemical constituents through shallow groundwater contributions may be important to microbial priming (Stalker et al.; 2009). Specifically, increases in labile, proteinaceous DOM from groundwater or in-stream autochthonous production may contribute to local bacterioplankton activity and lead to elevated bacterial carbon demand downstream in Biscayne Bay (Battin et al.; 2009).

2.5.3 Autochthonous Production Supports DOM Chemostasis

There is growing evidence of an urban priming effect where labile autochthonous DOM from anthropogenic sources facilitates microbial degradation of DOM (Fork et al.; 2020; Smith et al.; 2021). Increases in sources of bioavailable DOM may impact ecosystem metabolism and affect the quality of DOM exported downstream,

particularly in urban ecosystems (Bianchi; 2011). We found that sources of DOM from autochthonous production, as measured by S_R, BIX, and FI, are controlled, in part, by seasonal increases in stormwater runoff and tidal height (Fig. 2.8). These results may also suggest a compensatory mechanism where increased autochthonous production during the wet season balances decreased allochthonous DOM inputs during the dry season resulting in relatively stable DOM concentrations and high-quality DOM across the year (Parr et al.; 2015). Thus, the stabilization of DOM concentrations and quality, regardless of hydrologic influence, can help to maintain chemostasis during lower flows in large coastal waterways (Hosen et al.; 2021).

2.5.4 Shifts in Hydraulic Gradients Drive DOC Concentration and DOM Quality

Our observations of change in DOC and DOM related to the canal-to-marine hydraulic gradient suggest a variety of mechanisms are important for controlling seasonal export and processing rates. We observed elevated DOC concentrations in groundwater compared to surface water and changes in seasonal DOC corresponded to shifts in salinity. We also found that HIX, FI, and $SUVA_{254}$ were all significant DOM quality predictors of DOC concentration and all optical parameters showed a negative trend with CMHD (Table 2). In addition, dissolved nutrients originating from the canal reaches showed positive trends with NO3 ($r^2 = 0.22$, $p < 0.05$) and TP ($r^2 = 0.36$, $p < 0.05$) and may contribute to increases in downstream phytoplankton production (Fig. S4). Interestingly, we found a significant negative relationship between DOC and BIX during the dry season and during consecutive King Tide events in the wet season. These results support previous studies that observed coastal waterways as primary sources of DOC, particularly supplemented by

groundwater inputs, and that may contribute microbial DOM to increase in-stream metabolism downstream (Kim et al.; 2020).

2.5.5 Estimating DOM Source Using DOM Quality Indices

The combined isotope/DOM fluorescence method presented in this study shows promise for reliable estimations of DOM source using optical properties. This approach to DOM source tracing has the potential to better explain discrepancies among patterns in DOM concentration and quality resulting from differential flow paths and site-specific bioreactivity (Lee et al.; 2018; Yang and Hur; 2014). For example, $SUVA_{254}$ typically increases during periodic stormwater runoff events in the subtropical wet season (Fellman et al.; 2009) but may decrease with tidal extension during the dry season (Couturier et al.; 2016). Similarly, BIX can increase due to elevated in-stream production of autochthonous DOM but may also correspond to increases in FI associated with phytoplankton production (Kim et al.; 2020). Thus, incorporating multiple optical indices into mixing models that evaluate DOM source inputs from fresh and marine water sources allows for a more comprehensive and mechanistic understanding of DOM processing and transformation.

We cannot disregard the potential effects of photo- and biological degradation on the utility of organic matter properties for source tracking. While biodegradation heightens the possibility of under-estimating autochthonous DOM origins, indices such as BIX and FI are rather robust to changes in mineral absorption and can provide reliable estimates of DOM source (Lee et al.; 2018). However, this may not hold up in large-scale estuaries where residence time and sunlight exposure are increased. For example, Osburn et al. (2012) observed significant shifts in DOM composition upon biodegradation and exposure to sunlight in a coastal estuary. In

this study, canal stage was highly variable due to periodic fluctuations in stormwater flow, tidal height, and freshwater release from periodic tidal gate openings which further limited the possibility of degradation of optical indices.

2.6 Conclusions

As sea levels rise, seasonal and diurnal tidal forcing will continue to push the hydraulic gradient inland, shifting the fresh-saltwater boundary upward and upstream. Further, large inputs of terrigenous DOC can be introduced following significant precipitation (i.e., hurricane) events (Letourneau et al.; 2021), or during extreme high tide, as evidenced in this study. Taken together, these factors can lead to increases in annual groundwater contributions and seasonal pulsed inputs from stormwater runoff. This may result in larger seasonal differences in DOC concentrations and the contribution of DOM produced from within the canals and nearshore estuary will increase relative to that delivered from upstream sources. Net changes in DOC concentration versus DOM quality will influence the cycling of dissolved nutrients, bioavailability of allochthonous vs. autochthonous produced DOM, phytoplankton production, and the effect of light attenuation from DOM on phytoplankton ecology (Fellman et al.; 2011). Results presented here provide insight into the complex role of water source on in-stream reactions and the ultimate fate of riverine DOM in coastal environments. The combined isotope-DOM fluorescence mixing model used in this study could be applicable to any estuarine system and provides a sound method for differentiating among water source and flow paths in coastal systems. Our study highlights the relevance of groundwater contributions and in-stream DOM production on river carbon fluxes, which is often overlooked as it may support microbial metabolism and energy flow across trophic levels in coastal waters.

2.7 Bibliography

Arendt, C. A., Aciego, S. M. and Hetland, E. A. (2015). An open source b ayesian m onte c arlo isotope mixing model with applications in e arth surface processes, *Geochemistry, Geophysics, Geosystems* **16**(5): 1274–1292.

Asmala, E., Osburn, C. L., Paerl, R. W. and Paerl, H. W. (2021). Elevated organic carbon pulses persist in estuarine environment after major storm events, *Limnology and Oceanography Letters* **6**: 43–50.

Battin, T. J., Luyssaert, S., Kaplan, L. A., Aufdenkampe, A. K., Richter, A. and Tranvik, L. J. (2009). The boundless carbon cycle, *Nature Geoscience* **2**: 598–600.

Bernal, S., Lupon, A., Catalán, N., Castelar, S. and Martí, E. (2018). Decoupling of dissolved organic matter patterns between stream and riparian groundwater in a headwater forested catchment, *Hydrology and Earth System Sciences* **22**(3): 1897–1910.

Bianchi, T. S. (2011). The role of terrestrially derived organic carbon in the coastal ocean: A changing paradigm and the priming effect, *Proceedings of the National Academy of Sciences of the United States of America* **108**: 19473–19481.

Cable, J., Ogle, K. and Williams, D. (2011). Contribution of glacier meltwater to streamflow in the wind river range, wyoming, inferred via a bayesian mixing model applied to isotopic measurements, *Hydrological Processes* **25**: 2228–2236.

Casas-Ruiz, J. P., Catalán, N., Gómez-Gener, L., von Schiller, D., Obrador, B., Kothawala, D. N., López, P., Sabater, S. and Marcé, R. (2017). A tale of pipes and reactors: Controls on the in-stream dynamics of dissolved organic matter in rivers, *Limnology and Oceanography* **62**: S85–S94.

Couturier, M., Nozais, C. and Chaillou, G. (2016). Microtidal subterranean estuaries as a source of fresh terrestrial dissolved organic matter to the coastal ocean, *Marine Chemistry* **186**: 46–57.

Derrien, M., Kim, M. S., Ock, G., Hong, S., Cho, J., Shin, K. H. and Hur, J. (2018). Estimation of different source contributions to sediment organic matter in an agricultural-forested watershed using end member mixing analyses based on stable isotope ratios and fluorescence spectroscopy, *Science of the Total Environment* **618**: 569–578.

Fellman, J. B., Hood, E., Edwards, R. T. and D'Amore, D. V. (2009). Changes in the concentration, biodegradability, and fluorescent properties of dissolved organic matter during stormflows in coastal temperate watersheds, *Journal of Geophysical Research: Biogeosciences* **114**(G1).

Fellman, J. B., Petrone, K. C. and Grierson, P. F. (2011). Source, biogeochemical cycling, and fluorescence characteristics of dissolved organic matter in an agro-urban estuary, *Limnology and Oceanography* **56**: 243–256.

Fork, M. L., Osburn, C. L. and Heffernan, J. B. (2020). Bioavailability and compositional changes of dissolved organic matter in urban headwaters, *Aquatic Sciences* **82**(4): 1–15.

Hansen, A. M., Kraus, T. E., Pellerin, B. A., Fleck, J. A., Downing, B. D. and Bergamaschi, B. A. (2016). Optical properties of dissolved organic matter (dom): Effects of biological and photolytic degradation, *Limnology and oceanography* **61**(3): 1015–1032.

Helms, J. R., Stubbins, A., Ritchie, J. D., Minor, E. C., Kieber, D. J. and Mopper, K. (2008). Absorption spectral slopes and slope ratios as indicators of molecular

weight, source, and photobleaching of chromophoric dissolved organic matter, *Limnology and oceanography* **53**(3): 955–969.

Hosen, J. D., Aho, K. S., Fair, J. H., Kyzivat, E. D., Matt, S., Morrison, J., Stubbins, A., Weber, L. C., Yoon, B. and Raymond, P. A. (2021). Source switching maintains dissolved organic matter chemostasis across discharge levels in a large temperate river network, *Ecosystems* **24**: 227–247.

Jaffé, R., McKnight, D., Maie, N., Cory, R., McDowell, W. and Campbell, J. (2008). Spatial and temporal variations in dom composition in ecosystems: The importance of long-term monitoring of optical properties, *Journal of Geophysical Research: Biogeosciences* **113**(G4).

Kim, J., Kim, T.-H., Park, S. R., Lee, H. J. and Kim, J. K. (2020). Factors controlling the distributions of dissolved organic matter in the east china sea during summer, *Scientific reports* **10**(1): 1–10.

Lee, M. H., Osburn, C. L., Shin, K. H. and Hur, J. (2018). New insight into the applicability of spectroscopic indices for dissolved organic matter (dom) source discrimination in aquatic systems affected by biogeochemical processes, *Water Research* **147**: 164–176.

Letourneau, M. L., Schaefer, S. C., Chen, H., McKenna, A. M., Alber, M. and Medeiros, P. M. (2021). Spatio-temporal changes in dissolved organic matter composition along the salinity gradient of a marsh-influenced estuarine complex, *Limnology and Oceanography* **66**: 3040–3054.

Lunn, D., Spiegelhalter, D., Thomas, A. and Best, N. (2009). The bugs project: Evolution, critique and future directions, *Statistics in Medicine* **28**: 3049–3067.

Mcknight, D. M., Boyer, E. W., Westerhoff, P. K., Doran, P. T., Kulbe, T. and Andersen, D. T. (2001). Spectrofluorometric characterization of dissolved organic matter for indication of precursor organic material and aromaticity, *Limnol. Oceanogr* **46**: 38–48.

Menne, M. J., Durre, I., Vose, R. S., Gleason, B. E. and Houston, T. G. (2012). An overview of the global historical climatology network-daily database, *Journal of atmospheric and oceanic technology* **29**(7): 897–910.

Moore, W. S. (1999). The subterranean estuary: a reaction zone of ground water and sea water, *Marine Chemistry* **65**: 111–125.

Niencheski, L. F. H., Windom, H. L., Moore, W. S. and Jahnke, R. A. (2007). Submarine groundwater discharge of nutrients to the ocean along a coastal lagoon barrier, southern brazil, *Marine Chemistry* **106**: 546–561.

Parr, T. B., Cronan, C. S., Ohno, T., Findlay, S. E., Smith, S. M. and Simon, K. S. (2015). Urbanization changes the composition and bioavailability of dissolved organic matter in headwater streams, *Limnology and Oceanography* **60**: 885–900.

Raymond, P. A., Saiers, J. E. and Sobczak, W. V. (2016). Hydrological and biogeochemical controls on watershed dissolved organic matter transport: Pulse-shunt concept, *Ecology* **97**(1): 5–16.

Rodellas, V., Garcia-Orellana, J., Masqué, P., Feldman, M., Weinstein, Y. and Boyle, E. A. (2015). Submarine groundwater discharge as a major source of nutrients to the mediterranean sea, *Proceedings of the National Academy of Sciences of the United States of America* **112**: 3926–3930.

Rosenthal, J., Brooks, S., Gelman, A., Jones, G. and Meng, X. (2011). Handbook of markov chain monte carlo, *CRC Press, Boca Raton, FL, chapter Optimal Proposal Distributions and Adaptive* **2000**: 93–112.

Rudolph, J. C., Arendt, C. A., Hounshell, A. G., Paerl, H. W. and Osburn, C. L. (2020). Use of geospatial, hydrologic, and geochemical modeling to determine the influence of wetland-derived organic matter in coastal waters in response to extreme weather events, *Frontiers in Marine Science* **7**: 18.

Slomp, C. P. and Cappellen, P. V. (2004). Nutrient inputs to the coastal ocean through submarine groundwater discharge: Controls and potential impact, *Journal of Hydrology* **295**: 64–86.

Smith, M. A., Kominoski, J. S., Gaiser, E. E., Price, R. M. and Troxler, T. G. (2021). Stormwater runoff and tidal flooding transform dissolved organic matter composition and increase bioavailability in urban coastal ecosystems, *Journal of Geophysical Research: Biogeosciences* **126**(7): e2020JG006146.

Stalker, J. C., Price, R. M. and Swart, P. K. (2009). Determining spatial and temporal inputs of freshwater, including submarine groundwater discharge, to a subtropical estuary using geochemical tracers, biscayne bay, south florida, *Estuaries and coasts* **32**(4): 694–708.

Sukop, M. C., Rogers, M., Guannel, G., Infanti, J. M. and Hagemann, K. (2018). High temporal resolution modeling of the impact of rain, tides, and sea level rise on water table flooding in the arch creek basin, miami-dade county florida usa, *Science of the Total Environment* **616-617**: 1668–1688.

Wagner, S., Riedel, T., Niggemann, J., Vahatalo, A. V., Dittmar, T. and Jaffé, R. (2015). Linking the molecular signature of heteroatomic dissolved organic matter

to watershed characteristics in world rivers, *Environmental science & technology* **49**(23): 13798–13806.

Ward, N. D., Bianchi, T. S., Medeiros, P. M., Seidel, M., Richey, J. E., Keil, R. G. and Sawakuchi, H. O. (2017). Where carbon goes when water flows: carbon cycling across the aquatic continuum, *Frontiers in Marine Science* **4**: 7.

Weishaar, J. L., Aiken, G. R., Bergamaschi, B. A., Fram, M. S., Fujii, R. and Mopper, K. (2003). Evaluation of specific ultraviolet absorbance as an indicator of the chemical composition and reactivity of dissolved organic carbon, *Environmental science & technology* **37**(20): 4702–4708.

Yamashita, Y., Jaffé, R., Maie, N. and Tanoue, E. (n.d.). Yamashita, y., et al. assessing the dynamics of dissolved organic matter (dom) in coastal environments by excitation emission matrix fluorescence and parallel factor analysis (eem-parafac). limnol. oceanogr., 53(5), 2008, 1900–1908.

Yang, L., Chang, S. W., Shin, H. S. and Hur, J. (2015). Tracking the evolution of stream dom source during storm events using end member mixing analysis based on dom quality, *Journal of Hydrology* **523**: 333–341.

Yang, L. and Hur, J. (2014). Critical evaluation of spectroscopic indices for organic matter source tracing via end member mixing analysis based on two contrasting sources, *Water Research* **59**: 80–89.

2.8 Tables

Table 2.1: Mean (± standard deviation) values for hydrologic variables, water physicochemistry, and DOM optical properties in surface, ground, and marine water from June 2018 to May 2019

Covariate	Units	Wagner Creek (WC, *n*=48)	Little River (LR, *n*=48)	Coral Gables (CG, *n*=48)	Groundwater (*n*=12)	Marine Water (*n*=12)
Cum. Rainfall	mm	1115.5	1318.1	1209.5		
Tidal Amplitude	m	1.17	0.63	1.09		
Stage	m	0.36 (± 0.19)	0.49 (± 0.08)	0.37 (± 0.11)		
Temp	°C	28.9 (± 1.28)	26.2 (± 2.41)	25.2 (± 2.95)	27.0 (± 1.04)	26.17 (± 3.23)
DO	mg L^{-1}	3.6 (± 2.30)	4.4 (± 1.61)	5.4 (± 1.34)	0.41 (± 0.03)	6.29 (± 0.81)
Salinity	ppt	16.6 (± 10.98)	15.1 (± 15.22)	15.8 (± 15.95)	10.2 (± 5.63)	33.14 (± 2.79)
Turbidity	NTU	2.1 (± 1.54)	1.7 (± 1.06)	1.3 (± 0.60)		1.34 (± 0.73)
DOC	mg L^{-1}	3.5 (± 0.41)	9.3 (± 1.10)	4.3 (± 2.56)	6.80 (± 2.93)	4.35 (± 2.54)
TP	ug L^{-1}	46.3 (± 31.38)	18.5 (± 8.78)	22.4 (± 11.31)	60.0 (± 0.24)	10.1 (± 2.13)
NO_x-N	mg L^{-1}	0.1 (± 0.04)	0.2 (± 0.11)	0.1 (± 0.11)	0.03 (± 0.02)	0.02 (± 0.01)
TKN	mg L^{-1}	0.5 (± 0.15)	0.6 (± 0.28)	0.5 (± 0.21)	0.62 (± 0.30)	0.28 (± 0.17)
HIX	-	8.3 (± 1.03)	11.7 (± 4.26)	6.1 (± 3.05)	11.3 (± 1.40)	3.20 (± 0.32)
BIX	-	0.79 (± 0.02)	0.72 (± 0.01)	0.80 (± 0.02)	0.74 (± 0.03)	0.65 (± 0.03)
FI	-	1.54 (± 0.05)	1.51 (± 0.01)	1.60 (± 0.03)	1.65 (± 0.13)	1.82 (± 0.09)
$SUVA_{254}$	L mg^{-1} m^{-1}	1.76 (± 1.96)	0.93 (± 1.10)	1.09 (± 1.34)	0.05 (± 0.01)	0.05 (± 0.01)
N:P Molar Ratio	-	74.5 (± 91.4)	150.5(± 120.9)	89.5 (± 61.5)	38.0 (± 4.10)	24.0 (± 3.76)

Table 2.2: Coefficients, variance, and significance of multiple linear regression model to explain differences in DOC concentrations of surface canal waters.

Variable	Coefficient	Standard error	t	p
FI	-20.65	6.124	-3.373	**0.002**
BIX	8.474	5.218	1.624	*ns*
HIX	0.198	0.092	2.158	**0.037**
$SUVA_{254}$	-0.293	0.152	-1.927	**0.05**
^{18}O	0.425	0.158	2.697	**0.010**
2H	-0.128	0.077	-1.667	*ns*
f_{gw}	1.782	1.463	1.218	*ns*
CMHD	-14.03	3.434	-4.086	**<0.001**

$R^2 = 0.658$; F-statistic = 9.379; $p < 0.001$; n=164; *ns* = not significant

2.9 Figures

Fig. 2.1. Graphic representation of the various hydrologic (freshwater and saltwater) contributions to surface canals in an urban coastal karstic system.

Fig. 2.2. Map of canal surface water (red circles), groundwater (yellow circles), marine (blue circles), and rainwater collection sites in Miami, FL. Water control structures are represented by grey squares in each canal basin.

Fig. 2.3. Mean (a) canal stage (m; NGVD29) and surface flow (cfs) across three water control structures (G-93, S-26, S-27) and (b) mean groundwater level (m; NGVD29) at three USGS wells control structures (F-319, F-179, F-45) from June 1, 2018 to May 31, 2019.

Fig. 2.4. Stable isotopic composition (δ2H and δ18O) of surface waters in three canal drainage basins: Coral Gables (CG), Wagner Creek (WC), and Little River (LR). Also depicted are the $\delta^{18}O$ and $\delta^{2}H$ values of shallow groundwater (GW; gold diamonds), and marine water (MW; blue squares) relative to each canal basin. The bold black line represents the global meteoric water line (GMWL) with a slope of +8 and an intercept of +10 ‰. The thin gray line represents the best fit line for surface canal samples.

Fig. 2.5. Best fit fractional contributions of monthly mean groundwater (GW), marine water (MW), rainwater (RW), and stormwater (SW) from the Bayesian mixing model (2H/HIX/FI) across all study canal basins. Mean salinity (ppt) concentrations (± 0.95 C.I) are also represented.

Fig. 2.6. Relationships between distance upstream (m) and mean annual (a) dissolved organic carbon (DOC) concentrations, (b) humification index (HIX), (c) biological index (BIX), (d) fluorescence index (FI), and (e) fractional groundwater

contributions across all three coastal canals. Points represent the seasonal mean at each site (± SE, n = 6).

Fig. 2.7. The dashed horizontal line represents the mean GW contribution in the month of October (x = 0.215 ± 0.20) and the dotted line represents the annual mean GW contribution during the entire study period (x = 0.194 ± 0.20).

Fig. 2.8. Loadings and scores of principal components PC1 and PC2 for the composition of water source and quality parameters including water isotopes ($\delta^{18}O$ and $\delta^{2}H$), optical properties (HIX, BIX, FI), fractional source contributions of (GW, MW, RW, SW), and canal to marine head differential (CMHD). Axes are labeled with the percent variability explained by each principal component.

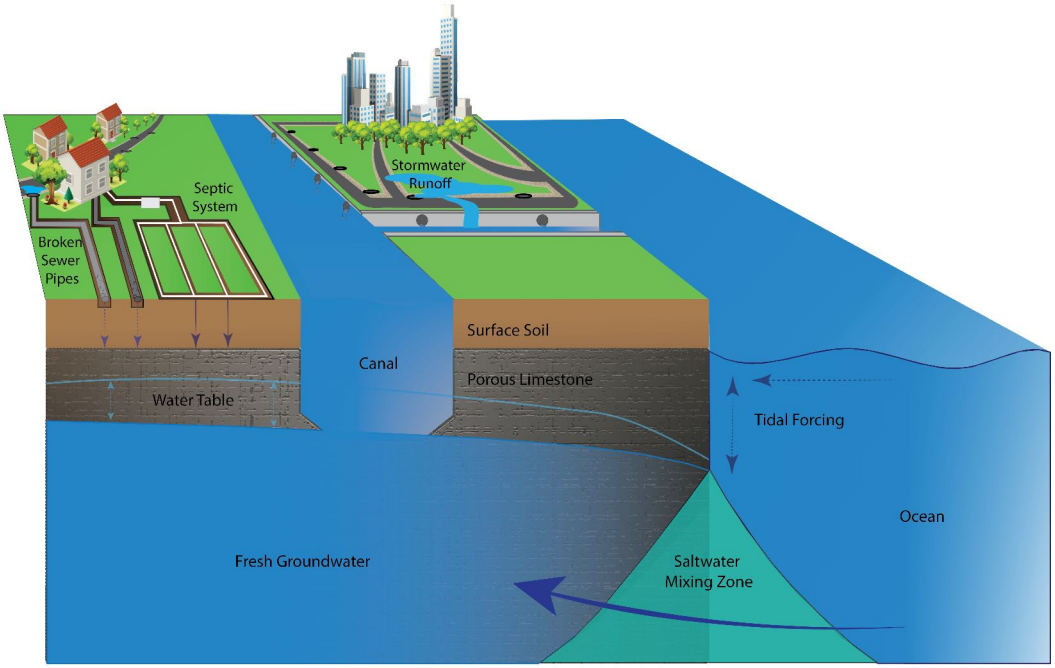

Figure 2.1: Graphic representation of the various hydrologic (freshwater and saltwater) contributions to surface canals in an urban coastal karstic system.

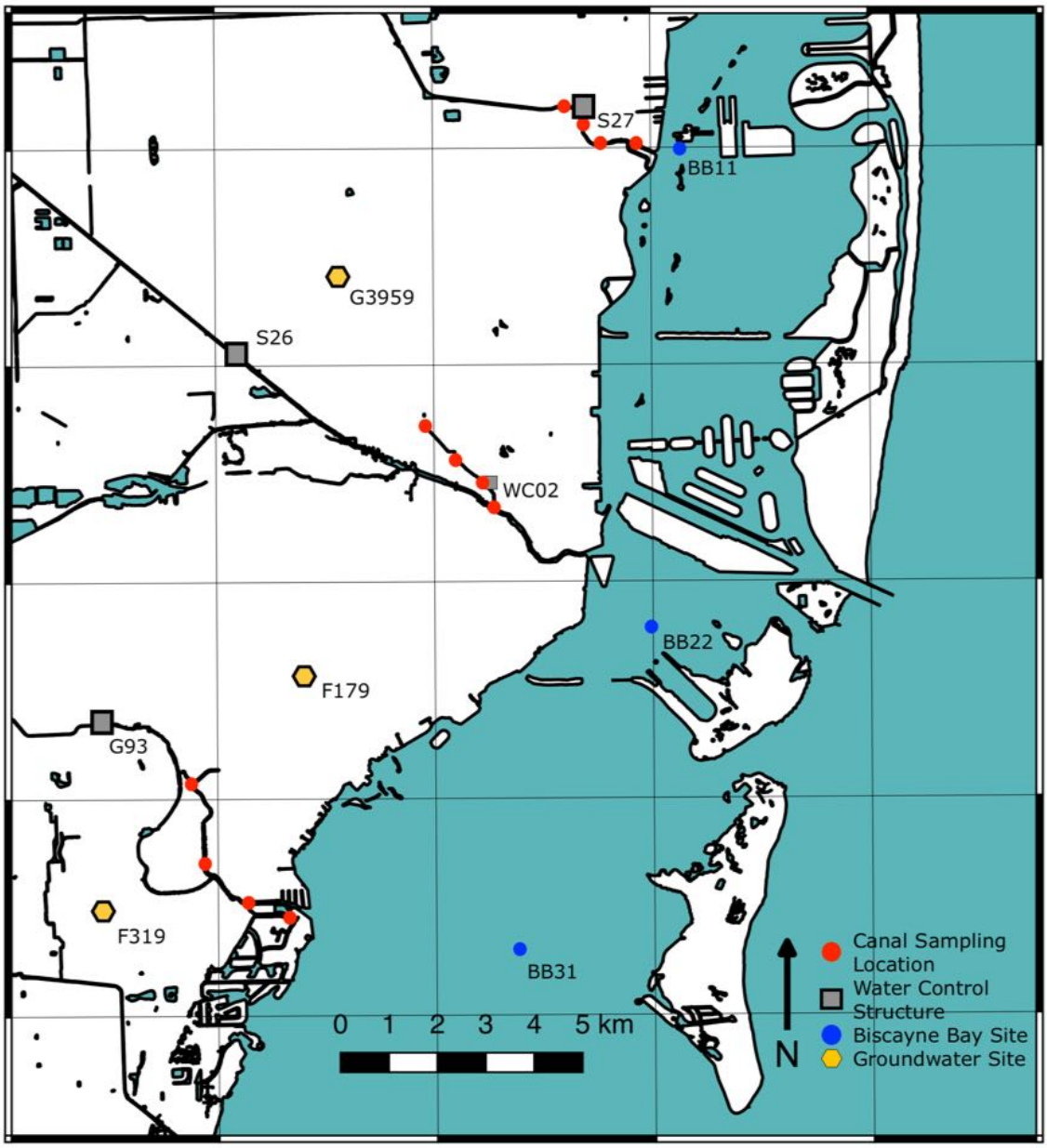

Figure 2.2: Map of canal surface water (red circles), groundwater (yellow circles), marine (blue circles), and rainwater collection sites in Miami, FL. Water control structures are represented by grey squares in each canal basin.

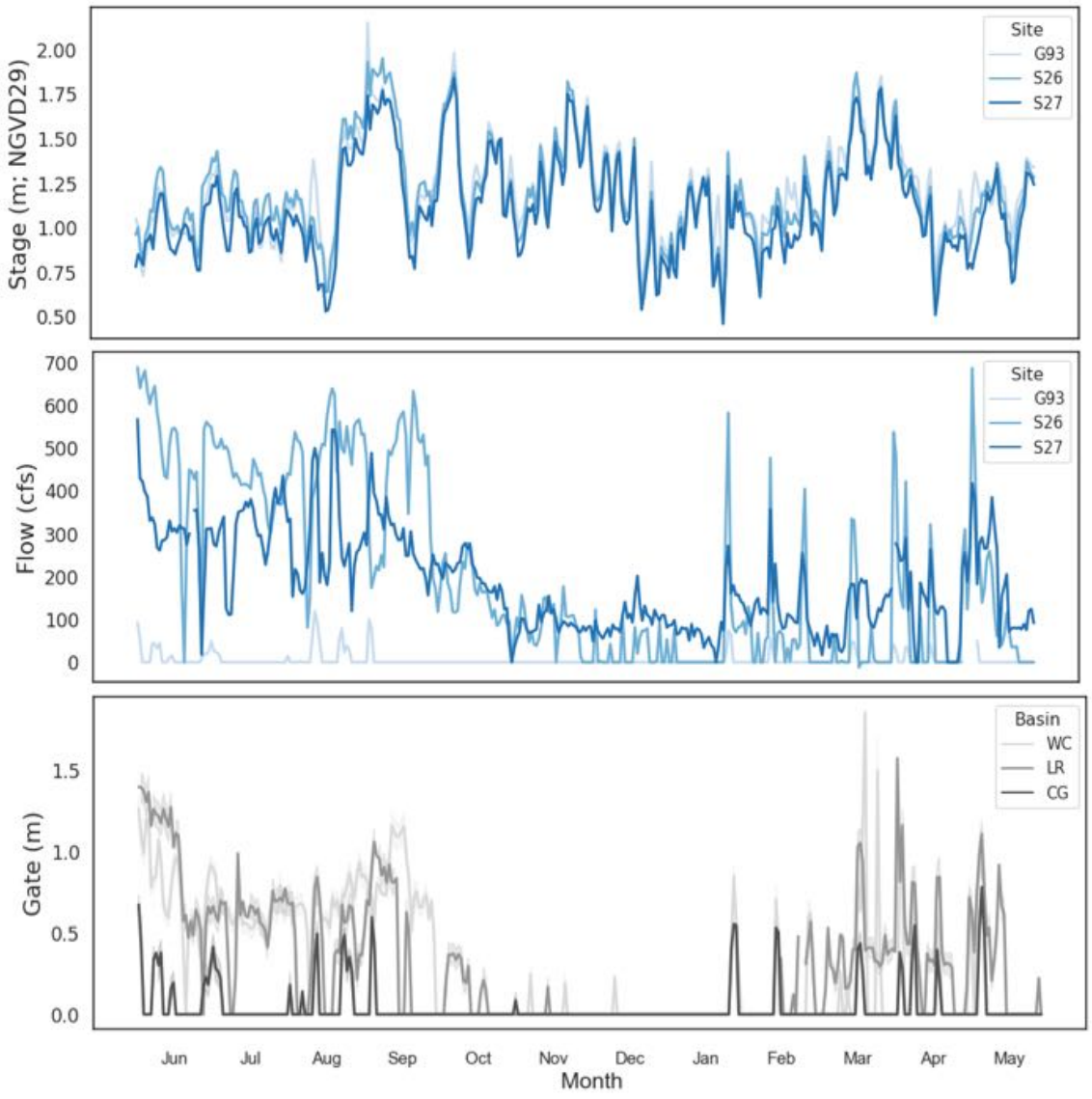

Figure 2.3: Mean (a) canal stage (m; NGVD29) and surface flow (cfs) across three water control structures (G-93, S-26, S-27) and (b) mean groundwater level (m; NGVD29) at three USGS wells control structures (F-319, F-179, F-45) from June 1, 2018 to May 31, 2019.

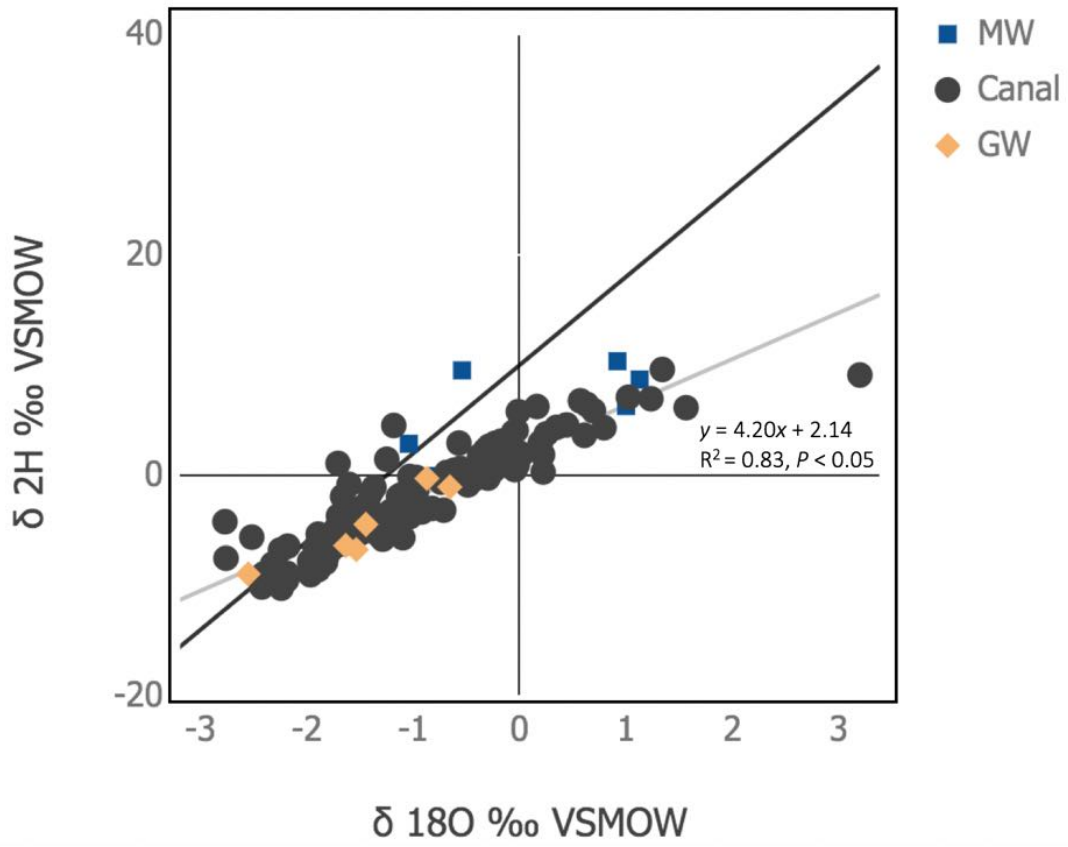

Figure 2.4: Stable isotopic composition ($\delta^{18}O$ and $\delta^{2}H$) of surface waters in three canal drainage basins: Coral Gables (CG), Wagner Creek (WC), and Little River (LR). Also depicted are the $\delta^{18}O$ and $\delta^{2}H$ values of shallow groundwater (GW; gold diamonds), and marine water (MW; blue squares) relative to each canal basin. The bold black line represents the global meteoric water line (GMWL) with a slope of +8 and an intercept of +10 ‰. The thin gray line represents the best fit line for surface canal samples.

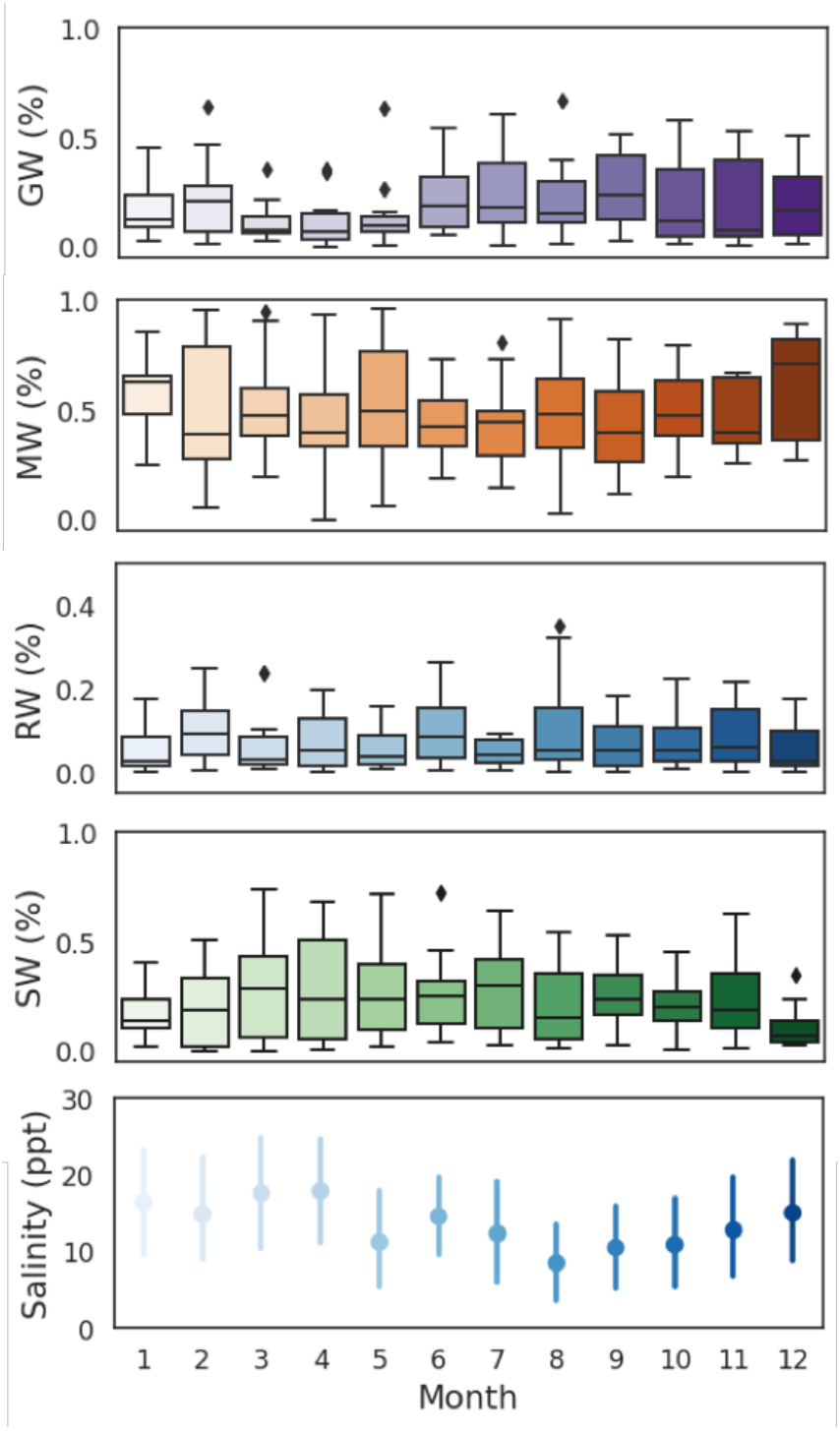

Figure 2.5: Best fit fractional contributions of monthly mean groundwater (GW), marine water (MW), rainwater (RW), and stormwater (SW) from the Bayesian mixing model (2H/HIX/FI) across all study canal basins. Mean salinity (ppt) concentrations (± 0.95 C.I) are also represented.

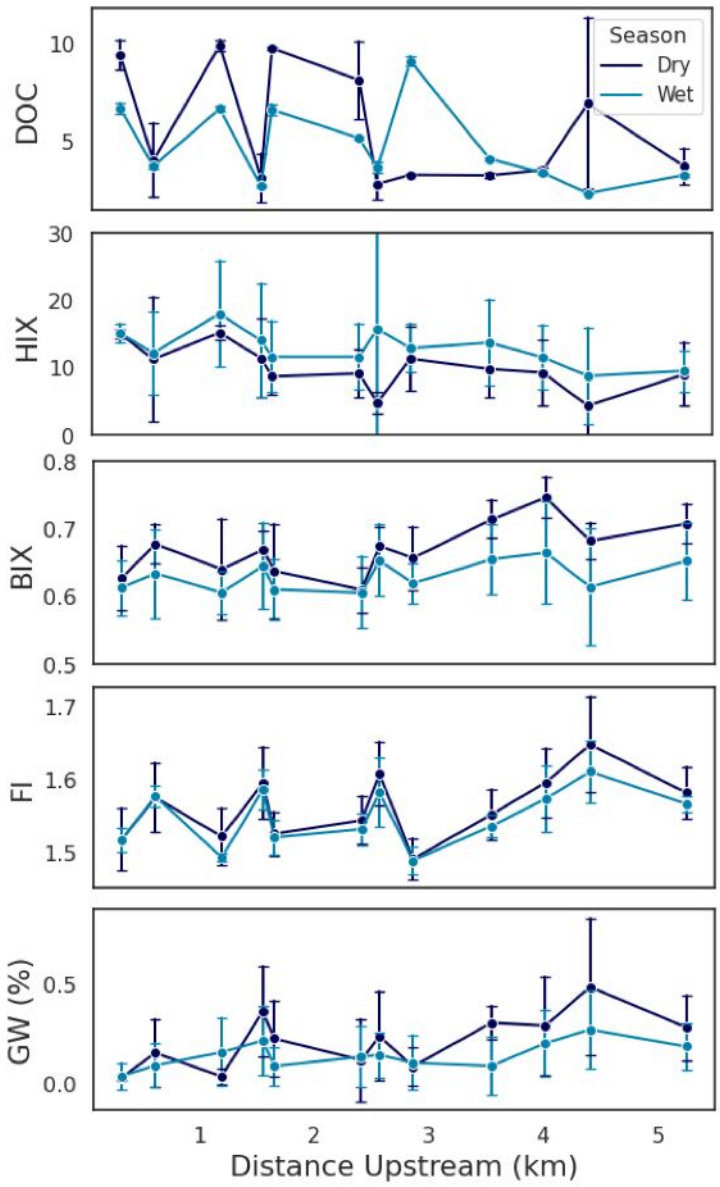

Figure 2.6: Relationships between distance upstream (m) and mean annual (a) dissolved organic carbon (DOC) concentrations, (b) humification index (HIX), (c) biological index (BIX), (d) fluorescence index (FI), and (e) fractional groundwater contributions across all three coastal canals. Points represent the seasonal mean at each site (± SE, n = 6).

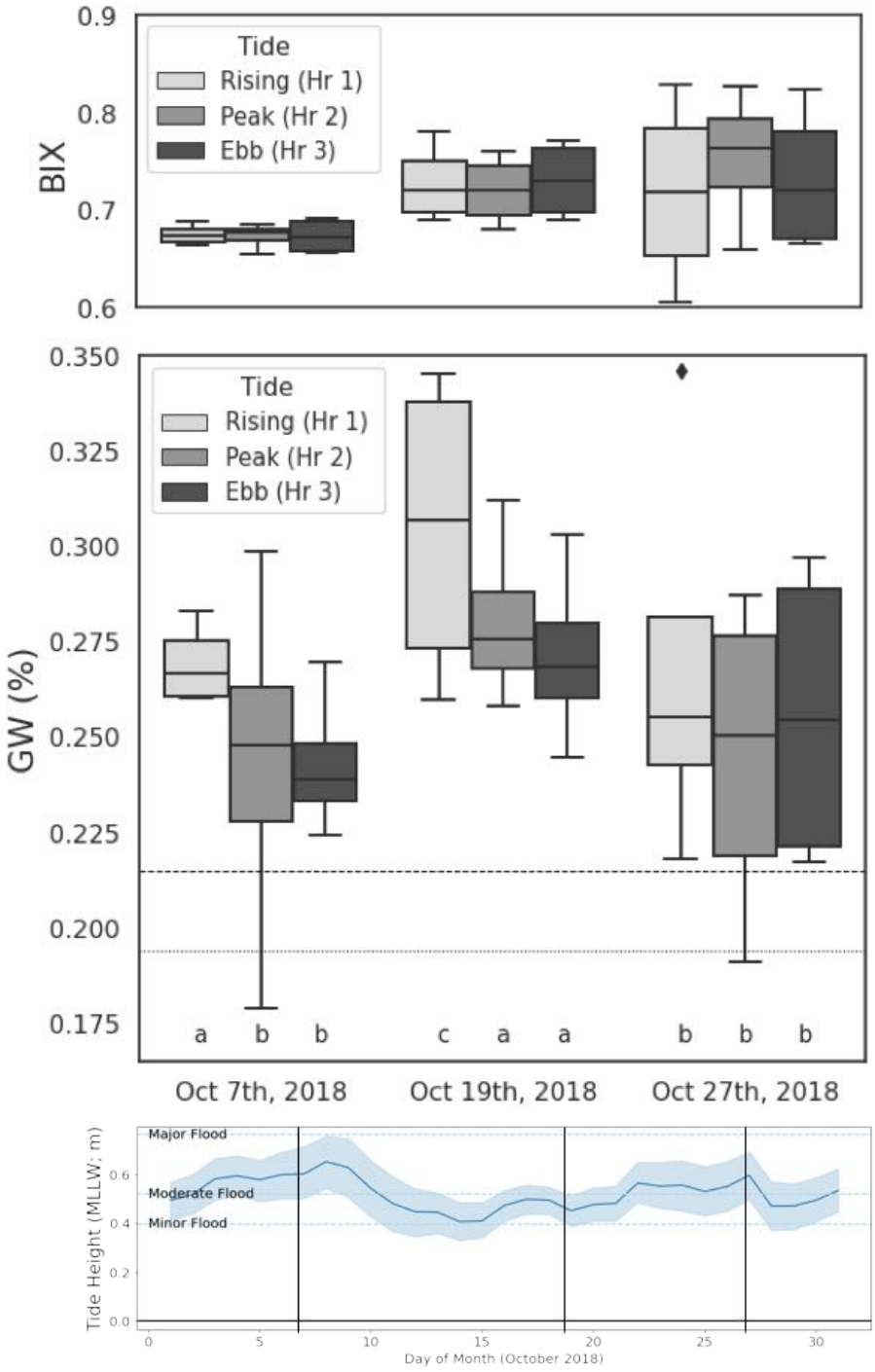

Figure 2.7: The dashed horizontal line represents the mean GW contribution to the Coral Gables (CG) canal during the month of October (x = 0.215 ± 0.20) and the dotted line represents the annual mean GW contribution during the entire study period (x = 0.194 ± 0.20).

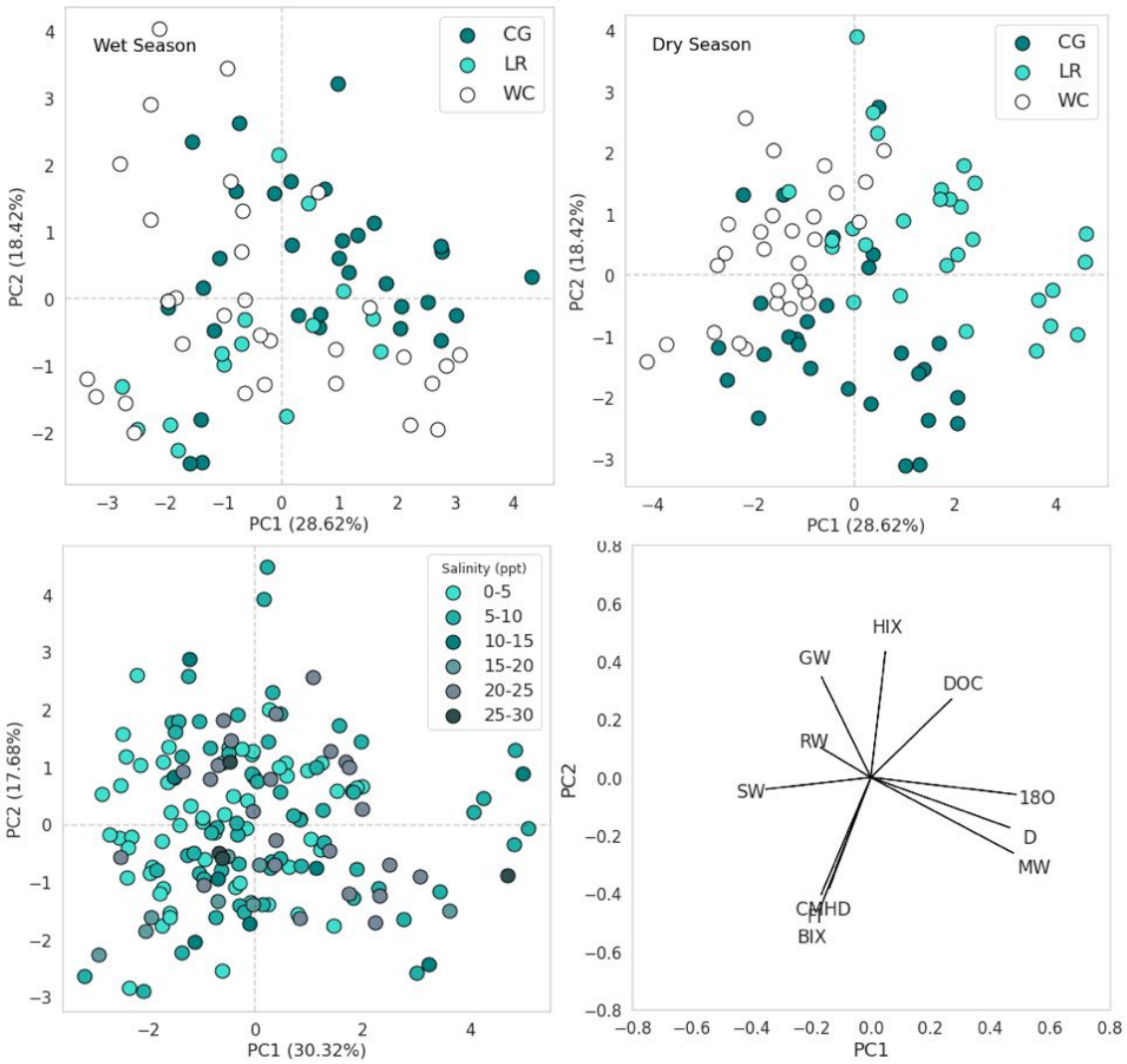

Figure 2.8: Results of a principal component analysis (PCA) represented by principal components (PC1 and PC2) scores during the (a) wet season, (b) dry season, (c) across a range of salinity (0-30 ppt), and (d) the model loadings. Model parameters include water isotopes ($\delta^{18}O$ and $\delta^{2}H$), optical properties (HIX, BIX, FI), fractional source contributions of (GW, MW, RW, SW), and canal to marine head differential (CMHD). Axes are labeled with the percent variability explained by each principal component.

2.10 Supplemental Information

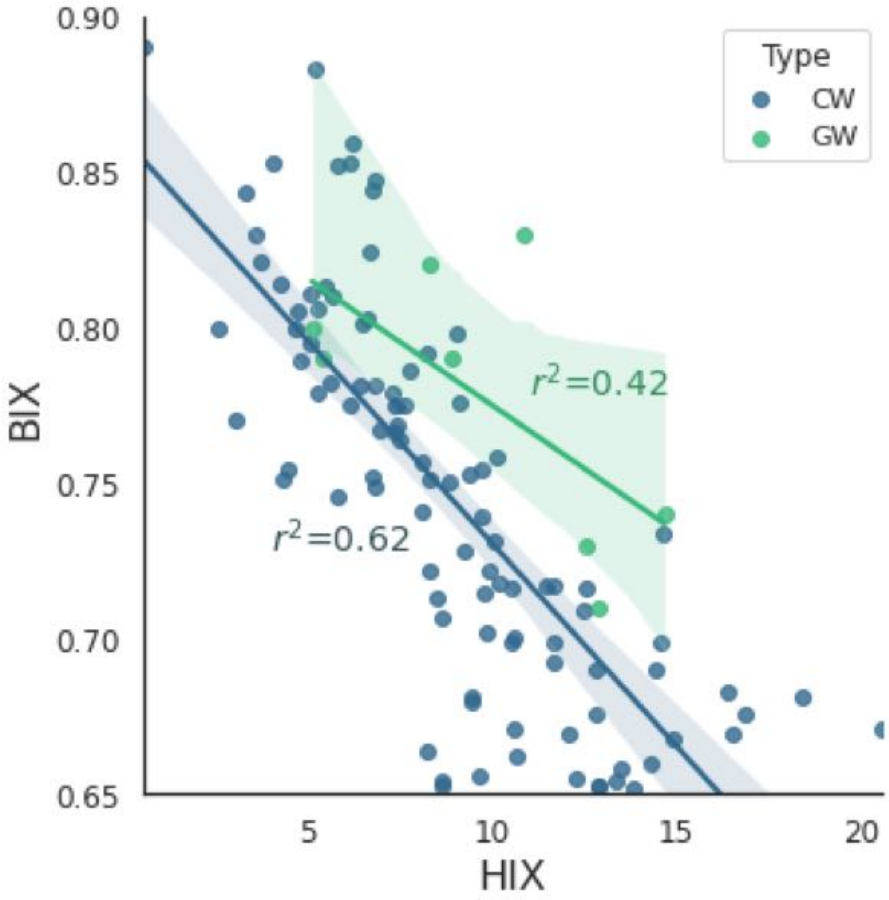

Figure 2.9: Relationship between HIX and BIX of DOM corresponding to canal water (CW) and groundwater (GW) samples. Shaded areas represent a 0.95 confidence interval.

[!ht]

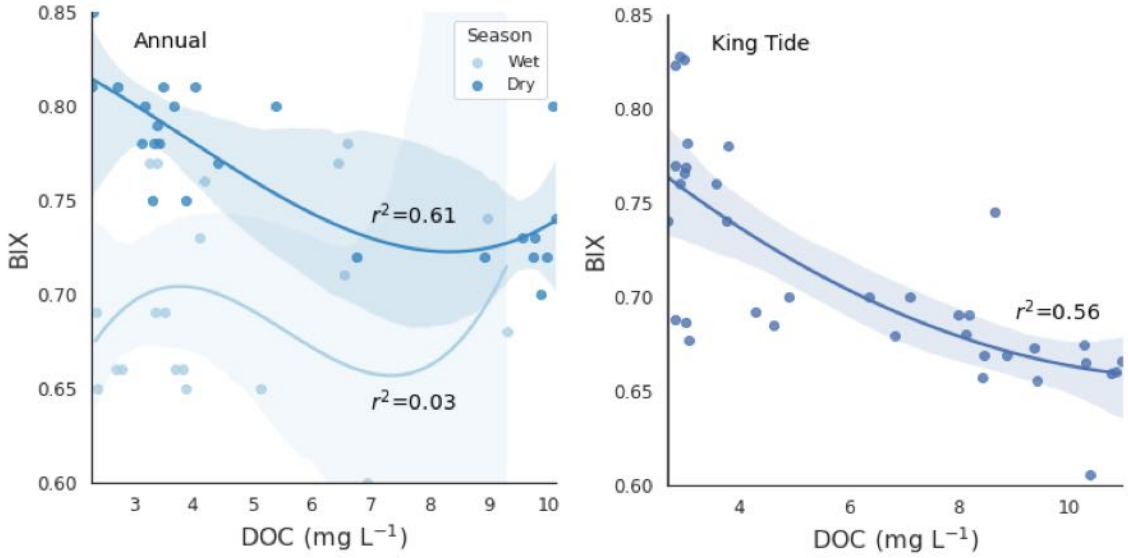

Figure 2.10: Relationships between DOC concentration and BIX during (a) wet and dry seasons I 2018-2019 and (b) three consecutive King Tide events in October 2018. The shaded area represents a 0.95 confidence interval.

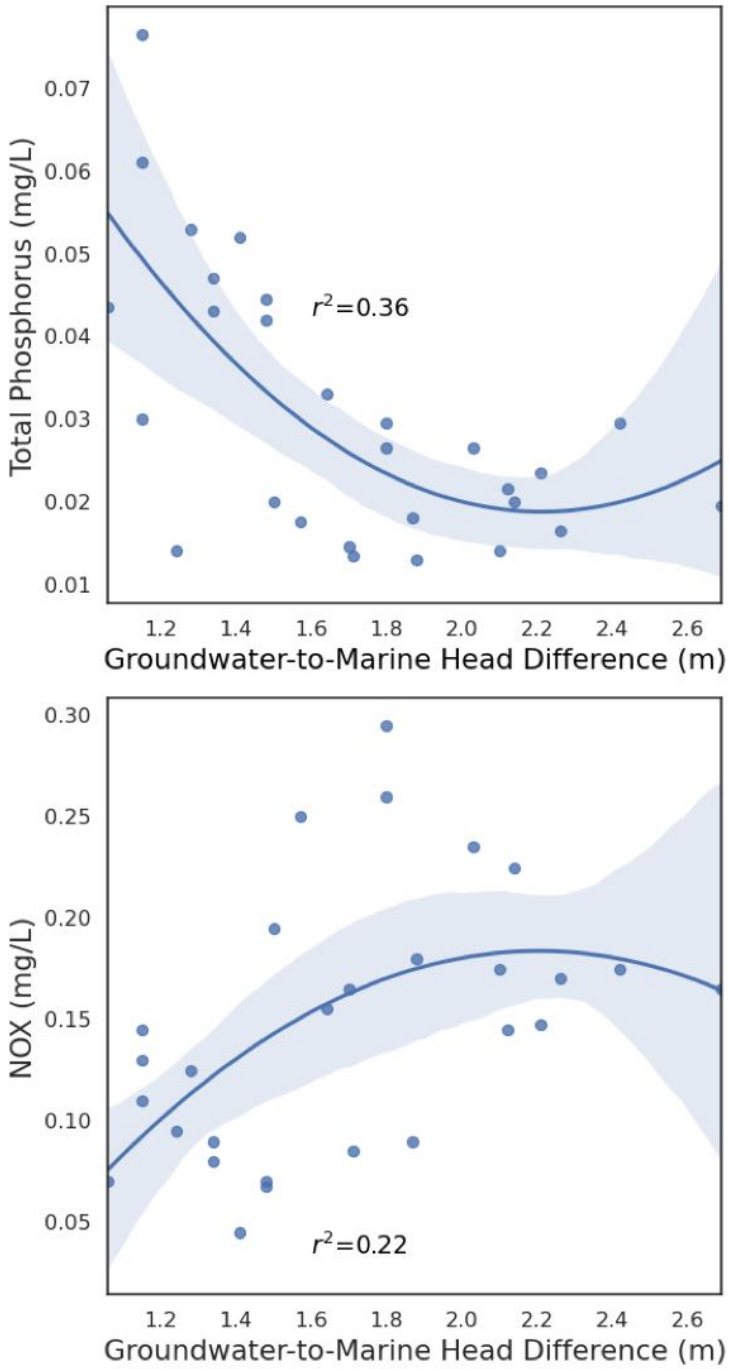

Figure 2.11: Relationship between the groundwater-to-marine head difference (m) and surface water nutrients in Biscayne Bay including (a) TP and (b) NOX. Significant R2 values are shown (P ¡ 0.05). Shaded regions represent 95% confidence intervals.

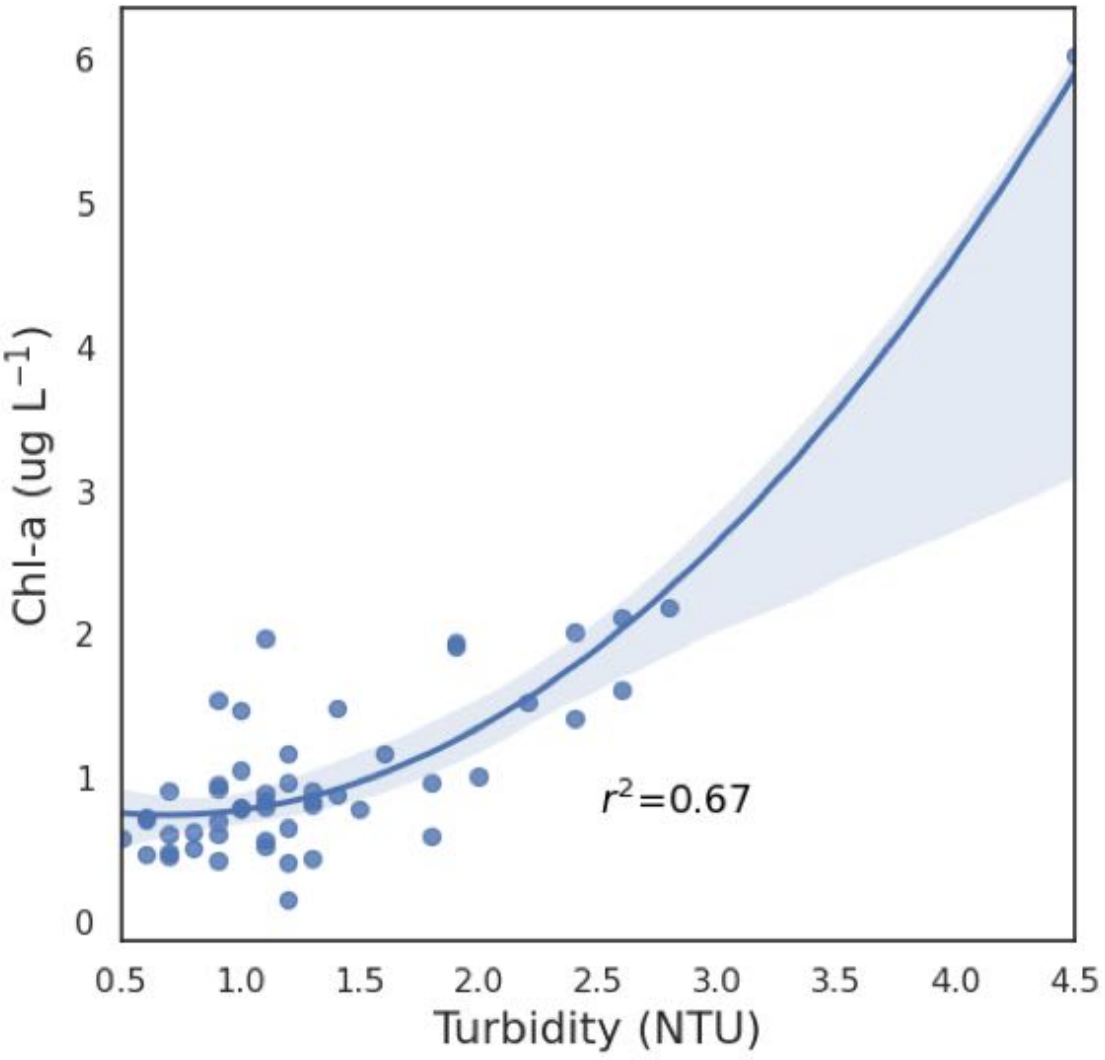

Figure 2.12: Relationship between turbidity and chlorophyll-a concentrations across three marine water sites in Biscayne Bay.

Table 2.3: List of USGS, SFWMD, NOAA, and Miami-Dade County DERM hydrologic variable collection sites for rainfall, groundwater, canal stage/flow, and marine water.

Site ID	Agency	Parameter	Latitude	Longitude
S27_R	SFWMD	Rainfall	25.851043	-80.188417
G93_R	SFWMD	Rainfall	25.738558	-80.286984
S26_R	SFWMD	Rainfall	25.807467	-80.260492
F-179	USGS (254444080144801)	Groundwater	25.745647	-80.246400
F-319	USGS (254217080171801)	Groundwater	25.704722	-80.288333
G-3959	USGS (254922080142701)	Groundwater	25.822917	-80.24-972
S27	SFWMD	Stage, Flow	25.851043	-80.188417
G93	SFWMD	Stage, Flow	25.738558	-80.286984
WC02*	-	Stage, Flow	25.784020	-80.210152
BB11	DERM	WQ		
BB22	DERM	WQ		
BB31	DERM	WQ		

**not a USGS gauge*

Table 2.4: DOM Fluorescence indices analyzed in this study, indicating the calculation and interpretation according to referenced literature.

Index	Calculation	Interpretation
$SUVA_{254}$	The normalization of UV absorbance at 254 nm by DOC concentration.	It indicates the DOM aromaticity (Weishaar et al., 2003).
E_2:E_3	The ratio of absorbances at 250 nm and 365 nm.	High values suggest a low average molecular size of DOM. (De Haan and De Boer, 1987).
S_R	The ratio of the log transformed absorbance spectra slope at 275–295 nm to that estimated in the range of 350–400 nm (Helms et al., 2008).	High values indicate a high proportion of the DOM molecular fraction with low molecular weight.
HIX	The sum of the fluorescence intensities between 300 and 345 nm divided by the sum of the intensities between 300 and 345 nm and between 435 and 480 nm, for an excitation wavelength of 254 nm (Ohno, 2002).	Higher values indicate a greater degree of DOM humification. (Zsolnay et al., 1999).
BIX	The ratio of the fluorescence intensity emitted at 380 nm, corresponding to the maximum of intensity of the β fluorophore, and that emitted at 430 nm, which corresponds to the maximum of the humic fraction at an excitation of 310 nm (Huguet et al., 2009).	The β fluorophore is typical of autochthonous recent DOM release (Parlanti et al., 2000). Therefore, high BIX values (> 1) suggest the presence of autochthonous and fresh DOM, whereas BIX values of 0.6–0.7 indicate a low or nil DOM autochthonous production.
FI	The ratio of emission intensities at 470 nm and 520 nm emitted at an excitation of 370 nm (Cory and McKnight, 2005).	It provides information about DOM sources; high values (≈ 1.8) suggest the prevalence of autochthonous DOM, and low values (≈ 1.3) suggest the prevalence of allochthonous DOM. (McKnight et al., 2001).

CHAPTER 3

Stormwater runoff and tidal flooding transform dissolved organic matter composition and increase bioavailability in urban coastal ecosystems

Matthew A. Smith[1], J.S. Kominoski[1], E.E. Gaiser[1], René M. Price[2], T.G. Troxler[2]

[1]Institute of Environment and Department of Biological Sciences, Florida International University, Miami, Florida 33199, USA

[2]Institute of Environment and Department of Earth Environment, Florida International University, Miami, Florida 33199, USA

3.1 Abstract

Coastal drainages contain multiple sources of dissolved organic matter (DOM) that influence OM transformation and fate along inland-to-marine gradients. Anthropogenic activities have altered DOM composition in urban drainages, thereby influencing in-stream breakdown rates, primary productivity, and downstream export. Yet, it is uncertain how hydrologic conditions (i.e., rainfall, tides, shallow groundwater) interact with different sources of DOM to regulate the transformation and export of DOM through urban coastal drainages. We characterized how seasonal changes in hydrologic conditions influence DOM composition and bioavailability in tidally-influenced drainages in Miami, FL, USA. We estimated the quality and bioavailability of DOM using compositional proxies based on fluorescence spectroscopy, including parallel factor analysis, and measured dissolved organic carbon (DOC) degradation during laboratory incubations containing a local bacterial community. Interactions between stormwater runoff and tidal amplitude increased the bioavailability of DOM and were positively correlated with predominantly humic-like components in the wet season and protein-like components in the dry season. Further, increases in tryptophan fluorescence intensity corresponded with elevated concentrations of Escherichia coli and enterococci – likely from waste-impacted groundwater – and contributed substantially to overall DOM bioavailability. Our results provide new evidence of an urban priming effect in which labile autochthonous DOM from anthropogenic sources facilitates microbial degradation of DOM that is driven by seasonal differences in stormwater runoff and tides. As hydrologic conditions in near-shore aquatic ecosystems shift with urbanization and climate-driven changes in sea level rise, increases in autochthonous sources of bioavailable DOM may impact ecosystem metabolism and affect the quality of DOM exported downstream.

3.2 Introduction

Dissolved organic matter (DOM) is a vital component of the aquatic carbon cycle and constitutes the majority of terrestrial organic carbon inputs from rivers to the ocean ((Hedges et al.; 1997; Battin et al.; 2008). Indeed, DOM controls a range of biogeochemical processes by regulating nutrient availability and microbial activities (Hullar et al.; 2006; Fellman et al.; 2008; Coble et al.; 2019). In coastal drainages, DOM originates from a range of allochthonous and autochthonous sources including terrestrial plants and soil, bacterial or algal production contributions, and exudates from marine phytoplankton (Sobczak et al.; 2002; Romera-Castillo et al.; n.d.; Asmala et al.; 2016). The role of DOM in biogeochemical cycling is a function of its composition (i.e., quality) and is driven by changes in land use (Wilson and Xenopoulos; 2009; Kaushal and Belt; 2012; Kominoski and Rosemond; 2012; Kelso and Baker; 2020) and hydrologic conditions, such as stormwater runoff and tidal mixing (Gardner et al.; 2005; Duan et al.; 2014; Hosen et al.; 2014). Despite the abundance of DOM in aquatic ecosystems, often only a small fraction is bioavailable (i.e., easily degradable; Parr et al. (2015)). Autochthonous DOM is widely considered to be higher quality (lower C:nutrient) and more bioavailable than allochthonous DOM potentially stimulating heterotrophic metabolism in aquatic ecosystems (McCallister and Giorgio; 2012; Epstein et al.; 2016). Changes in the relatively small pool of bioavailable DOM may significantly alter ecosystem functions (Findlay and Parr; 2017) and ultimately determine how much DOM is transported downstream, enters aquatic food webs, or is metabolized and released in gaseous forms (Søndergaard et al.; 2003). Quantifying how changes in land use and hydrologic conditions (e.g., water level, tidal amplitude) influence DOM composition and bioavailability is needed to

understand DOM processing and downstream export in urbanizing drainages (Parr et al.; 2015).

Urbanization alters aquatic DOM composition and processing rates by changing stormwater flow paths and surface-subsurface connectivity (Hosen et al.; 2014). Urban landscapes contain unique sources of DOM such as petroleum products (e.g., oil, gas), debris from ornamental vegetation, pet waste, and sewage from leaky septic or sewer systems (Walsh et al.; 2005; Hale et al.; 2016; Fork et al.; 2018). Enhanced hydrologic connectivity among streets, storm sewer drains, and subsurface pipe networks results in high infrastructure drainage densities (i.e., stream or pipe length per unit watershed area) in urban watersheds (Baruch et al.; 2018; Kelso and Baker; 2020). In turn, runoff from highly urbanized landscapes increases loading of terrestrial allochthonous organic matter and nutrients (nitrogen, N; phosphorus, P) which may also increase autochthonous DOM production and stimulate microbial activity. Non-point source inputs of DOM mobilized by stormwater runoff are much less constrained to a particular chemical composition yet are often differentiated from distinct terrestrial and marine endmembers

Recent findings suggest that urbanization can increase autochthonous production and bioavailability of DOM inputs to streams particularly during warm and/or wet months when runoff is increased (Asmala et al.; 2013; Fork et al.; 2020; Kelso and Baker; 2020). However, in some coastal drainages, diurnal and seasonal tides can interact with runoff, which may influence the timing, quality, and bioavailability of DOM. Changes in DOM composition and relative source in coastal urban drainages are uncertain but can be better understood using compositional proxies including those based on fluorescence spectroscopy, such as the humification index (HIX) and autochthonous index (BIX) (Yang et al.; 2015). By decomposing the complex mixture of fluorescence signatures into discrete compositional features, we can begin

to understand the source and biogeochemical function of DOM in coastal urban ecosystems.

In low-lying coastal urban drainages, tidal influence on shallow groundwater is a potentially important but overlooked source of DOM (Zhou et al.; 2019). Shallow groundwater often consists of lower density fresh water residing above higher density, saline water (Rochelle-Newall et al.; 2014). The water table in unconfined aquifers is dynamically connected to mean sea level, fluctuates with diurnal and lunar (perigean) spring tides, and tidal amplitudes decrease exponentially with distance from the coast (Rotzoll and Fletcher; 2013; Sukop et al.; 2018). As sea levels rise, the boundary between fresh and saline groundwater moves inland and elevates the water table, leading to land surface inundation during high tide events in low-lying areas (Abarca et al.; 2013; Befus et al.; 2020). Anthropogenic sources accumulate in shallow aquifers in urban drainage basins, relative to stormwater runoff that is discharged during seasonal storm events (McKenzie et al.; 2021). Previous studies in urban drainages have noted increased bioavailability of anthropogenic DOM and microbial processing rates in wastewater-impacted streams or shallow groundwater (Kalscheur et al.; 2012; Meng et al.; 2013; Parr et al.; 2015). High perigean spring tides and episodic storm events that come onshore can force marine water to intrude further into the aquifer, causing the water table and labile DOM to interact with surface water in coastal urban drainages (McKenzie et al.; 2021). Therefore, understanding the combined influence of seasonal stormwater runoff, groundwater infiltration, and marine forcings (i.e., sea level rise, tidal flooding) on the concentration and composition of DOM in coastal aquatic ecosystems is critical to define ecosystem function and predict ecosystem responses to shifting environmental conditions (Medeiros et al.; 2017).

Our goal was to quantify changes in DOM concentration, composition, and bioavailability driven by seasonal stormwater runoff and daily or seasonal tidal flooding in coastal urban drainages. We characterized DOM composition and bioavailability in three urban canal basins draining into a near-shore estuarine environment strongly influenced by the ocean. Specifically, we asked: (1) how do seasonal changes in stormwater runoff and tidal amplitude influence DOM composition and bioavailability in coastal urban drainages, and (2) how do increases in anthropogenic sources influence DOM bioavailability and autochthonous production? We hypothesized that DOM from terrestrial sources in stormwater runoff would be more aromatic and less readily used by microbial communities compared to DOM from marine, fresh groundwater, or anthropogenic sources. We also hypothesized that the frequency and timing of seasonal runoff would have a stronger influence on DOM bioavailability and stimulate DOM processing via increased microbial activities as compared to daily or seasonal tidal influences alone. Finally, we hypothesized that increases in protein-like DOM from anthropogenic sources in shallow groundwater would increase overall DOM bioavailability and rates of autochthonous production with increasing tidal amplitude. As hydrologic conditions are anticipated to shift in response to climate change and coastal watershed urbanization, understanding the complex linkages of urban DOM and hydrology is critical to predict how carbon processing and aquatic ecosystem function will respond to rising sea levels and saltwater intrusion.

3.3 Methods

3.3.1 Study Design and Hydrology

Study Design and Hydrology We conducted our analysis in three coastal drainage basins of Miami, FL (USA). Each drainage basin contained a canal that discharges into Biscayne Bay. We collected water samples at four locations along inland-to-coastal gradients of three canals (Wagner Creek, WC; Coral Gables, CG; Little River, LR; n = 12; Fig. 3.1). The three drainages represent a range of imperviousness (33-50%), land use, total drainage area, and drainage density among surface and subsurface stormwater infrastructure (Table 1). Canal stage (meters; NGVD29) was monitored continuously at 15-minute intervals for the duration of the study period (June 1, 2018 – May 31, 2019) and was collected from South Florida Water Management District (SFWMD) water control structures in each drainage basin (Fig. 3.1; Table S1; SFWMD, 2008). Daily cumulative precipitation (mm) was also recorded at a local rain gage in each basin (n = 3; Fig. 3.1).

3.3.2 Land-Use/Land Cover Analysis

Land-Use/Land Cover Analysis Drainage basins were delineated based on the piped stormwater drainage network identified by the South Florida Water Management District (SFWMD, 2008). Total imperviousness, canopy cover, and land use data were calculated using the 2016 National Land Cover Dataset (Dewitz, 2016). Land use categories included (1) road/parking density, (2) residential, (3) commercial, (4) industrial, and (5) vacant land (Table 1). Stormwater sub-basins were further characterized by drainage density (calculated by total length of stormwater pipes divided by total drainage area), number of storm drains, and number of outfall

locations (Table 1). We calculated a septic:stormwater ratio as the number of septic systems within a drainage basin divided by the total number of stormwater outfall locations to indicate the drainage-specific differences in hydrologic inputs from septic release versus stormwater runoff to each canal. Septic system data were obtained from the Miami-Dade County Open Data Hub (MDC, 2017). All geospatial analyses were conducted using ArcGIS 10.8.

3.3.3 Water Chemistry Analysis

Surface water grab samples were collected quarterly from twelve canal locations at baseflow during low and high tide in a diurnal cycle in the subtropical (1) wet season (August, October 2018) and (2) dry season (February, April 2019) (Fig. 3.2; n = 144). High tide flooding in the wet season was captured during a high perigean spring tide, otherwise known as "King tide," on October 27, 2018. For the purposes of this study, we collected samples during periods no less than 24 h after a rain event to remove the direct influence of rainfall-driven effects on streamflow and first-flush water quality. Surface grab water samples were collected within 3 h of each other on sampling days. In addition, two groundwater wells were sampled for baseline groundwater quality on four occasions (n = 8; Table S1). Both wells were pre-existing and installed by the United States Geological Survey (USGS). One well was completed to a depth of 6 m (USGS F-319, Table S1) to sample shallow groundwater and one well was completed to a depth of 23.5 m (USGS F-179, Table S1). Prior to sampling, the groundwater wells were purged of at least three standing well volumes. All samples were filtered in the field using Whatman 0.7-µm glass fiber filter (GF/F) that were pre-combusted at 500^{o}C and collected in acid-washed, amber HDPE bottles. Samples were transported to the laboratory on ice and stored at 4°C

and analyzed within seven days of collection. Samples were analyzed for dissolved organic carbon (DOC) on a Shimadzu TOC-V total organic carbon analyzer after acidification and purging to remove inorganic C. At each sampling location, we also measured water physicochemical parameters [temperature, dissolved oxygen (DO), conductivity, and pH with a YSI multiparameter handheld sonde (YSI Company, Yellow Springs, OH, USA).

Other water chemistry parameters, including total phosphorus (TP; mg L-1), total Kjeldahl nitrogen (TKN; mg L-1), nitrate + nitrite-nitrogen (NOx-N; mg L-1), Escherichia coli (E. coli; MPN 100 mL-1) and enterococci (MPN 100 mL-1) concentrations were collected and analyzed by the Miami-Dade County Department of Environmental Resources Management (DERM; Lietz, 1999) at the most upstream and downstream sites of this study. Water quality analyses were analyzed at DERM using EPA methods 365.1, 353.2, 351.4, 1603, and 1600 for TP, TKN, NOx, E. coli, and enterococci respectively (U.S. EPA, 2018). Heterotrophic bacterial abundance (BA; 106 cells mL-1) and bacterial productivity (BP, µg C L h-1) were measured at each collection period at the most upstream and downstream locations in each canal to relate ambient bacterial activities with changes in DOM bioavailability (n = 24). Total bacteria counts were measured using DAPI (4',6-diamndino-2-phenylindole; fluorescent stain) epifluorescence (Porter Feig, 1980). Bacterial production was estimated from rates of biosynthesis using the tracer 3H-thymidine (Findlay, 1993). Unfiltered samples were collected and processed within 24 h of collection, incubated for 1 h with tracer addition, and measured for unincorporated label (Kemp et al.; 1993).

3.3.4 DOM Bioavailability Assays

To quantify DOM bioavailability, bioavailable dissolved organic carbon (BDOC) degradation assays were conducted following standard methods (Servais et al.; 1989; Fellman et al.; 2008) in August 2018, October 2018, February 2019, and April 2019. In this study, we refer to BDOC as the proportion of total DOC that is utilized by heterotrophic bacteria through one of two processes: (1) mineralization of C for energy or (2) incorporation of C into bacterial biomass (Fellman et al.; 2008). Net loss of DOC through bacterial production and respiration was measured over 28-day chamber incubations (Eckard et al.; 2017). Triplicate 500-mL water samples were collected and filtered using 0.22-µm sterilized filters (Millipore Corporation, Burlington, Massachusetts) within 24 h of field collection. A small aliquot of unfiltered canal water was collected from each sample location for use as a microbial inoculum. In this study, the local microbial community was comprised of both bacterial and algal microbes. A total of 450 mL of filter-sterilized canal water and 22 mL of microbial inoculum (5% total volume) were combined and gently mixed in 500-mL amber polypropylene bottles. Samples were loosely capped to allow airflow and stored in the dark at 20°C for the duration of the experiment. Samples were regularly agitated every 3 d to prevent anoxia. Subsamples were taken at 0, 1, 3, 7, 14, and 28 d to measure the time-specific percent BDOC and change in DOM properties. Net loss of bulk DOC was measured at each time step by from depletion of total DOC concentration over time. For the purposes of this study, incubations were conducted without amending nutrient concentrations of nitrogen (N) or phosphorus (P) to prevent nutrient limitation (McDowell et al.; 2006). Molar N:P ratios were compared to the Redfield ratio of 16:1 to assess either N or P limitation. Triplicate control samples were included in the experiment using Ultrapure water and dosed with the same microbial inoculum from each site.

To measure biofilm biomass over the incubation period, a quarter section of a pre-combusted Whatman 0.7-µm glass fiber filter (GF/F) was added to each bottle. After 28 d, filters were dried (60^{o}C), weighed for dry mass (DM), and then combusted (500^{o}C for 8 h) to provide the ash-free dry mass (AFDM). For each sample, the ratio between AFDM and DM was quantified to indicate the relative proportion of organic content in the total biofilm (Paule et al.; 2009).

3.3.5 Fluorescence spectroscopy of DOM

DOM fluorescence spectroscopy was conducted on all samples to determine relative abundance and chemical composition. Fluorescence excitation-emission matrices (EEMs) were collected with a Horiba Aqualog (Jobin Yvon Horiba, France). EEMs were measured from samples at room temperature (approximately 21^{o}C) every 3 nm over excitation wavelength intervals between 240 and 455 nm, and an emission wavelength range of ex + 10 nm to ex + 250 nm in a 1 cm quartz cuvette. EEMs were corrected for instruments optics, Raman normalized, and blank subtracted using MATLAB R2019a (Mathworks, Natick, MA). Three fluorescence indices were calculated including the fluorescence index (FI) indicating proportion of microbial DOM sources, biological index (BIX) indicating proportion of recently produced DOM, and humification index (HIX) indicating proportion of terrestrial derived DOM (Jaffé et al.; 2008). Specific ultraviolet absorbance at a wavelength of 254 nm (SUVA254), which is the ratio of UV absorbance at a 254 nm wavelength divided by the DOC concentration, has been used to estimate the aromaticity of DOM (Weishaar et al.; 2003) and the type of environmental degradation (Hansen et al., 2016). Higher SUVA254 values (3-5) are considered an indicator of more aromatic ring structures. The spectral slope ratio (S_R) was calculated by dividing

the natural log of the slope of absorbance spectra between two primary wavelength ranges ($S_{275-295}$, $S_{350-400}$). S_R values are a qualitative indicator of molecular weight, with larger values indicating lower molecular weight (Helms et al.; n.d.).

3.3.6 Statistical Analyses

Processing of absorbance and fluorescence data and parallel-factor analysis (PARAFAC) modeling were carried out using the DrEEM 3.0 toolbox in MATLAB R2019a (Murphy et al.; 2013). First, we normalized EEMs by total sample fluorescence, and then we fit a PARAFAC model to n = 150 EEMs as described by Stedmon and Markager (2005). We validated the model using split-half validation (Fig. S5), random initialization tests, and visual examination of the residuals. To compare across components, we compared the intensity (Fmax) of each component normalized by total fluorescence in each sample. Pearson's bivariate correlation (r) and linear regression analysis (R2) were used to calculate significant relationships between environmental/landscape variables, DOM optical properties, and water quality parameters using Bonferroni corrections to account for multiple pairwise comparisons. One- and two-way repeated measures analysis of variance (ANOVA) were used to test significant (= 0.05) main and interactive effects of season and tide on DOM fluorescence and bioavailability, followed by Tukey's honest significant difference (HSD) post hoc tests. Principal component analysis (PCA) was used to reduce the dimensionality of the dataset and determine the primary sources of variability in water chemistry across seasons and tides. PCA was conducted using the scikit-learn package in Python (3.6). Relative abundance scores (% Fmax) were used for PARAFAC components in regression analyses. Prior to statistical analysis, an alpha level of 0.05 was set for all analyses and some data were

log-transformed to meet the assumptions of normality and homoscedasticity. We also performed an analysis of covariance (ANCOVA) to determine how PARAFAC components influence DOM bioavailability (% BDOC). The ANCOVA test included a linear model with % BDOC as a dependent variable and PARAFAC components indices as independent variables across season, tide, and canal location.

3.4 Results

3.4.1 Hydrology and Water Quality

Local hydrologic conditions and water chemistry varied considerably across sites, drainage basins, and seasons (Table S1). Daily average rainfall was between 2 and 5 times higher in the wet than dry season across all drainage basins (Fig. 3.2). Sub-hourly measurements of water level show distinct differences in tidal amplitude during diurnal tidal cycles and seasonal high tide events across drainage basins (Fig. 3.2, Table 2). The WC drainage had the greatest tidal amplitude whereas tidal amplitude in LR was relatively low. Average canal surface water temperatures were significantly different across seasons and basins with highest temperatures in WC between 28.9°C (dry season) and 29.1°C (wet season; Table 2). Salinity varied between 0 and 32 ppt along the three inland-coastal gradients and displayed distinct seasonal differences in average salinity within each drainage (Table S1). Turbidity was relatively low (<10 NTU) and did not display any trends across seasons or drainage basin. DOC concentrations (mg/L) ranged between 2.03 to 10.11 mg L-1. DOC was negatively correlated with imperviousness ($P < 0.05$), highest in upstream locations and was different between seasons and drainage basins (two-way ANOVA, $F(2,42)= 8.30$, $P < 0.001$; Table S2).

Concentrations of TP, NOx, and TKN in surface water were similar among sites and between seasons. Overall, N:P molar ratios ranged between 15 to 567 indicating slight to moderate P limitation at all sites. N:P molar ratios were elevated downstream compared to upstream locations, particularly in CG and WC basins, but mean N:P molar ratios did not differ between seasons or basins. However, molar ratios of N:P increased when moving downstream during the wet season and decreased when moving downstream during the dry season reflecting the influence of stormwater runoff on nutrient availability (Fig. S2). TP concentrations were highest in WC sites which corresponded with relatively low inorganic NOx and high TKN concentrations. N:P molar ratios ranged from 16 to 154 during the dry season and 20 to 567 during the wet season, indicating moderate to severe P limitation across all canal locations. E. coli concentrations were different between basins with values reaching 6,900 MPN 100 ml-1 in the wet season in WC at high tide (ANOVA, $F(2,42) = 5.04$, $P < 0.01$; Table 2,). Similarly, enterococci concentrations varied significantly between basins (two-way ANOVA, $F(2,13) = 5.73$, $P < 0.01$; Table 2). Heterotrophic bacterial abundance (BA) was different between basins (ANOVA, $F(2,33) = 5.30$, $P < 0.05$; Table 2) and highest values were observed in the CG basin. Mean bacterial productivity (BP) was significantly different between basins (ANOVA, $F(2,33) = 3.39$, $P < 0.05$) with highest values in the CG basin (3.14 µg C L h-1) but did not differ between seasons.

Relative to surface water, groundwater showed lower mean TP (0.12 mg L-1) and NOx (0.015 mg L-1) concentrations (Table 2). Molar ratios of N:P increased with depth and mean values ranged from 6.0 (F-319) to 38.0 (F-179). Deeper groundwater was enriched with DOC (10.50 mg L-1; F-179) compared to shallow groundwater (1.65 mg L-1; F-319). Salinity ranged between 0.25 and 19.2 ppt with highest values in deeper groundwater.

3.4.2 DOM Bioavailability Assays

During 28-d incubations, BDOC concentrations ranged between 0 to 22.83% of the total DOC with the highest concentrations in the wet season at low tide (Fig. 3.3). Overall, % BDOC increased with septic:stormwater ratio across all drainage basins and varied between seasons and tides (Fig. 3.3, Fig. S4). There was no relationship between BDOC and initial DOC concentrations. BDOC was greatest in CG during the wet season and during the dry season in LR. BDOC was greatest during low tide in CG and LR drainage basins while BDOC in the WC basin was mixed. Results of a two-way ANOVA shows an interaction between % BDOC and season*tide (two-way ANOVA, $F(1,44) = 3.58$, $P < 0.05$), but no influence of season or tide alone (Fig. 3.3; Table 3). Biofilm biomass, measured by AFDM, varied between seasons ($P = 0.05$) and drainage basins ($P = 0.03$). AFDM was very low in LR, particularly during the dry season, (0.16-1.09 g.m-2) compared to other sites (Table 2). Ratios of BA and BP with % BDOC increase when moving upstream in CG and LR canals while a decreasing trend is observed in the smaller tributary of WC (Fig. 3.3). Highest BDOC:BA and BDOC:BP ratios were observed in downstream section of CG (CGCP).

3.4.3 DOM Fluorescence Indices

HIX values ranged from 2.73 in the dry season at high tide and 29.93 in wet season at high tide, with a mean value of 10.45 (Table 2). SUVA254 ranged between 1.05 and 12.92 L mg-1 m-1, suggesting that canal DOM was a mixture of aromatic (humic) substances and more protein-like DOM. We observed an increase in SUVA254 during the wet season (4.67 L mg-1 m-1) compared to the dry season (1.26 L mg-1 m-1; Table 2). HIX values increased with SUVA254 and AFDM but not with DOC

concentration, suggesting a mixture of terrestrial and marine carbon in the DOC pool. FI ranged between 1.45 and 1.67 and reflect a mixture of terrestrial derived, lignin rich DOM with marine derived protein-like DOM. FI values increased during high tide and decreased during low tide but did not differ between wet and dry season. Generally, upstream sites had higher FI values compared to downstream sites but decreased with imperviousness, suggesting an autochthonous source of DOM. Fresh groundwater was characterized by high BIX (0.71-0.83) and FI (1.61-1.83) values compared to mixed canal samples (0.58 – 0.81, 1.45 – 1.67; Table 2). HIX values in groundwater were low ranging from 0.8 – 1.3 compared to surface water (2.6 – 18.2). Similarly, SUVA254 in groundwater was generally low with a mean value of 0.37 L mg-1 m-1 (Table 2). The minimum value of S_R was 0.92 in surface canal water samples while the maximum S_R of 2.21 was found in in groundwater. Mean S_R in both surface and groundwater samples were comparable to S_R from riverine samples in other studies (Helms et al.; n.d.) and did not differ between basins or seasons. $S_{275-295}$ values ranged between 0.0124 nm-1 and 0.0209 nm-1 and did not differ between basins or seasons.

3.4.4 EEM-PARAFAC Components

Three humic-like and two-protein-like components were identified in the EEM-PARAFAC model (Table 4; Fig. 3.4). Humic-like component 1 (C1; Ex: 333 nm /Em: 440 nm) reflects humic acids derived from processing of DOM by terrestrial or aquatic microbes (Yamashita et al.; 2013; Hosen et al.; 2014). Humic-like component 2 (C2) has peaks at Ex: <250, 303 nm/Em: 380 nm and is a humic-like component that is ubiquitous in marine environments with biological activity (Yamashita et al.; n.d.; Fellman et al.; 2010). Humic-like component 3 (C3) has a peak

at Ex: 267 nm/Em: 460-480 nm and a secondary peak at Ex: 381 nm/Em: 460-480 nm is related to organic humic substances or marine-like humic substances (Murphy et al.; 2011). C3 is related to autochthonous production and/or influence from anthropogenic sources (Meng et al.; 2013). Protein-like components C4 (Ex: 276 nm/Em: 335-345) and C5 (Ex: 270 nm/Em: 305) are indicative of the presence of tryptophan-like and tyrosine-like proteins, respectively (Elliott et al.; 2006; Hudson et al.; 2007; Nowicki et al.; 2019). C4 is common in waters subject to anthropogenic influence and areas of high primary productivity (Williams et al.; 2010). Tryptophan components (230-280/330-360 nm) like C4, generally contribute the highest intensity peaks in wastewaters, even in treated effluents, compared with background levels in natural surface and groundwaters (Reynolds and Ahmad; 1997; Fox et al.; 2017). C5 is protein-like and shares spectral properties with wastewater-impacted DOM and is often associated with high nutrient content and high autochthonous production (Murphy et al.; 2011; Fork et al.; 2020).

The proportional abundances of individual PARAFAC components were related to the septic:stormwater ratio in each urban drainage basin (Fig. S6). C1, C2 were positively correlated ($r = 0.33$, $P = 0.02$; $r = 0.30$, $P = 0.03$) and C4 was negatively correlated ($r = -0.38$, $P < 0.01$) with imperviousness while C5 showed no significant relationship (Fig. 3.4). Two-way ANCOVA results revealed C1, C2, and C4 differed across seasons and tides while C5 also differed across upstream and downstream locations (Table 5). Components associated with humic substances (i.e., C1, C2, C3) had a greater mean Fmax (1.86, 1.07, 0.70) than protein-like components (i.e., C4, C5; 0.25, 0.16) which implies that humics were important contributors to DOM pool in these urban waterways (Fig. S6). Humic-like components (C1, C3) and protein-like component (C4) were significantly different across wet and dry seasons as well as high and low tide (Fig. S7). Proportions of the humic component C2

were highest in fresh groundwater (25-29%) compared to surface water. Results of an ANCOVA test show that the relative proportion of humic component C1 and protein component C4 were significantly related to % BDOC across season, tide, and upstream-downstream location (Table 5). Trends between % BDOC and C5 were only significant between upstream and downstream locations. Component C4 was positively correlated with BIX and $S_{R]}$, indicating recent origin and low molecular weight (Fig. 3.5).

The composition of DOM varied between wet and dry seasons, less between tidal flooding events (Fig. 3.5). Variables corresponding to humic or refractory substances (HIX, SUVA254) were closely associated with principal component (PC) axis 1 and represent the majority of DOM in the wet season (Fig. 3.5). Variables that represent recently produced, proteinaceous DOM (BIX, FI, S_R) and PARAFAC component C4 were grouped on the opposite end of PC1 and characterized the majority of DOM in the dry season. PC2 was closely aligned with % BDOC and PARAFAC component C5 and corresponds with wet season DOM composition. Humic-like components C1, C2, and C3 grouped together with DOC concentration but with no clear trend between season or tide. Fresh groundwater unimpacted by wastewater grouped separately from mixed samples and was characterized by high BIX and FI values (Fig. 3.5). Tidal differences in DOM character were less clear, however, the majority of DOM collected at high tide corresponds with increases in humic-like, high molecular weight material.

We observed a positive correlation between tryptophan-like C4 and % BDOC in the wet season (R2 = 0.18, P $<$ 0.05) and a negative correlation in the dry season (R2 = 0.15, P ¡ 0.05; Fig. 3.6). No significant correlations between tyrosine-like C5 and % BDOC were observed. Fecal indicator bacteria showed positive trends with protein-like fluorescence, particularly in the wet season (Fig. 3.6). E.coli concentrations were

positively related with C5 during the wet season ($R2 = 0.20$, $P < 0.05$). Enterococci concentrations were positively correlated with C4 during wet ($R2 = 0.52$, $P < 0.001$) and dry seasons ($R2 = 0.26$, $P < 0.001$) and also with C5 during the wet season only ($R2 = 0.22$, $P < 0.05$). Elevated concentrations of protein-like fluorescence may indicate high quality DOM and nutrient composition but may also reflect breakdown products of lignin (Aiken, 2014). Overall, proteinaceous DOM signatures, including indicators of tryptophan-like (C4) and tyrosine-like (C5) fluorescence, can be related to sources of anthropogenic waste (Nowicki et al., 2019).

3.5 Discussion

Urbanization in coastal environments has led to ecosystems with distinct biogeochemical characteristics (Kaye et al.; 2006; Parr et al.; 2015). We provide evidence of distinct seasonal shifts in urban DOM sources, composition, and bioavailability driven by seasonal runoff and tidal flooding. Our data show that DOM contributions from urban runoff, marine water, and fresh groundwater are thoroughly mixed during the wet season, whereas individual sources of DOM are distinct during the dry season (Fig. 3.5). Our results agree with previous studies in urban ecosystems that found DOM bioavailability increases with anthropogenically-sourced, autochthonous DOM during the wet season when stormwater runoff is increased (Hosen et al.; 2014; Parr et al.; 2015). Additionally, we found that elevated indicators of autochthonous production increased the proportion of bioavailable DOM and were related to sources of anthropogenic waste signified by tryptophan-like fluorescence (Osburn et al.; 2012; Kelso and Baker; 2020); Fig. 3.6). Interestingly, elevated heterotrophic bacterial abundance and activities during the wet season, when the water table is high, led to shifts in microbial utilization of C from allochthonous sources to autochthonous

sources. Overall, the combined effects of seasonal runoff and tidal flooding suggest an urban priming effect where labile autochthonous DOM from anthropogenic sources facilitate microbial degradation of humic DOM in coastal waters (Guenet et al.; 2010; Bianchi; 2011; Fork et al.; 2020).

3.5.1 Role of Hydrology on DOM Composition

Seasonal variation in hydrologic conditions drives shifts in DOC concentration and DOM composition. Our results highlight changes in the timing and distribution of fresh and marine water driven by seasonal runoff and tidal amplitude (Fig. 3.2). Interactive effects of seasonal runoff (e.g., overland flow, stormwater conveyance) and drainage-level landscape characteristics (e.g., imperviousness, drainage density) determine the concentration and biodegradation of DOC in urban drainages. In turn, the timing and magnitude of stormwater runoff ultimately determine the proportion of labile and recalcitrant humic substances in receiving water bodies, as seen in previous studies (Hosen et al.; 2014; Dalmagro et al.; 2017; Fork et al.; 2020). We found that optical measures of aromaticity and humic-like components (HIX, SUVA254, C1-3) were strongly correlated with bioavailability in the wet season and indices of marine-derived, recently produced, proteinaceous DOM (BIX, C4, C5) were the determining factor of bioavailability in the dry season. Similar to previous studies, we observed a notable shift in DOM composition away from humic-like components to more fulvic-acid and protein-like DOM suggesting that more readily used forms of protein-like DOM are processed more quickly (Hosen et al.; 2014; Williams et al.; 2016). Elevated concentrations of protein-like fluorescence may indicate high quality DOM and nutrient composition but may also reflect breakdown products of lignin or residual effects of photodegradation (Helms et al.;

2013; Aiken; 2014). The coupled influence of seasonal runoff and tidal amplitude dictate the extent of shallow groundwater inputs to surface waterways, thereby driving increases in anthropogenically-sourced DOM. Together, these results suggest an urban priming effect in which labile autochthonous DOM from anthropogenic sources facilitates microbial degradation of DOM that is driven by seasonal differences in stormwater runoff and tides (Bianchi; 2011). We may also have observed a compensatory mechanism where increased autochthonous production balances loss of allochthonous DOM inputs during the dry season resulting in relatively consistent BDOC concentrations and high-quality DOM across the year (Parr et al.; 2015). Overall, seasonal canal stage and increasing tidal amplitude shift the composition of the DOM pool to reflect increasing anthropogenic, protein-like DOM signatures in the water column.

The composition of DOM in coastal urban waters is influenced by runoff and tidal flooding. Our results partially support the second hypothesis that DOM composition and bioavailability is driven by seasonal stormwater runoff to a greater degree than tidal amplitude. Sources of DOM during low and high tide are diffuse but suggest multiple inputs of bioavailable DOM from (1) in-stream autochthonous production and/or (2) shallow groundwater inputs impacted by anthropogenic waste. The transition from flood (high) to ebb (low) tides shifts DOM sources from seawater with low DOC to fresh surface water or shallow groundwater with tryptophan-rich, bioavailable DOM as seen in other studies (Lønborg et al.; 2010; Zhou et al.; 2019). At low tide, large quantities of nutrients and DOM may be released to the water column from surficial sediments due to a hydraulic pressure gradient from tidal forcing (Wu et al.; 2018). This influx of carbon and nutrient availability can stimulate in-stream autochthonous production and lead to rapid processing of newly introduced DOM when tides turnover. At high tide, decreased freshwater pressure may

enhance saltwater intrusion and mobilize humic- or protein-like DOM from shallow soils into surface flow paths. Mobilization of shallow soil-borne DOM is supported by the observation that PARAFAC components C3 (low molecular weight; humic) and C4 (recently produced; protein-like) increased in with septic:stormwater and suggest that low tides enhance combined terrestrial and anthropogenic DOM signatures. Although the extent of surface-subsurface connectivity was not measured in this study, it can influence DOM composition (Chen et al.; 2010; Zhang et al.; 2020).

Variation in residence time along urban stream networks is an important factor in determining the rate and extent of DOM processing (Battin et al.; 2008). Urban water systems are characterized by flashy hydrology and short water residence time. However, pulsed inputs of stormwater to urban drainages result in the flushing of leaf litter, DOC, and anthropogenic waste into storm drains during the wet season contributing to a 'gutter subsidy' of organic matter to urban streams (Kaushal and Belt; 2012). This flushing effect introduces elevated nutrients and organic matter that may stimulate microbial activities and associated DOM processing rates when flows or tidal amplitude are low. This seasonal and/or event-driven flushing effect may also mobilize other anthropogenic carbon sources including particulates, polyaromatic cyclic hydrocarbons, oil, and grease to urban canals, which may further affect DOM bioavailability]Badin et al. (2008).

Relative location to upstream and downstream water sources drive variation in bioavailability of DOC along coastal urban drainages. One possible explanation for our observed differences in % BDOC is the increased heterotrophic processing and autotrophic production at downstream locations directly connected to the ocean. Biofilm biomass (AFDM), representing increased heterotrophic bacterial production, was positively correlated with % BDOC and was greatest in downstream loca-

tions where N:P molar ratios were low. However, we observed seasonal increases in nutrient availability during the wet season via stormwater runoff that temporarily alleviated nutrient limitation and increase dissolved oxygen (DO) at upstream sites, providing ideal conditions for in-stream production. These findings are supported by the observation that % BDOC increases with the proportion of protein-like fluorescence (Fig. 3.6).

3.5.2 Urban Sources of Bioavailable DOM

Our data suggest that the DOM pool in this coastal urban system is dominated by humic-like DOM that is periodically supplied by proteinaceous DOM when autochthonous production is increased. Typically, urban DOM is represented by lower molecular weight and aromaticity compared to DOM found in non-urban stream ecosystems (Asmala et al.; 2013; Parr et al.; 2015). Of particular interest is the observation that protein-like component C4 correlated with % BDOC across seasons, tides, and upstream-downstream location (Table 5). C4, a tryptophan-like fluorescence related to autochthonous production and wastewater impacted streams, displayed strong positive relationships with BIX and S_R highlighting its recent production and simple, low molecular weight composition. Similarly, increasing proportions of C4 relative to humic-like fluorescence are significantly correlated to DOM bioavailability (Fig. 3.6). Protein-like fluorescence (C4, C5) was positively correlated with log-transformed E. coli concentrations in the wet season with highest bacterial loads at high tide (Fig. 3.6). These findings support the notion that tryptophan-like fluorescence intensity may be used as a proxy for degraded water quality determination in wastewater impacted streams (Baker and Inverarity; 2004; Gu et al.; 2020; Mendoza et al.; 2020; Sorensen et al.; 2020). We found that likely diffuse sources of

anthropogenic waste (e.g., septic release, pet waste), indicated by increased bacterial loads, including E. coli, and associated DOM composition, may result in increased microbial utilization of DOM and processing rates in the water column.

Point sources of anthropogenic DOM in urban canals are attributed to wastewater effluent from leaky wastewater systems (Kalscheur et al.; 2012). Large numbers of septic systems (n = 4101) in the CG drainage basin are likely contributing high quality (low C:N), labile DOM to shallow groundwaters following significant runoff or tidal events. These contributions may explain some of the elevated bacterial abundance/productivity, E. coli concentrations, and rates of biodegradation in CG sites (Table 2). Our findings support the third hypothesis that labile DOM from wastewater impacted subsurface flow (and septic effluent) contributes bioavailable DOM to surface flows and, when coupled with elevated nutrients and bacterial productivity, leads to rapid biodegradation of DOC. In drainage basins with greater imperviousness and hydrologic connectivity via stormwater outfalls (WC, LR), other petroleum-based hydrocarbons may also contribute small, labile fractions of DOM from urbanized landscapes, similar to contributions seen with C3.

3.5.3 Ecosystem Implications for Urban DOM Processing

Urbanization has the potential to modulate microbial processing rates in urban aquatic ecosystems by altering the biotic (e.g., microbial community composition) and abiotic (e.g., light exposure) conditions along the urban drainage continuum (Walsh et al.; 2005; Parr et al.; 2015). Previous studies have demonstrated that engineered headwaters may act both as locations of significant DOM processing and as sources of fresh DOM when surface-subsurface connectivity is increased during stormwater runoff events (Fork et al.; 2020). In turn, DOM found in surface

canal water reflect multiple simultaneous processes, including algal and microbial production and consumption, input of fresh allochthonous DOM, and photodegradation (Hosen et al.; 2021). In urban headwaters, the role of photodegradation in DOM processing is limited since flow and in-channel storage occurs underground (Cory et al.; 2018). As DOM moves downstream to surface channels, the role of photodegradation in DOM processing becomes increasingly important as algal resources supplement the microbial DOM pool (Cory et al.; 2018). Optical indices, including $S_{275-295}$ and S_R, have been used to deconvolute the relative proportions of photobleached versus fresh microbial DOM in ocean waters (Helms et al.; 2013). We observed a significant increase in mean SUVA254 during the wet season while mean S_R did not change, suggesting seasonal shifts in aromaticity but no notable changes in molecular size of DOM. Given that our experiment excluded irradiation of DOM, our results largely reflect the continual microbial recycling of existing DOM, which decreased in bioavailability over time with flocculation processes. Overall, the urban DOM pool appears to shift away from humic-like DOM from terrestrial, allochthonous sources to protein-like DOM from autochthonous, in-stream production in urban drainages (Parr et al.; 2015; Williams et al.; 2016; Hosen et al.; 2018).

Seasonal differences in hydrology interact with urban infrastructure to influence DOM sources and bioavailability. During warm, wet months, we found that the proportion of labile DOM increases due to more frequent contributions from terrigenous humic substances in stormwater runoff. Autochthonous DOM (indicated by greater values of BIX, C4, C5) may also facilitate microbial degradation of more humic DOM via a priming effect (Bianchi; 2011; Fork et al.; 2020). Increased microbial processing of urban DOM may result in a more aromatic and/or recalcitrant DOM pool when autochthonous production is low. However, increases in dissolved oxygen conditions in open channel urban waterways during stormwater runoff events can stimulate

rates of in-stream primary production (Gold et al.; 2020). Overall, seasonal runoff and tidal cycles appear to regulate the balance between humic and proteinaceous DOM inputs, but increases in urban DOM from more frequent or intense runoff and tidal events may lead to changes in ecosystem metabolism. Therefore, quantifying the timing and relative proportion of DOM inputs from stormwater runoff, marine, and shallow groundwater resources is critical to determine the extent of bacterial, nutrient, and metabolic controls on stream ecosystem function.

3.6 Conclusions

Our findings highlight a complex system of processes that control DOM source, transformation, and export in coastal urban ecosystems. The timing and magnitude of water inputs from stormwater runoff, marine water, and shallow groundwater determine the quantity and composition of DOM that is released from the landscape. Increases in labile, microbially sourced DOM from septic release and in-stream autochthonous production are introduced during peak stormwater runoff or tidal events when the underlying water table connects with surface flow paths. Despite smaller proportions of anthropogenically sourced, protein-like components compared to terrestrial matter, they constitute a significant portion of bioavailable DOM (Fig. S6). Specifically, increases in tryptophan-like fluorescence may indicate an increased capacity for in-stream production and lead to rapid microbial degradation of humic DOC, as well as the conversion of nutrients to more bioavailable forms in downstream locations.

As sea levels rise, saltwater intrusion will lead to more frequent and longer inundation of surface flow paths with groundwater. More frequent and spatially robust groundwater monitoring of organic matter composition is needed to evaluate the

short-term effects of tidal fluctuations on potentially harmful release from urban wastewater systems. Future work should attempt to collect high temporal resolution measurements of tryptophan-like fluorescence during seasonal rainfall and tidal events to understand the full extent of effect of urbanization and sea level rise on coastal riverine DOM processing. Understanding the spatiotemporal linkages among seasonal hydrology and DOM composition in coastal urban ecosystems will inform future assessments on the influence of DOM composition on microbial processing and food web interactions in coastal urban ecosystems.

3.7 Bibliography

Abarca, E., Karam, H., Hemond, H. F. and Harvey, C. F. (2013). Transient groundwater dynamics in a coastal aquifer: The effects of tides, the lunar cycle, and the beach profile, *Water Resources Research* **49**: 2473–2488.

Aiken, G. (2014). Fluorescence and dissolved organic matter: a chemist's perspective, *Aquatic organic matter fluorescence* **35**.

Asmala, E., Autio, R., Kaartokallio, H., Pitk¨anen, L., Stedmon, C. and Thomas, D. (2013). Bioavailability of riverine dissolved organic matter in three baltic sea estuaries and the effect of catchment land use, *Biogeosciences* **10**(11): 6969–6986.

Asmala, E., Kaartokallio, H., Carstensen, J. and Thomas, D. N. (2016). Variation in riverine inputs affect dissolved organic matter characteristics throughout the estuarine gradient, *Frontiers in Marine Science* **2**.

Badin, A. L., Faure, P., Bedell, J. P. and Delolme, C. (2008). Distribution of organic pollutants and natural organic matter in urban storm water sediments as a function of grain size, *Science of the Total Environment* **403**: 178–187.

Baker, A. and Inverarity, R. (2004). Protein-like fluorescence intensity as a possible tool for determining river water quality, *Hydrological Processes* **18**: 2927–2945.

Baruch, E. M., Voss, K. A., Blaszczak, J. R., Delesantro, J., Urban, D. L. and Bernhardt, E. S. (2018). Not all pavements lead to streams: Variation in impervious surface connectivity affects urban stream ecosystems, *Freshwater Science* **37**: 673–684.

Battin, T. J., Kaplan, L. A., Findlay, S., Hopkinson, C. S., Marti, E., Packman, A. I., Newbold, J. D. and Sabater, F. (2008). Biophysical controls on organic carbon fluxes in fluvial networks, *Nature geoscience* **1**(2): 95–100.

Befus, K. M., Barnard, P. L., Hoover, D. J., Hart, J. A. F. and Voss, C. I. (2020). Increasing threat of coastal groundwater hazards from sea-level rise in california, *Nature Climate Change* **10**: 946–952.

Bianchi, T. S. (2011). The role of terrestrially derived organic carbon in the coastal ocean: A changing paradigm and the priming effect, *Proceedings of the National Academy of Sciences of the United States of America* **108**: 19473–19481.

Chen, M., Price, R. M., Yamashita, Y. and Jaffé, R. (2010). Comparative study of dissolved organic matter from groundwater and surface water in the florida coastal everglades using multi-dimensional spectrofluorometry combined with multivariate statistics, *Applied Geochemistry* **25**: 872–880.

Coble, A. A., Koenig, L. E., Potter, J. D., Parham, L. M. and McDowell, W. H. (2019). Homogenization of dissolved organic matter within a river network occurs in the smallest headwaters, *Biogeochemistry* **143**: 85–104.

Cory, R. M., Kling, G. W., Stanley, E. and Giorgio, P. D. (2018). Special issue-current evidence interactions between sunlight and microorganisms influence dissolved organic matter degradation along the aquatic continuum, *Limnology and Oceanography Letters* **3**: 102–116.
URL: *https://arcticdata.io/catalog/view/doi:10.18739/*

Dalmagro, H. J., Johnson, M. S., de Musis, C. R., Lathuilli`ere, M. J., Graesser, J., Pinto-J´unior, O. B. and Couto, E. G. (2017). Spatial patterns of doc concentration and dom optical properties in a brazilian tropical river-wetland system, *Journal of Geophysical Research: Biogeosciences* **122**: 1883–1902.

Duan, S., Amon, R. M. and Brinkmeyer, R. L. (2014). Tracing sources of organic matter in adjacent urban streams having different degrees of channel modification, *Science of the Total Environment* **485-486**: 252–262.

Eckard, R. S., Pellerin, B. A., Bergamaschi, B. A., Bachand, P. A., Bachand, S. M., Spencer, R. G. and Hernes, P. J. (2017). Dissolved organic matter compositional change and biolability during two storm runoff events in a small agricultural watershed, *Journal of Geophysical Research: Biogeosciences* **122**: 2634–2650.

Elliott, S., Lead, J. R. and Baker, A. (2006). Characterisation of the fluorescence from freshwater, planktonic bacteria, *Water Research* **40**: 2075–2083.

Epstein, D. M., Kelso, J. E. and Baker, M. A. (2016). Beyond the urban stream syndrome: organic matter budget for diagnostics and restoration of an impaired urban river, *Urban Ecosystems* **19**: 1623–1643.

Fellman, J. B., D'Amore, D. V., Hood, E. and Boone, R. D. (2008). Fluorescence characteristics and biodegradability of dissolved organic matter in forest and wetland soils from coastal temperate watersheds in southeast alaska, *Biogeochemistry* **88**: 169–184.

Fellman, J. B., Hood, E. and Spencer, R. G. (2010). Fluorescence spectroscopy opens new windows into dissolved organic matter dynamics in freshwater ecosystems: A review, *Limnology and Oceanography* **55**: 2452–2462.

Findlay, S. E. and Parr, T. B. (2017). Dissolved organic matter, *Methods in Stream Ecology: Third Edition* **2**: 21–36.

Fork, M. L., Blaszczak, J. R., Delesantro, J. M. and Heffernan, J. B. (2018). Engineered headwaters can act as sources of dissolved organic matter and nitrogen to urban stream networks, *Limnology and Oceanography Letters* **3**: 215–224.

Fork, M. L., Osburn, C. L. and Heffernan, J. B. (2020). Bioavailability and compositional changes of dissolved organic matter in urban headwaters, *Aquatic Sciences* **82**(4): 1–15.

Fox, B. G., Thorn, R. M., Anesio, A. M. and Reynolds, D. M. (2017). The in situ bacterial production of fluorescent organic matter; an investigation at a species level, *Water Research* **125**: 350–359.

Gardner, G. B., Chen, R. F. and Berry, A. (2005). High-resolution measurements of chromophoric dissolved organic matter (cdom) in the neponset river estuary, boston harbor, ma, *Marine Chemistry* **96**: 137–154.

Gold, A. C., Thompson, S. P., Magel, C. L. and Piehler, M. F. (2020). Urbanization alters coastal plain stream carbon export and dissolved oxygen dynamics, *Science of The Total Environment* **747**: 141132.

Gu, N., Song, Q., Yang, X., Yu, X., Li, X. and Li, G. (2020). Fluorescence characteristics and biodegradability of dissolved organic matter (dom) leached from non-point sources in southeastern china, *Environmental Pollution* **258**: 113807.

Guenet, B., Danger, M., Abbadie, L., , Gé and Lacroix, R. (2010). Priming effect: bridging the gap between terrestrial and aquatic ecology, *CONCEPTS SYNTHESIS EMPHASIZING NEW IDEAS TO STIMULATE RESEARCH IN ECOLOGY Ecology* **91**: 2850–2861.

Hale, R. L., Scoggins, M., Smucker, N. J. and Suchy, A. (2016). Effects of climate on the expression of the urban stream syndrome, *Freshwater Science* **35**: 421–428.

Hedges, J. I., Keil, R. G. and Benner, R. (1997). What happens to terrestrial organic matter in the ocean?, *Organic geochemistry* **27**(5-6): 195–212.

Helms, J. R., Stubbins, A., Perdue, E. M., Green, N. W., Chen, H. and Mopper, K. (2013). Photochemical bleaching of oceanic dissolved organic matter and its effect on absorption spectral slope and fluorescence, *Marine Chemistry* **155**: 81–91.

Helms, J. R., Stubbins, A., Ritchie, J. D., Minor, E. C., Kieber, D. J. and Mopper, K. (n.d.). Helms, j.r., et al. absorption spectral slopes and slope ratios as indicators of molecular weight, source, and photobleaching of chromophoric dissolved organic matter. limnol. oceanogr., 53(3), 2008, 955–969.

Hosen, J. D., Aho, K. S., Fair, J. H., Kyzivat, E. D., Matt, S., Morrison, J., Stubbins, A., Weber, L. C., Yoon, B. and Raymond, P. A. (2021). Source switching maintains dissolved organic matter chemostasis across discharge levels in a large temperate river network, *Ecosystems* **24**: 227–247.

Hosen, J. D., Armstrong, A. W. and Palmer, M. A. (2018). Dissolved organic matter variations in coastal plain wetland watersheds: The integrated role of hydrological connectivity, land use, and seasonality, *Hydrological Processes* **32**: 1664–1681.

Hosen, J. D., McDonough, O. T., Febria, C. M. and Palmer, M. A. (2014). Dissolved organic matter quality and bioavailability changes across an urbanization gradient in headwater streams, *Environmental Science and Technology* **48**: 7817–7824.

Hudson, N., Baker, A. and Reynolds, D. (2007). Fluorescence analysis of dissolved organic matter in natural, waste and polluted waters - a review, *River Research and Applications* **23**: 631–649.

Hullar, M. A., Kaplan, L. A. and Stahl, D. A. (2006). Recurring seasonal dynamics of microbial communities in stream habitats, *Applied and Environmental Microbiology* **72**: 713–722.

Jaffé, R., McKnight, D., Maie, N., Cory, R., McDowell, W. and Campbell, J. (2008). Spatial and temporal variations in dom composition in ecosystems: The importance of long-term monitoring of optical properties, *Journal of Geophysical Research: Biogeosciences* **113**(G4).

Kalscheur, K. N., Penskar, R. R., Daley, A. D., Pechauer, S. M., Kelly, J. J., Peterson, C. G. and Gray, K. A. (2012). Effects of anthropogenic inputs on the organic quality of urbanized streams, *Water Research* **46**: 2515–2524.

Kaushal, S. S. and Belt, K. T. (2012). The urban watershed continuum: Evolving spatial and temporal dimensions, *Urban Ecosystems* **15**: 409–435.

Kaye, J. P., Groffman, P. M., Grimm, N. B., Baker, L. A. and Pouyat, R. V. (2006). A distinct urban biogeochemistry?, *Trends in Ecology and Evolution* **21**: 192–199.

Kelso, J. E. and Baker, M. A. (2020). Organic matter is a mixture of terrestrial, autochthonous, and wastewater effluent in an urban river, *Frontiers in Environmental Science* **7**: 202.

Kemp, P. F., Cole, J. J., Sherr, B. F. and Sherr, E. B. (1993). *Handbook of methods in aquatic microbial ecology*, CRC press.

Kominoski, J. S. and Rosemond, A. D. (2012). Conservation from the bottom up: Forecasting effects of global change on dynamics of organic matter and management needs for river networks, *Freshwater Science* **31**: 51–68.

Lønborg, C., Álvarez Salgado, X. A., Davidson, K., Martínez-García, S. and Teira, E. (2010). Assessing the microbial bioavailability and degradation rate constants of dissolved organic matter by fluorescence spectroscopy in the coastal upwelling system of the ría de vigo, *Marine Chemistry* **119**: 121–129.

McCallister, S. L. and Giorgio, P. A. D. (2012). Evidence for the respiration of ancient terrestrial organic c in northern temperate lakes and streams, *Proceedings of the National Academy of Sciences of the United States of America* **109**: 16963–16968.

McDowell, W. H., Zsolnay, A., Aitkenhead-Peterson, J. A., Gregorich, E. G., Jones, D. L., Jödemann, D., Kalbitz, K., Marschner, B. and Schwesig, D. (2006). A comparison of methods to determine the biodegradable dissolved organic carbon from different terrestrial sources, *Soil Biology and Biochemistry* **38**: 1933–1942.

McKenzie, T., Habel, S. and Dulai, H. (2021). Sea-level rise drives wastewater leakage to coastal waters and storm drains, *Limnology and Oceanography Letters* **6**: 154–163.

Medeiros, P. M., Seidel, M., Gifford, S. M., Ballantyne, F., Dittmar, T., Whitman, W. B. and Moran, M. A. (2017). Microbially-mediated transformations of estuarine dissolved organic matter, *Frontiers in Marine Science* **4**: 69.

Mendoza, L. M., Mladenov, N., Kinoshita, A. M., Pinongcos, F., Verbyla, M. E. and Gersberg, R. (2020). Fluorescence-based monitoring of anthropogenic pollutant inputs to an urban stream in southern california, usa, *Science of the Total Environment* **718**: 137206.

Meng, F., Huang, G., Yang, X., Li, Z., Li, J., Cao, J., Wang, Z. and Sun, L. (2013). Identifying the sources and fate of anthropogenically impacted dissolved organic matter (dom) in urbanized rivers, *Water Research* **47**: 5027–5039.

Murphy, K. R., Hambly, A., Singh, S., Henderson, R. K., Baker, A., Stuetz, R. and Khan, S. J. (2011). Organic matter fluorescence in municipal water recycling schemes: Toward a unified parafac model, *Environmental Science and Technology* **45**: 2909–2916.

Murphy, K. R., Stedmon, C. A., Graeber, D. and Bro, R. (2013). Fluorescence spectroscopy and multi-way techniques. parafac, *Analytical Methods* **5**: 6557–6566.

Nowicki, S., Lapworth, D. J., Ward, J. S., Thomson, P. and Charles, K. (2019). Tryptophan-like fluorescence as a measure of microbial contamination risk in groundwater, *Science of the Total Environment* **646**: 782–791.

Osburn, C. L., Handsel, L. T., Mikan, M. P., Paerl, H. W. and Montgomery, M. T. (2012). Fluorescence tracking of dissolved and particulate organic matter quality in a river-dominated estuary, *Environmental Science and Technology* **46**: 8628–8636.

Parr, T. B., Cronan, C. S., Ohno, T., Findlay, S. E., Smith, S. M. and Simon, K. S. (2015). Urbanization changes the composition and bioavailability of dissolved organic matter in headwater streams, *Limnology and Oceanography* **60**: 885–900.

Paule, A., Émilie Lyautey, Garabetian, F. and Rols, J. L. (2009). Autogenic versus environmental control during development of river biofilm, *Annales de Limnologie* **45**: 1–10.

Reynolds, D. M. and Ahmad, S. R. (1997). Rapid and direct determination of wastewater bod values using a fluorescence technique, *Wat. Res* **31**: 2012–2018.

Rochelle-Newall, E., Hulot, F. D., Janeau, J. L. and Merroune, A. (2014). Cdom fluorescence as a proxy of doc concentration in natural waters: A comparison of four contrasting tropical systems, *Environmental Monitoring and Assessment* **186**: 589–596.

Romera-Castillo, C., Sarmento, H., Antó, X., Lvarez-Salgado, A. , Gasol, J. M. and Marrasé, C. (n.d.). Production of chromophoric dissolved organic matter by marine phytoplankton.
URL: *https://ccmp.bigelow.*

Rotzoll, K. and Fletcher, C. H. (2013). Assessment of groundwater inundation as a consequence of sea-level rise, *Nature Climate Change* **3**: 477–481.

Servais, P., Anzil, A. and Ventresque, C. (1989). Simple method for determination of biodegradable dissolved organic carbon in water, *APPLIED AND ENVIRONMENTAL MICROBIOLOGY* **55**: 2732–2734.

Sobczak, W. V., Cloern, J. E., Jassby, A. D. and Müller-Solger, A. B. (2002). Bioavailability of organic matter in a highly disturbed estuary: The role of detrital and algal resources, *Proceedings of the National Academy of Sciences* **99**(12): 8101–8105.

Sorensen, J. P., Carr, A. F., Nayebare, J., Diongue, D. M., Pouye, A., Roffo, R., Gwengweya, G., Ward, J. S., Kanoti, J., Okotto-Okotto, J. et al. (2020). Tryptophan-like and humic-like fluorophores are extracellular in groundwater: implications as real-time faecal indicators, *Scientific reports* **10**(1): 1–9.

Stedmon, C. A. and Markager, S. (2005). Resolving the variability in dissolved organic matter fluorescence in a temperate estuary and its catchment using parafac analysis, *Limnology and oceanography* **50**(2): 686–697.

Sukop, M. C., Rogers, M., Guannel, G., Infanti, J. M. and Hagemann, K. (2018). High temporal resolution modeling of the impact of rain, tides, and sea level rise on water table flooding in the arch creek basin, miami-dade county florida usa, *Science of the Total Environment* **616-617**: 1668–1688.

Søndergaard, M., Stedmon, C. A. and Borch, N. H. (2003). Fate of terrigenous dissolved organic matter (dom) in estuaries: Aggregation and bioavailability, *Ophelia* **57**: 161–176.

Walsh, C. J., Roy, A. H., Feminella, J. W., Cottingham, P. D., Groffman, P. M. and Ii, R. P. M. (2005). The urban stream syndrome: current knowledge and the search for a cure, *Am. Benthol. Soc* **24**: 706–723.

Weishaar, J. L., Aiken, G. R., Bergamaschi, B. A., Fram, M. S., Fujii, R. and Mopper, K. (2003). Evaluation of specific ultraviolet absorbance as an indicator of the chemical composition and reactivity of dissolved organic carbon, *Environmental Science and Technology* **37**: 4702–4708.

Williams, C. J., Frost, P. C., Morales-Williams, A. M., Larson, J. H., Richardson, W. B., Chiandet, A. S. and Xenopoulos, M. A. (2016). Human activities cause distinct dissolved organic matter composition across freshwater ecosystems, *Global Change Biology* **22**: 613–626.

Williams, C. J., Yamashita, Y., Wilson, H. F., Jaffe, R. and Xenopoulos, M. A. (2010). Unraveling the role of land use and microbial activity in shaping dissolved organic matter characteristics in stream ecosystems, *Limnology and Oceanography* **55**: 1159–1171.

Wilson, H. F. and Xenopoulos, M. A. (2009). Effects of agricultural land use on the composition of fluvial dissolved organic matter, *Nature Geoscience* **2**: 37–41.

Wu, W., Meador, T. and Hinrichs, K. U. (2018). Production and turnover of microbial organic matter in surface intertidal sediments, *Organic Geochemistry* **121**: 104–113.

Yamashita, Y., Boyer, J. N. and Jaffé, R. (2013). Evaluating the distribution of terrestrial dissolved organic matter in a complex coastal ecosystem using fluorescence spectroscopy, *Continental Shelf Research* **66**: 136–144.

Yamashita, Y., Jaffé, R., Maie, N. and Tanoue, E. (n.d.). Yamashita, y., et al. assessing the dynamics of dissolved organic matter (dom) in coastal environments by excitation emission matrix fluorescence and parallel factor analysis (eem-parafac). limnol. oceanogr., 53(5), 2008, 1900–1908.

Yang, L., Chang, S. W., Shin, H. S. and Hur, J. (2015). Tracking the evolution of stream dom source during storm events using end member mixing analysis based on dom quality, *Journal of Hydrology* **523**: 333–341.

Zhang, L., Fang, W., Li, X., Lu, W. and Li, J. (2020). Strong linkages between dissolved organic matter and the aquatic bacterial community in an urban river, *Water Research* **184**.

Zhou, Y., Li, Y., Yao, X., Ding, W., Zhang, Y., Jeppesen, E., Zhang, Y., Podgorski, D. C., Chen, C., Ding, Y., Wu, H. and Spencer, R. G. (2019). Response of chromophoric dissolved organic matter dynamics to tidal oscillations and anthropogenic disturbances in a large subtropical estuary, *Science of the Total Environment* **662**: 769–778.

3.8 Tables

Table 3.1: Land use and cover characteristics of canal drainage basins in Miami, FL, USA.

Land Use (%)	Wagner Creek (WC)	Little River (LR)	Coral Gables (CG)
Impervious Cover*	43.52	49.77	33.41
Canopy Cover*	8.87	7.17	18.20
Road/Parking*	38.86	22.83	38.36
Residential*	26.65	29.12	42.05
Commercial/Institutional*	15.72	7.89	9.25
Industrial*	8.46	5.39	1.17
Vacant*	7.53	2.24	6.98
# Septic Systems	30	1001	4101
# Stormwater Outfalls	60	24	7
Drainage Density (km km^{-2})†	36.17	7.48	2.25
Septic:Stormwater Ratio‡	0.5	42	586

Data were obtained from the National Land Cover Database (NLCD) 2016 and the Miami-Dade County Open Data Hub (https://gis-mdc.opendata.arcgis.com/)
* percent coverage of land cover within coastal portion of primary canal drainage basin
† drainage density calculated as the total length of the stormwater piped network by the total drainage area
‡ calculated ratio of the number of septic systems within study basins divided by the total number of stormwater outfall locations

Table 3.2: Mean (± standard deviation) values for hydrologic variables, water physicochemistry, optical properties, and autotrophic and heterotrophic biological stocks including process rates in surface water and groundwater during dry (November-April) and wet (May-October) seasons from June 2018 to May 2019.

		Wagner Creek (WC)		Little River (LR)		Coral Gables (CG)		Groundwater	
Covariate	Units	Dry Season	Wet Season	Dry Season	Wet Season	Dry Season	Wet Season	F-179	F-319
Cum. Rainfall	mm	481.8	633.7	396.3	921.8	310.1	899.4		
Tidal Amplitude	m	1.25	1.09	0.60	0.65	1.07	1.11		
Stage	m	0.36 (± 0.19)	0.38 (± 0.16)	0.49 (± 0.08)	0.43 (± 0.09)	0.37 (± 0.11)	0.41 (± 0.13)		
Temp	°C	28.9 (± 1.28)	29.1 (± 1.52)	26.2 (± 2.41)	26.9 (± 2.08)	25.2 (± 2.95)	25.7 (± 2.87)	27.7 (± 1.02)	27.8 (± 0.79)
DO	mg L^{-1}	3.6 (± 2.30)	3.0 (± 1.80)	4.4 (± 1.61)	3.6 (± 1.55)	5.4 (± 1.34)	4.3 (± 1.84)	0.37 (± 0.02)	0.28 (± 0.06)
Salinity	ppt	16.6 (± 10.98)	9.1 (± 11.48)	15.1 (± 15.22)	11.5 (± 13.04)	15.8 (± 15.95)	14.4 (± 14.53)	19.2 (± 0.78)	0.25 (± 0.01)
Turbidity	NTU	2.1 (± 1.54)	3.0 (± 4.58)	1.7 (± 1.06)	2.5 (± 1.38)	1.3 (± 0.60)	1.83 (± 1.11)		
DOC	mg L^{-1}	3.5 (± 0.41)	5.0 (± 2.57)	9.3 (± 1.10)	6.3 (± 0.71)	4.3 (± 2.56)	3.2 (± 0.65)	10.5 (± 0.63)	1.65 (± 0.21)
TP	µg L^{-1}	46.3 (± 31.38)	48.0 (± 45.16)	18.5 (± 8.78)	22.4 (± 7.09)	22.4 (± 11.31)	24.8 (± 15.45)	0.06 (± 0.01)	0.11 (± 0.07)
NO_x-N	mg L^{-1}	0.1 (± 0.04)	0.1 (± 0.05)	0.2 (± 0.11)	0.2 (± 0.08)	0.1 (± 0.11)	0.2 (± 0.15)	0.03 (± 0.02)	0.01 (± 0.01)
TKN	mg L^{-1}	0.5 (± 0.15)	0.7 (± 0.21)	0.6 (± 0.28)	1.0 (± 0.59)	0.5 (± 0.21)	0.4 (± 0.15)	0.95 (± 0.05)	0.29 (± 0.01)
HIX	-	8.3 (± 1.03)	13.7 (± 5.40)	11.7 (± 4.26)	13.7 (± 2.01)	6.1 (± 3.05)	12.1 (± 9.73)	11.3 (± 1.40)	0.84 (± 0.12)
BIX	-	0.79 (± 0.02)	0.74 (± 0.03)	0.72 (± 0.01)	0.66 (± 0.08)	0.80 (± 0.02)	0.66 (± 0.02)	0.74 (± 0.03)	0.81 (± 0.05)
FI	-	1.54 (± 0.05)	1.54 (± 0.04)	1.51 (± 0.01)	1.51 (± 0.03)	1.60 (± 0.03)	1.55 (± 0.04)	1.65 (± 0.13)	1.75 (± 0.18)
$SUVA_{254}$	L mg^{-1} m^{-1}	1.76 (± 1.96)	4.74 (± 2.60)	0.93 (± 1.10)	3.31 (± 0.72)	1.09 (± 1.34)	5.96 (± 4.68)	0.05 (± 0.01)	0.07 (± 0.01)
N:P Molar Ratio	-	74.5 (± 91.4)	74.0 (± 70.5)	150.5(± 120.9)	140.3 (± 63.2)	89.5 (± 61.5)	65.6 (± 19.5)	38.0 (± 4.10)	6.0 (± 2.40)
BA	10^6 cells mL^{-1}	1.37 (± 0.47)	0.48 (± 0.08)	1.75 (± 0.45)	0.53 (± 0.12)	2.34 (± 1.51)	1.60 (± 0.10)		
BP	µg C L h^{-1}	1.67 (± 0.04)	0.71 (± 0.78)	0.88 (± 0.48)	1.67 (± 0.59)	3.14 (± 3.10)	1.87 (± 0.10)		
E. coli	MPN 100 mL^{-1}	682 (± 1083)	2511 (± 3126)	267 (± 222)	303 (± 104)	182 (± 66)	318 (± 301)		
Enterococci	MPN 100 mL^{-1}	140 (± 61.5)	144 (± 16.3)	340 (± 221)	69.0 (± 8.48)	36.5 (± 37.5)	20.5 (± 14.8)		
Biofilm AFDM	g m^{-2}	1.23 (± 1.97)	1.58 (± 2.10)	0.16 (± 0.39)	1.09 (± 1.77)	1.08 (± 1.67)	1.83 (± 1.63)		
AFDM:DM	-	32 (± 15)	48 (± 0.21)	25 (± 22)	49 (± 25)	26 (± 12)	86 (± 32)		

DO, dissolved oxygen; DOC, dissolved organic carbon; TP, total phosphorous; NO_x-N, oxidized nitrogen; TKN, total Kjeldahl nitrogen; HIX, humification index; FI, fluorescence index; $SUVA_{254}$, specific UV absorbance at 254nm; BA, bacterial abundance; BP, bacterial productivity; AFDM, ash-free dry mass; DM, dry mass; AI, autotrophic index; MPN, most probable number

Table 3.3: Results of two-way ANOVA with balanced design of effects of tide and season on % BDOC.

Source of variation	df	SS	F	*P*
Stage	13	923.34	2.719	**0.02**
Basin	13	81.53	1.15	*ns*
Tide	22	33.02	0.971	*ns*
Season	22	12.91	0.379	*ns*
Tide*Season	10	121.83	3.582	**0.05**

ns = not significant ($p > 0.05$); df, degrees of freedom; SS, sum of squares

Table 3.4: Emission and excitation maxima and characteristics of modeled EEM-PARAFAC components

Component	Excitation maxima (nm)	Emission maxima (nm)	Description
C1	333	440	Humic-like fluorophore of terrestrial origin; derived from processing of DOM by terrestrial or aquatic microbes in forested streams, wetlands, and agriculturally influenced streams (Yamashita et al., 2013; Hosen et al., 2014)
C2	<250, 303	380	ubiquitous humic-like substances of low-molecular weight; common in marine environments with biological activity (Fellman et al., 2010; ; Murphy et al., 2011; Meng et al., 2013)
C3	267, 385	460-490	Represents protein-like and microbial humic-like fluorescence; autochthonous production or derived from anthropogenic sources or wastewater impacted streams (Murphy et al., 2011; Meng et al., 2013).
C4	276	335-345	tryptophan-like, protein-like fluorescence, indicates recent production; often found in anthropogenically affected watersheds (Parr et al., 2009; Williams et al., 2010)
C5	270	305	tyrosine-like, protein-like fluorescence present in marine waters (Hudson et al., 2007)

Table 3.5: Statistical comparisons of EEM-PARAFAC components across seasons, tides, and location with percent bioavailable DOC (BDOC) as a covariate using two-way repeated measures analysis of covariance (ANCOVA).

	Season		Tide		Location*	
	F	*P*	F	*P*	F	*P*
% C1	4.91	**0.03**	4.55	**0.04**	5.54	**0.02**
% C2	3.75	**0.05**	3.53	*ns*	4.36	**0.04**
% C3	3.21	*ns*	3.11	*ns*	3.71	*ns*
% C4	4.29	**0.04**	4.16	**0.05**	5.02	**0.03**
% C5	3.71	*ns*	3.48	*ns*	4.27	**0.04**

*position along inland-to-coastal gradient (i.e., upstream, downstream)
ns = not significant ($P > 0.05$)

3.9 Figures

Figure 3.1. Map of sampling locations and land use/cover in three canal drainage basins including Coral Gables (CG), Wagner Creek (WC), and Little River (LR). Grab sampling locations are designated by yellow circles (n=12). Coordinates are presented in decimal degrees.

Figure 3.2. Daily cumulative rainfall and canal stage in three study canals from June 2018 to May 2019. Data represent stage (m; NAVD29) measured at (1) 15-minute intervals and (2) 3-day moving average. Four sampling events are represented by solid black lines.

Figure 3.3. Comparison of (a) dissolved organic carbon (DOC), (b) percent bioavailable DOC (BDOC), and ratios of % BDOC to (c) bacterial abundance (BA; 106 cells mL-1) and (d) bacterial productivity (BP, µg C L d-1). Drainage basins are ordered by increasing septic:stormwater (WC, LR, CG). The direction of arrows indicates the upstream-downstream location within each canal.

Figure 3.4. Excitation-emission plots of five EEM-PARAFAC components (C1, C2, C3, C4, C5) validated in this study. Orange hues indicate higher and blue hues lower fluorescence intensities.

Figure 3.5. Principal component analysis (PCA) for water quality parameters. PCA score plots show differences (a) wet and dry season versus (b) high and low tide. PCA loading plot (c) depicts the distribution of variables including EEM-PARAFAC components, DOM fluorescence indices, and % BDOC. Axes are labeled with the percent variability explained by each principal component.

Figure 3.6. Seasonal relationships between the standardized percentage of PARAFAC components and (a,b) % BDOC, (c,d) $\log_{10}$ Escherichia coli (E. coli) concentrations, as well as fluorescence intensity in raman units (RU) with (d,f) $\log_{10}$

Enterococci concentrations. Significant R^2 values are shown ($P < 0.05$). Shaded regions represent 95% confidence intervals.

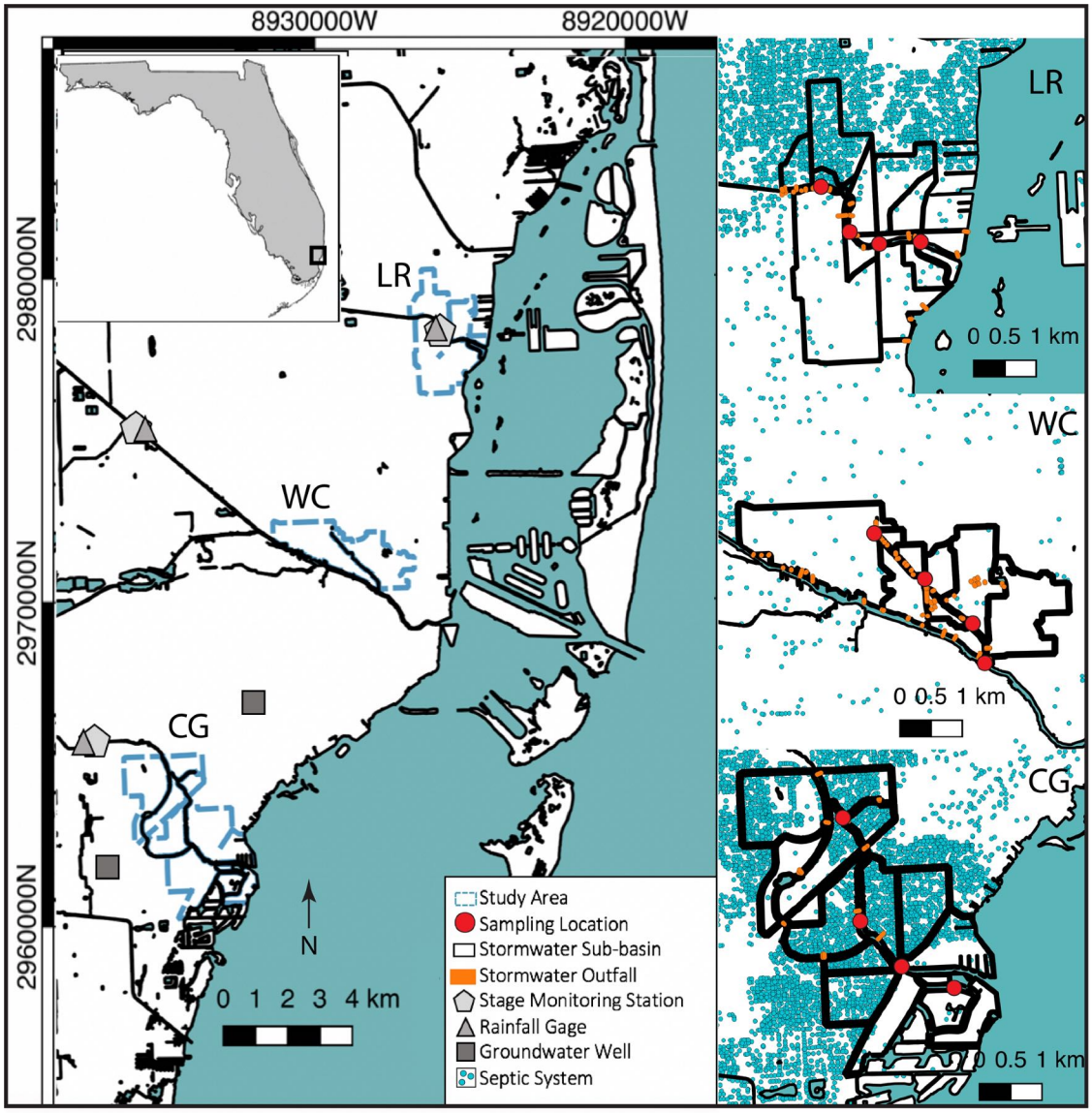

Figure 3.1: Map of sampling locations and land use/cover in three canal drainage basins including Coral Gables (CG), Wagner Creek (WC), and Little River (LR). Grab sampling locations are designated by yellow circles (n=12). Coordinates are presented in decimal degrees.

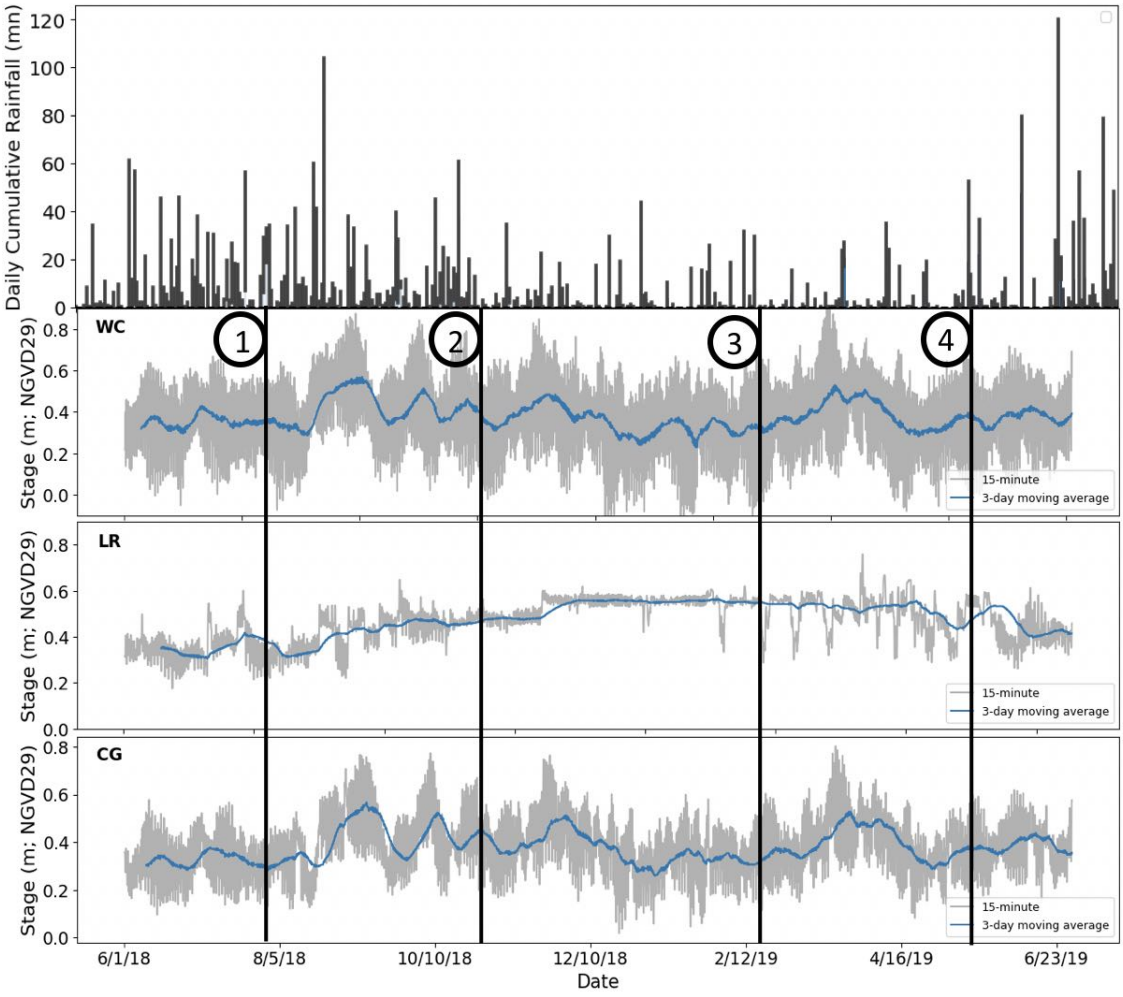

Figure 3.2: Daily cumulative rainfall and canal stage in three study canals from June 2018 to May 2019. Data represent stage (m; NAVD29) measured at (1) 15-minute intervals and (2) 3-day moving average. Four sampling events are represented by solid black lines.

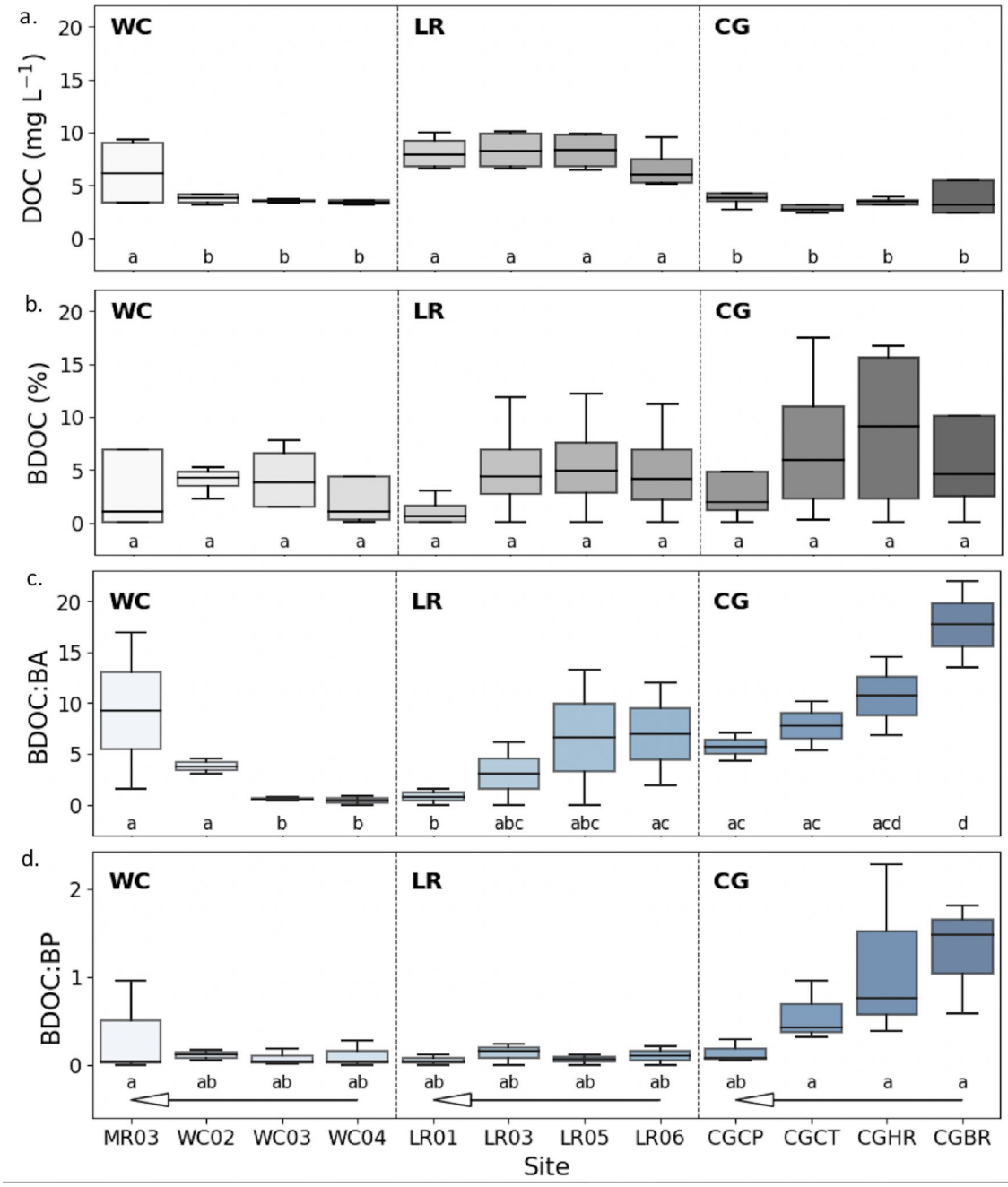

Figure 3.3: Comparison of (a) dissolved organic carbon (DOC), (b) percent bioavailable DOC (BDOC), and ratios of % BDOC to (c) bacterial abundance (BA; 106 cells mL^{-1}) and (d) bacterial productivity (BP, µg C L d^{-1}). Drainage basins are ordered by increasing septic:stormwater (WC, LR, CG). The direction of arrows indicates the upstream-downstream location within each canal.

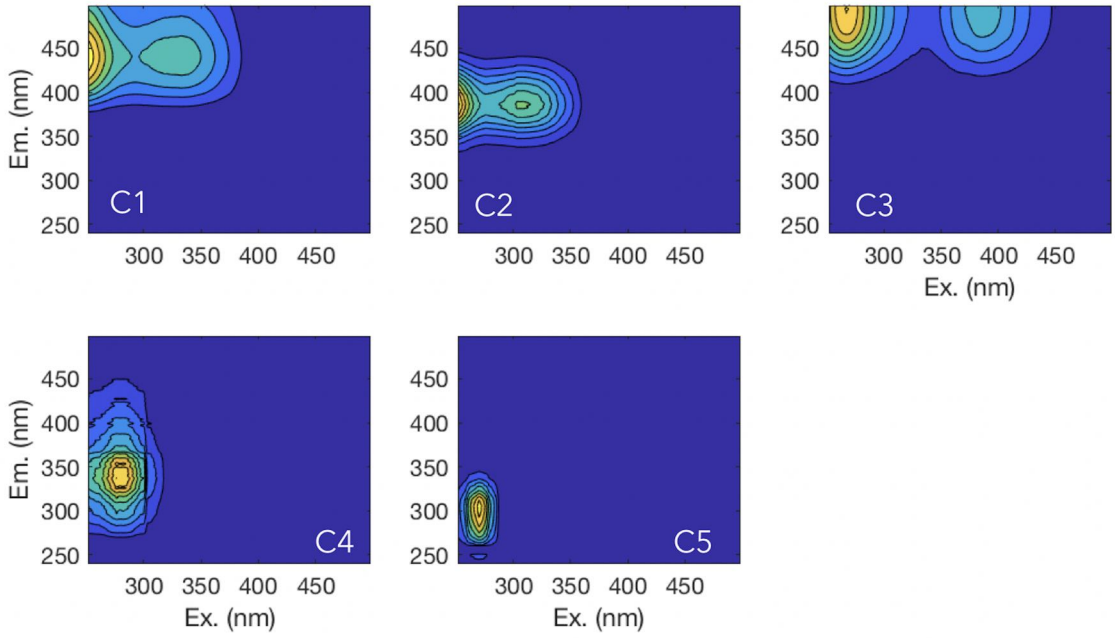

Figure 3.4: Excitation-emission plots of five EEM-PARAFAC components (C1, C2, C3, C4, C5) validated in this study. Orange hues indicate higher and blue hues lower fluorescence intensities.

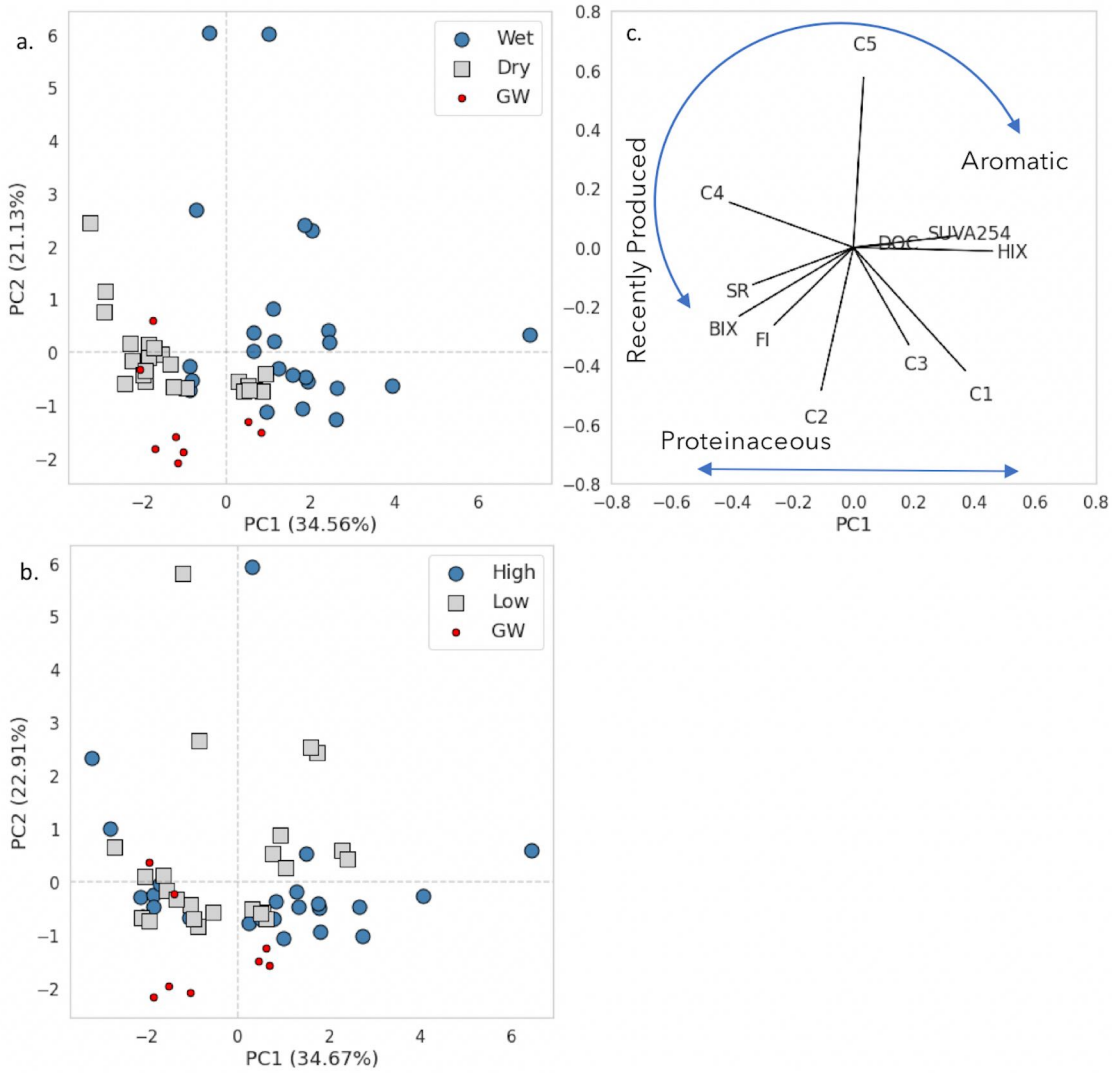

Figure 3.5: Principal component analysis (PCA) for water quality parameters. PCA score plots show differences (a) wet and dry season versus (b) high and low tide. PCA loading plot (c) depicts the distribution of variables including EEM-PARAFAC components, DOM fluorescence indices, and % BDOC. Axes are labeled with the percent variability explained by each principal component.

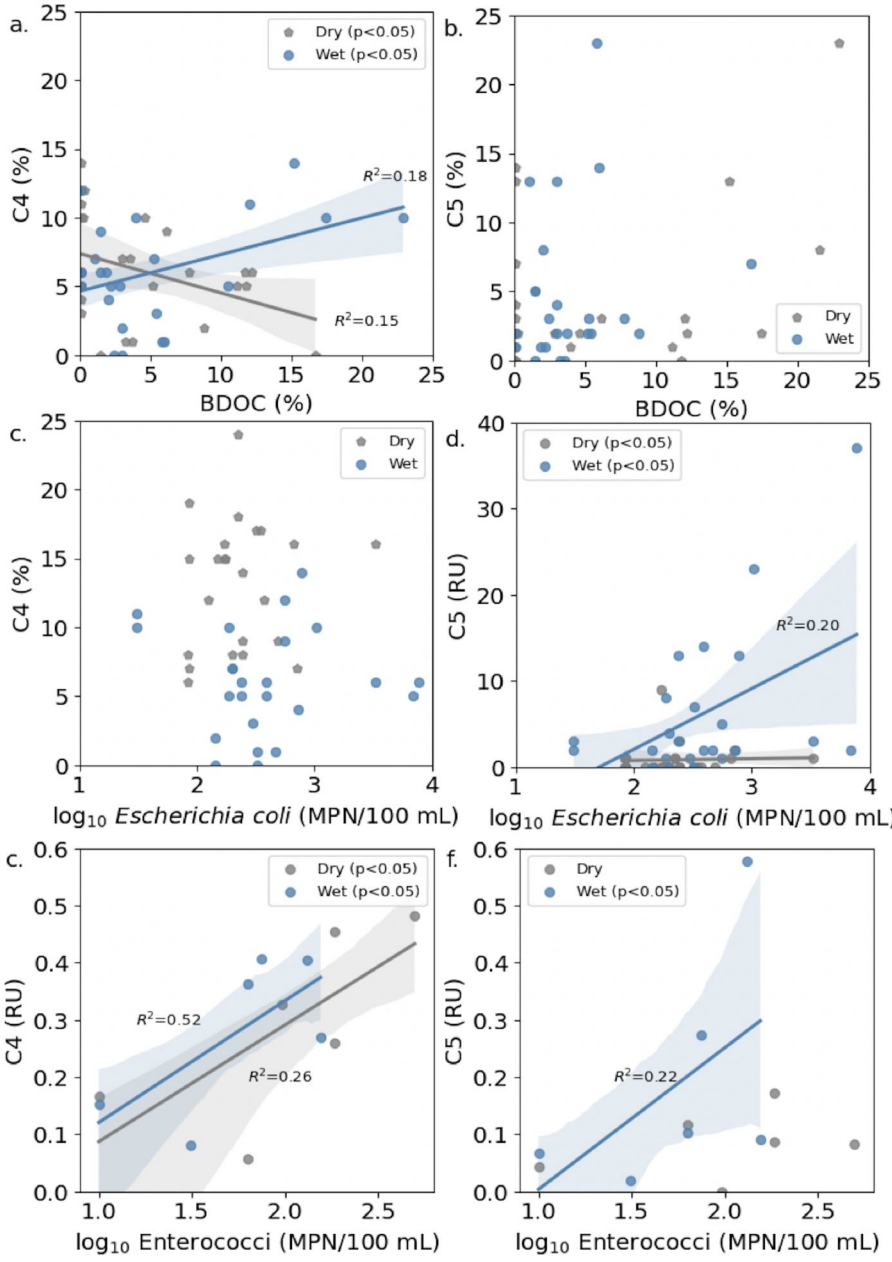

Figure 3.6: Seasonal relationships between the standardized percentage of components and (a,b) % BDOC, (c,d) log10 Escherichia coli (E. coli) concentrations, as well as fluorescence intensity in raman units (RU) with (d,f) $\log_{10}$ Enterococci concentrations. Significant R^2 values are shown ($P < 0.05$). Shaded regions represent 95% confidence intervals.

3.10 Supplemental Information

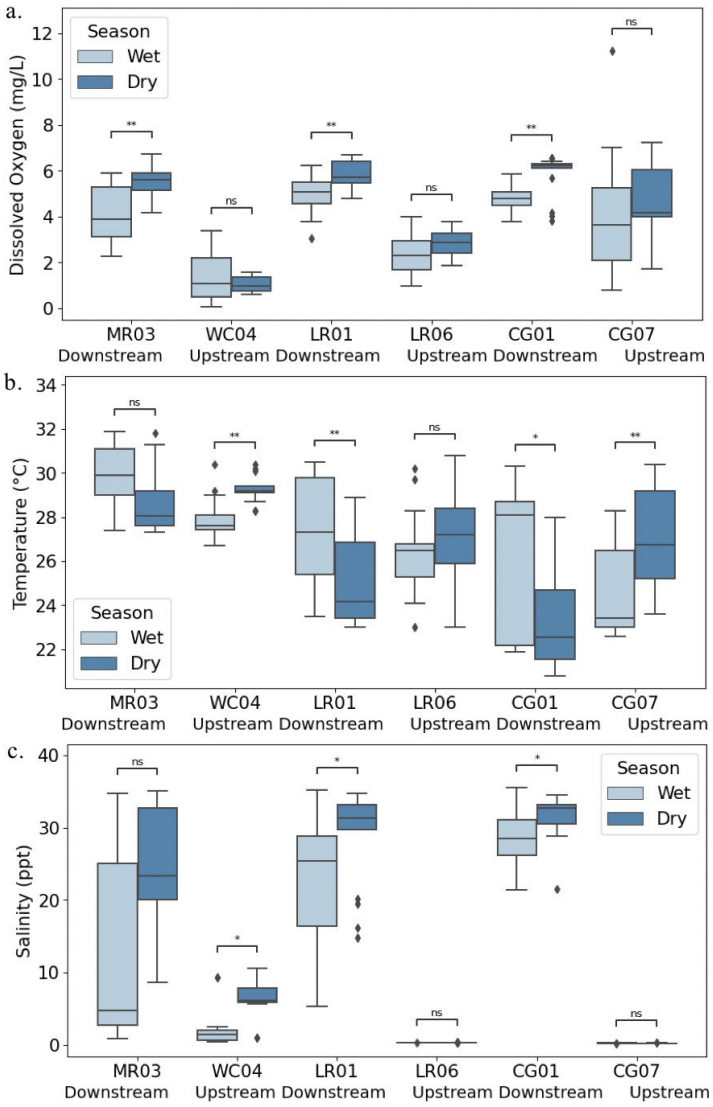

Figure 3.7: Seasonal average (a) salinity (ppt), (b) surface water temperature (deg C), and (c) dissolved oxygen (mg/L) in upstream and downstream locations in three drainage basins of Miami, FL from June 2018 to May 2019. Significant seasonal differences were observed in salinity ($P < 0.05$) while differences in surface water temperature and dissolved oxygen and were seen across seasons and basins ($P < 0.01$). Significant interactions between season and basin were observed with temperature ($P < 0.01$).

[!ht]

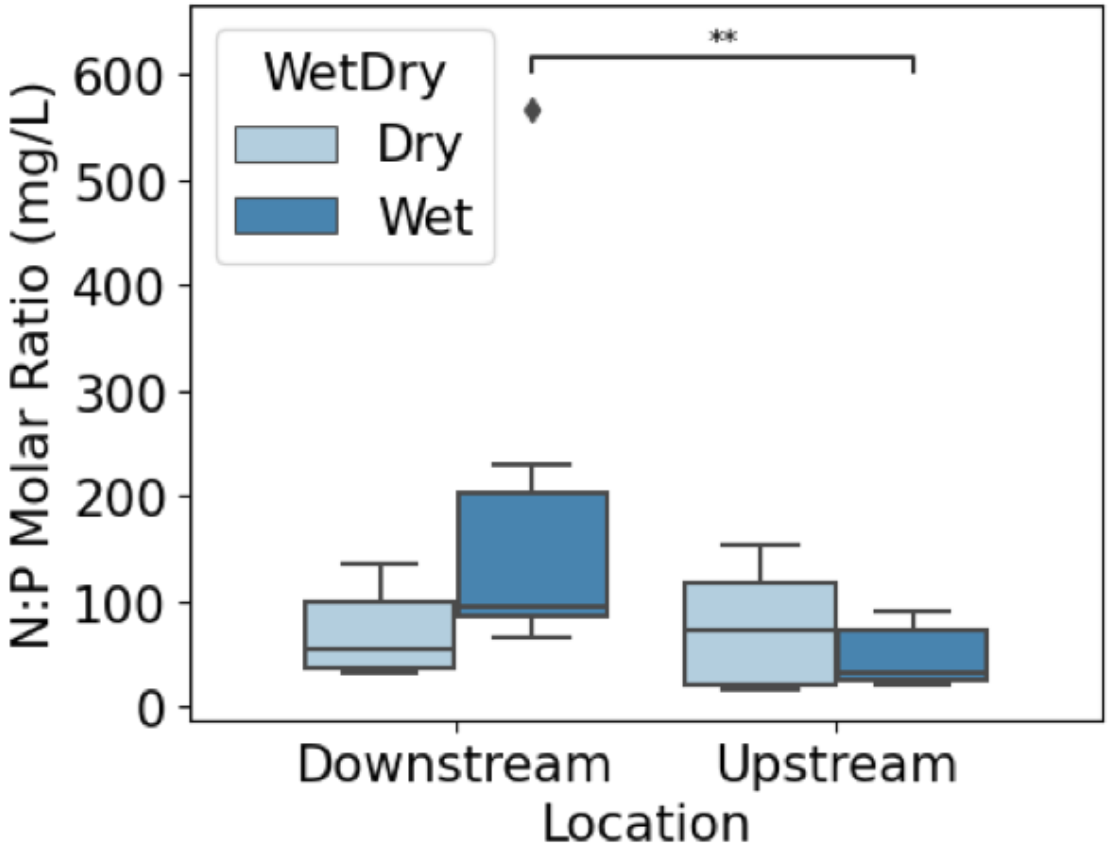

Figure 3.8: Comparison of dissolved N:P molar ratios in surface water samples. Samples were analyzed by canal location along an inland-coastal gradient (upstream-downstream) and by season (wet and dry). Repeated measures ANOVA followed by Tukey's honest significant differences (HSD) post hoc test showed a significant difference among locations ($P = 0.04$), but not seasons ($P > 0.05$). A significant interaction among location*season was observed ($F_{1,34} = 4.90$; $P = 0.03$).

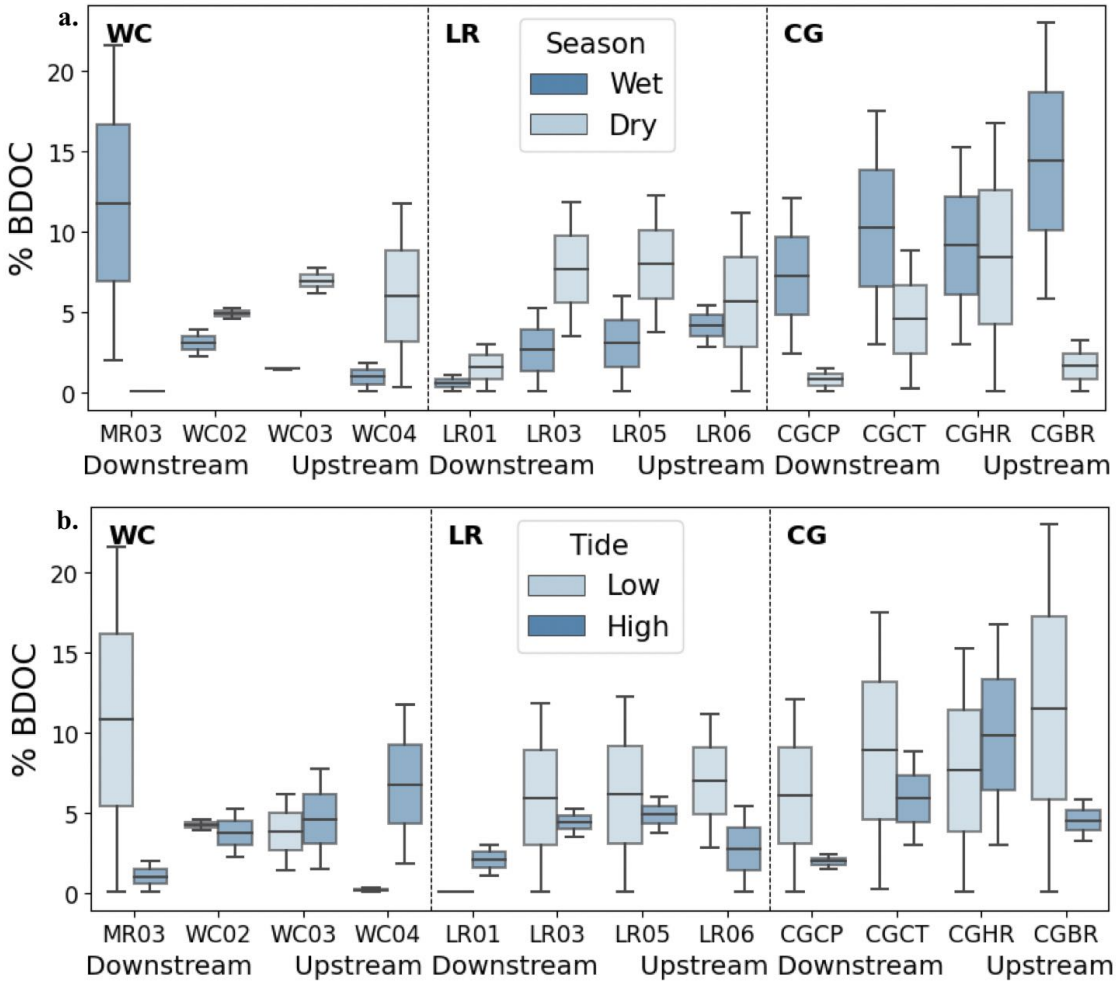

Figure 3.9: Average % BDOC proportions across all 12 sites in (a) wet and dry seasons and (b) low and high tides. Drainage basins are ordered by their respective septic:stormwater ratio (WC, LR, CG).

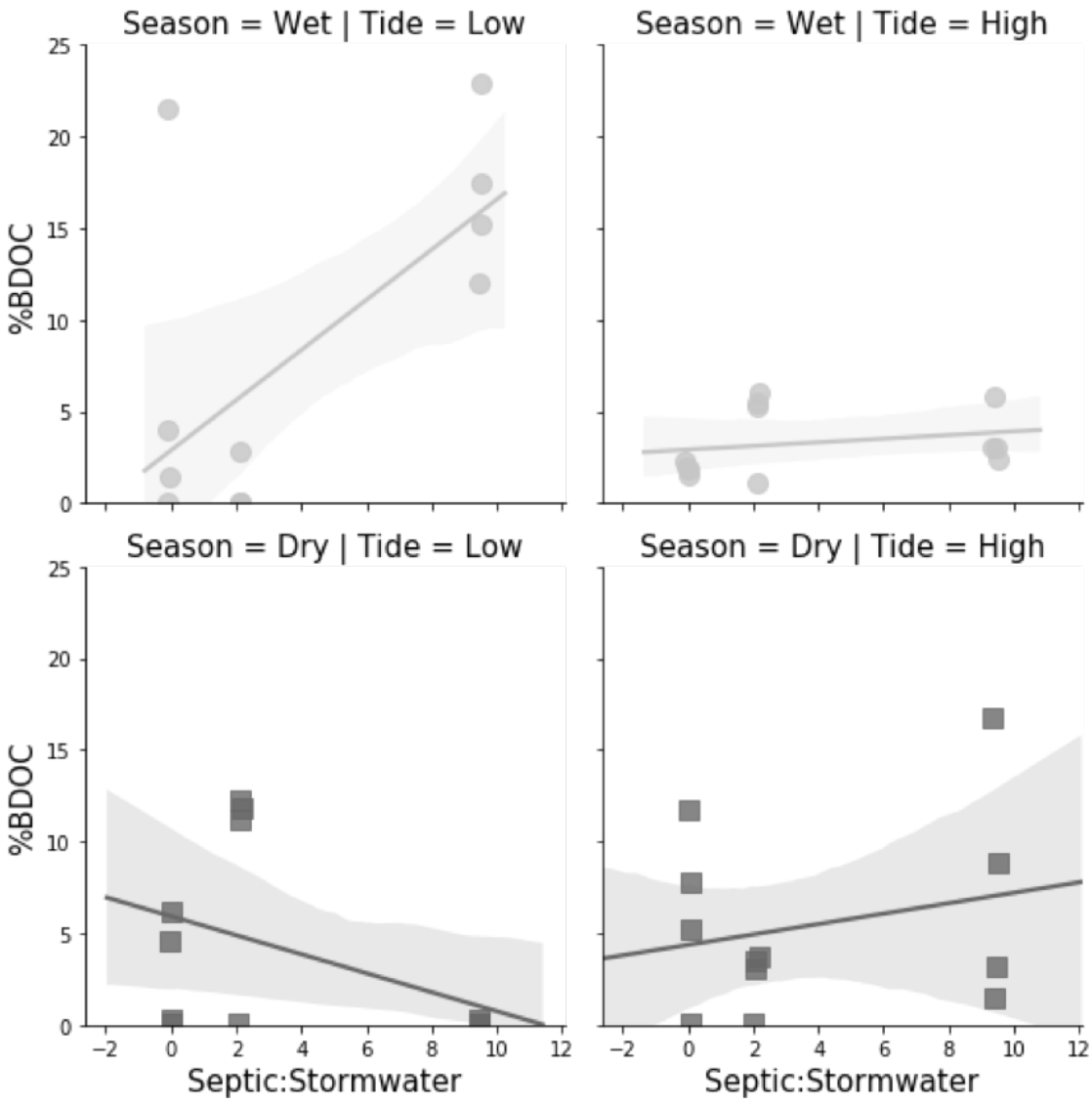

Figure 3.10: Seasonal rainfall and tidal relationships between Septic:Stormwater ratios and bioavailable DOC (BDOC; %).

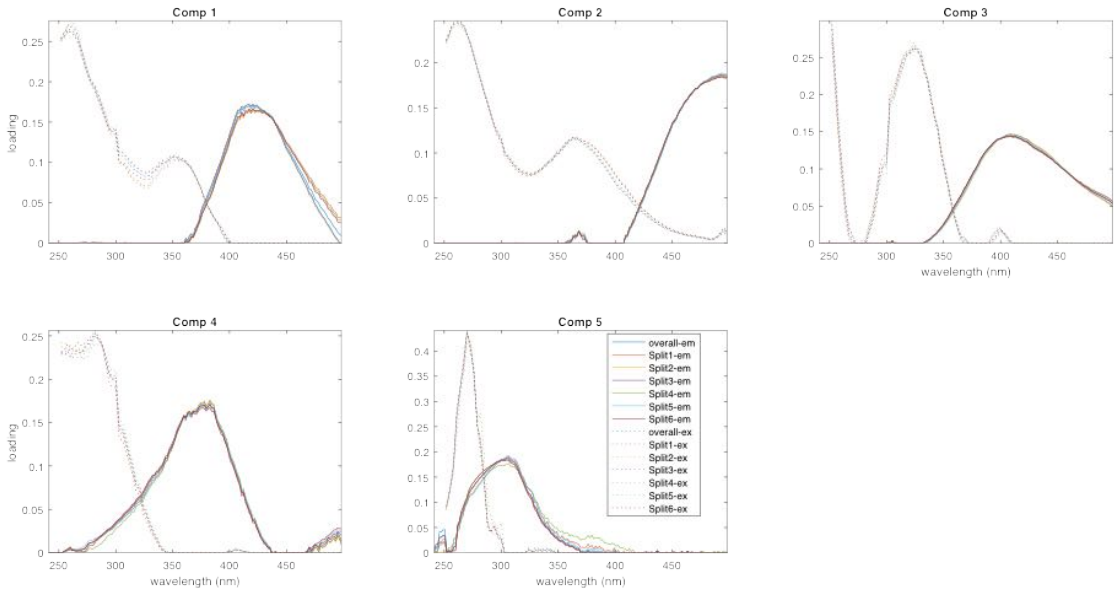

Figure 3.11: Emission and excitation loadings from splits used in split-half analysis of the 5-component PARAFAC model (Fig. 5) validated for 146 samples.

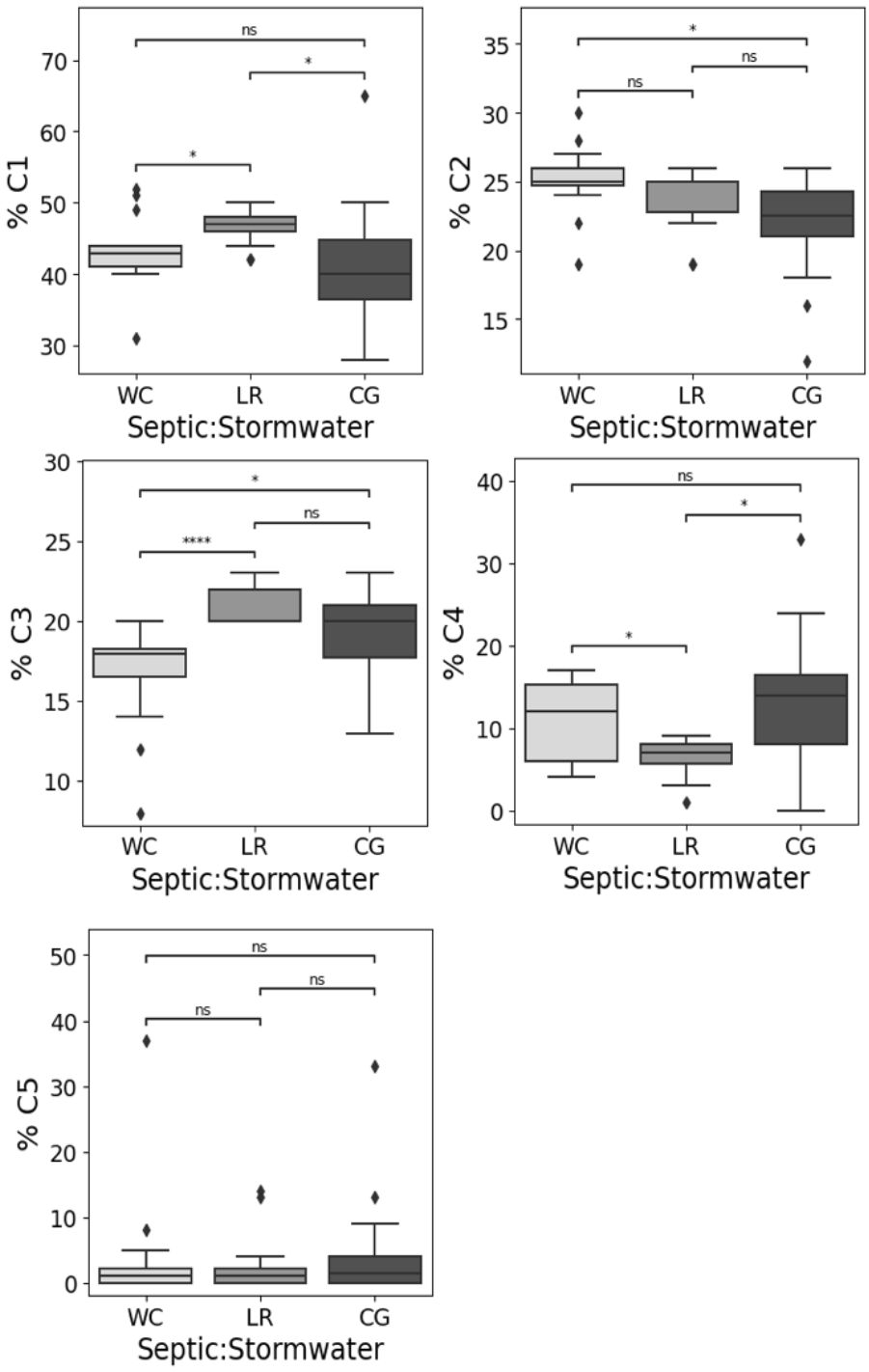

Figure 3.12: Relationships between percent contributions of five components across a gradient of septic:stormwater.

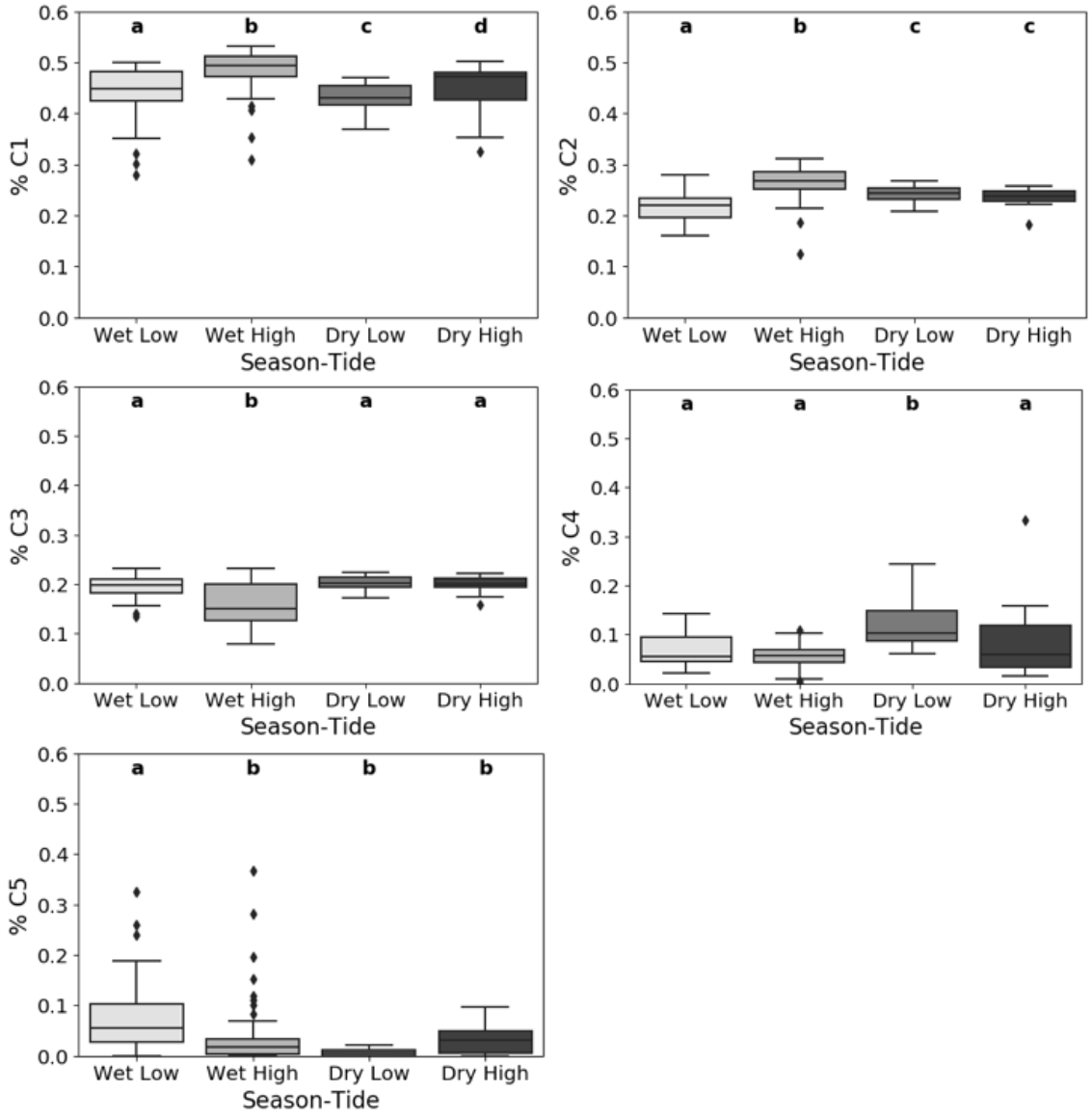

Figure 3.13: Comparison of PARAFAC components across season and tide. Significant differences were determined by two-way repeated measures ANOVA with Tukey's HSD.

Table 3.6: List of USGS/SFWMD collection sites for canal stage/flow, groundwater, and rainfall.

Site ID	Agency	Parameter	Latitude	Longitude
S27_R	SFWMD	Rainfall	25.851043	-80.188417
G93_R	SFWMD	Rainfall	25.738558	-80.286984
S26_R	SFWMD	Rainfall	25.807467	-80.260492
F-179	USGS (254444080144801)	Groundwater	25.745647	-80.246400
F-319	USGS (254217080171801)	Groundwater	25.704722	-80.288333
S27	SFWMD	Stage, Flow	25.851043	-80.188417
G93	SFWMD	Stage, Flow	25.738558	-80.286984
WC02*	-	Stage, Flow	25.784020	-80.210152

**not a USGS gauge*

Table 3.7: Results of two-way repeated measures ANOVA on mean values for water physicochemistry and autotrophic and heterotrophic biological stocks and process rates in each canal basin during dry (November-April) and wet (May-October) season between June 2018 to May 2019.

Covariate	Units	Season		Basin		Interaction	
		F	*P*	F	*P*	F	*P*
Cum. Rainfall	mm	12.21	**<0.0001**	0.22	*ns*	1.22	*ns*
Stage	m	129.40	**<0.001**	1547.13	**<0.0001**	123.54	**<0.0001**
Temp	°C	2.47	**<0.001**	44.84	**<0.001**	0.31	**<0.001**
DO	mg L^{-1}	12.05	**<0.001**	13.25	**<0.001**	0.34	*ns*
Salinity	ppt	4.67	**0.03**	0.67	*ns*	0.91	*ns*
Turbidity	NTU	2.30	*ns*	1.36	*ns*	0.06	*ns*
DOC	mg L^{-1}	3.79	**<0.001**	95.99	**<0.001**	8.30	**<0.001**
TP	µg L^{-1}	0.23	*ns*	9.14	**<0.001**	0.14	*ns*
NO_x	mg L^{-1}	1.60	*ns*	8.83	**<0.001**	0.41	*ns*
TKN	mg L^{-1}	3.10	*ns*	3.18	**0.05**	1.24	*ns*
HIX	-	63.24	**<0.001**	5.43	**<0.001**	6.79	**<0.001**
BIX	-	36.09	**<0.001**	20.04	**<0.001**	9.48	**<0.001**
FI	-	8.71	**<0.001**	16.84	**<0.001**	3.43	**<0.001**
$SUVA_{254}$	L mg^{-1} m^{-1}	23.24	**<0.001**	1.47	*ns*	1.12	*ns*
BA	10^6 cells mL^{-1}	5.30	**0.05**	2.39	*ns*	0.12	*ns*
BP	µg C L^{-1} h^{-1}	0.37	*ns*	3.39	**0.05**	0.65	*ns*
N:P Molar Ratio	-	1.99	*ns*	2.34	*ns*	1.98	*ns*
E. coli	MPN 100 mL^{-1}	2.88	*ns*	5.04	**<0.01**	2.19	*ns*
Enterococci	MPN 100 mL^{-1}	2.92	*ns*	3.48	*ns*	2.57	*ns*
Biofilm AFDM	g m^{-2}	3.80	**0.05**	3.65	**0.03**	1.71	*ns*
AFDM:DM	-	5.20	**0.05**	3.91	**0.05**	1.25	*ns*

DO, dissolved oxygen; DOC, dissolved organic carbon; TP, total phosphorous; NO_x-N, oxidized nitrogen; TKN, total Kjeldahl nitrogen; HIX, humification index; FI, fluorescence index; $SUVA_{254}$, specific UV absorbance at 254nm; BA, bacterial abundance; BP, bacterial productivity; AFDM, ash-free dry mass; DM, dry mass; AI, autotrophic index; MPN, most probable number

CHAPTER 4

Dissolved organic matter composition and phosphorus limitation mediate water-column and whole-system nutrient uptake in urban wetlands

Matthew A. Smith[1], John S. Kominoski[1], Olga Barbosa[2], Elizabeth Cook[3], Stephen Elser[4], Nancy B. Grimm[4], Jennifer Mors[5], Jason Sauer[4], Tearsa Saffell[4]

[1]Institute of Environment and Department of Biological Sciences, Florida International University, Miami, FL, 33199 USA

[2]Instituto de Ciencias Ambientales y Evolutivas, Facultad de Ciencias, Universidad Austral de Chile, Valdivia, Chile

[3]Environmental Science Department, Barnard College, New York, NY, USA

[4]School of Life Sciences and Julie Ann Wrigley Global Institute of Sustainability, Arizona State University, Tempe, AZ, USA

[5]Department of Environmental Science Management, Portland State University; P.O. Box 751; Portland, OR USA

4.1 Abstract

Wetlands are key transitional areas between terrestrial and aquatic ecosystems that serve as critical carbon and nutrient sinks, but our understanding of wetland biogeochemistry in urban settings is limited. Urban development alters the timing and magnitude of hydrologic and geomorphic processes of wetlands, thereby influencing the source and composition of dissolved organic matter (DOM) and concentrations of dissolved organic carbon (DOC) and nutrients [nitrogen (N) and phosphorus (P)]. Our objective was to quantify the influence of ambient DOC and nutrient concentrations, landscape physiography, and dissolved organic matter (DOM) composition on water-column and whole-system nutrient uptake capacity in freshwater wetlands along a gradient of imperviousness in Valdivia, Chile. We added elevated dissolved inorganic nitrogen ($NO3^-$ + $NH4^+$) and soluble reactive phosphorus (SRP; PO43-) to open water areas in wetlands (n = 9) along a gradient of watershed imperviousness. We quantified $NO3^-$, $NH4^+$, and SRP loss rates (k), uptake velocities (v_f) and total daily maximum uptake rates (U_{vol}) from severely P-limited (N:P = 110-2954) wetlands. We found that water column uptake of NO3- and SRP represents a significant proportion of total uptake, particularly in small urban wetlands supplied with labile, proteinaceous carbon and with short water residence time. Overall, our study shows that increases in the stoichiometric availability of labile organic carbon can stimulate sequestration of NO3- and SRP in nutrient polluted or nutrient limited urban wetlands. Results of this study provide evidence for the need to identify thresholds for various hydrologic and landscape variables beyond which water column and/or whole system nutrient uptake can be increased.

4.2 Introduction

Wetlands function as biogeochemical control points (i.e., a point in time and/or space of disproportionate biogeochemical significance) and serve as critical carbon and nutrient sinks (Verhoeven et al.; 2006; Jordan et al.; 2011). Freshwater wetlands have long been recognized as important regulators of excess nitrogen (N) and phosphorus (P) in surface waters (Mulholland; 1992; Cheng and Basu; 2017), and there is growing evidence that small wetlands can provide effective nutrient removal relative to total watershed area (Howarth et al.; 1996; Wollheim et al.; 2014). Nutrients entering freshwater wetlands are either removed completely (i.e., via denitrification) or are removed from the water column via microbially-mediated processes and temporarily stored as particulate or dissolved organic matter (Mulholland et al.; 2008). The relative importance of water column versus benthic contributions to whole-system nutrient uptake depends upon the extent of reactive surface area, water residence time, and nutrient loading rates (Reisinger et al.; 2015; Wollheim et al.; 2018). For example, low topographic, fluvial wetlands may be consistently inundated but connected to surface flow, whereas floodplain wetlands are connected to river and stream mainstems under high-flow conditions. These isolated wetland areas provide significant capacity for nutrient retention and/or uptake by increasing reactive surface area, heterotrophic processes and storage or organic matter, and unique redox conditions that promote denitrification (Forshay and Stanley; 2005; Wollheim et al.; 2014). Wetlands contribute to significant N and P removal from the system (McClain et al.; 2003; Wollheim et al.; 2008), but may be limited by the amount and composition of dissolved organic matter (DOM) inputs (Tank et al.; 2008; Reisinger et al.; 2015).

The importance of DOM concentrations in supporting wetland biogeochemical processing is well understood (Tank et al.; 2010; Ghosh and Leff; 2013), but little is known about how changes in DOM composition alter the rate and magnitude of nutrient uptake wetlands among different land use types. Disturbances to hydrologic regimes via changes in land use can alter water-column mediated nutrient transport and/or uptake of N and P that contribute to nutrient removal capacity at the whole-system level (Johnston et al.; 1984; Ashkenas et al.; 2004; Bernot et al.; 2006). Additions of labile carbon (C) can increase bacterial production (i.e., biomass) (Bernhardt and Likens; 2002), transformed inorganic nitrogen (Johnson et al.; 2009), and increased phosphorus (P) demand (Oviedo-Vargas et al.; 2013). DOM composition and dissolved organic carbon (DOC) concentrations are linked to changes in watershed imperviousness, catchment area, and wetland coverage (Parr et al.; 2015; Singh et al.; 2017). Similarly, urban watersheds exhibit a distinct biogeochemistry with the majority of DOM from labile, proteinaceous sources (Williams et al.; 2016). Elemental stoichiometry controls benthic uptake processes where great potential for microbial processing and sedimentation exists (Battin et al.; 2008; Coble et al.; 2016; Stutter et al.; 2020). Therefore, pulsed inputs of elevated DOM (including DOC), N and P concentrations, and N:P molar ratios may differentially influence water column versus whole-system nutrient removal capacity (Stelzer et al.; 2003; Larson et al.; 2014), especially in urban wetlands.

Globally, wetland ecosystems are under pressure from rapidly expanding urban development (Ehrenfeld; 2000; Lee et al.; 2006). Urban landscapes are characterized by elevated nutrient loading rates and variable forms of labile or allochthonous DOM across longitudinal (upstream-downstream) and vertical (surface-subsurface) gradients (Fork et al.; 2020). In turn, the capacity of wetlands to regulate N and P inputs may decline as nutrient loading increases with urbanization, particularly in

wetlands with short water residence time (Hogan and Walbridge; 2007; Palta et al.; 2017; Wollheim et al.; 2018). Recent findings suggest that urbanization can increase autochthonous production and bioavailability of DOM inputs to downstream water bodies, including wetlands (Asmala et al.; 2013; Kelso and Baker; 2020). The availability of inorganic N (N; nitrate; $NO3^-$ and ammonium; $NH4^+$) and soluble reactive P (SRP; PO4-3) in urban runoff influences water-column N and P uptake based on the extent of nutrient limitation (Bechtold et al.; 2012; Coble et al.; 2016). Despite differences in nutrient composition, nutrient loss rates typically decline with increasing water depth (Alexander et al.; 2007) and exceedingly high nutrient loads (O'Brien et al.; 2007). Therefore, the capacity of small wetlands to remove N and P depends on their relative position within the watershed (i.e., upstream-downstream), as well as surrounding land use and ambient N and P concentrations and N:P molar ratios (Cheng and Basu; 2017). In turn, small freshwater wetlands located close to upstream nutrient sources can drive significant nutrient removal, particularly following significant runoff events (Schmadel et al.; 2019).

Most studies that address nutrient uptake functionality in wetlands have focused on linking nutrient uptake to a limited range of hydrological, chemical or biological attributes, often for constructed wetlands (Fink and Mitsch; 2004; Laterra et al.; 2018). Additionally, few studies address the importance of water-column relative to whole-system N and P uptake. An alternative to whole-system measurements of nutrient uptake is to measure processing rates in specific compartments of the ecosystem directly. Water-column nutrient uptake can be estimated using short-term incubation experiments where the conversion rate of inorganic dissolved N and P to organic forms is measured (Reisinger et al.; 2015; Larson et al.; 2019). Estimations of water-column nutrient uptake can be modeled at the scale of the larger wetland if water residence time is known (Larson et al.; 2019). Understanding the capacity

for water-column relative to whole-system nutrient uptake is becoming increasingly important as wetlands decrease in size and residence time with urbanization.

To better understand the influence of DOM composition and nutrient availability on uptake dynamics, we quantified water-column uptake of $NO3^-$, $NH4^-$, and SRP along a gradient of impervious cover and N:P limitation. We employed a combination of whole system (in situ) nutrient manipulations and water column (ex situ) chamber measurements to address the following questions: (1) How do water-column and whole-system nutrient uptake compare along a gradient of urbanization? (2) How do different indicators of DOC composition and quality influence total nutrient uptake? and (3) How does the relative extent of N and P limitation influence water column and whole system nutrient uptake? We predicted that (1) water-column nutrient uptake and demand of N and P would be higher in wetlands with low to moderate ambient nutrient concentrations and optimal redox conditions [driving $NO3^-$ relative to $NH4^+$ loss], (2) increased concentrations of labile DOC would result in accelerate metabolism and transformation of naturally occurring DOC and nutrients via a priming effect , and (3) decreasing water-column and whole system uptake with increasing P-limitation existing nutrient limitation would drive water-column uptake.

4.3 Methods

4.3.1 Study Locations

We quantified water-column and whole-system nutrient uptake in wetlands of Valdivia, Chile (Fig. 4.2; 39° 81' 96 S, 73° 24' 52 W). Study sites were located within 90 km of the coast and all wetlands were characterized as freshwater (salinity < 2

ppt). Valdivia exhibits a temperate rainforest climate with significant annual precipitation (109 – 250 cm y-1) during a distinct wet season (April – October). The local geology is dominated by a volcanic lithology and soils are comprised of organic matter of a recent origin (Heusser; 1976; Sable and Wohl; 2006). The potential abiotic adsorption of P to underlying bedrock and surficial sediments was considered to play a role in nutrient uptake (Patil et al.; 2013). However, short water residence time (e.g., $<$ 24 h) and the presence of shallow bedrock suggest that hyporheic zone biological processes rather than geochemical adsorption drive nutrient uptake dynamics (Ensign and Doyle; 2006).

4.3.2 Wetland Characteristics

Nine wetlands were selected for nutrient addition experiments along a gradient of imperviousness (1 – 58 %) in January – February 2018 and 2020 (n = 18). In each wetland, a shallow, isolated pool was selected to conduct the experiment that represents the larger wetland ecosystem (Table 1). For statistical comparison, watershed imperviousness was classified into three categories including high (>40%), medium (20-40%), and low (<20%) percent imperviousness. Land use type (i.e., residential, commercial, industrial, parking, open land) was also considered for statistical comparison of nutrient uptake dynamics but was not considered as part of the initial site selection. Hydrologically modified stormwater retention ponds, bioswales, or other stormwater features were not considered as part of this study. We also collected data on wetland vegetation structure during the study period in 2018 (Table S1). Individuals counts of vegetation species were used to compute species richness and vegetation density (relative to total wetland area). Catchments draining to each wetland were characterized using a modified digital elevation model (DEM; 15 ft

resolution) and computed using the 'Pysheds' package in Python (Python 3.6.0). Catchment boundaries were used to clip land use and land cover data gathered from the National Land Cover Database (NLCD, 2014). All geospatial analyses were conducted using ArcGIS 10.8 (Esri Corporation, Redlands, CA, USA).

4.3.3 Water Chemistry

Ambient concentrations of NO3-, NH4+, SRP, DOC, and Chloride (Cl-) were measured in all wetlands one week prior to addition experiments. Other water quality parameters including pH, temperature, dissolved oxygen, and specific conductivity were also measured at the time of collection as well as during the duration of each nutrient addition experiment. DOM composition and source characterization were measured on 0.45 um-filtered water samples collected during each site collection and stored in amber HDPE containers. Triplicate samples were collected at each site and refrigerated (4 °C) until analysis using excitation-emission matrix fluorescence spectroscopy. Fluorescence excitation-emission matrices (EEMs) were collected with a Horiba Aqualog (Jobin Yvon Horiba, France) using the methods of Yamashita et al. (2010). EEMs were collected on room temperature samples every 3 nm over excitation wavelength intervals between 240 and 455nm, and an emission wavelength range of ex + 10 nm to ex + 250 nm in a 1 cm quartz cuvette. EEMs were corrected for instruments optics, Raman normalized, and blank subtracted using MATLAB version 2019 software. We calculated several fluorescence indices of DOM composition including a fluorescence index (FI) indicating proportion of microbial DOM sources, biological index (BIX) indicating proportion of recently produced DOM, and humification index (HIX) indicating proportion of terrestrial derived DOM Jaffé et al. (2008). We also calculated the specific ultraviolet absorbance at a wavelength of 254

nm ($SUVA_{254}$) which provides a measure of the relative amount of chromophoric C in a sample and is correlated with percent aromaticity of DOM (Weishaar et al.; 2003). Spectral slopes were calculated for two primary wavelength ranges ($S_{275-295}$, $S_{350-400}$) using nonlinear least-squares fit for each spectral range where higher S values indicate low molecular weight or decreasing aromaticity (Hansen et al.; 2016). Spectral slope ratio (SR) was calculated as $S_{275-295}$ divided by $S_{350-400}$ where ratios are negatively correlated to DOM molecular weight (Helms et al.; n.d.).

4.3.4 Whole System Nutrient Addition Experiments

We measured whole-column nutrient uptake in isolated wetland pools using a modified nutrient addition method (Forshay and Stanley; 2005) and calculations derived from Wollheim et al., 2014. Wetland pools were small areas of inundation that were disconnected from surface flow in the larger wetland. Wetlands ranged in length of water residence time (0.5 - 8 hours) and amount of P limitation ranging in molar N:P ratios from 110 to 2954 (Table 1). Water-column nutrient uptake of $NO3^-$, $NH4^-$, and SRP was measured using short-term additions (based on estimated residence time) of reactive solutes with a conservative tracer using standard methods (Wollheim et al.; 2014). Residence times were estimated from wetland pool dimensions and depletion of a conservative tracer (Cl^-) over the course of 8h. Residence times were used to calculate a solute breakthrough curve (Covino et al.; 2010) and determine the timing and total number of samples needed for each addition experiment. Background solute concentrations of $NO3^-$, $NH4^+$, and SRP were sampled in each wetland and used to calculate the amount of solute added to each chamber. We increased dissolved inorganic N (DIN; $NO3^-$ + $NH4^+$) 2 times and soluble reactive phosphorus (SRP) 4 times above ambient concentrations. Solutions were

prepared with the corresponding amount of $KNO3^{-}$ and KPO_4^3 for each wetland along with a conservative tracer (Cl^{-}). In each wetland, the solution was applied to the surface using a backpack sprayer and subsampled from the center across the breakthrough curve, or depletion of the conservative tracer (n = 12-20). We continuously collected 60-mL grab samples until the conservative tracer reached a constant concentration. Samples were stored on frozen until analysis. We quantified dissolved inorganic N ($NO3^{-}$ + $NH4^{+}$) using the phenol-hypoclorite colorimetric method (Solorzano, 1967) and SRP using the ascorbic acid method (Murphy and Riley; 1962) followed by colorimetric analysis with a flow injection analyzer (Quikchem 8100, Lachat Instruments, Milwaukee, Wisconsin, USA).

4.3.5 Water-Column Nutrient Addition Experiments

We quantified water-column NO3-, NH4+, and SRP uptake rates using chamber incubations in the laboratory following standard methods (Harrison et al.; 1989). Triplicate 1-L glass containers were filled with surface water from each of 9 wetland sites. As in the previous experiment, nutrient amendment solutions were created to increase DIN by 2 times and SRP by 4 times above ambient. Subsamples (60 mL) subsamples were collected and filtered (0.45-µm Millipore, City, Country) at hours 0, 1, 2, 3, 4, 6, and 8. Chambers were agitated prior to each sampling to ensure homogeneity of sample. We repeatedly collected 60-mL grab samples until the conservative tracer reached a constant concentration. Samples were stored on frozen until analysis following the analytical procedures outlined above.

4.3.6 Calculation of Nutrient Uptake

We calculated maximum nutrient uptake (U_{vol}) using a modified Tracer Additions for Spiraling Curve Characterization (TASCC) approach, substituting time for distance (Wollheim et al.; 2014). Time-specific uptake rates (k_w; h^{-1}) were calculated for each time point of collection: kw = [ln(N - N addition)/Cl addition) - (ln(N - N baseline)/Cl baseline)]/ T (1) where N - Naddition and Claddition are the concentrations of solute and tracer in the addition solution (mg L^{-1}), N - Nbaseline and Clbaseline and the background corrected solute and tracer concentrations (mg L^{-1}), and T is the time since initial nutrient addition (h). Uptake velocity (v_f; cm h^{-1}) for each time point was also calculated as: $v_f = k_w$ * h (2) where v_f represents biological demand relative to baseline nutrient concentrations (m h $^{-1}$.) and h is the mean depth of the wetland pool (cm). To compare uptake velocities across wetlands, we standardized values to unite of m $year^{-1}$. We accounted for dilution based on the disappearance of the Cl^- tracer indicating the physical exchange of surface and subsurface water, less removal from the wetland itself. Velocities were related to the geometric mean solute concentration for each sample point: N - Ngeomean = (N - N_{obs} * N - N_{cons}) (3) where N - N_{obs} is the observed time-specific solute concentration and N - N_{cons} is the time-specific solute concentration expected from dilution only, calculated as [Cl_{obs} * N - N-addition- Cl-addition]. Total areal uptake was calculated for each time point and represents combined oxic -anoxic processes (assimilation and denitrification): U = v_f * N - Ngeomean *1000 (4) We evaluated first-order kinetics of nutrient uptake across wetlands (Newbold et al.; 1983). We calculated maximum nutrient uptake (U_{vol}) using the linear form of the exponential model: ln Nx = ln N_0 - ax (5) where N_0 is the initial nutrient concentration at the application site, N_0 is the nutrient concentration at time point (x). We assumed that gross uptake over the study period approximates total net system uptake capacity

at elevated concentrations. This was, in part, validated by approaching saturation in most wetland sites without actually reaching total nutrient saturation.

4.3.7 Statistical Analyses

We used one-way analysis of variance (ANOVA) to test general differences in distributions of NO3-, NH4 and SRP ambient concentrations across sites followed by Tukey's Honest Significant Difference (HSD) tests. For the majority of uptake experiments, we evaluated uptake kinetics using a first order decay function. In cases of low ambient nutrient concentrations, linear correlations were used without indication of nutrient saturation. For all other cases of non-linearity, we tested the fit of second-order, nonlinear, or efficiency-loss (EL) curves. EL is the dominant form of uptake kinetics in small aquatic fluvial systems (i.e., rivers, streams) that experience chronic nitrate inputs (O'Brien et al.; 2007; Hall et al.; 2013; Wollheim et al.; 2014).

We built structural equation models (SEM) to estimate hypothesized correlations between landscape variables, nutrient concentrations, DOM fluorescence metrics, and nutrient uptake kinetics (Fig. 4.2). Our goal was to quantify landscape and wetland specific variables to explain variation in nutrient uptake metrics across a gradient of watershed imperviousness. We chose to use SEM instead of traditional statistical comparisons because it allows for specific system-level network hypotheses and a suite of covariates (Schweiger et al.; 2016). We tested the fit of the conceptual model to predict water column (WC) and whole system (WS) $NO3^{-}$ and SRP uptake using maximum likelihood estimation. We used 12 predictor variables that include breakdown rates (k), uptake velocity (v_f), and maximum uptake (U_{vol}; Fig. 4.2). We included water column k, vf, and U_{vol} as covariates nested in the larger whole system model to account for the proportional influence of uptake in the water column alone.

Non-significant parameter estimates were excluded from the models to reduce model overfitting and maximize parsimony. We evaluated the several performance metrics of each model including chi-square goodness of fit, CFI, RMSEA, and Akaike's Information Criterion (AIC). We incorporated both study years (2018, 2020) in the whole system uptake model as well as triplicate samples collected in 2020 for the laboratory uptake model. An alpha value of 0.05 for significance was used for all observations and statistical analyses were conducted using Python programming language (Python 3.6.0).

4.4 Results

4.4.1 Water Chemistry and Environmental Characteristics

Ambient DOC and nutrient concentrations differed in wetlands across the gradient of imperviousness. NO3- concentrations were consistently high in the most urbanized catchments in both with mean concentrations of 2.34 mg L-1 while SRP concentrations were exceedingly low leading to significant P limitation (Table 1,2). $NH4^+$ concentrations ranged from 20 to 735 µg L^{-1} across sites with highest concentrations in wetlands of low impervious natural catchments. DOC concentrations decreased with percent imperviousness (one-way ANOVA, $F_{2,15} = 6.86$, $P < 0.01$; Fig. 4.3). N:P was different among groups of imperviousness ($F_{2,15}$=3.76, $P < 0.05$) and greatest N:P was observed in watersheds with medium imperviousness. Although watershed area decreased with imperviousness, individual pool volume remained relatively consistent across sites (Table 1). Vegetation was dominated by five macrophyte species including *Juncus acutiflorus*, *Ranunculusr Repens*, *Schoenoplectus califrnicus*, *Lotus pedunculatus*, and *Holcus lanatus* (Table S1). *Juncus acutiflorus* dominated indi-

vidual species counts while *Lotus pedunculatus* was represented at all wetland sites. Vegetation density and species richness increased with imperviousness ($R^2 = 0.57$; $R^2 = 0.37$; $P < 0.05$). Individual species counts were not included in statistical comparison of nutrient uptake metrics.

4.4.2 DOM Composition

DOM composition was variable across sites and levels of imperviousness (Fig. 4.3). FI tended to increase with imperviousness (F=3.76, df=2,15, $p < 0.05$). HIX and BIX were not significantly different across sites, suggesting a mixture of terrestrial derived OM and labile, proteinaceous DOM at all sites. $SUVA_{254}$, an indicator of aromaticity, ranged from 0.87 to 7.16 L mg^{-1} m^{-1} and greatest $SUVA_{254}$ values were observed in moderately urbanized watersheds (Table 2). SR values, an indication of DOM molecular weight, were variable across wetlands (0.56-0.90) with lowest values at the least urbanized sites (Table 2). Overall, we found that fluorescence indicators of DOM quality (BIX and FI) were highly correlated with ambient concentrations of $NO3^-$, $NH4^+$, and SRP, whereas indicators of low molecular weight, recalcitrant DOM (HIX and S_R) strongly correlated with DOC.

4.4.3 Comparing Water-Column and Whole-System Nutrient Uptake

At the whole system level, first-order loss rates (k) of NO3- varied significantly among sites. NO3- k at the whole system level ranged from 0.066 to 12.264 h^{-1} and SRP k ranged from 0.032 to 26.662 h^{-1} (Table 4.3). NO3- k increased with imperviousness, but SRP k did not differ with imperviousness. Water column k exhibited

a similar range for NO3 (0.769 – 13.155 h^{-1}), but SRP k was an order of magnitude smaller (0.001 – 0.284 h^{-1}) compared to whole system uptake (Table 4.3). Of the 36 samples measured for water column k, we were unable to measure significant uptake of SRP in 4 samples. Samples with no significant SRP uptake were at sites with low ambient SRP and high ambient NO3- concentrations. Uptake velocity (v_f), representing nutrient demand relative to concentration, were variable between solutes NO3- (2.59 ± 3.42) and SRP (± 2.77 ± 6.61). Greatest NO3- and NH4+ demand was seen in high impervious catchments (Table 4). We observed considerable variability in v_f among sites, but was less variable than U_{vol}, suggesting that differences in U_{vol} were driven by ambient concentrations of N and P. Consequently, v_f showed a strong negative correlation with increasing P-limitation (N:P molar ratio) in whole-system nutrient additions. Measurements of v_f were not comparable with water-column experiments as ex situ chamber incubations did not accurately represent differences in pool depth. Water column volumetric uptake (U_{vol}) varied significantly between sites and among solutes (Fig. 4.4. Maximum daily uptake of $NO3^-$ (U_{vol}-NO3; 0.001 – 2.63 mg $NO3^-$ m^{-3} d^{-1}) was an order of magnitude greater than SRP (U_{vol}-SRP; 0.0001 – 0.0463 mg SRP m^{-3} d^{-1}). U_{vol}-SRP ranged from 0.002 to 1.776 mg $NH4^+$ m^{-3} d^{-1}. A first order decay model was used to fit the data for uptake measurements of significant linear decline in concentration and report average R^2 values of 0.54, and 0.63 for $NO3^-$ and SRP, respectively. The highest uptake estimates of U_{vol}-NO3 (13.155 m^{-3} d^{-1}) and U_{vol}-SRP (0.284 m-3 d-1) were recorded in small, high impervious catchments (Fig. 4.4). Interestingly, U_{vol}-NO3 was greater in the water column compared to the whole system level (Fig. 4.4), likely due to the increased U_{vol}-NH4 in whole system experiments.

4.4.4 Stoichiometric Controls on Nutrient Uptake

Nutrient ratios of N:P were important predictor variables of whole-system level uptake, particularly SRP, across all wetlands. Interestingly, stoichiometric ratios were positively correlated with increasing % imperviousness, likely due to differences in site-specific SRP removal (assimilatory vs. dissimilatory) at the catchment scale. Uptake of NO3- and NH4 were tightly coupled in whole-system measurements but this relationship did hold true in the water column due to variable rates of uptake velocity (v_f). SRP uptake was also strongly (positively) correlated with both $NO3^-$ and $NH4^+$ uptake ($R^2 = 0.73$, $P < 0.05$) at the whole-system level suggesting that higher SRP is supported by NO3- concentrations is receiving waters. Overall, greatest SRP uptake (U_{vol}) occurred in severely P-limited wetland pools (N:P molar ratio > 2500), whereas wetlands exhibiting moderate P-limitation (> 108) did not significantly correlate with other solute uptake metrics, but did correlate with total N and P concentration ($P = 0.05$; $P = 0.04$, respectively).

4.4.5 Structural Equation Models

Structural equation modeling identified causal relationships between predictor variables and whole-system nutrient uptake metrics. The resulting NO3- and SRP models were consistent with the data and performed well (NO3- χ^2 test $P = 0.36$, df = 78; Fig. 4.5) (SRP χ^2 test $P = 0.08$, df = 78; Fig. 4.6) explaining 73.53% and 69.38% of the variance in Uvol, respectively (Table 4). Ambient nutrient concentrations of $NO3^-$ were negatively correlated (0.67, -1.39) with k $NO3^-$, but was not correlated for SRP, suggesting strong influence of stoichiometric ratios and exogenous factors on SRP uptake (Figs. 4.5, 4.6). DOC concentrations were not significantly correlated with U_{vol} of $NO3^-$ or SRP, suggesting the composition of carbon is more

influential on uptake than is concentration. DOC was also negatively correlated with N:P ratios in both models (Fig. 4.5, 4.6). Imperviousness was positively correlated with k NO3- (0.42) although not correlated with k SRP. Water column UNO3 was negatively correlated with v_f, representing nutrient demand, of both $NO3^-$ (-0.45) and SRP (-0.35). Additionally, water-column breakdown rates (k) were a significant predictor variable of SRP k at the whole system level (1.23; Fig. 4.6). Water column U_{SRP} was positively correlated with HIX (0.28) and BIX (0.10), but not correlated with any uptake metrics at the whole system level. SR, with larger values representing lower molecular weight of DOM, was positively correlated with water column k NO3- (0.16), U_{vol} $NO3^-$ (0.21), and k SRP (0.13). Not all metrics of DOM composition (HIX, BIX, FI) at the whole system level were significant in this model, perhaps because of a large degree of variance in measurement during limited time scales.

4.5 Discussion

Using a comparative approach of water-column and whole-system nutrient uptake dynamics, we measured significant proportions of water-column nutrient uptake compared to system level removal. We observed that water column nutrient uptake represents a significant portion of total uptake, particularly in wetlands with nutrient limiting conditions, high DOC concentrations and autochthonous DOM. Further, increases in labile DOM appear to correlate with elevated uptake of SRP while water column conditions that support transformation of inorganic N correlate with increased NO3- uptake. Overall, our findings correspond with similar studies of whole-system uptake in natural riparian wetlands (Wollheim et al.; 2014), but we provide newfound estimates of significant water column uptake in urban-

ized wetlands. We estimated a significant proportion of total uptake was driven by water column processes that are mediated by N:P molar ratios and DOM composition. Here, we discuss the details of these relationships and how findings signify the importance of water-column nutrient uptake in relation to whole-system nutrient dynamics.

4.5.1 DOM characteristics as predictors of water-column nutrient uptake

We found strong influence of DOC concentration and DOM composition on nutrient demand and maximum uptake at all sites, particularly in the water column. We found that fluorescence indices of DOC quality (BIX and FI) were strongly related to the availability of NO3- and SRP across all study wetlands. Overall, DOC composition interacts with v_f to a stronger degree than Uvol, where DOC concentrations are the strongest limiting factor. BIX and FI were also important predictors of both the velocity and magnitude of $NH4^+$ and SRP uptake in the water column and not at the whole-system level. The range of FI in the water column (1.43-1.98) represent a significant range with greater FI values at the most urban sites compared to other aquatic ecosystems (Table 2). Higher FI in urban wetlands may prime DOM for microbial processing, increasing rates of turnover and demand for $NH4^+$ and SRP where uptake occurs. The priming effect observed here is consistent with previous studies showing increased autochthonous DOM bioavailability and quick conversion of N from inorganic to organic forms with increasing urbanization (McElmurry et al.; 2014; Hosen et al.; 2014). Although these fluorescence metrics were not significant predictors of nutrient uptake at the whole system level, low-molecular weight DOM (S_R) was positively correlated with uptake of $NO3^-$ and SRP in the water column.

These results suggest that DOM composition plays a role in mediating water column uptake while benthic processes and other site specific factors, including vegetation type and density and redox potential, control uptake at the system level. Our findings partially support the first and second hypotheses that greater uptake occurs in urban wetlands primarily due to increased production of microbially sourced DOM, as seen in other studies (Thouin et al.; 2009; Robbins et al.; 2017). Further, we demonstrate how indices of DOM quality can be used to reasonably predict nutrient uptake capacity in the water column of urban wetlands.

4.5.2 Environmental and Stoichiometric Controls on Nutrient Uptake

Relationships among solute uptake and concentration may be strongly affected by seasonal patterns of precipitation and discharge. Nutrient addition experiments were conducted during the transition from wet to dry season, a period typified by high water levels and short water residence time that influence gross primary production and aquatic ecosystem respiration (Gibson et al.; 2015). It is likely that relationships among nutrient loading and subsequent nutrient uptake are strongest during the wet season and shortly thereafter, compared to the dry season when there is less lateral hydrologic connectivity (Griffiths and Mitsch; 2017). Similarly, physical conditions of temperature, dissolved oxygen, and pH likely exert strong control over rates of microbial metabolism, particularly in summer months. When biological activity in the water column is high, elemental stoichiometric requirements of biological uptake processes are likely to link N and P uptake through tightly coupled co-limitation (Gibson and O'Reilly; 2012; Hall et al.; 2013). Therefore, uptake measurements

during periods of high hydrologic turnover may best approximate actual nutrient uptake capacity.

Generally, solute uptake was tightly coupled with ambient concentrations and Uvol of other nutrients. In most cases, NO3- uptake was tightly correlated with SRP. uptake suggesting short-term potential alleviation of P limitation. There was no apparent correlation of N:P molar ratios with uptake capacity in the water column alone. Interestingly, neither SRP nor NO3- reached full saturation despite exceedingly high total concentrations (> 5 mg L^{-1}). Cases of significant linear uptake kinetics over short time periods may result from alleviation of other limiting factors including light availability, water depth, or ecosystem respiration in reference to biological (microbial) activities. Although we did not measure these factors in this study, it is important to note the influence of site-specific landscape controls on nutrient uptake, especially at the whole-system level.

Ambient nutrient concentrations and elemental stoichiometry were significant predictor of the rate and magnitude of uptake in the water column and whole system level. High demand for both NO3- and SRP suggest strong co-limitation in Valdivian wetlands, signified by a tight coupling of ambient N:P molar ratios and uptake rate. Yet, a consistent lack of relationship between uptake velocity and single nutrient concentration suggests that site-specific biological and physical variations in the wetland itself may overwhelm the uptake response and biological communities may respond differentially to change in nutrient loads (Gibson et al.; 2015). Changes in the relative composition and availability of nutrients (NO3- : NH4) may also contribute to the weak relationship between uptake velocity and concentration.

4.5.3 Wetlands as Urban Watershed Biogeochemical Control Points

The role of urban wetlands as nutrient sources or sinks depends on the differential capacity for water column versus whole system uptake of excess nutrients. As urbanization increases, wetland coverage decreases, residence time shortens, and nutrient loading rates become more dependent on seasonal runoff from impervious surfaces. Such urban wetlands rely on optimal nutrient concentrations and water column conditions (e.g., light, dissolved oxygen, vegetation) to transform or sequester carbon and nutrients over short time periods. Our study highlights the significant capacity for nutrient uptake in the water column on short time scales, relative to the whole system level. However, the rate and volumetric uptake of N and P is highly dependent upon stoichiometric relationships of C:N:P and the chemical compositions and/or autochthonous versus allochthonous DOM. Despite relatively low concentrations of DOC in urbanized wetlands, increases in low-molecular weight DOM, as evidenced by high SR values, are needed to stimulate removal of nutrients, particularly N, at exceedingly high concentrations. In this study, we found that the total reactive surface area of wetlands (i.e., both water column and benthic sediments) combined with alleviation of P limitation were vital for wetlands to remove nutrients without reaching total saturation. This information is critical to support effective nutrient removal in urban wetlands with short water residence time where microbially-sourced DOM supports rapid conversion of N and P from inorganic to organic forms and removal from the system. These findings highlight the importance of understanding the relationships between catchment scale landscape characteristics and DOM – nutrient composition to elucidate the timing and magnitude of nutrient uptake in urban wetland ecosystems. A mechanistic understanding of the

controls on nutrient uptake from urban wetlands is essential for efficient water quality mitigation in response to urban stormwater pollution.

4.5.4 Implications for Urban Wetland Management

Results of this study suggest that current estimates of nutrient removal in urban wetlands are underestimated and less well understood compared to non-urban wetlands. Traditionally, there has been a focus on the importance of benthic nutrient processing in assessing whole-system nutrient uptake rather than with isolated measurements of water column uptake (Alexander et al.; 2007). Although benthic processes are likely to drive total uptake capacity, microbially-driven nutrient processing in the water column of urban wetlands is likely higher than natural wetlands due to a greater proportion of bioavailable dissolved nutrients and relatively short water residence time (< 4 h).

Most non-constructed urban wetlands are optimized for flood mitigation and stormwater management, but few are altered to maximize water column nutrient removal rates. Results of this study suggest that optimal vegetation type and density, seasonal water residence time, and relative location within the larger watershed are all critical factors in determining nutrient uptake capacity. Most importantly, the spatial distribution and composition of small wetlands along a hydrologic network will influence how network-scale N and P fluxes respond to increased non-point N loading from urbanization and changes in climate variability (Wollheim et al.; 2014). For example, increasing the number and spatial coverage of smaller headwater wetlands can improve total reactive surface area in the watershed, increase lateral hydrologic connectivity, and improve watershed scale efficiency of N or P removal. Results of this study provide evidence for the need to identify thresholds for various

hydrologic and landscape variables beyond which water column and/or whole system nutrient uptake can be increased. Further investigation on the specific transformative pathways that determine the ultimate fate of nutrients in exported waters is needed to validate the biogeochemical value of urban wetlands.

4.6 Conclusions

In this study, we build upon our understanding of nutrient uptake in aquatic ecosystems and show how wetland nutrient uptake compares to lake and stream/river nutrient uptake capacities. Our results indicate that wetlands are able to function under different nutrient loading conditions because of the hydrological, organic matter storage, and biogeochemical differences between wetlands and other aquatic ecosystems. Specifically, urban wetlands show great capacity for nutrient uptake in the water column and represents a significant portion of total uptake. Further, we show that increases in the stoichiometric availability of labile carbon can stimulate sequestration of nitrate and phosphorus in nutrient-polluted or nutrient-limited urban wetlands. Given the modular nature of urban wetlands, the ability to modify water residence time and nutrient and organic matter delivery may maximize nutrient processing and uptake rates compared to natural wetlands. However, further investigation on the specific transformative pathways that determine the ultimate fate of nutrients in exported waters is needed to validate the true biogeochemical value of urban wetlands.

4.7 Bibliography

Alexander, R. B., Boyer, E. W., Smith, R. A., Schwarz, G. E. and Moore, R. B. (2007). The role of headwater streams in downstream water quality, *Journal of the American Water Resources Association* **43**: 41–59.

Ashkenas, L. R., Johnson, S. L., Gregory, S. V., Tank, J. L. and Wollheim, W. M. (2004). A stable isotope tracer study of nitrogen uptake and transformation in an old-growth forest stream, *Ecology* **85**(6): 1725–1739.

Asmala, E., Autio, R., Kaartokallio, H., Pitkänen, L., Stedmon, C. and Thomas, D. (2013). Bioavailability of riverine dissolved organic matter in three baltic sea estuaries and the effect of catchment land use, *Biogeosciences* **10**(11): 6969–6986.

Battin, T. J., Kaplan, L. A., Findlay, S., Hopkinson, C. S., Marti, E., Packman, A. I., Newbold, J. D. and Sabater, F. (2008). Biophysical controls on organic carbon fluxes in fluvial networks, *Nature geoscience* **1**(2): 95–100.

Bechtold, H. A., Marcarelli, A. M., Baxter, C. V. and Inouye, R. S. (2012). Effects of n, p, and organic carbon on stream biofilm nutrient limitation and uptake in a semi-arid watershed, *Limnology and Oceanography* **57**(5): 1544–1554.

Bernhardt, E. S. and Likens, G. E. (2002). Dissolved organic carbon enrichment alters nitrogen dynamics in a forest stream, *Ecology* **83**: 1689–1700.

Bernot, M. J., Tank, J. L., Royer, T. V. and David, M. B. (2006). Nutrient uptake in streams draining agricultural catchments of the midwestern united states, *Freshwater Biology* **51**(3): 499–509.

Cheng, F. Y. and Basu, N. B. (2017). Biogeochemical hotspots: Role of small water bodies in landscape nutrient processing, *Water Resources Research* **53**: 5038–5056.

Coble, A. A., Marcarelli, A. M., Kane, E. S. and Huckins, C. J. (2016). Uptake of ammonium and soluble reactive phosphorus in forested streams: influence of dissolved organic matter composition, *Biogeochemistry* **131**: 355–372.

Covino, T. P., McGlynn, B. L. and McNamara, R. A. (2010). Tracer additions for spiraling curve characterization (tascc): Quantifying stream nutrient uptake kinetics from ambient to saturation, *Limnology and Oceanography: methods* **8**(9): 484–498.

Ehrenfeld, J. G. (2000). Evaluating wetlands within an urban context, **4**: 69–85.

Ensign, S. H. and Doyle, M. W. (2006). Nutrient spiraling in streams and river networks, *Journal of Geophysical Research: Biogeosciences* **111**(G4).

Fink, D. F. and Mitsch, W. J. (2004). Seasonal and storm event nutrient removal by a created wetland in an agricultural watershed, *Ecological Engineering* **23**: 313–325.

Fork, M. L., Osburn, C. L. and Heffernan, J. B. (2020). Bioavailability and compositional changes of dissolved organic matter in urban headwaters, *Aquatic Sciences* **82**.

Forshay, K. J. and Stanley, E. H. (2005). Rapid nitrate loss and denitrification in a temperate river floodplain, *Biogeochemistry* **75**: 43–64.

Ghosh, S. and Leff, L. G. (2013). Impacts of labile organic carbon concentration on organic and inorganic nitrogen utilization by a stream biofilm bacterial community, *Applied and Environmental Microbiology* **79**: 7130–7141.

Gibson, C. A. and O'Reilly, C. M. (2012). Organic matter stoichiometry influences nitrogen and phosphorus uptake in a headwater stream, *Freshwater Science* **31**: 395–407.

Gibson, C. A., O'Reilly, C. M., Conine, A. L. and Lipshutz, S. M. (2015). Nutrient uptake dynamics across a gradient of nutrient concentrations and ratios at the landscape scale, *Journal of Geophysical Research G: Biogeosciences* **120**: 326–340.

Griffiths, L. N. and Mitsch, W. J. (2017). Removal of nutrients from urban stormwater runoff by storm-pulsed and seasonally pulsed created wetlands in the subtropics, *Ecological Engineering* **108**: 414–424.

Hall, R. O., Baker, M. A., Rosi-Marshall, E. J., Tank, J. L. and Newbold, J. D. (2013). Solute-specific scaling of inorganic nitrogen and phosphorus uptake in streams, *Biogeosciences* **10**: 7323–7331.

Hansen, A. M., Kraus, T. E., Pellerin, B. A., Fleck, J. A., Downing, B. D. and Bergamaschi, B. A. (2016). Optical properties of dissolved organic matter (dom): Effects of biological and photolytic degradation, *Limnology and Oceanography* **61**: 1015–1032.

Harrison, P. J., Parslow, J. S. and Conway, H. L. (1989). Determination of nutrient uptake kinetic parameters: a comparison of methods, *Source: Marine Ecology Progress Series* **52**: 301–312.

Helms, J. R., Stubbins, A., Ritchie, J. D., Minor, E. C., Kieber, D. J. and Mopper, K. (n.d.). Helms, j.r., et al. absorption spectral slopes and slope ratios as indicators of molecular weight, source, and photobleaching of chromophoric dissolved organic matter. limnol. oceanogr., 53(3), 2008, 955–969.

Heusser, C. J. (1976). Palynology and depositional environment of the río ignao nonglacial deposit, province of valdivia, chile, *Quaternary Research* **6**(2): 273–279.

Hogan, D. M. and Walbridge, M. R. (2007). Urbanization and nutrient retention in freshwater riparian wetlands, *Ecological Applications* **17**: 1142–1155.

Hosen, J. D., McDonough, O. T., Febria, C. M. and Palmer, M. A. (2014). Dissolved organic matter quality and bioavailability changes across an urbanization gradient in headwater streams, *Environmental Science and Technology* **48**: 7817–7824.

Howarth, R. W., Billen, G., Swaney, D., Townsend, A., Jaworski, N., Lajtha, K., Downing, J. A., Elmgren, R., Caraco, N., Jordan, T. et al. (1996). Regional nitrogen budgets and riverine n & p fluxes for the drainages to the north atlantic ocean: Natural and human influences, pp. 75–139.

Jaffé, R., McKnight, D., Maie, N., Cory, R., McDowell, W. and Campbell, J. (2008). Spatial and temporal variations in dom composition in ecosystems: The importance of long-term monitoring of optical properties, *Journal of Geophysical Research: Biogeosciences* **113**(G4).

Johnson, L. T., Tank, J. L. and Arango, C. P. (2009). The effect of land use on dissolved organic carbon and nitrogen uptake in streams, *Freshwater Biology* **54**: 2335–2350.

Johnston, C. A., Bubenzer, G., Lee, G., Madison, F. and Mc Henry, J. (1984). Nutrient trapping by sediment deposition in a seasonally flooded lakeside wetland.

Jordan, S. J., Stoffer, J. and Nestlerode, J. A. (2011). Wetlands as sinks for reactive nitrogen at continental and global scales: A meta-analysis, *Ecosystems* **14**: 144–155.

Kelso, J. E. and Baker, M. A. (2020). Organic matter is a mixture of terrestrial, autochthonous, and wastewater effluent in an urban river, *Frontiers in Environmental Science* **7**: 202.

Larson, J. H., Evans, M. A., Fitzpatrick, F. A., Frost, P. C., Bailey, S., Kennedy, R., James, W. F., Richardson, W. B. and Reneau, P. C. (2019). Water column nutrient processing rates in rivermouths of green bay (lake michigan), *Biogeochemistry* **142**: 73–93.

Larson, J. H., Frost, P. C., Xenopoulos, M. A., Williams, C. J., Morales-Williams, A. M., Vallazza, J. M., Nelson, J. C. and Richardson, W. B. (2014). Relationships between land cover and dissolved organic matter change along the river to lake transition, *Ecosystems* **17**.

Laterra, P., Booman, G. C., Picone, L., Videla, C. and Orúe, M. E. (2018). Indicators of nutrient removal efficiency for riverine wetlands in agricultural landscapes of argentine pampas, *Journal of Environmental Management* **222**: 148–154.

Lee, S. Y., Dunn, R. J., Young, R. A., Connolly, R. M., Dale, P. E., Dehayr, R., Lemckert, C. J., McKinnon, S., Powell, B., Teasdale, P. R. and Welsh, D. T. (2006). Impact of urbanization on coastal wetland structure and function, *Austral Ecology* **31**: 149–163.

McClain, M. E., Boyer, E. W., Dent, C. L., Gergel, S. E., Grimm, N. B., Groffman, P. M., Hart, S. C., Harvey, J. W., Johnston, C. A., Mayorga, E. et al. (2003). Biogeochemical hot spots and hot moments at the interface of terrestrial and aquatic ecosystems, *Ecosystems* pp. 301–312.

McElmurry, S. P., Long, D. T. and Voice, T. C. (2014). Stormwater dissolved organic matter: Influence of land cover and environmental factors, *Environmental Science and Technology* **48**: 45–53.

Mulholland, P. J. (1992). Regulation of nutrient concentrations in a temperate forest stream: Roles of upland, riparian, and instream processes, *Limnol. Oceanogr* **37**: 1512–1526.

Mulholland, P. J., Helton, A. M., Poole, G. C., Hall, R. O., Hamilton, S. K., Peterson, B. J., Tank, J. L., Ashkenas, L. R., Cooper, L. W., Dahm, C. N., Dodds, W. K., Findlay, S. E., Gregory, S. V., Grimm, N. B., Johnson, S. L., McDowell, W. H., Meyer, J. L., Valett, H. M., Webster, J. R., Arango, C. P., Beaulieu, J. J., Bernot, M. J., Burgin, A. J., Crenshaw, C. L., Johnson, L. T., Niederlehner, B. R., O'Brien, J. M., Potter, J. D., Sheibley, R. W., Sobota, D. J. and Thomas, S. M. (2008). Stream denitrification across biomes and its response to anthropogenic nitrate loading, *Nature* **452**: 202–205.

Murphy, J. and Riley, J. (1962). Determination of dissolved reactive phosphorus by the ascorbic acid method, *Anal Chim Acta* **27**: 31–36.

Newbold, J., Elwood, J., O'neill, R. and Sheldon, A. (1983). Phosphorus dynamics in a woodland stream ecosystem: a study of nutrient spiralling, *Ecology* **64**(5): 1249–1265.

Oviedo-Vargas, D., Royer, T. V. and Johnson, L. T. (2013). Dissolved organic carbon manipulation reveals coupled cycling of carbon, nitrogen, and phosphorus in a nitrogen-rich stream, *Limnology and Oceanography* **58**(4): 1196–1206.

O'Brien, J. M., Dodds, W. K., Wilson, K. C., Murdock, J. N. and Eichmiller, J. (2007). The saturation of n cycling in central plains streams: 15 n experiments across a broad gradient of nitrate concentrations, *Biogeochemistry* **84**(1): 31–49.

Palta, M. M., Grimm, N. B. and Groffman, P. M. (2017). "accidental" urban wetlands: ecosystem functions in unexpected places, *Frontiers in Ecology and the Environment* **15**(5): 248–256.

Parr, T. B., Cronan, C. S., Ohno, T., Findlay, S. E., Smith, S. M. and Simon, K. S. (2015). Urbanization changes the composition and bioavailability of dissolved organic matter in headwater streams, *Limnology and Oceanography* **60**: 885–900.

Patil, S., Covino, T. P., Packman, A. I., McGlynn, B. L., Drummond, J. D., Payn, R. A. and Schumer, R. (2013). Intrastream variability in solute transport: Hydrologic and geomorphic controls on solute retention, *Journal of Geophysical Research: Earth Surface* **118**: 413–422.

Reisinger, A. J., Tank, J. L., Rosi-Marshall, E. J., Hall, R. O. and Baker, M. A. (2015). The varying role of water column nutrient uptake along river continua in contrasting landscapes, *Biogeochemistry* **125**(1): 115–131.

Robbins, C. J., King, R. S., Yeager, A. D., Walker, C. M., Back, J. A., Doyle, R. D. and Whigham, D. F. (2017). Low-level addition of dissolved organic carbon increases basal ecosystem function in a boreal headwater stream, *Ecosphere* **8**(4): e01739.

Sable, K. A. and Wohl, E. (2006). The relationship of lithology and watershed characteristics to fine sediment deposition in streams of the oregon coast range, *Environmental Management* **37**: 659–670.

Schmadel, N. M., Harvey, J. W., Schwarz, G. E., Alexander, R. B., Gomez-Velez, J. D., Scott, D. and Ator, S. W. (2019). Small ponds in headwater catchments are a dominant influence on regional nutrient and sediment budgets, *Geophysical Research Letters* **46**: 9669–9677.

Schweiger, E. W., Grace, J. B., Cooper, D., Bobowski, B. and Britten, M. (2016). Using structural equation modeling to link human activities to wetland ecological integrity, *Ecosphere* **7**(11): e01548.

Singh, S., Dash, P., Silwal, S., Feng, G., Adeli, A. and Moorhead, R. J. (2017). Influence of land use and land cover on the spatial variability of dissolved organic matter in multiple aquatic environments, *Environmental Science and Pollution Research* **24**: 14124–14141.

Stelzer, R. S., Heffernan, J. and Likens, G. E. (2003). The influence of dissolved nutrients and particulate organic matter quality on microbial respiration and biomass in a forest stream, *Freshwater Biology* **48**(11): 1925–1937.

Stutter, M., Graeber, D. and Weigelhofer, G. (2020). Available dissolved organic carbon alters uptake and recycling of phosphorus and nitrogen from river sediments, *Water* **12**(12): 3321.

Tank, J. L., Rosi-Marshall, E. J., Baker, M. A. and Hall, R. O. (2008). Are rivers just big streams? a pulse method to quantify nitrogen demand in a large river, *Ecology* **89**(10): 2935–2945.

Tank, J. L., Rosi-Marshall, E. J., Griffiths, N. A., Entrekin, S. A. and Stephen, M. L. (2010). A review of allochthonous organic matter dynamics and metabolism in streams, *Journal of the North American Benthological Society* **29**(1): 118–146.

Thouin, J. A., Wollheim, W. M., Vörösmarty, C. J., Jacobs, J. M. and McDowell, W. H. (2009). The biogeochemical influences of no32, dissolved o2, and dissolved organic c on stream no32 uptake, *Journal of the North American Benthological Society* **28**: 894–907.

Verhoeven, J. T., Arheimer, B., Yin, C. and Hefting, M. M. (2006). Regional and global concerns over wetlands and water quality, *Trends in Ecology and Evolution* **21**: 96–103.

Weishaar, J. L., Aiken, G. R., Bergamaschi, B. A., Fram, M. S., Fujii, R. and Mopper, K. (2003). Evaluation of specific ultraviolet absorbance as an indicator of the chemical composition and reactivity of dissolved organic carbon, *Environmental Science and Technology* **37**: 4702–4708.

Williams, C. J., Frost, P. C., Morales-Williams, A. M., Larson, J. H., Richardson, W. B., Chiandet, A. S. and Xenopoulos, M. A. (2016). Human activities cause distinct dissolved organic matter composition across freshwater ecosystems, *Global Change Biology* **22**: 613–626.

Wollheim, W. M., Bernal, S., Burns, D. A., Czuba, J., Driscoll, C., Hansen, A., Hensley, R., Hosen, J., Inamdar, S., Kaushal, S. et al. (2018). River network saturation concept: factors influencing the balance of biogeochemical supply and demand of river networks, *Biogeochemistry* **141**(3): 503–521.

Wollheim, W. M., Harms, T. K., Peterson, B. J., Morkeski, K., Hopkinson, C. S., Stewart, R. J., Gooseff, M. N. and Briggs, M. A. (2014). Nitrate uptake dynamics of surface transient storage in stream channels and fluvial wetlands, *Biogeochemistry* **120**: 239–257.

Wollheim, W. M., Peterson, B. J., Thomas, S., Hopkinson, C. and Vörösmarty, C. (2008). Dynamics of n removal over annual time periods in a suburban river network, *Journal of Geophysical Research: Biogeosciences* **113**(G3).

4.8 Tables

Table 4.1: Physicochemical characteristics of urban wetland sites in Valdivia, Chile.

Site	% Imp[a]	Area (km^2)	Pool Volume (m^3)	DOC[b] (mg/L^{-1})	NO_3^--N[b] ($\mu g/L^{-1}$)	NH_4^+-N[b] ($\mu g/L^{-1}$)	SRP[b] ($\mu g/L^{-1}$)	Molar N:P
VAL1	12.16	10.60	15	3.43	2653	23	10	1458
VAL2	47.83	3.26	7.4	2.03	4094	207	46	246
VAL3	34.92	12.24	13	3.91	2	20	5	1181
VAL4	23.77	3.26	10	7.60	6	574	8	141
VAL5	0.04	1.63	76.4	2.55	236	44	18	588
VAL6	51.52	0.82	10.2	0.94	7	225	66	110
VAL7	48.32	0.84	10	3.31	2291	735	44	2954
VAL8	40.19	61.19	9.4	1.81	645	98	2	1109
VAL9	35.63	20.42	10.6	1.34	62	340	25	2104

[a]watershed percent imperviousness (% Imp)

[b]ambient dissolved organic carbon (DOC), nitrate (NO_3^--N), ammonium (NH_4^+-N), and soluble reactive phosphorus (SRP) concentrations

Table 4.2: Fluorescence excitation-emission matrices of dissolved organic carbon (DOC) in riparian wetlands.

Site	HIX	BIX	FI	$SUVA_{254}$ ($L\ mg^{-1}\ m^{-1}$)	Spectral Slope Ratio (S_R)	E2:E3
VAL1	6.50	1.53	1.69	7.29	0.72	5.66
VAL2	3.78	0.90	1.72	11.82	1.42	2.78
VAL3	2.27	1.93	1.78	2.81	0.61	4.59
VAL4	3.95	1.91	1.67	2.76	1.03	2.74
VAL5	4.28	1.39	1.73	3.53	0.76	4.78
VAL6	7.57	0.86	1.76	6.38	0.99	6.15
VAL7	2.65	3.07	2.05	1.51	0.93	5.13
VAL8	2.78	2.17	1.83	2.21	0.61	7.07
VAL9	5.34	1.43	1.87	8.21	1.07	5.92

Table 4.3: First-order loss rates (k; h-1) for field and water column uptake of nitrate ($NO3^{-}$), ammonium ($NH4^{+}$), and soluble reactive phosphorus (SRP) across a gradient of watershed imperviousness.

NO_3^- *k* (h^{-1})		NH_4^+ *k* (h^{-1})		SRP *k* (h^{-1})	
WS	*WC*	*WS*	*WC*	*WS*	*WC*
2.30 (3.40)	3.94 (4.24)	0.30 (0.38)	0.001 (0.001)	2.87 (6.40)	0.10 (0.11)

Loss rates for water column experiments are means (± 1SE) from replicate chambers ($n = 3$).

Table 4.4: Structural equation modeling fit statistics of whole system (WS) and water column (WC) uptake of nitrate ($NO3^{-}$) and soluble reactive phosphorus (SRP).

Model	χ^2	χ^2 p-value	CFI	RMSEA	AIC
WS+WC NO_3^-	109.49	0.34	0.980	0.052	87.57
WS+WC SRP	104.34	0.08	0.867	0.108	44.41

CFI = comparative fit index; RMSEA = root mean square error of approximation ; AIC = akaike information criteria

4.9 Figures

Figure 4.1. Wetland study locations along a gradient of imperviousness in Valdivia, Chile (n = 9).

Figure 4.2. Conceptual causal model linking land use and ambient biogeochemistry to nutrient uptake through direct and indirect links in shallow urban and non-urban wetlands.

Figure 4.3. Water chemistry and dissolved organic matter composition variables in wetlands represented by low, medium, and high levels of watershed imperviousness. Grey-scale shading used on boxplots to indicate increasing imperviousness. Describe the box plots (median, upper and lower quartiles, and 95% confidence intervals as error bars).

Figure 4.4. Comparison of whole system maximum (n=18) and water column (n=36) daily nutrient uptake (U_{vol}; mg m^{-3} d^{-1}) of (a) nitrate ($NO3^{-}$) and soluble reactive phosphorus (SRP) in wetlands along a gradient of watershed imperviousness. Circles represent mean values and error bars represent ± SD.

Figure 4.5. The best-supported model for nitrate (NO3-) in water column and whole system uptake experiments of wetlands along a gradient of imperviousness. Standardized coefficients are reported, and the sign of the coefficient indicates the direction of the correlation between variables. Nonsignificant variables and coefficients were not included in the model (P ¿ 0.05).

Figure 4.6. The best-supported model for soluble reactive phosphorus (SRP) in water column and whole system uptake experiments of wetlands along a gradient of imperviousness. Standardized coefficients are reported, and the sign of the coefficient indicates the direction of the correlation between variables. Non-significant variables and coefficients were not included in the model (P ¿ 0.05).

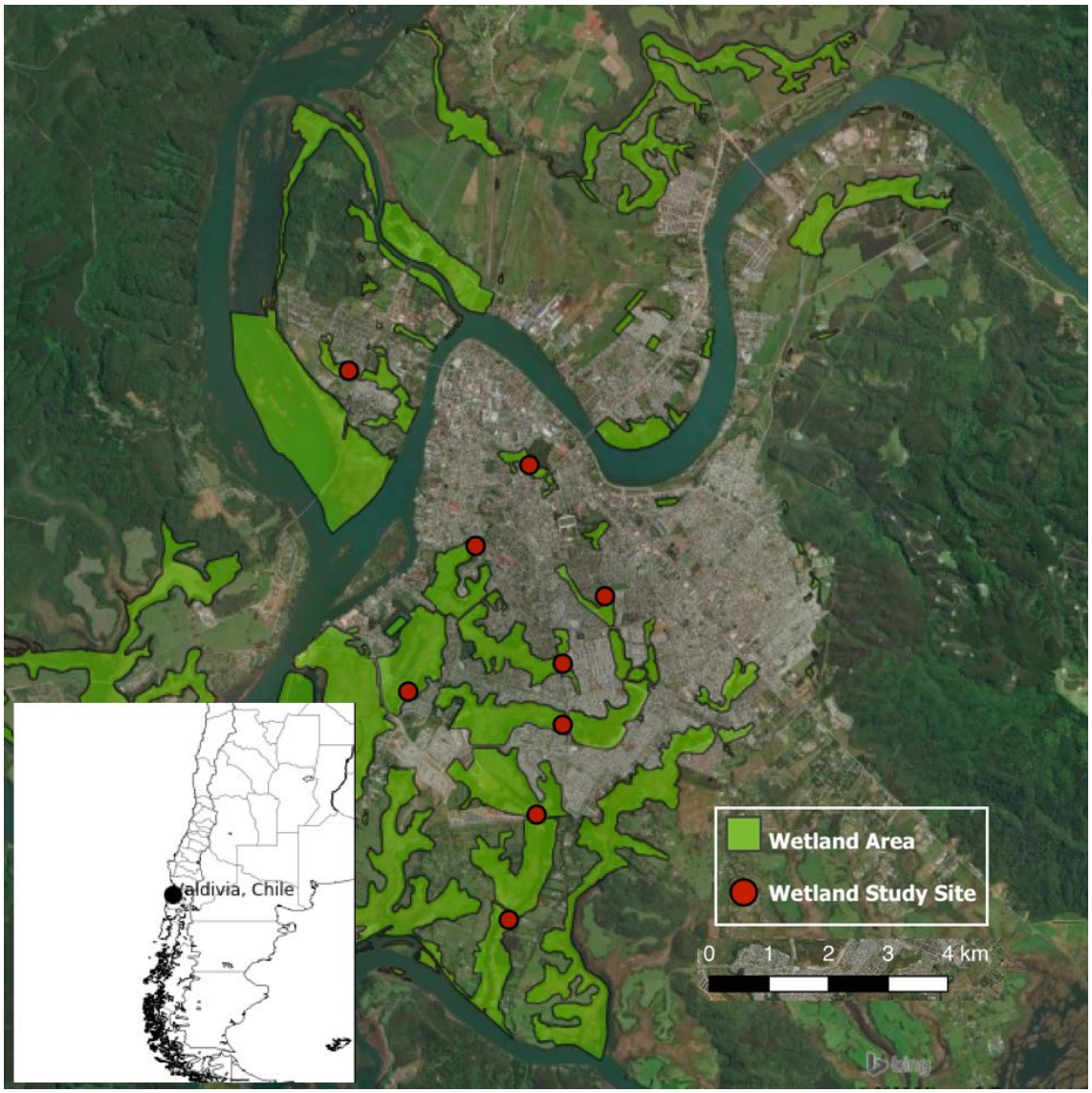

Figure 4.1: Wetland study locations along a gradient of imperviousness in Valdivia, Chile (n = 9).

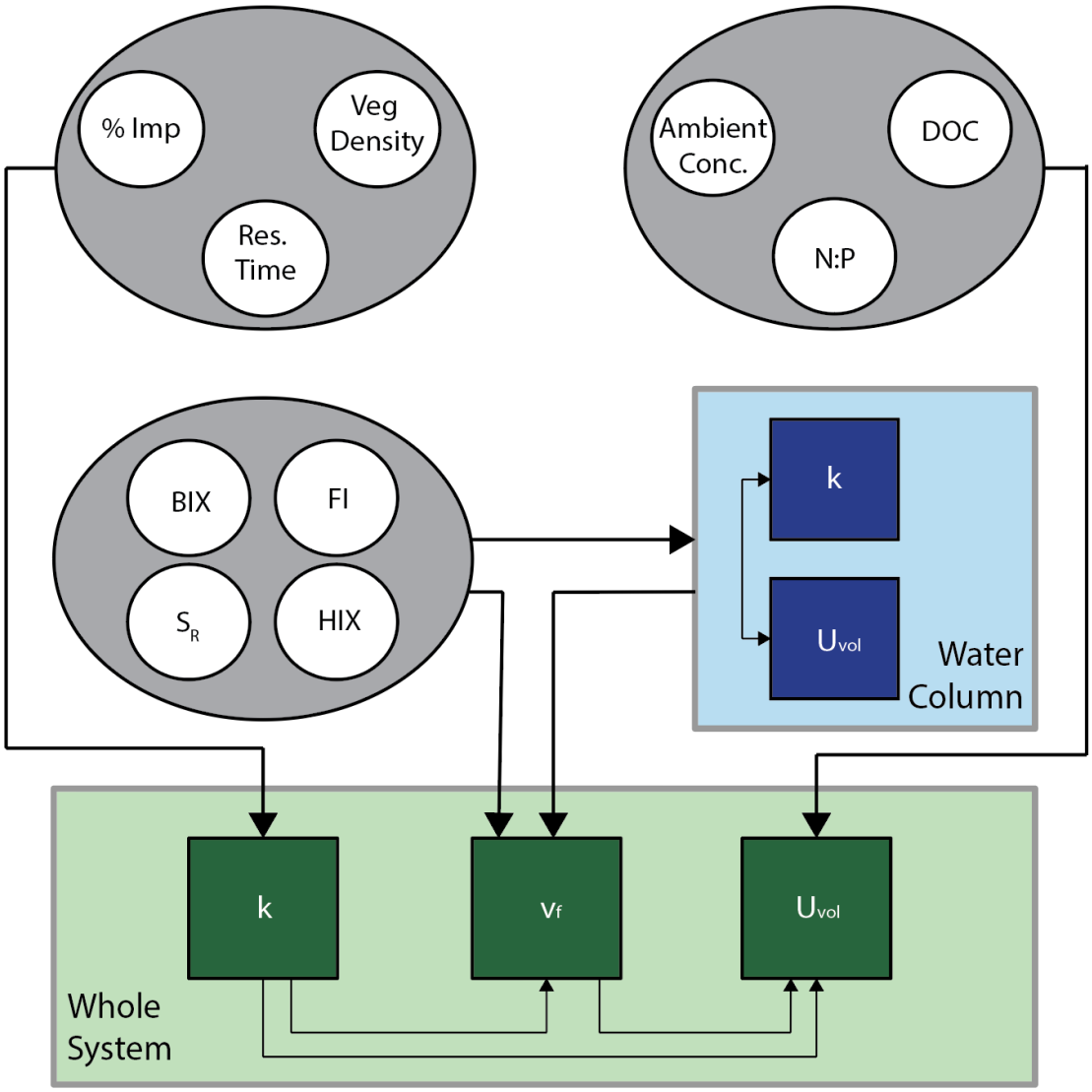

Figure 4.2: Conceptual causal model linking land use and ambient biogeochemistry to nutrient uptake through direct and indirect links in shallow urban and non-urban wetlands.

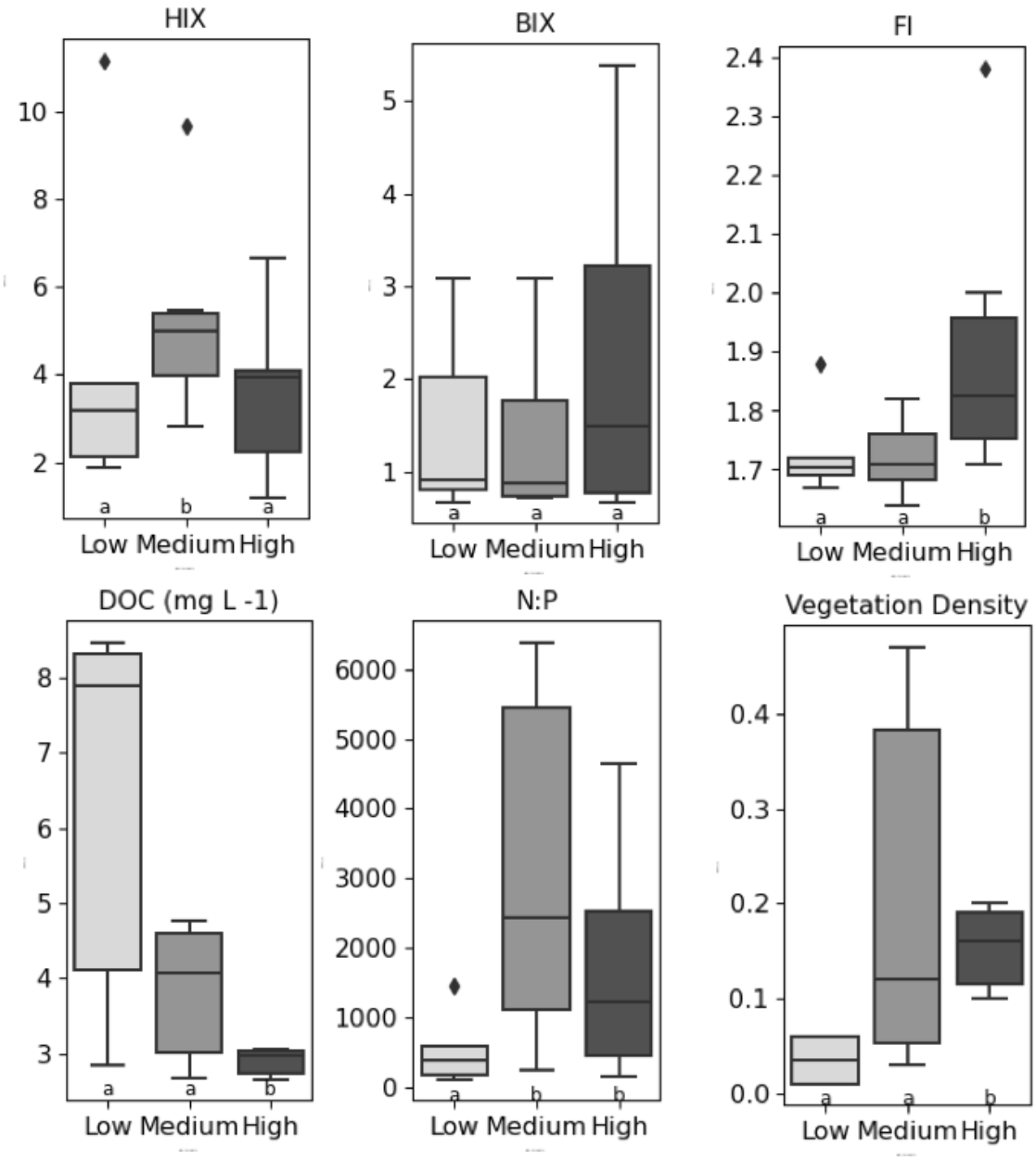

Figure 4.3: Water chemistry and dissolved organic matter composition variables in wetlands represented by low, medium, and high levels of watershed imperviousness. Grey-scale shading used on boxplots to indicate increasing imperviousness. Describe the box plots (median, upper and lower quartiles, and 95% confidence intervals as error bars).

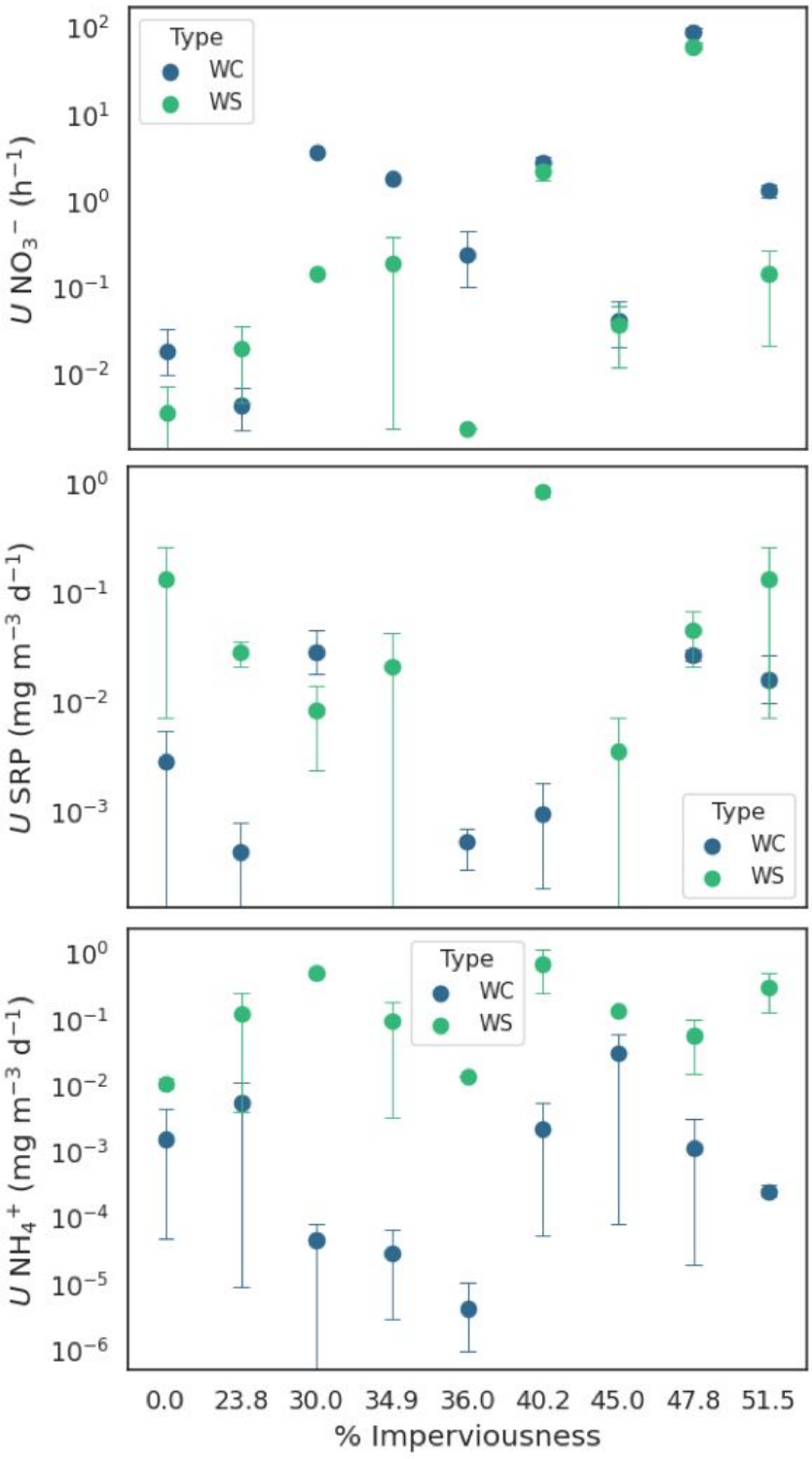

Figure 4.4: Comparison of whole system maximum (n=18) and water column (n=36) daily nutrient uptake (U_{vol}; mg m^{-3} d^{-1}) of (a) nitrate (NO3-) and soluble reactive phosphorus (SRP) in wetlands along a gradient of watershed imperviousness. Circles represent mean values and error bars represent ± SD.

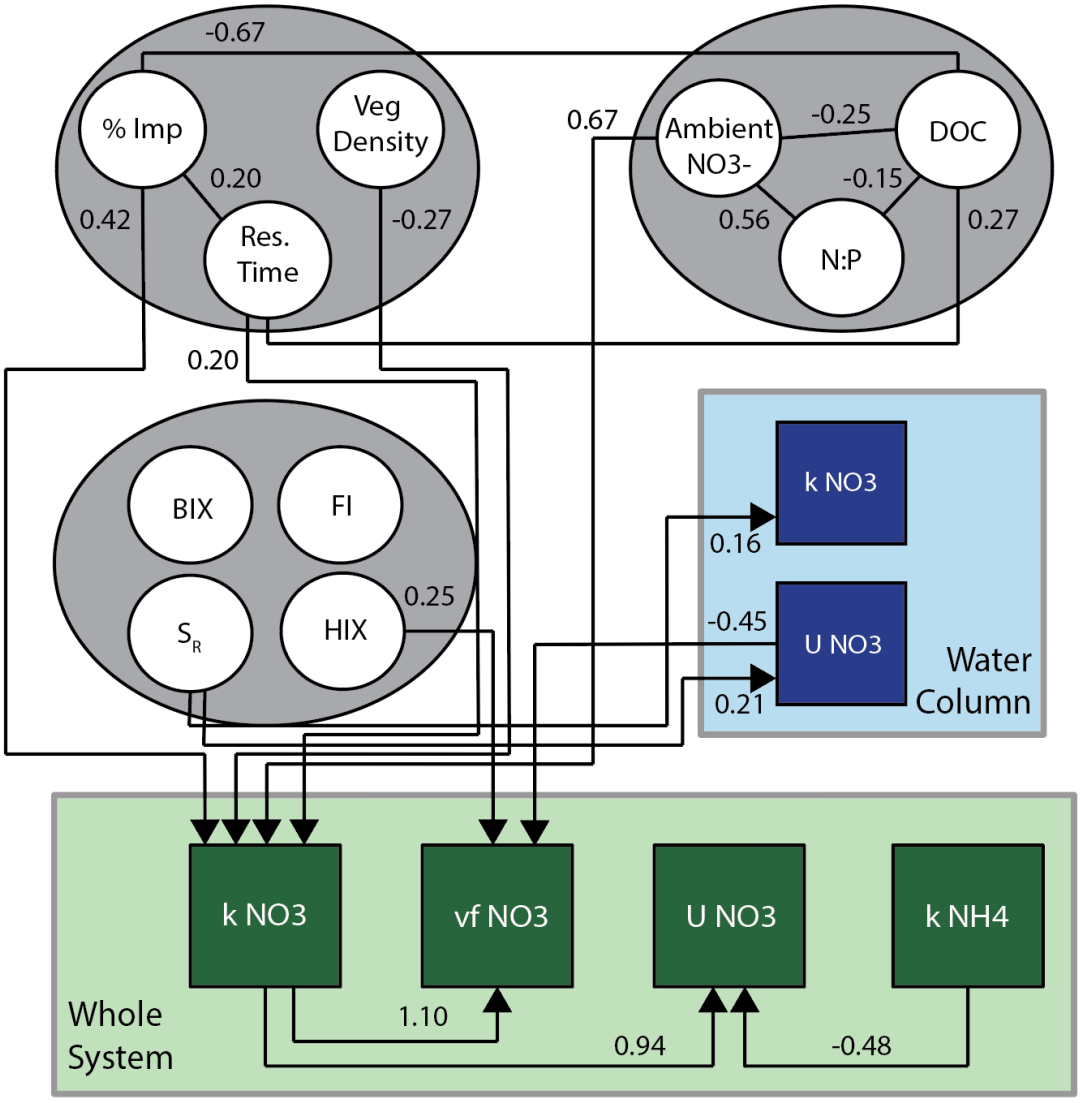

Figure 4.5: The best-supported model for nitrate ($NO3^{-}$) in water column and whole system uptake experiments of wetlands along a gradient of imperviousness. Standardized coefficients are reported, and the sign of the coefficient indicates the direction of the correlation between variables. Nonsignificant variables and coefficients were not included in the model (P ¿ 0.05).

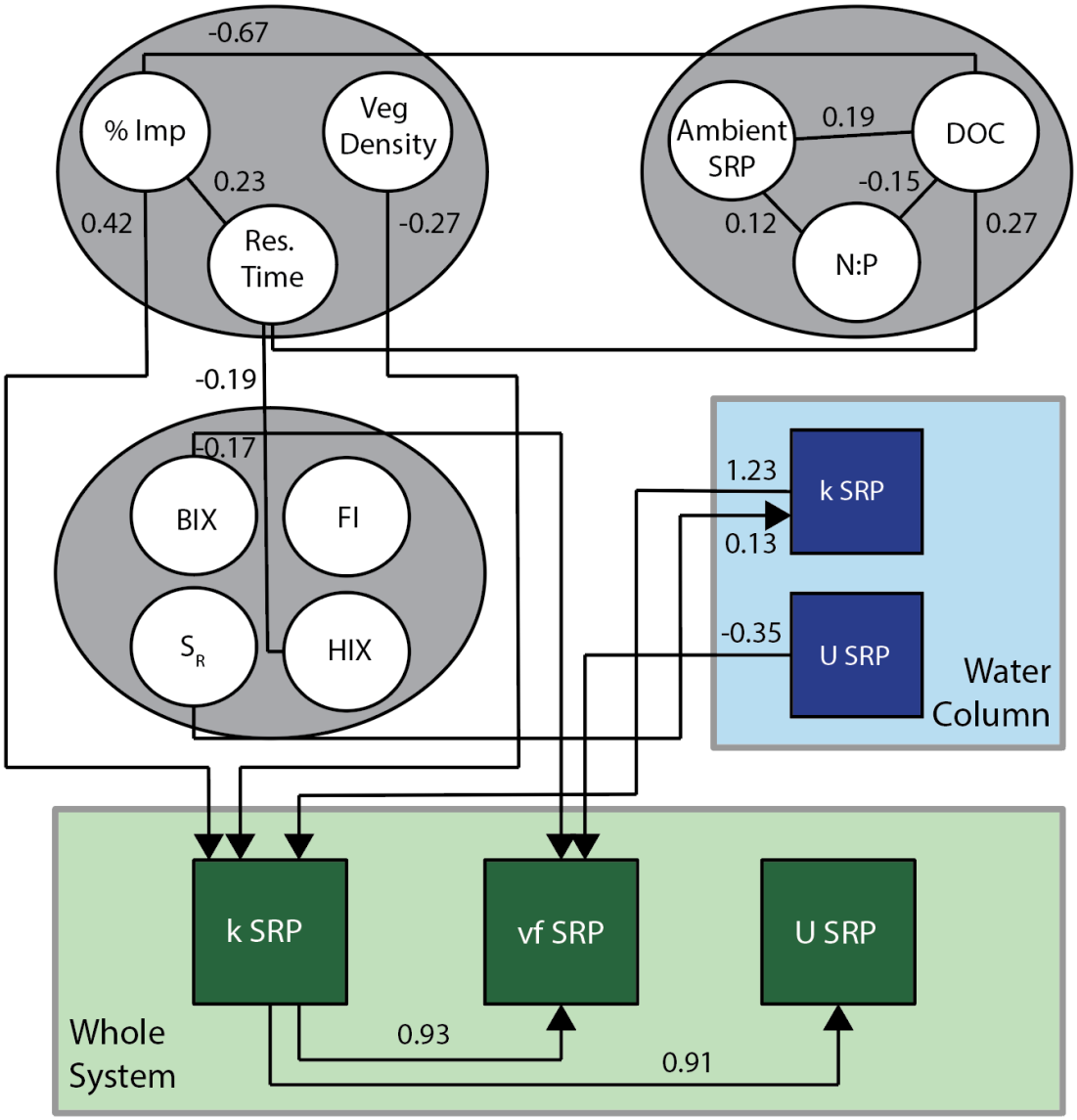

Figure 4.6: The best-supported model for soluble reactive phosphorus (SRP) in water column and whole system uptake experiments of wetlands along a gradient of imperviousness. Standardized coefficients are reported, and the sign of the coefficient indicates the direction of the correlation between variables. Non-significant variables and coefficients were not included in the model (P ¿ 0.05).

CHAPTER 5

Synchronizing hydrology in urban watersheds: flow-shunt flood-pulse concept

Matthew A. Smith[1], J.S. Kominoski[1], E.E. Gaiser[1], N.B. Grimm[2], McPhillips, L.[3], Rosenzweig, B.[4], A. Ruhi[5], T.G. Troxler[6]

[1]Institute of Environment and Department of Biological Sciences, Florida International University, Miami, Florida 33199, USA

[2]School of Sustainability, Arizona State University, Tempe, Arizona 85287, USA

[3]Department of Civil and Environmental Engineering, Department of Agricultural and Biological Engineering, Pennsylvania State University, University Park, Pennsylvania 16802, USA

[4]Environmental Sciences Initiative, Advanced Science Research Center at the Graduate Center, City University of New York, New York, New York 10031, USA

[5]Department of Environmental Science, Policy, and Management, University of California, Berkeley, California 94720, USA

[6]Department of Earth and Environment, Florida International University, Miami, Florida 33199, USA

5.1 Abstract

Climate-driven changes in flow frequency and magnitude directly impact urban ecosystems worldwide. Shifts in regional precipitation interact with heterogeneous urban infrastructure to increase stream discharge variability not explained by river-floodplain hydrology in larger-order rivers and aquatic ecosystems. Increased urban development and stormwater runoff conveyance enhance pulsed hydrologic connectivity that can exacerbate vulnerability – and likely the timing and scale – of climate-related flooding. We analyzed recent (2000-2020) discharge records from n = 360 watersheds and found discharge in urban streams was less persistent day-to-day but had greater temporal synchrony during annual peak flood events in urban compared to non-urban streams. Flood synchrony scale (i.e., distance over which multiple rivers flood simultaneously) decreased with urbanization, reflecting smaller drainage areas and increased connectivity in urban watersheds. We merge these ideas into the "flow-shunt flood-pulse concept" (FSFP) to explain and quantify how climate change and urban water infrastructure across different biomes increase and synchronize flooding at smaller scales than in non-urban watersheds of the same geographic distribution. As the frequency and magnitude of storm events shift with climate change, urban water infrastructure and flood management will require mitigation strategies that address how surface water conveyance that "shunts" urban runoff feeds back onto spatiotemporal patterns of flooding that don't follow watershed boundaries. Our results and expanded theoretical framework have large implications for the transport of carbon and nutrients across longitudinal gradients in urban ecosystems.

5.2 Introduction

The Flood-Pulse Concept proposed that rivers and adjacent floodplains are integral components of a single dynamic ecosystem supported by interactions among biophysical, hydrological, and ecological processes (Junk et al.; 1989). The major driving force of these interactions is the pulsing of river discharge and expansion–contraction cycles that occur below flood stage ("flow pulse") and discharge exceedance events above flood stage ("flood pulse") (Tockner et al.; n.d.). Both flow magnitude and variability determine the degree of hydrologic connectivity across longitudinal gradients that support the ecological integrity of riverine environments (Poff et al.; 1997). In natural flow regimes, discharge patterns generally reflect the climate of a river's upstream drainage area, where low-order streams (i.e., headwaters and tributaries) exhibit frequent irregular flood peaks that are directly influenced by local precipitation (Junk et al.; 1989; Poff et al.; 1997; Sponseller et al.; 2013). This climatic influence on stream discharge typically diminishes with increasing drainage area and this scaling has profound ecological consequences spanning many levels of biological organization (Sabo et al.; 2010). However, our ability to predict the frequency and magnitude offlood pulse regimes relies on understanding the influence of land use change on stream discharge under changing climatic conditions (Niel and Willems; 2019; Dudley et al.; 2020; Hall et al.; 2014).

Urbanization has led to significant alterations in the timing and magnitude of natural flood pulse regimes (Gori et al.; 2019; Grimm et al.; 2008; Montz and Gruntfest; 1986; Pickett et al.; 2008). Increasing high-flow magnitude and flashiness are well documented in urban ecosystems (Hopkins et al.; 2015; Ntelekos et al.; 2007; Willems et al.; 2012), but the frequency and duration of these events vary greatly across hydrogeologic setting and level of urbanization (Booth and Konrad; 2017;

Hale et al.; 2015). Urban streams are often disconnected laterally, longitudinally, and vertically, where channelization and incision disrupt lateral connections, dams, and surface water withdrawals, or returns interrupts longitudinal connectivity, and changes in recharge and baseflow contributions to urban streams disrupt vertical connectivity with groundwater (Fig. 5.1). Previous studies have observed that the climatic influence on localized flooding is dampened through complex interactions between infiltration losses and surface water management (Hopkins et al.; 2020; Poff et al.; 2007). Hydrologic alterations (i.e., dams, channel modification) can result in the homogenization of regional flow variability by modifying or controlling flood stage, and the magnitude and timing components of low and high flows (McManamay et al.; 2012; Poff et al.; 2007; Violin et al.; 2011). However, it is not known whether the consequences of flow alterations from dams, surface water management, or flood control measures could have a parallel in the context of urbanization.

Recent evidence suggests that urban watersheds have distinct microclimates that are increasingly decoupled from seasonal and multi-annual precipitation patterns of the surrounding region (Jain and Lall; 2001; Willems et al.; 2012; Pathirana et al.; 2014; Zhang et al.; 2018). In large metropolitan areas, urban heat islands (i.e., spatially concentrated high temperatures) can force thermally driven circulation patterns, leading to enhance convergence of atmospheric moisture and convective precipitation over a city (Freitag et al.; 2018). The type and strength of climatic events vary across the U.S. but unanimously drive increased magnitude differences between low and high flow events in urban areas. Further, as air temperatures warm, the intensity of extreme precipitation (>95% percentile) is expected to increase due to the enhanced water vapor-holding capacity of warm air according to the Clausius-Clapeyron relation (Ali et al.; 2018; Slater et al.; 2021). However, there is little evidence that increases in heavy rainfall evens at higher temperatures translate into

similar increases in streamflow, due to other landscape-level factors such as catchment size, vegetation cover, and antecedent soil moisture (Wasko and Nathan; 2019; Wasko et al.; 2020). Thus, quantifying the spatiotemporal variability in regional climate relative to local landscape variables will allow us to understand the universal consequences of urban flow alterations on stream discharge patterns and ecosystem.

Here, we quantified the various scales of spatiotemporal flood synchrony within and across ten major metropolitan areas of the U.S. Our goal was to identify the phenomenon of converging high flow patterns in urban watersheds despite differences in regional climate. We used historical analysis of stream discharge and precipitation time series to evaluate relationships between climate, land cover and use, and hydrology metrics. We tested three research questions: (1) How do seasonal changes in precipitation and soil moisture influence low- and high-flow patterns in urban and non-urban watersheds?, (2) How does the periodicity and amplitude of stream discharge differ among urban and non-urban watersheds, and (3) Do streams in urban watersheds have higher spatiotemporal synchrony of peak annual flood events compared to non-urban watersheds? We hypothesized that discharge in urban watersheds would be more variable and have higher amplitude between low and high flows compared to non-urban watersheds. We also anticipated greater spatial synchrony of high flow events in urban watersheds owing to increased hydrologic connectivity of urban stormwater systems.

5.3 Methods

5.3.1 Watershed Characterization

We quantified high-flow discharge patterns at N = 361 USGS stream gages across n = 10 metropolitan areas of the U.S. (Table 1) using daily discharge data from 2000 – 2019 (U.S. Geological Survey [USGS] Hydrologic Unit Code 10-12 [HUC10,12]). All watersheds that fell within the statistical metropolitan area of each major U.S. city were included in this study (Fig. 5.2). Watersheds were selected to span a gradient of % impervious land cover (1- 69%) and limited drainage area (<500 km^2). Land use and land cover were quantified for each watershed, and we collected streamflow data were gathered from the GAGES II dataset (Falcone; 2011). Sites that did not have continuous discharge records were removed from analysis.

5.3.2 Hydrometeorological Variables

Daily stream discharge records were collected from 361 USGS stream gages that fell within each metropolitan area. We calculated several hydrologic-condition metrics (McMahon et al.; 2003) for each water year (e.g., October 1, 2010 – September 30, 2011). For comparison of annual peak discharge across watersheds of different drainage area, were used normalized discharge per unit area (km2) for statistical analysis. Median annual daily streamflow was used to provide a conservative upper bound below which flow anomalies are considered "low" (i.e., flow pulse) while discharge exceeding the 75th percentile of annual flows was considered "high (i.e., flood pulse) (Smakhtin; 2001).

Gridded monthly mean precipitation was derived from the Daymet Version 4 monthly climate summaries dataset at 1 km x 1 km spatial resolution from the Oak

Ridge National Laboratory Distributed Active Archive Center (Thornton et al.; 2020). Monthly mean soil moisture data were gathered at 0.25 x 0.25 degree spatial resolution from the Copernicus Climate Change Service. The soil moisture estimates were generated by blending passive and active microwave soil moisture retrievals as a weighted average with the weights being proportional to the signal-to-noise ratio (SNR) of the data sets.

5.3.3 High-Flow Pattern Analysis

The aim of this trend analysis was to quantify historical changes in frequency and amplitude difference among low-flow and high-flow (flood) pulse extremes (i.e., anomalies) in streams, as well as determine significant correlations with precipitation or level of urbanization.

The following fundamental properties of streamflow signal (FDSS) statistics were computed from daily flow time series at each of the study gages: (1) mean discharge; (2) coefficient of variation; (3) skewness; (4) kurtosis; (5) the autoregressive lag-one (AR-1) correlation coefficient; (6) flow amplitude; and (7) the phase of the seasonal signal (Archfield et al.; 2014). These streamflow statistics were chosen to characterize the varies properties of daily streamflow generation and distribution across space and time, as described byPoff et al. (1997). Specifically, the metrics of streamflow distribution streamflow (FDSS 1-4) describe the magnitude of flows while the AR(1) correlation coefficient (FDSS 5) describes the persistence of streamflow from 1 day to the next and, could be considered a proxy for the duration and rate of change in streamflow. Further, the seasonal signal (FDSS 6-7) could be related to the timing of streamflow events. FDSS metrics were compared between watershed type (urban and non-urban) within each metropolitan area as well as among cities

and ecoregions (Fig. 5.2). Auto- and cross-correlation analyses were performed on pairwise comparisons of total daily precipitation and daily mean stream discharge. Stream discharge covariates were also identified among all hydrologic metrics to remove potentially confounding variables.

5.3.4 Flood Spatial Synchrony Scale

We calculated a flood synchrony scale to estimate the spatial extent of annual peak flood events occurring (near) simultaneously. The flood synchrony scale is defined as the maximum radius around a stream gage within which at least half of the other stream gages also record flooding within a specific time window (Berghuijs et al.; 2019). Flood synchrony scales were calculated for all watersheds in this study during the years 2000 and 2019. We first determined the total number of gages that flooded simultaneously as a function of distance from each individual reference gage:

$f(1) = \sum_{i=1}^{n(l)} f_i = 1$

Where n is the number of gages within a distance (l) of the central gage and fi represents whether an annual flood event at gage 1 occurs within (fi = 1) or outside (fi = 0) during a specific time interval (t) from the initial date of flooding at the central gage. We chose a temporal window of t = 4 days (i.e., ± 2 days) to capture instantaneous flood responses as well as moderately lagged responses that arise from differences in site-specific drainage area and hydrologic connectivity. A hierarchical clustering technique was also used to measure similarity (or dissimilarity) of flood synchrony scales across watersheds along a gradient of urbanization (Thyne et al.; n.d.).

5.3.5 Statistical Analyses

Stream discharge anomalies were compared among watersheds within each city, as well as across cities and climate ecoregions. The associations between (1) climate and hydrologic metrics and (2) landscape and hydrologic metrics were assessed across seasons, years, and ecoregions. Impervious cover was used as a representative variable for urbanization in this study. We computed seasonal Pearson's correlation coefficients to determine the strength of relationship among hydrologic and landscape variables. Selected hydrologic metrics were calculated using the discharge package (https://cran.r-project.org/web/packages/discharge/index.html in R (R Development Core Team, 2020). Metrics were used to explain the relationship between predictable, seasonal flow patterns relative to stochastic (or episodic) flow variability. Auto- and cross-correlation analyses were performed on pairwise comparisons of total daily precipitation and daily mean stream discharge. Stream discharge covariates were also identified among all hydrologic metrics to remove potentially confounding variables.

5.4 Results

5.4.1 Relationship Between Precipitation and Soil Moisture

Pearson correlation coefficients between monthly mean precipitation and antecedent soil moisture revealed distinct seasonal patterns across ecoregions (Fig. 5.3). Generally, there was a strong association between elevated precipitation and elevated antecedent soil moisture levels in most ecoregions, with the exception of Northern Forests (Fig. 5.3). We observed a significant influence of season on the strength of this relationship with the strongest correlation during 2000 in spring ($R^2 = 0.53$)

and during 2020 in autumn ($R^2 = 0.52$). As seen in other studies, we observed that drier, less vegetated climate regions showed a highly linear relationship between soil moisture and rainfall (Sehler et al., 2020). Interestingly, coefficient of variance (CV) in the seasonal relationship between precipitation and soil moisture shifted between 2000 and 2020. Variance in autumn and spring 2000 (CV = 1.44, 0.98) decreased in 2020 (CV = 0.54, 0.49) while variance increased during Summer (0.62 – 0.76) and Winter (0.91-1.35) months.

5.4.2 Long-Term Hydrometeorological Trends

Distributions of peak flow magnitudes varied significantly across all ten cities with clear differences between urban and non-urban watersheds (Fig. 5.4). Overall, urban streamflows were more variable and showed lower flow amplitude across daily and seasonal time scales than non-urban streamflows. Annual peak flow z scores were more variable in urban watersheds and had more frequent high-flow anomalies compared to non-urban watersheds. Mean periodicity of urban discharge in mesic climates (0.40-0.67) was less than in non-urban watersheds (0.42-0.91), with the exceptions of DAL and PDX (Fig. 5.5). Urban watersheds in mesic climates were characterized by high signal-to-noise ratio (SNR) compared to urban and non-urban watersheds in semi-arid climates. AR(1) lag correlations coefficients, describing the persistence of daily streamflow and a proxy for rates of change in streamflow, decreased with imperviousness ($R^2 = 0.21$; Fig. 5.4). Coefficient of variation (CV) of stream discharge slightly increased with % imperviousness ($R^2 = 0.20$). FDSS metrics for skewness (i.e., asymmetry of stream discharge) and kurtosis (i.e., sharpness in stream discharge) slightly increased with imperviousness. Flow amplitude also decreased with % imperviousness ($R^2 = 0.09$), although not significant.

5.4.3 Flood Synchrony Scales in Urban and Non-Urban Watersheds

Flood synchrony - the distance over which multiple rivers flood synchronously - decreased with urbanization across all sites and climate regions. Spatial patterns of flood synchrony scales varied significantly across cities, with western cities (PHX, PDX) exhibiting higher overall synchrony of peak flood events compared to eastern cities in both 2000 and 2020 (Fig. 5.7. Flood synchrony scales ranged between 2.7 km (ATL) and 154 km (PHX) with an average of 46.72 km across all sites. Floods that occurred around the same time (± 2 days, i.e., 30 June to 4 July) correlated over larger distances in the western longitudes compared to those in the east, with flood synchrony scales exceeding 70 km2 in PHX and PDX watersheds (Fig. 5.7). The average flood synchrony scale represented a total watershed area of approximately 6,850 km2, which is an order of magnitude larger than the typical watershed evaluated in eastern cities.

Overall, spatial synchrony of high-flow anomalies decreased from 2000 to 2020, while the total number of synchronous flood gages increased, indicating more frequent localized flooding in recent years (Fig. 5.7). A positive relationship was observed between flood synchrony scales and drainage area ($R^2 = 0.21$), particularly in watersheds with greater than 30% imperviousness (Fig. 5.8. Watersheds with low imperviousness (<4%) showed the highest flood synchrony scales but varied with total drainage area compared to high impervious sites. Overall, we found that repetitive widespread precipitation events (> Q95) may drive the spatial synchrony of flood events as opposed to watershed-level landscape characteristics alone.

5.5 Discussion

We tested relationships between the timing and magnitude of annual peak flood events in urban compared to non-urban stream ecosystems in order to predict how flow anomalies are driven by changes in climate and urbanization. We explored how interactions between precipitation and soil moisture can modulate stream discharge signals, particularly during severe rain events. In our investigation of nonstationarity, we observed that flood timing is more variable in summer and winter months, consistent with changes in mean and extreme rainfall and shifts in soil moisture due changes in urbanization. These interactions suggest hydrologic connectivity and land use influence low-flow anomalies and relate to the timing and magnitude of extreme flooding in urban and non-urban watersheds. We found that urban discharge was strongly linked with sub-annual precipitation patterns that drive more frequent, high-magnitude, peak-flow events of short duration compared to non-urban watersheds. Over two decades of daily discharge data spanning ecoregions showed that urban streams showed decreased variability in high-flow discharge that reflected site-specific landscape factors. Overall, changes in local weather and landscape factors modulate the rainfall-runoff response and exhibit strong influence on the spatial connectedness of resulting floods throughout the year.

5.5.1 Climatic and Landscape Drivers of Flood Pulse Response

Changes in precipitation extremes due to climate change will continue to increase the frequency and magnitude of high-flow events in streams and rivers (Sharma et al.; 2018; Vogel et al.; 2011). In this study, we observed positive flood trends

in urban watersheds that were increasingly linked to short-term precipitation patterns that resulted in spatiotemporal synchronization of high-flow anomalies across metropolitan regions. Seasonal precipitation trends appear to drive lower periodicity discharge signals in urban watersheds, likely due to decreased lag time and increased flashiness (Fig. 5.5). Our results agree with those of other long-term hydrological assessments that highlight increased frequency and magnitude of peak flow events in urban watersheds, primarily driven by changes in imperviousness (Smith et al.; 2013; Yang et al.; 2015). However, variability in the amount and persistence of urban discharge may be caused by differences in regional stormwater management practices and surface water availability, which determine the strength of relationship between hydrology and urbanization (Brown et al.; 2009; Jefferson et al.; 2017).

We highlight several climate-driven mechanisms of flow variability and anomalies along a gradient of urbanization. Seasonal precipitation patterns interact with antecedent soil moisture to modulate (1) antecedent stream conditions (e.g., low flow persistence), (2) time-sensitive interactions with landscape characteristics to affect the magnitude of flow versus flood conditions, and (3) compounding peak flow via increased surface connectivity (Fig. 5.8). Low-flow responses to urbanization are nonlinear and depend upon a suite of site-specific factors (e.g., point source discharge, groundwater contributions, surface water evaporation; Roy and Shuster (2009). These findings are consistent with other studies showing strong associations between seasonal precipitation, soil moisture, and flood periodicity (Berghuijs et al.; 2019; Brunner et al.; 2020). We observed a notable decrease from 2000 to 2020 in the variation of precipitation versus soil moisture which signifies a paradigm shift in the presence and connectivity of stormwater management that support more direct rainfall-runoff relationships in urban watersheds. As evidenced in other studies, soil moisture anomalies can influence the magnitude of flooding as well as shape

the spatial dependence of floods by modulating the role of the driving atmospheric (i.e., precipitation) forcing (Brunner et al.; 2020). This information, coupled with decreasing patterns of signal persistence in discharge anomalies, or AR(1) correlation coefficients, further supports the idea that interactions between climate and urbanization amplify flood peak frequency but dampen flood duration.

Across the globe, annual minimum and maximum temperatures have increased at faster rates in recent decades, with direct influence on the frequency and duration and extreme weather (Hansen et al.; 2012; Zobel et al.; 2017). Climate extremes can exacerbate the variability and unpredictability of urban hydro-climatological regimes (Fadhel et al.; 2018; Hopkins et al.; 2020). These events place stress on cities to modify freshwater delivery during low flow periods (i.e., drought) and increase surface water connectivity and longitudinal transport of stormwater during high flow events (Marshall et al.; 2001). In turn, urban watersheds will be increasingly sensitive to precipitation inputs and discharge patterns will reflect the heightened stormwater connectivity across basins (Pathirana et al.; 2014). However, there remains a clear distinction between discharge anomalies in mesic and semi-arid climates across the U.S. In mesic climates, watershed flood response to urbanization is highly variable. In semi-arid mountainous regions (e.g., Phoenix, Arizona), urbanization leads to increased water retention and decreased flood variability, as shown in previous studies (McPhillips et al.; 2019). These patterns underscore the importance of storm type (i.e., duration, intensity) and antecedent landscape conditions (e.g., soil moisture) that vary with urban development (Sharma et al.; 2018; Smith et al.; 2013). Thus, antecedent climate and landscape hydrologic conditions during dry months may influence the magnitude of low-flow pulse anomalies, which can either dampen or intensify future high-flow anomaly detection.

5.5.2 Ecological and Biogeochemical Implications of Flood Pulses

Projecting nonstationary trends in urban discharge is complex and requires a robust yet flexible scientific framework to guide process-based experiments of flow-ecology relationships (Junk and Wantzen; 2004; Olden et al.; 2012; Poff; 2018; Tashie et al.; 2020). The natural flow regime paradigm, which holds that minimum flows and periodic flooding are critical to maintain ecological integrity, is often presented as the benchmark for river and stream ecosystem management (Acreman et al.; 2014). This type of management is intended to correct impacts of imperviousness and bring an ecosystem back to 'pre-development' conditions. We found that low-flow conditions become more variable with urbanization, while peak-flow magnitudes, but not durations, increase and the scale at which flood synchronization occurs is reduced. Recent studies have asserted that the full (natural) range of hydrological and ecological processes cannot be restored in urban streams, but biological communities will nevertheless become more diverse and often more resilient to changes in flow patterns (Konrad and Booth; 2005). Other ecological repercussions are expected in regions where surface water and/or shallow groundwater are used for domestic water supplies. Ultimately, biological communities may benefit from the redistribution of water availability and residence time by optimizing water storage capacity and surface water conveyance in cities. In this study, we find that estimates of variable baseflow conditions are linked to more synchronous flood pulses that, when managed accordingly, can provide ample opportunities for beneficial nutrient, matter, and organismal transport (Bogan et al.; 2013; Lewis et al.; 2001; Stromberg et al.; 2007). In turn, understanding regional patterns of low-flow pulse regimes and surface hydrologic connectivity can increase the overall resilience of urban aquatic commu-

nities to anticipated changes in precipitation from climate change (Thorp et al.; 2006; Baruch et al.; 2018).

5.5.3 Adapting the Pulse-Shunt Concept for Urban Flow Regimes

Hydrologic connectivity in urban ecosystems is driven, in part, by the timing and magnitude of pulsing via stream discharge. Our study reveals that urbanization leads to increased inter- and intra-basin spatiotemporal connectedness of annual peak flood events. In consideration of the original Pulse-Shunt Concept, the high spatiotemporal variability of high-flow urban discharge patterns due to increased frequency and intensity of rain events may lead to discrepancies among estimates of flood pulse magnitude and duration (Fig. 5.8). Accordingly, we call for a new perspective of the PSC in urban ecosystems: once that emphasizes the increasing spatial and temporal connectedness of flow patterns during high flow discharge events that may lead to the homogenization of high-flow patterns across regional climates.

Below, we summarize the major postulates of the new concept that could form the basis for a new urban-centric perspective of carbon and nutrient transport following significant discharge events:

1. Antecedent stream conditions (e.g., low flow persistence) and soil moisture prime or dampen the correlation between precipitation and stream discharge. This observation trends with increases in impervious cover by way of urbanization.

2. Time-sensitive interactions between precipitation event intensity and duration combined with local water storage capacity affect the magnitude of flow versus flood conditions

3. Compounding peak flow via increased surface and subsurface connectivity during high-flow discharge exceedance events result in high spatiotemporal synchrony of flood magnitude and duration.

Recent studies have suggested that urbanization results in a tightly constrained range of hydrographic characteristics within watersheds across US cities (Hale et al.; 2015; Steele et al.; 2014). The existing paradigm of river-floodplain hydrology described runoff generation and variability in flood response to shifting climate and land use as a continuum. However, a recent paradigm shift in urban hydrology describes urban flood response as a network of threshold-mediated, connectivity-controlled processes that are driven by heterogeneity of low-flow pulse regimes and landscape physiography (Loperfido et al.; 2014; Spence; 2010). As cities continue to increase the spatial extent and hydrologic connectivity of stormwater management, we can expect significant improvements in water storage capacity and low flows that converge across increasing spatial scales.

5.6 Conclusions

The frequency and magnitude of flood pulses have increased with urbanization over the past few decades but are synchronizing across more localized spatial scales in recent years. We found that the relationship between precipitation and antecedent soil moisture plays a key role in stream discharge response and variability. Decreased variation among these two variables suggests the potential for urbanization to dampen the relationship between seasonal precipitation and discharge to ho-

mogenize with other urbanized watershed response across regional climates. This is evidenced by the stronger coupling of precipitation and urban discharge in mesic climates but not in semi-arid climates where urbanization appears to modulate peak flow anomalies. Further, we observed heterogeneity in urban stream discharge during low to moderate flow magnitude and heightened synchronization of flood pulses across smaller, more localized scales following extreme precipitation. Therefore, the spatial connectedness of peak flood events is driven by land-surface processes such as soil moisture, impervious cover, and stormwater management that shift with increasing urbanization. Overall, our findings suggest that surface water conveyance "shunts" urban runoff onto spatiotemporal patterns of flooding that don't follow traditional watershed boundaries. The newly adapted framework of the urban flow-shunt flood-pulse concept can lead to a deeper understanding of interactive effects among climate and landscape characteristics that differ between flow-shunt and flood-pulse events in urbanizing ecosystems.

5.7 Bibliography

Acreman, M., Arthington, A. H., Colloff, M. J., Couch, C., Crossman, N. D., Dyer, F., Overton, I., Pollino, C. A., Stewardson, M. J. and Young, W. (2014). Environmental flows for natural, hybrid, and novel riverine ecosystems in a changing world, *Frontiers in Ecology and the Environment* **12**: 466–473.

Ali, H., Fowler, H. J. and Mishra, V. (2018). Global observational evidence of strong linkage between dew point temperature and precipitation extremes, *Geophysical Research Letters* **45**(22): 12–320.

Archfield, S. A., Kennen, J. G., Carlisle, D. M. and Wolock, D. M. (2014). An objective and parsimonious approach for classifying natural flow regimes at a continental scale, *River Research and Applications* **30**: 1166–1183.

Baruch, E. M., Voss, K. A., Blaszczak, J. R., Delesantro, J., Urban, D. L. and Bernhardt, E. S. (2018). Not all pavements lead to streams: Variation in impervious surface connectivity affects urban stream ecosystems, *Freshwater Science* **37**: 673–684.

Berghuijs, W. R., Allen, S. T., Harrigan, S. and Kirchner, J. W. (2019). Growing spatial scales of synchronous river flooding in europe, *Geophysical Research Letters* **46**: 1423–1428.

Bogan, M. T., Boersma, K. S. and Lytle, D. A. (2013). Flow intermittency alters longitudinal patterns of invertebrate diversity and assemblage composition in an arid-land stream network, *Freshwater Biology* **58**(5): 1016–1028.

Booth, D. B. and Konrad, C. P. (2017). Hydrologic metrics for status-and-trends monitoring in urban and urbanizing watersheds, *Hydrological Processes* **31**: 4507–4519.

Brown, L. R., Cuffney, T. F., Coles, J. F., Fitzpatrick, F., McMahon, G., Steuer, J., Bell, A. H. and May, J. T. (2009). Urban streams across the usa: Lessons learned from studies in 9 metropolitan areas, *Journal of the North American Benthological Society* **28**: 1051–1069.

Brunner, M. I., Gilleland, E., Wood, A., Swain, D. L. and Clark, M. (2020). Spatial dependence of floods shaped by spatiotemporal variations in meteorological and land-surface processes, *Geophysical Research Letters* **47**(13): e2020GL088000.

Dudley, R., Hirsch, R. M., Archfield, S. A., Blum, A. G. and Renard, B. (2020). Low streamflow trends at human-impacted and reference basins in the united states, *Journal of Hydrology* **580**: 124254.

Fadhel, S., Rico-Ramirez, M. A. and Han, D. (2018). Sensitivity of peak flow to the change of rainfall temporal pattern due to warmer climate, *Journal of Hydrology* **560**: 546–559.

Falcone, J. A. (2011). Gages-ii: Geospatial attributes of gages for evaluating streamflow, *Technical report*, US Geological Survey.

Freitag, B. M., Nair, U. S. and Niyogi, D. (2018). Urban modification of convection and rainfall in complex terrain, *Geophysical Research Letters* **45**: 2507–2515.

Gori, A., Blessing, R., Juan, A., Brody, S. and Bedient, P. (2019). Characterizing urbanization impacts on floodplain through integrated land use, hydrologic, and hydraulic modeling, *Journal of Hydrology* **568**: 82–95.

Grimm, N. B., Faeth, S. H., Golubiewski, N. E., Redman, C. L., Wu, J., Bai, X. and Briggs, J. M. (2008). Global change and the ecology of cities, *New Series* **319**: 756–760.

Hale, R. L., Turnbull, L., Earl, S. R., Childers, D. L. and Grimm, N. B. (2015). Stormwater infrastructure controls runoff and dissolved material export from arid urban watersheds, *Ecosystems* **18**(1): 62–75.

Hall, J., Arheimer, B., Borga, M., Brázdil, R., Claps, P., Kiss, A., Kjeldsen, T. R., Kriaučiūnienė, J., Kundzewicz, Z. W., Lang, M., Llasat, M. C., Macdonald, N., McIntyre, N., Mediero, L., Merz, B., Merz, R., Molnar, P., Montanari, A., Neuhold, C., Parajka, J., Perdigão, R. A., Plavcová, L., Rogger, M., Salinas, J. L., Sauquet, E., Schär, C., Szolgay, J., Viglione, A. and Blöschl, G. (2014). Understanding flood regime changes in europe: A state-of-the-art assessment, *Hydrology and Earth System Sciences* **18**: 2735–2772.

Hansen, J., Sato, M. and Ruedy, R. (2012). Perception of climate change, *Proceedings of the National Academy of Sciences* **109**(37): E2415–E2423.

Hopkins, K. G., Bhaskar, A. S., Woznicki, S. A. and Fanelli, R. M. (2020). Changes in event-based streamflow magnitude and timing after suburban development with infiltration-based stormwater management, *Hydrological Processes* **34**: 387–403.

Hopkins, K. G., Morse, N. B., Bain, D. J., Bettez, N. D., Grimm, N. B., Morse, J. L., Palta, M. M., Zak, D. R. and Groffman, P. M. (2015). Type and timing of stream flow changes in urbanizing watersheds in the eastern us stream flow changes in urban watersheds, *Elementa: Science of the Anthropocene* **3**.

Jain, S. and Lall, U. (2001). Floods in a changing climate: Does the past represent the future?, *Water Resources Research* **37**: 3193–3205.

Jefferson, A. J., Bhaskar, A. S., Hopkins, K. G., Fanelli, R., Avellaneda, P. M. and McMillan, S. K. (2017). Stormwater management network effectiveness and implications for urban watershed function: A critical review, *Hydrological Processes* **31**(23): 4056–4080.

Junk, W. J., Bayley, P. B., Sparks, R. E. et al. (1989). The flood pulse concept in river-floodplain systems, *Canadian special publication of fisheries and aquatic sciences* **106**(1): 110–127.

Junk, W. J. and Wantzen, K. M. (2004). The flood pulse concept: new aspects, approaches and applications-an update, *Second international symposium on the management of large rivers for fisheries*, Food and Agriculture Organization and Mekong River Commission, FAO Regional . . . , pp. 117–149.

Konrad, C. P. and Booth, D. B. (2005). Hydrologic changes in urban streams and their ecological significance, *American Fisheries Society Symposium*, Vol. 47, p. 17.

Lewis, W. M., Hamilton, S. K., Rodri´guez, M. A., Rodri´guez, R., Saunders, J. F. and Lasi, M. A. (2001). Foodweb analysis of the orinoco floodplain based on production estimates and stable isotope data, *Am. Benthol. Soc* **20**: 241–254.

Loperfido, J. V., Noe, G. B., Jarnagin, S. T. and Hogan, D. M. (2014). Effects of distributed and centralized stormwater best management practices and land cover on urban stream hydrology at the catchment scale, *Journal of Hydrology* **519**: 2584–2595.

Marshall, J., Kushnir, Y., Battisti, D., Chang, P., Czaja, A., Dickson, R., Hurrell, J., McCartney, M., Saravanan, R. and Visbeck, M. (2001). North atlantic cli-

mate variability: Phenomena, impacts and mechanisms, *International Journal of Climatology* **21**: 1863–1898.

McMahon, G., Bales, J. D., Coles, J. F., Giddings, E. M. and Zappia, H. (2003). Use of stage data to characterize hydrologic conditions in an urbanizing environment 1, *JAWRA Journal of the American Water Resources Association* **39**(6): 1529–1546.

McManamay, R. A., Orth, D. J. and Dolloff, C. A. (2012). Revisiting the homogenization of dammed rivers in the southeastern us, *Journal of Hydrology* **424-425**: 217–237.

McPhillips, L. E., Earl, S. R., Hale, R. L. and Grimm, N. B. (2019). Urbanization in arid central arizona watersheds results in decreased stream flashiness, *Water Resources Research* **55**: 9436–9453.

Montz, B. and Gruntfest, E. C. (1986). Changes in american urban floodplain occupancy since 1958: the experiences of nine cities, *Applied Geography* **6**(4): 325–338.

Niel, J. D. and Willems, P. (2019). Climate or land cover variations: what is driving observed changes in river peak flows? a data-based attribution study, *Hydrology and Earth System Sciences* **23**(2): 871–882.

Ntelekos, A. A., Smith, J. A. and Krajewski, W. F. (2007). Climatological analyses of thunderstorms and flash floods in the baltimore metropolitan region, *Journal of Hydrometeorology* **8**: 88–101.

Olden, J. D., Kennard, M. J. and Pusey, B. J. (2012). A framework for hydrologic classification with a review of methodologies and applications in ecohydrology, *Ecohydrology* **5**(4): 503–518.

Pathirana, A., Denekew, H. B., Veerbeek, W., Zevenbergen, C. and Banda, A. T. (2014). Impact of urban growth-driven landuse change on microclimate and extreme precipitation - a sensitivity study, *Atmospheric Research* **138**: 59–72.

Pickett, S. T., Cadenasso, M. L., Grove, J. M., Groffman, P. M., Band, L. E., Boone, C. G., Burch, W. R., Grimmond, C. S. B., Hom, J., Jenkins, J. C. et al. (2008). Beyond urban legends: an emerging framework of urban ecology, as illustrated by the baltimore ecosystem study, *BioScience* **58**(2): 139–150.

Poff, N. L., Allan, J. D., Bain, M. B., Karr, J. R., Prestegaard, K. L., Richter, B. D., Sparks, R. E. and Stromberg, J. C. (1997). The natural flow regime, **47**: 769–784.

Poff, N. L., Olden, J. D., Merritt, D. M. and Pepin, D. M. (2007). Homogenization of regional river dynamics by dams and global biodiversity implications.
URL: *www.pnas.orgcgidoi10.1073pnas.0609812104*

Poff, N. L. R. (2018). Beyond the natural flow regime? broadening the hydro-ecological foundation to meet environmental flows challenges in a non-stationary world, Vol. 63, Blackwell Publishing Ltd, pp. 1011–1021.

Roy, A. H. and Shuster, W. D. (2009). Assessing impervious surface connectivity and applications for watershed management 1, *JAWRA Journal of the American Water Resources Association* **45**(1): 198–209.

Sabo, J. L., Finlay, J. C., Kennedy, T. and Post, D. M. (2010). The role of discharge variation in scaling of drainage area and food chain length in rivers, *science* **330**(6006): 965–967.

Sharma, A., Wasko, C. and Lettenmaier, D. P. (2018). If precipitation extremes are increasing, why aren't floods?, *Water Resources Research* **54**: 8545–8551.

Slater, L. J., Anderson, B., Buechel, M., Dadson, S., Han, S., Harrigan, S., Kelder, T., Kowal, K., Lees, T., Matthews, T. et al. (2021). Nonstationary weather and water extremes: a review of methods for their detection, attribution, and management, *Hydrology and Earth System Sciences* **25**(7): 3897–3935.

Smakhtin, V. U. (2001). Low flow hydrology: a review, *Journal of hydrology* **240**(3-4): 147–186.

Smith, B. K., Smith, J. A., Baeck, M. L., Villarini, G. and Wright, D. B. (2013). Spectrum of storm event hydrologic response in urban watersheds, *Water Resources Research* **49**: 2649–2663.

Spence, C. (2010). A paradigm shift in hydrology: Storage thresholds across scales influence catchment runoff generation, *Geography Compass* **4**: 819–833.

Sponseller, R. A., Heffernan, J. B. and Fisher, S. G. (2013). On the multiple ecological roles of water in river networks, *Ecosphere* **4**(2): 1–14.

Steele, M. K., Heffernan, J. B., Bettez, N., Cavender-Bares, J., Groffman, P. M., Grove, J. M., Hall, S., Hobbie, S. E., Larson, K., Morse, J. L., Neill, C., Nelson, K. C., O'Neil-Dunne, J., Ogden, L., Pataki, D. E., Polsky, C. and Chowdhury, R. R. (2014). Convergent surface water distributions in u.s. cities, *Ecosystems* **17**: 685–697.

Stromberg, J. C., Beauchamp, V. B., Dixon, M. D., Lite, S. J. and Paradzick, C. (2007). Importance of low-flow and high-flow characteristics to restoration of riparian vegetation along rivers in arid south-western united states, *Freshwater Biology* **52**: 651–679.

Tashie, A., Pavelsky, T. and Emanuel, R. E. (2020). Spatial and temporal patterns in baseflow recession in the continental united states, *Water Resources Research* **56**.

Thornton, M., Wei, Y., Thornton, P., Shrestha, R., Kao, S. and Wilson, B. (2020). Daymet: Station-level inputs and cross-validation result for north america, version 4. ornl daac, oak ridge, tennessee, usa.

Thorp, J. H., Thoms, M. C. and Delong, M. D. (2006). The riverine ecosystem synthesis: Biocomplexity in river networks across space and time, *River Research and Applications* **22**: 123–147.

Thyne, G., Güler, C. and Poeter, E. (n.d.). Introduction sequential analysis of hydrochemical data for watershed characterization, **42**: 711–723.

Tockner, K., Malard, F. and Ward, J. V. (n.d.). An extension of the ¯ood pulse concept.

Violin, C. R., Cada, P., Sudduth, E. B., Hassett, B. A., Penrose, D. L. and Bernhardt, E. S. (2011). Effects of urbanization and urban stream restoration on the physical and biological structure of stream ecosystems, *Ecological Applications* **21**(6): 1932–1949.

Vogel, R. M., Yaindl, C. and Walter, M. (2011). Nonstationarity: Flood magnification and recurrence reduction factors in the united states, *Journal of the American Water Resources Association* **47**: 464–474.

Wasko, C. and Nathan, R. (2019). Influence of changes in rainfall and soil moisture on trends in flooding, *Journal of Hydrology* **575**: 432–441.

Wasko, C., Nathan, R. and Peel, M. C. (2020). Changes in antecedent soil moisture modulate flood seasonality in a changing climate, *Water Resources Research* **56**(3): e2019WR026300.

Willems, P., Arnbjerg-Nielsen, K., Olsson, J. and Nguyen, V. T. (2012). Climate change impact assessment on urban rainfall extremes and urban drainage: Methods and shortcomings, *Atmospheric Research* **103**: 106–118.

Yang, L., Tian, F. and Niyogi, D. (2015). A need to revisit hydrologic responses to urbanization by incorporating the feedback on spatial rainfall patterns, *Urban Climate* **12**: 128–140.

Zhang, W., Villarini, G., Vecchi, G. A. and Smith, J. A. (2018). Urbanization exacerbated the rainfall and flooding caused by hurricane harvey in houston, *Nature* **563**: 384–388.

Zobel, Z., Wang, J., Wuebbles, D. J. and Kotamarthi, V. R. (2017). High-resolution dynamical downscaling ensemble projections of future extreme temperature distributions for the united states, *Earth's Future* **5**: 1234–1251.

5.8 Tables

Table 5.1: Watershed characteristics of non-urban and urban watersheds using NLCD 2016 and GAGESII dataset information.

Metropolitan Area		State	Elevation (m)	Mean Annual Precipitation (mm)	Mean Annual Temperature (ºC)	Mean Drainage Area (km^2)	Mean Imperviousness (%)
ATL	Atlanta	GA	261.0	1263	16.3	616.0	40.9
BAL	Baltimore	MD	84.7	1034	13.0	5.51	42.6
DAL	Dallas	TX	121.9	942	19.3	172.0	24.0
DEN	Denver	CO	1578.9		9.7	1061.9	21.9
NYC	New York	NJ, NY, PA	26.6	1174	11.9	66.3	23.3
PHX	Phoenix	AZ	704.1	211	22.6	176.9	5.0
PDX	Portland	OR, WA	69.6	915	11.3	69.4	13.7
SYR	Syracuse	NY	122.3	1039	8.6	246.0	5.0
TPA	Tampa	FL	<1.0	1295	22.4	414.4	25.3
DC	Washington DC	D.C., MD, VA, WV	75.9	1290	14.4	859.9	31.7

5.9 Figures

Figure 5.1. Diagram illustrating the basic tenets of the flow-shunt concept adapted from Raymond et al. (2016).

Figure 5.2. Study metropolitan areas of the continental United States including Portland, OR; Syracuse, NY; New York City, NY; Baltimore, MD; Denver, CO; Washington, DC; Phoenix, AZ; Atlanta, GA; Dallas, TX; and Tampa, FL. Level I Ecoregions are represented and study sites are represented white circles.

Figure 5.3. Pearson correlation coefficients for the observed relationship between seasonal antecedent soil moisture and precipitation in (a) 2000 and (b) 2020 across Level I Ecoregions.

Figure 5.4. Calculated metrics of stream discharge time series for (a) periodicity of statistically significant power spectra (95% C.I.), (b) signal-to-noise ratios (SNR), (c) lag-one auto-correlation, and (d) cross-correlation (r) coefficients between daily precipitation and stream discharge in urban and non-urban watersheds from 2000 to 2020. See Table 1 for city abbreviations.

Figure 5.5. Mean values of the seven fundamental daily streamflow statistics (FDSS) with changes in % imperviousness across all study gauges. Shaded regions represent a 95% confidence interval (C.I.).

Figure 5.6. Calculated Flood Synchrony Scale (FSS; sq km) during 2000 (left) and 2020 (right) in (a) Portland, Oregon, (b) Baltimore, Maryland, and (c) Phoenix, Arizona. Darker hues indicate higher FSS values.

Figure 5.7. Relationship between Flood Synchrony Scale (FSS; sq km) and (a) change (Δ) in percent watershed imperviousness and (b) total drainage area (sq km) across all study sites.

Figure 5.8. Conceptual diagram illustrating the the influence of urbanization on the timing, frequency, and magnitude of streamflow anomalies during high-flow flood events.

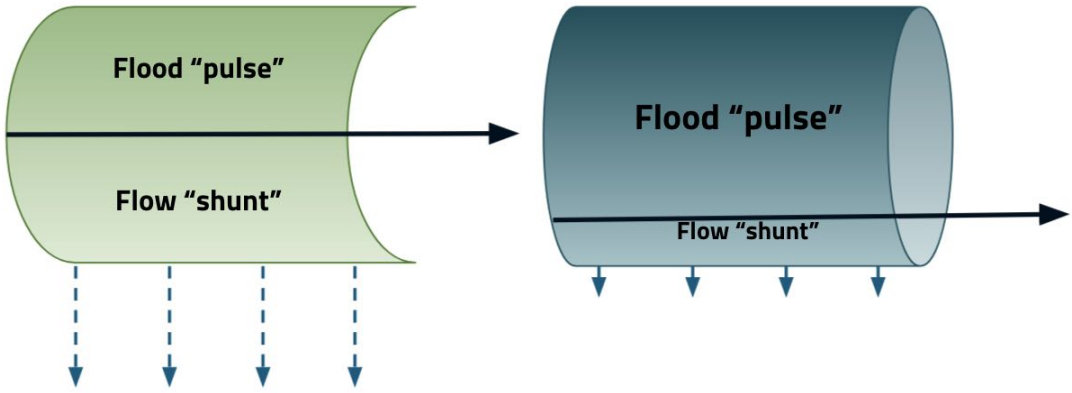

Figure 5.1: Diagram illustrating the basic tenets of the flow-shunt concept adapted from Raymond et al. (2016).

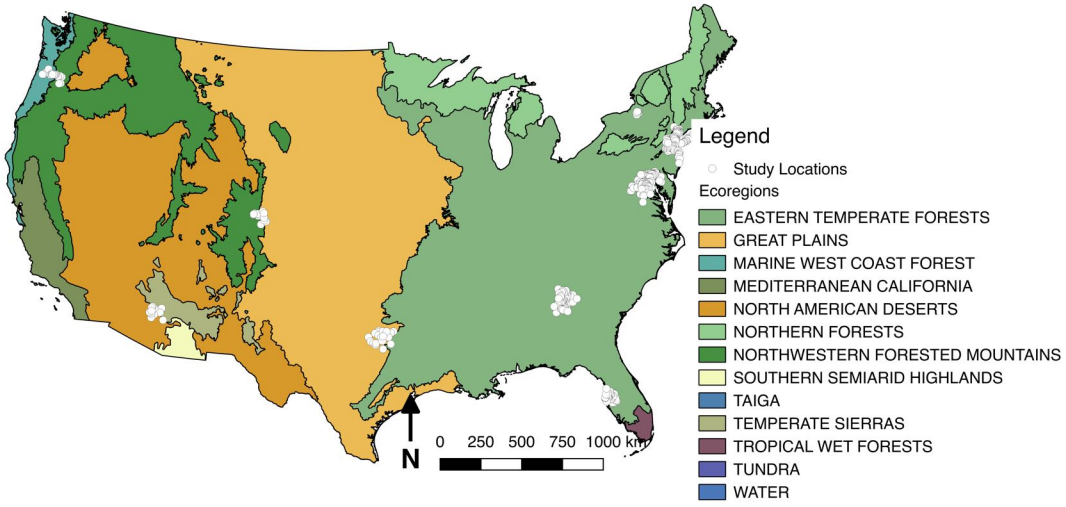

Figure 5.2: Study metropolitan areas of the continental United States including Portland, OR; Syracuse, NY; New York City, NY; Baltimore, MD; Denver, CO; Washington, DC; Phoenix, AZ; Atlanta, GA; Dallas, TX; and Tampa, FL. Level I Ecoregions are represented and study sites are represented white circles.

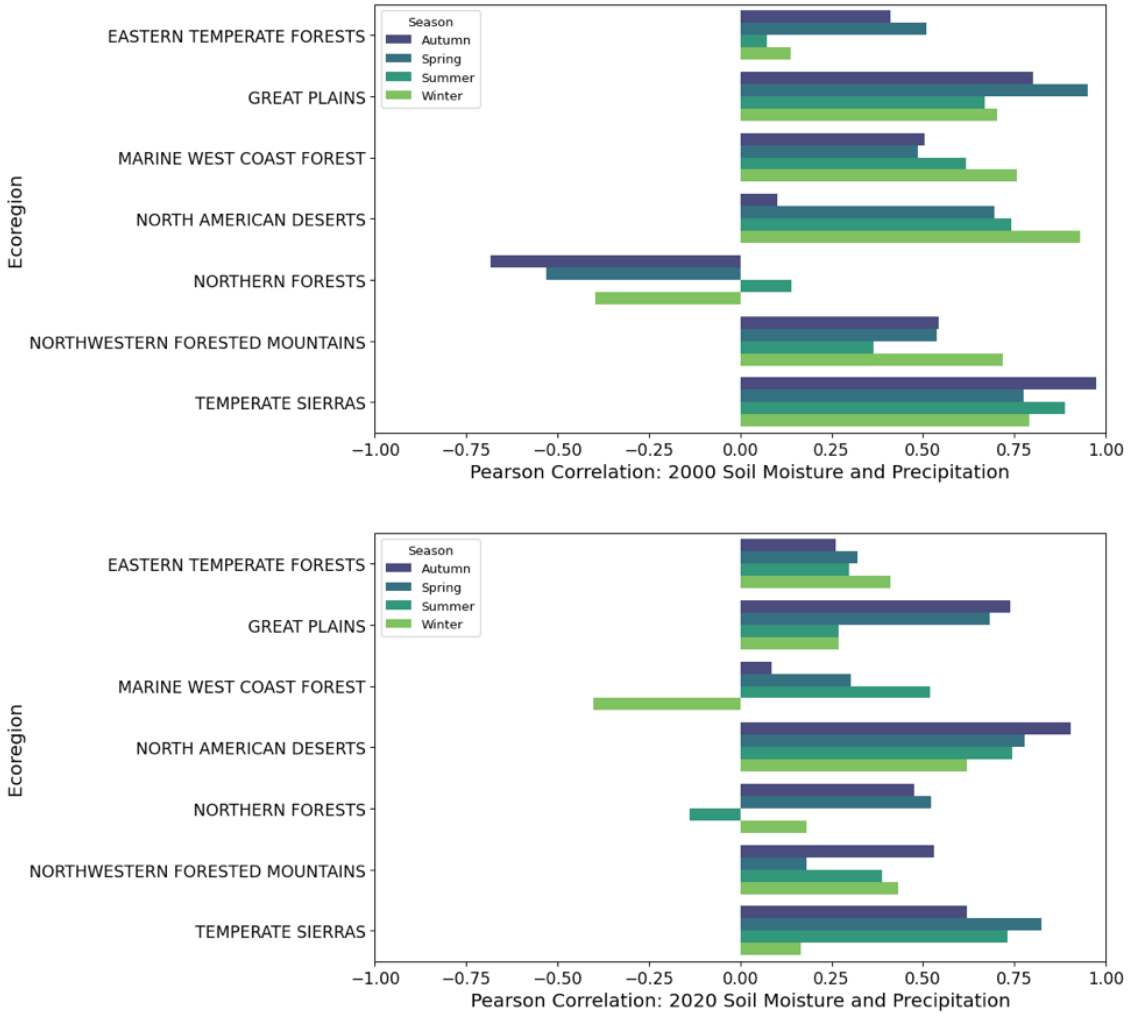

Figure 5.3: Pearson correlation coefficients for the observed relationship between seasonal antecedent soil moisture and precipitation in (a) 2000 and (b) 2020 across Level I Ecoregions.

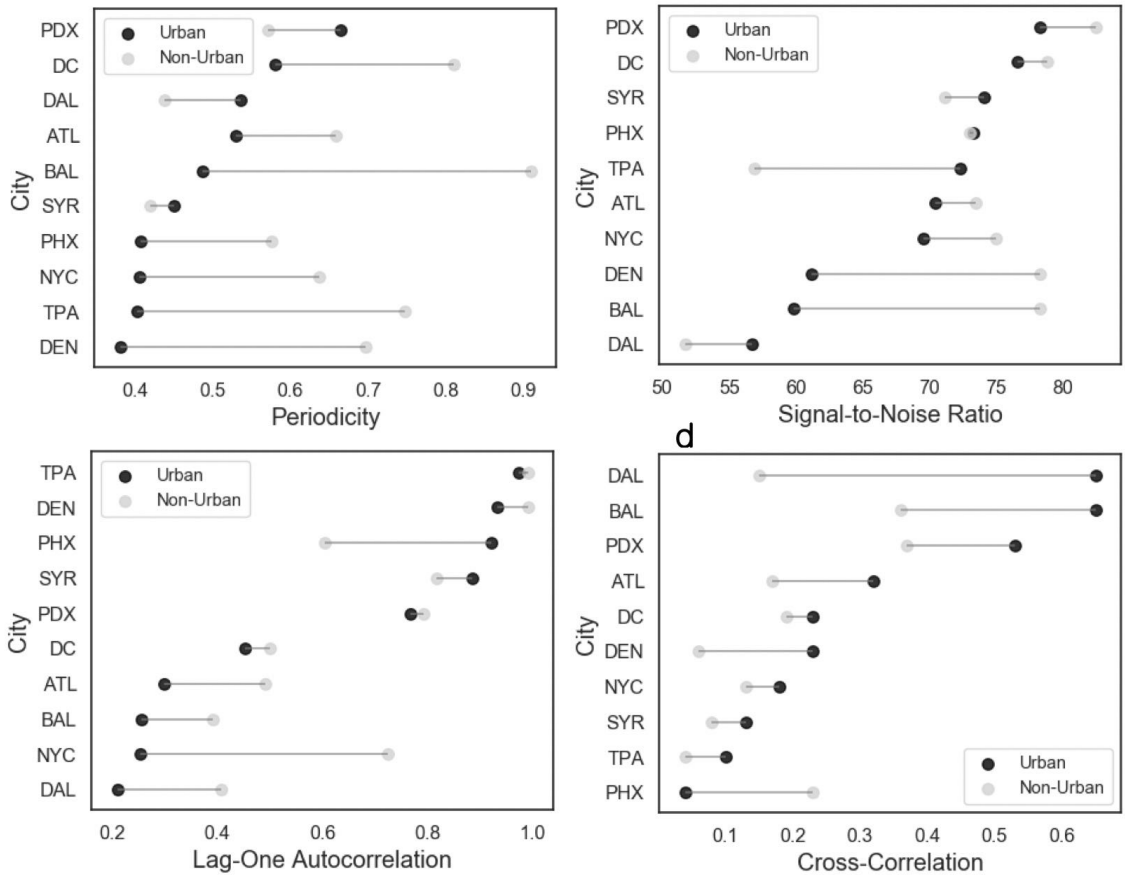

Figure 5.4: Calculated metrics of stream discharge time series for (a) periodicity of statistically significant power spectra (95% C.I.), (b) signal-to-noise ratios (SNR), (c) lag-one auto-correlation, and (d) cross-correlation (r) coefficients between daily precipitation and stream discharge in urban and non-urban watersheds from 2000 to 2020. See Table 1 for city abbreviations.

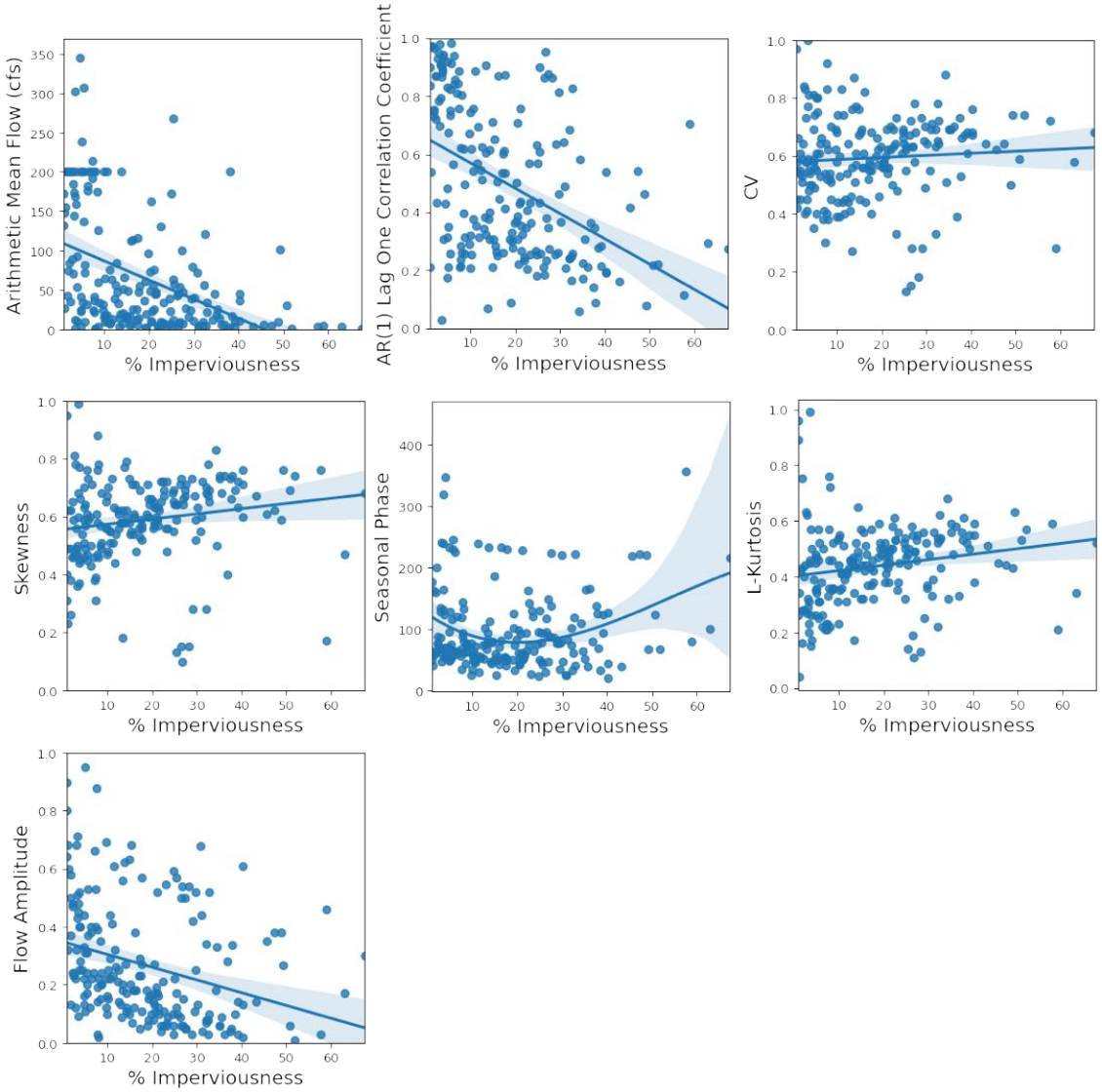

Figure 5.5: Mean values of the seven fundamental daily streamflow statistics (FDSS) with changes in % imperviousness across all study gauges. Shaded regions represent a 95% confidence interval (C.I.).

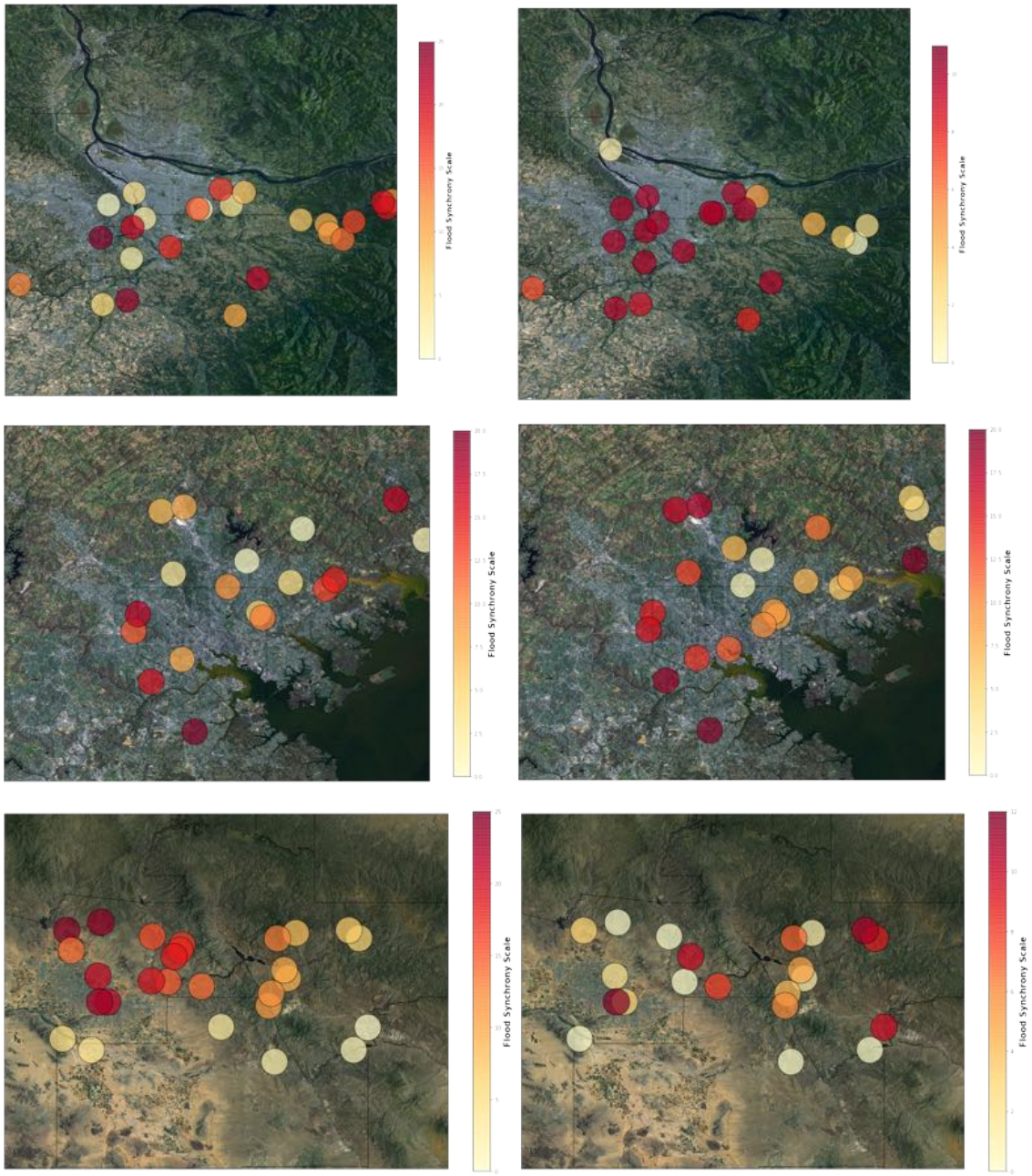

Figure 5.6: Calculated Flood Synchrony Scale (FSS; sq km) during 2000 (left) and 2020 (right) in (a) Portland, Oregon, (b) Baltimore, Maryland, and (c) Phoenix, Arizona. Darker hues indicate higher FSS values.

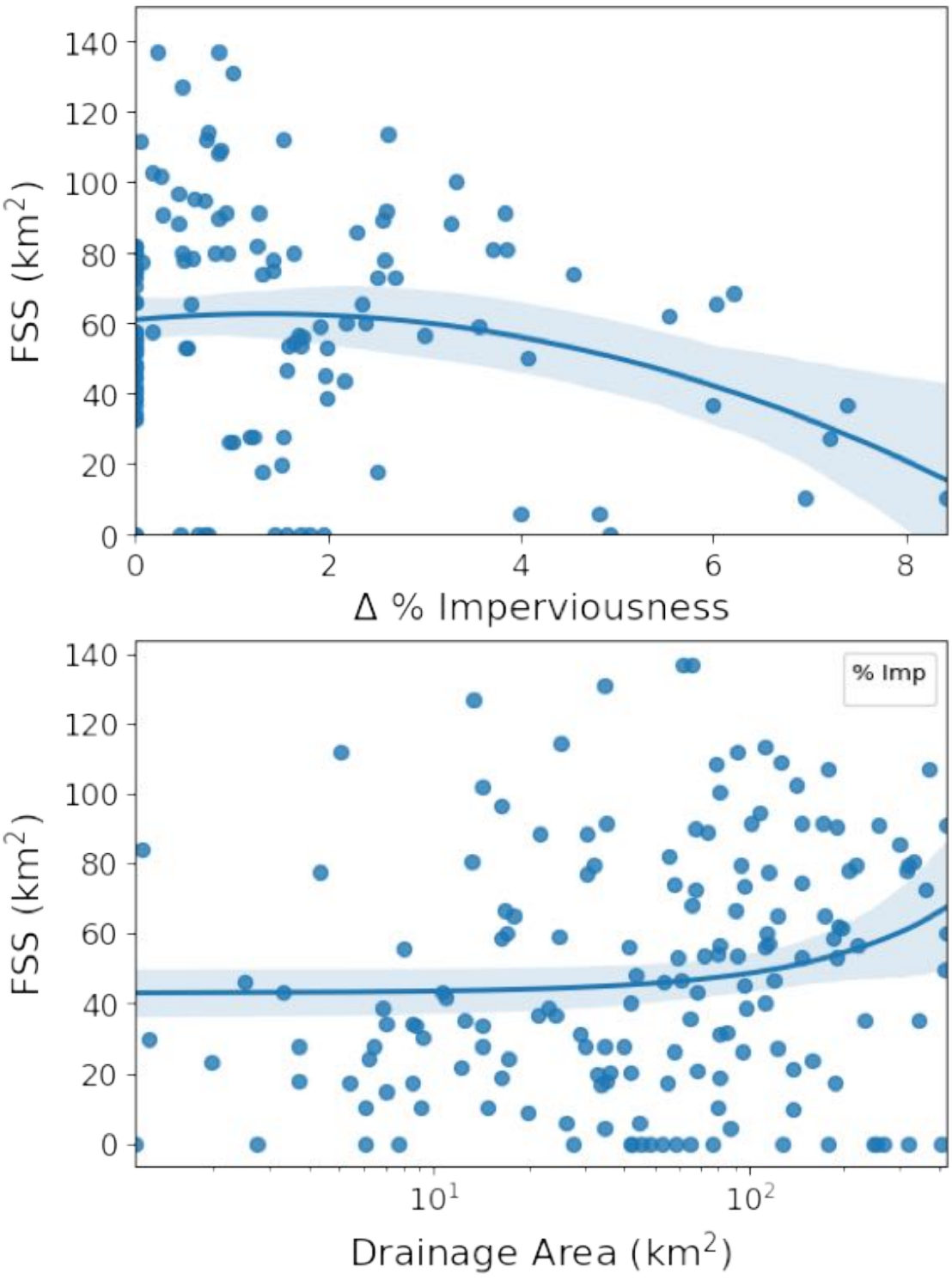

Figure 5.7: Relationship between Flood Synchrony Scale (FSS; sq km) and (a) change (Δ) in percent watershed imperviousness and (b) total drainage area (sq km) across all study sites.

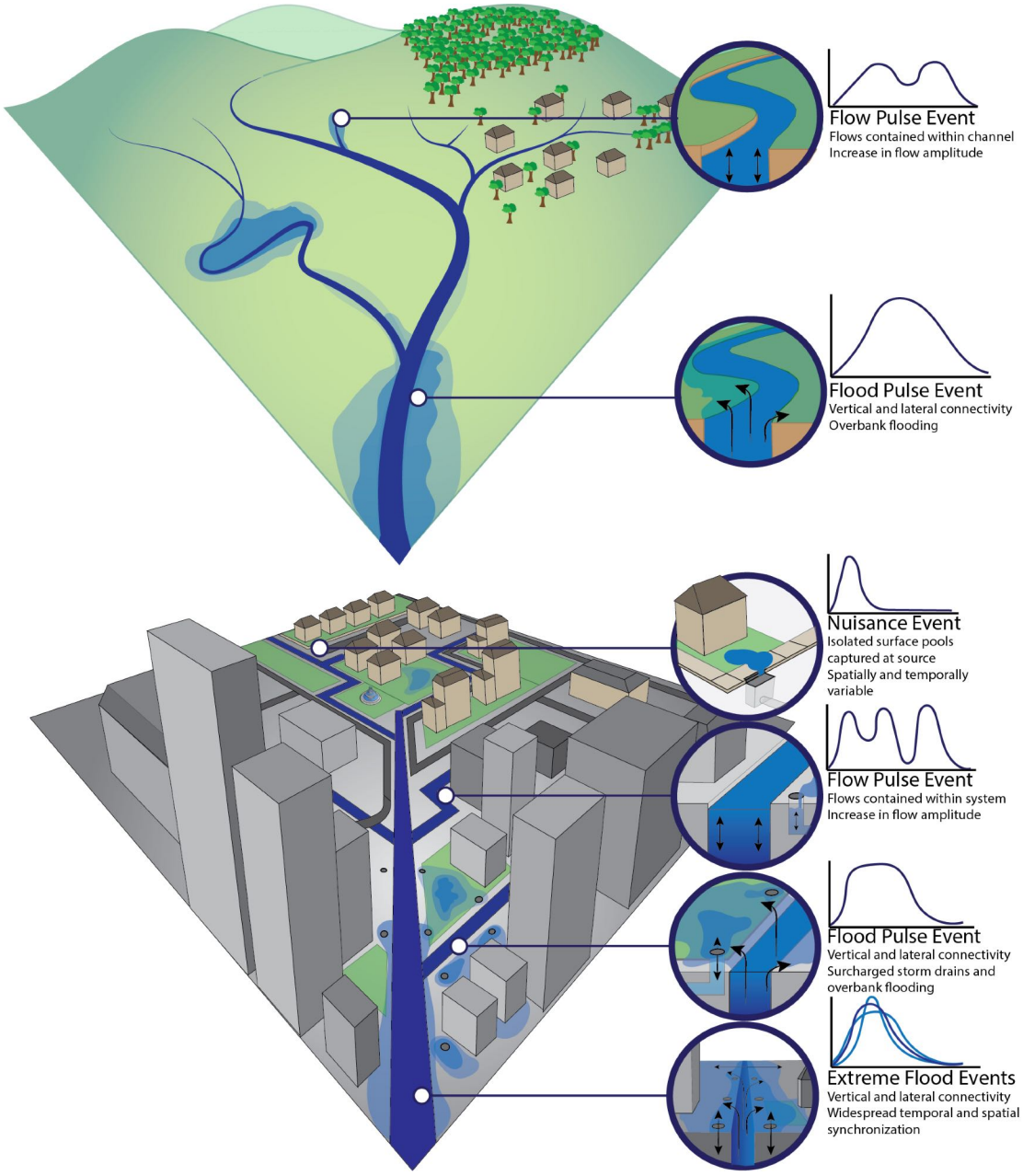

Figure 5.8: Conceptual diagram illustrating the the influence of urbanization on the timing, frequency, and magnitude of streamflow anomalies during high-flow flood events.

5.10 Supplemental Information

Table 5.2: List of streamflow statistics from Archfeld et al. (2013)

Statistic ID	Hydrologic Metric	Statistical Description (from Archfield *et al.* (2013))
lam1	mean	arithmetic mean of stream discharge series
tau2	cov	coefficient of variance in stream discharge series
tau3	skewness	asymmetry of stream discharge series
tau4	kurtosis	measure of sharpness in distribution of stream discharge series
ar1	AR(1)	Lag-one correlation coefficient
amp	amplitude	Amplitude of seasonal discharge signal
phase	phase	Phase of seasonal discharge signal

[ht!]

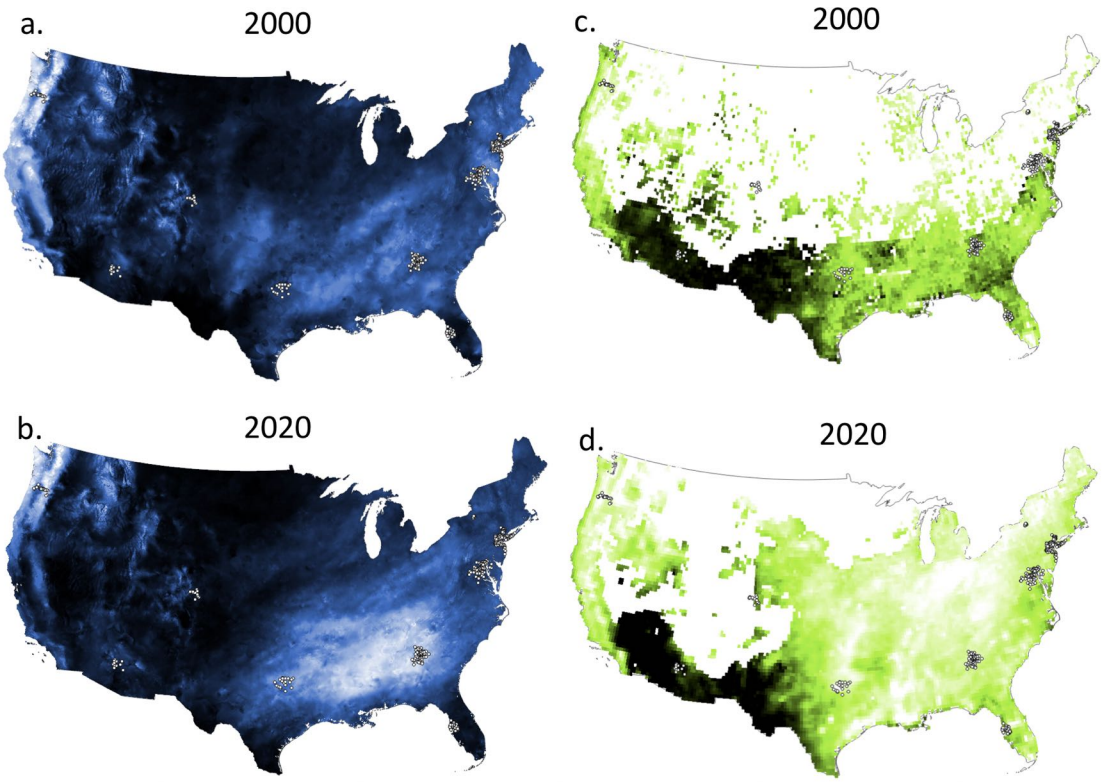

Figure 5.9: Comparison of of monthly mean values of gridded precipitation (blue; a,b) and antecedent soil moisture (green; c,d) in January 2000 and January 2020 in the continguous United States. Darker hues indicate higher values. Study locations are represented by white circles.

CHAPTER 6

CONCLUSIONS

Coastal urban aquatic ecosystems are biogeochemical hotspots that support prime conditions for the processing and transformation of carbon and nutrients from headwater streams to receiving estuaries (Basu et al.; 2010; Kroeze et al.; 2013). Human activities in urban environments can change the source, timing, and quality of DOC and DOM in coastal waters, thereby altering the capacity for in-stream processing and impact the ultimate fate of carbon and nutrients downstream. Additionally, accelerated SLR and adaptive stormwater management is driving increases in more bioavailable DOM and nutrients, particularly from groundwater sources, that can arise during significant flow or flood pulse events. Together, these changes in hydrologic and land use conditions have substantial impact on the health and productivity of coastal aquatic ecosystems.

The determination of water source contributions to coastal canals presented in Chapter 2 clearly demonstrates the importance of seasonal groundwater contributions of DOC, DOM and nutrients to coastal waterways. Chapter 2 also demonstrates the utility of a combined isotope-fDOM tracer mixing model to estimate water source contributions and relative DOM source.

Chapter 3 explored interactions between seasonal stormwater runoff and tidal extension that lead to increased DOM bioavailability from anthropogenic sources in the wet season at high tide. We provide evidence of an urban priming effect in which labile autochthonous DOM can facilitate microbial degradation of DOM and may affect overall ecosystem metabolism.

In Chapter 4, we demonstrate the relative importance of water column processing of inorganic nutrients in urban wetlands that contain high proportions of labile, easily degradable DOM. Specifically, we suggest that smaller, short-residence

time urban wetlands may have significant capacity to uptake nutrients before being exported downstream.

Finally, Chapter 5 introduces the urban flow-shunt flood-pulse concept in which high-flow discharge events in urban watersheds tend to synchronize across smaller spatial but more frequent temporal scales compared to non-urban watersheds. Further, we observed similar flow patterns across temperate regional climates that contrasted those in mountainous or arid watersheds where flow synchronization decreased with urbanization.

6.0.1 The combined influence of runoff and tides on carbon and nutrient cycling

This dissertation adds to our understanding of the biogeochemical complexity of carbon and nutrient processing in coastal urban ecosystems under changing climatic and hydrological conditions. We provide evidence that the processing of carbon and nutrients are heavily influenced by the timing and magnitude of seasonal stormwater runoff and tidal extension. Further, the combined influence of climate, landscape hydrology, and coastal dynamics may not only elevate the concentration of DOC and dissolved nutrients, but also impact the ultimate fate of constituents in downstream waters.

Our results suggest that there is a strong connection between upstream freshwater, subsurface (ground) brackish water, and coastal saltwater during the wet season at high tide. Given the high spatial connectedness of urban stormwater systems, water moves freely between surface and subsurface systems resulting in a thoroughly mixed DOM and nutrient pool (Walsh et al.; 2012; Hale et al.; 2016). Kaushal and Belt (2012) suggested that aging urban water infrastructure can behave as an "urban karst" with the water they carry interacting with other pipes and shallow ground-

water. Results from Chapter 2 and 3 suggest the increasing presence of groundwater in surface canals and may contribute labile DOM to the larger DOM pool, as seen in other studies (Stalker et al.; 2009; Santos et al.; 2021). Similarly, results from Chapter 4 suggest that sources of labile and/or proteinaceous DOM, often supplied by groundwater, can stimulate the processing of more recalcitrant DOM and influence the uptake of dissolved nutrients in the water column. Together, However, more evidence is needed regarding

6.0.2 Urban coastal waterways serve as biogeochemical control points

The work of this dissertation supports the conclusion that the sources of carbon and nutrients in coastal urban ecosystems are unique and support evidence of an urban priming effect in response to significant hydrologic and/or tidal events. The coastal waterways presented here are active biogeochemical transformers that support processing of DOC, DOM and nutrients from both surface and subsurface hydrologic flowpaths. While the results of this research highlight the immense capacity for instream processing and transformation, we may still be underestimating the role of urban sourced DOM in regional biogeochemical budgets (Parr et al.; 2015). Conceptualizing coastal urban waterways as active corridors for flow-shunt and flood-pulse processes can lead to better understanding of catchment biogeochemical budgets and the rising influence of coastal groundwater with SLR.

6.1 Bibliography

Basu, N. B., Destouni, G., Jawitz, J. W., Thompson, S. E., Loukinova, N. V., Darracq, A., Zanardo, S., Yaeger, M., Sivapalan, M., Rinaldo, A. et al. (2010). Nutrient loads exported from managed catchments reveal emergent biogeochemical stationarity, *Geophysical Research Letters* **37**(23).

Hale, R. L., Scoggins, M., Smucker, N. J. and Suchy, A. (2016). Effects of climate on the expression of the urban stream syndrome, *Freshwater Science* **35**: 421–428.

Kaushal, S. S. and Belt, K. T. (2012). The urban watershed continuum: Evolving spatial and temporal dimensions, *Urban Ecosystems* **15**: 409–435.

Kroeze, C., Hofstra, N., Ivens, W., Löhr, A., Strokal, M. and van Wijnen, J. (2013). The links between global carbon, water and nutrient cycles in an urbanizing world - the case of coastal eutrophication, *Current Opinion in Environmental Sustainability* **5**: 566–572.

Parr, T. B., Cronan, C. S., Ohno, T., Findlay, S. E., Smith, S. M. and Simon, K. S. (2015). Urbanization changes the composition and bioavailability of dissolved organic matter in headwater streams, *Limnology and Oceanography* **60**: 885–900.

Santos, I. R., Chen, X., Lecher, A. L., Sawyer, A. H., Moosdorf, N., Rodellas, V., Tamborski, J., Cho, H.-M., Dimova, N., Sugimoto, R., Bonaglia, S., Li, H., Hajati, M.-C. and Li, L. (2021). Submarine groundwater discharge impacts on coastal nutrient biogeochemistry, *Nature Reviews Earth Environment* **2**: 307–323.

Stalker, J. C., Price, R. M. and Swart, P. K. (2009). Determining spatial and temporal inputs of freshwater, including submarine groundwater discharge, to a

subtropical estuary using geochemical tracers, biscayne bay, south florida, *Estuaries and coasts* **32**(4): 694–708.

Walsh, C. J., Fletcher, T. D. and Burns, M. J. (2012). Urban stormwater runoff: a new class of environmental flow problem.

VITA

MATTHEW SMITH

October 25, 1992	Born, Baltimore, Maryland
2014	B.S., Biology York College of Pennsylvania York, Pennsylvania
2014-2016	Research Associate Texas A&M University College Station, Texas
2018	M.S., Biological Sciences Florida International University Miami, Florida
2016-2019	Graduate Research Fellow Urban Resilience to Extremes SRN Miami, Florida
2018-2020	Graduate Research Fellow SESYNC Annapolis, Maryland
2018-2020	Knauss Fellow NOAA Sea Grant Washington, D.C.
2016-2021	Doctoral Candidate Florida International University Miami, Florida

PUBLICATIONS AND PRESENTATIONS

Smith, M.A., Kominoski, J.S., Gaiser, E.E., Price, R.M., Troxler, T.G. (2021). Stormwater runoff and tidal flooding transform dissolved organic matter composition and increase bioavailability in urban coastal ecosystems. *Journal of Geophysical Research: Biogeosciences*, 126 (7), e2020JG006146.

Li, J., West, J.B., Hart, A., Wegrzyn, J.L., Smith, M.A., Domec, C., Loopstra, C.A., Casola, C. (2021). Extensive variation in drought-induced gene expression changes between loblolly pine genotypes. *Frontiers in Genetics: Plant Genetics*

and Genomics, 12, 659.

Smith, M.A., Abellera, M., Greenfeld, B., Molnar, M. (2021). Exploring the challenges and opportunities for effective benefit-cost analysis of nature-based solutions in coastal resilience planning. American Shore and Beach Preservation Association (ASBPA) National Coastal Conference, New Orleans, LA.

Smith, M.A., Kominoski, J.S., Gaiser, E.E., Grimm, N.B., McPhillips, L.E., Rosenzweig, B.R., Ruhi, A., Troxler, T.G. (2021). Synchronizing hydrology in urban watersheds: flow-shunt flood-pulse concept. Association for the Sciences of Limnology and Oceanography, virtual

Smith, M.A., Kominoski, J.S., Price, R.M., Gaiser, E.E., Troxler, T.G. (2020) Evaluating spatiotemporal variation in water source contributions to coastal urban canal networks using an endmember mixing model. Ecological Society of America, virtual

Smith, M.A., Balderas-Guzman, C., Wang, R., Muellerklein, O., Eger, C. (2020) Decrypting stormwater pollution: Identifying urban watershed typologies using machine learning. National Watershed and Stormwater Conference, virtual

Smith, M.A., Kominoski, J.S., Price, R.M., Gaiser, E.E., Troxler, T.G. (2019) The urban flood pulse concept: defining spatiotemporal periodicity and synchrony of flood pulse dynamics in urban ecosystems. American Geophysical Union, San Francisco, CA

Smith, M.A., Kominoski, J.S., Barbosa, O., Chang, H., Morse, J.L., Gaiser, E.E., Grimm, N.B., Troxler, T.G., Williams, T. (2019) A comparison of nutrient uptake dynamics in urban wetlands across different regional climates. Invited talk at the Ecological Society of America, Louisville, KY